# Developing Therapeutic Interventions for Influenza Virus Infection: Targeting Host Factors and Characterizing T-Cell Epitopes

**Dissertation**

der Mathematisch-Naturwissenschaftlichen Fakultät

der Eberhard Karls Universität Tübingen

zur Erlangung des Grades eines

Doktors der Naturwissenschaften

(Dr. rer. nat.)

vorgelegt von

M.Sc. Hazem Ahmed Hamza Ewess

aus Giza, Ägypten

Tübingen

2024

Gedruckt mit Genehmigung der Mathematisch-Naturwissenschaftlichen Fakultät der Eberhard Karls Universität Tübingen.

| | |
|---|---|
| Tag der mündlichen Qualifikation: | 23.09.2024 |
| Dekan: | Prof. Dr. Thilo Stehle |
| 1. Berichterstatter: | Prof. Dr. Oliver Planz |
| 2. Berichterstatter: | Prof. Dr. Hans-Georg Rammensee |
| 3. Berichterstatterin: | Prof. Dr. Cécile Gouttefangeas |

Printed with the support of the German Academic Exchange Service (DAAD)

*für meine Eltern, die mir allweil ein Lächeln ins Gesicht zaubern.*

# Table of Contents


**SUMMARY** 1

**ZUSAMMENFASSUNG** 2

**GENERAL INTRODUCTION** 3

**Taxonomy and genome structure** 4

**Evolution and host range** 5

**Therapeutic approaches for management of Influenza** 7

**Influenza Vaccines and recent advances** 7

Seasonal influenza vaccines 7

Recent advances in influenza vaccines development 8

Headless HA vaccines 8

Chimeric HA vaccines 8

COBRA approach 9

mRNA vaccines 9

T cell-based vaccines 11

**Broadly neutralizing antibodies-based therapeutics** 11

Immune plasma 12

Anti-HA monoclonal antibodies 13

Anti-NA monoclonal antibodies 13

**Antiviral drugs** 14

Direct-acting antiviral drugs 14

M2 ion channel inhibitors 14

Neuraminidase inhibitors 15

Polymerase inhibitors 16

Host-targeted antiviral drugs 16

Targeting the Raf/MEK/ERK Pathway 17

**References** 19

**OBJECTIVES** 39

**RESULTS** 40

## *Table of Contents*

**Part I** **41**

**Chapter 1** **43**

**Antiviral Efficacy Against Influenza Virus and Pharmacokinetic Analysis of a Novel MEK-Inhibitor, ATR-002, in Cell Culture and in the Mouse Model** **43**

Disclosure of authorship contribution 44

Abstract 45

Introduction 45

Materials and methods 47

Results 52

Discussion 64

References 68

Supplementary materials 73

**Chapter 2** **75**

**Improved *in vitro* Efficacy of Baloxavir Marboxil Against Influenza A Virus Infection by Combination Treatment with the MEK Inhibitor ATR-002** **75**

Disclosure of authorship contribution 76

Abstract 77

Introduction 77

Materials and methods 79

Results 82

Discussion 90

References 94

Supplementary materials 100

**Chapter 3** **103**

**Antiviral and Immunomodulatory Effect of Zapnometinib in Animal Models and Hospitalized COVID-19 Patients** **103**

Disclosure of authorship contribution 104

Abstract 105

Introduction 107

Materials and methods 109

Results 119

Discussion 132

References 138

Supplementary material 148

**Part II** **163**

**Chapter 4** **165**

**Identification and Relative Abundance of Naturally Presented and Cross-Reactive Influenza A Virus MHC Class I-Restricted T Cell Epitopes** **165**

Disclosure of authorship contribution 166

Abstract 167

Introduction 167

Materials and methods 169

Results 175

Discussion 190

References 194

Supplementary materials 200

**GENERAL DISCUSSION** **205**

**ABBREVIATIONS** **215**

**ACKNOWLEDGEMENTS** **218**

# Summary

The development of vaccines and antiviral drugs are the pillars for preventing and treating influenza. Currently available vaccines as well as direct-acting antiviral drugs are prone to resistance due to the continuous emergence of new variants. Accordingly, there is an urgent demand for developing alternative approaches. Lessons learned from previous pandemics are people with a preexisting cellular immune response either protected or less severe against the infection. Also, Influenza viruses rely on cellular signaling pathways that enhance efficient replication. These observations lead to the proposal of new approaches that target either cellular factors or activation of cellular immune response against influenza viruses.

In this context, the results in part I address the development of MEK inhibitor, zapnometinib, as a host-targeted antiviral drug against Influenza A virus (IAV). **Chapter 1 and Chapter 2** emphasize that zapnometinib can effectively impair the replication of different IAV subtypes, including baloxavir-resistant strains, via nuclear retention of influenza vRNP. Moreover, **Chapter 2** extends the investigations by showing that the combinatorial treatment of zapnometinib and baloxavir marboxil results in synergistic effect when used at lower concentrations than when used individually. **Chapter 3** sheds light on the dual therapeutic potential of zapnometinib by modulating rather than fully suppressing the immune response using acute lung injury (ALI) model. Taken together, the results highlight important findings that can help progress the development of zapnometinib as a potential therapeutic option for treating influenza virus infection.

In Part II, **chapter 4** focuses on implementing a mass spectrometry-based immunopeptidomics approach to identify and further characterize naturally presented IAV-derived MHC-I restricted epitopes. The immunopeptidomic analysis alongside functional characterization unveiled novel nine epitopes comprising different viral protein segments restricted to different HLA allotypes, HLA-A*24:02, HLA-A*68:01, HLA-B*07:02, and HLA-B*51:01. Conservation analysis revealed that most epitopes are highly conserved among zoonotic reservoirs, with potential single amino acid substitutions in the vicinity of anchor residues that do not significantly affect binding affinity. These findings demonstrate how the identified epitopes can confer heterosubtypic protection and represent potential targets for vaccination.

# Zusammenfassung

Die Entwicklung von Impfstoffen und antiviralen Medikamenten sind die Eckpfeiler der Grippeprävention und -behandlung. Derzeit verfügbare Impfstoffe und antivirale Medikamente sind anfällig für Resistenz, da weiterhin neue Stämme auftauchen. Dementsprechend ist es dringend erforderlich, Alternativen zu entwickeln. Erkenntnisse aus früheren Pandemien zeigen, dass Menschen mit einer vorbestehenden zellulären Immunantwort entweder geschützt sind oder die Infektion weniger schwer verläuft. Auch Influenzaviren sind auf zellbasierte Signalwege angewiesen, um sich effizient zu vermehren. Diese Beobachtungen führten zum Vorschlag neuer Ansätze, die sich mit zellulären Faktoren gegen Influenzaviren befassen.

In diesem Zusammenhang befassen sich die Ergebnisse in Teil I mit der Entwicklung des MEK-Inhibitors Zapnometinib als Wirtszell-gerichtetes antivirales Medikament gegen das Influenza-A-Virus (IAV). **Kapitel 1** und **Kapitel 2** betonen, dass Zapnometinib die Replikation verschiedener Influenzaviren Stämme stören kann, einschließlich Baloxavir-resistenter Stämme, indem es die Influenza-vRNP nukleare Retention bewirkt. Darüber hinaus erweitert Kapitel 2 detailliert Untersuchungen, die zeigen, dass die Kombination von Zapnometinib und Baloxavir marboxil eine synergistische Wirkung hat, wenn sie in geringeren Dosen als bei alleiniger Anwendung eingesetzt wird. **Kapitel 3** stellt das doppelte therapeutische Potenzial von Zapnometinib vor, indem es die Immunantwort moduliert, anstatt sie vollständig zu unterdrücken, und verwendet dazu ein Modell für akuten Lungenverletzungsmodell (ALI). Insgesamt heben die Ergebnisse wichtige Erkenntnisse hervor, die die Entwicklung von Zapnometinib zur Behandlung von Influenzaviren Infektionen voranzutreiben.

In Teil II stellt sich **Kapitel 4** auf die Anwendung eines massenspektrometrischen Ansatzes zur Identifizierung und weiteren Charakterisierung natürlich präsentierter IAV-abgeleiteter MHC-I Epitope. Die funktionelle Charakterisierung enthüllte neun neuartige Epitope, die verschiedene virale Proteinsegmente umfassen und auf verschiedene HLA-Allele, HLA-A*24:02, HLA-A*68:01, HLA-B*07:02 und HLA-B*51:01, restringiert sind. Konservierungsanalyse zeigten, dass die meisten Epitope hoch konserviert sind, wobei mögliche Substitutionen nur einer Aminosäure in der Nähe des Ankerrests möglich sind, ohne dass die Bindungsaffinität wesentlich beeinträchtigt wird. Diese Erkenntnisse zeigt, wie identifizierte Epitope heterosubtypischen Schutz verleihen und potenzielle Ziele für die Impfung darstellen können.

# General Introduction

Influenza is an acute respiratory tract infection caused by Influenza viruses circulating worldwide. Influenza virus infection poses a major public health concern and significant morbidity and mortality. Annually, seasonal epidemics are estimated to result in about 3 to 5 million cases of severe illness and about 290 000 to 650 000 respiratory deaths among adults [1-4]. The incidence rate in children is estimated at 90 million cases and 100,000 deaths annually in children younger than 5 years [2,5,6].

Every 10 to 50 years, sporadic and global pandemic outbreaks also occur and are characterized by the introduction of new influenza A virus (IAV) strains that are antigenically different from the circulating strains and may involve strains of zoonotic origin. The virulence of pandemic strain and the lack of pre-existing immunity in humans are often associated with the severity of infection and mortality rates [3]. During pandemics, the features of the viral surface glycoproteins, hemagglutinin (HA) and neuraminidase (NA), are relatively naïve to the immune system. This was the case during the Spanish flu in 1918, which killed at least 50 million people worldwide, caused by the IAV H1N1 subtype when the majority of the population lacked immunity to the HA and NA as well as in 1958 when the H2N2 was newly introduced [7]. However, IAV avian strains whose proteins (except HA and NA) differ by less than 10 amino acids (AA) from the 1918 Spanish H1N1 strain are still circulating in nature [8].

In 1968, during the H3N2 pandemic, only the H3 was introduced to humans while the H2 was derived from previously circulating H2N2 [7,9]. In 2009, despite the circulation of seasonal H1N1 in humans, the swine-origin H1N1 pandemic strain had distinct H1 and N1 surface glycoproteins [10]. The genomic analysis of this pandemic strain revealed that the swine-origin virus arose from triple reassortments between the Eurasian avian-like swine viruses and the North American swine viruses [11]. Widespread infections during the pandemic phase induce population immunity and within a few years, the pandemic strains had become seasonal viruses with a lower fatality rate [12]. Currently, the major disease burden is caused by seasonal epidemics of IAV (H1N1 and H3N2) and influenza B virus (IBV) co-circulating in humans, but IAV H2N2 was circulating between 1957 to 1968 in humans. These IAV subtypes as well as the two IBV lineages represent the formulation backbone of the human seasonal influenza vaccines [3].

## Taxonomy and genome structure

Influenza viruses belong to the Orthomyxoviridae family which comprises seven genera, including four genera of influenza viruses, Alpha-, Beta-, Gamma-, and Deltainfluenzavirus (Influenzavirus A, Influenzavirus B, Influenzavirus C, and Influenzavirus D) and three non-influenza viruses [13,14].

IAV can be further classified into subtypes according to their antigenic determinants; HA and NA glycoproteins. Based on sequences similarity, IAVs are classified into 18 HA subtypes (H1-H18) and 11 NA (N1-N11) in various combinations. Unlike IAV, IBV does not exhibit distinct HA or NA subtypes. Instead, IBV are diverged into two antigenically different lineages (B/Yamagata/16/1988-like and B/Victoria/2/1987-like) [3,15,16].

Influenza viruses are defined as single-stranded, negative-sense RNA viruses with segmented RNA genome that replicate in the nucleus of infected cells. IAV and IBV contain eight viral RNA (vRNA) segments, whereas Influenza C and D viruses only have seven segments. The viral genome segments encode at least ten essential viral proteins (PB2, PB1, PA, HA, NP, NA, M1, M2, NS1, and NS2). IAV and IBV have the ability to increase the coding capacity of their genomes and express additional auxiliary proteins e.g. PB1-F2, PB2-S1, PB1-N40, and PA-X that fulfill a wide range of functions during viral infection and remain unknown to be incorporated into the virion. These accessory proteins are encoded by some but not all strains either by using alternative open reading frames or via splicing [16,17].

The transmembrane glycoprotein HA is initially synthesized as an inactive form called HA0. To be fully active, it is further cleaved into HA1 and HA2 subunits through a proteolytic process. HA is assembled as trimers which comprise the head domain, which contains the receptor-binding site (RBS), and the stalk domain, which harbors the fusion peptide. HA facilitates viral entry through the binding to the cell surface receptors sialyloligosaccharides and in membrane fusion. The NA glycoprotein possesses sialidase activity, facilitating both the viral entry and release of virus progeny from the cell surface by cleavage of sialic acid [16]. It is essential to consider the glycosylation of HA and NA, as it can influence immune recognition, receptor binding affinity, and enzyme function. Alterations in the extent of HA glycosylation may also influence the virus's potential for inter-species transmission [18,19].

Each vRNA segment surrounds an oligomeric Nucleoprotein (NP) structure, and the promotor is bound to a heterotrimeric polymerase structure of Influenza polymerase basic 1 (PB1), Influenza polymerase basic 2 (PB2), and Polymerase acidic (PA) proteins, known as RNA-dependent RNA polymerase (RdRp) complex. The PA subunit contains the endonuclease that cleaves the CAP-structure (cap-snatching) from cellular mRNAs, which is then utilized by the RdRp to generate capped primers for viral mRNA synthesis [20-22]. These structures form together the biologically active viral ribonucleoproteins (vRNP) complex which transcribes and replicates the viral genome within the nucleus of the infected cell [13,23,24].

## Evolution and host range

The enormous reservoir of IAV in waterfowl plays a critical role in providing unlimited gene pools. These gene pools have the potential to give rise to new variants capable of infecting humans, thereby posing a major pandemic threat [13,25,26].

The virus can escape selective pressures as the RdRp lacks a proofreading function. Through the accumulation of point mutations constantly alters the genome sequence, allowing the virus to generate a multitude of genetic and antigenic variants [27]. Owing to the segmented nature of the influenza virus genome, genetic reassortment events can take place by interchanging RNA segments between two viruses of the same type. This process provides additional mechanisms of genetic adaptation. However, there have been no reports of reassortment events occurring between the members of the four influenza virus genera [14]. Throughout history, the Asian H2N2 influenza outbreak in 1957 as well as the Hong Kong H3N2 influenza outbreak in 1968 exemplify how reassortment events can give rise to novel influenza virus strains with significant implications for global health [3,13,28]. This was also the case for the emergence of swine flu pandemic H1N1 in 2009 by triple reassortment events between avian, human and swine viruses [29,30]. Moreover, the highly pathogenic avian influenza (HPAI) H7N9 emerged in 2013 as a result of multiple reassortment events involving different avian influenza viruses (AIV) strains [31,32].

Certain influenza viruses are adapted to infect various birds (chicken, quail, and turkeys), as well as mammals (e.g. swine, equine, and humans). Such Inter-species transmissions often coincide with viral genetic adaptations to the new host, influenced by the error-prone nature

of the viral RNA polymerase. Viral adaptation to a new host is a multifactorial process and may require AA substitutions in the RBS. These substitutions are necessary for optimizing receptor binding, improving the ability of HA to become activated at varying pH levels, and fine-tuning the balance between the HA binding activity and NA destroying activity [33-36]. The ensuing intra-host viral quasispecies result in a swarm of viral mutants that promote adaption to the selection pressure, and quasispecies may become the dominant virus population. Various viral variants are transmitted between animals, and low-fitness variants can be retained, presumably, by the aid of fitter variants within a host [3,14,37].

The glycosylation of HA glycoprotein plays a crucial role in influenza viruses' evolution. The virulence of influenza viruses as well as the host range may be influenced by the location and number of oligosaccharide side chains. Furthermore, glycosylation is a critical factor in the immune evasion tactics employed by influenza viruses. The addition of glycans to the globular domain has been demonstrated to directly inhibit the neutralization of HA by both monoclonal (mABs) and polyclonal (pABs) antibodies [38-41]. These side chains are not consistent among different influenza virus strains or subtypes. For the H1N1 and H3N2 subtypes, the number of N-glycosylation sites has increased since their introduction into humans. Also, the H5 and H7 isolates from terrestrial birds exhibit greater number of glycosylation sites compared to isolates from wild birds. The HPAI H7N9, which emerged in China in 2013, naturally lacks a glycosylation site from $HA_{158}$ to $HA_{160}$ (H3 numbering). This particular glycosylation site is critical for respiratory transmission [14,18,32,42].

The host range varies between the four influenza virus types. A unique characteristic of IAV lies in its ability to circulate across a wide range of host species. This includes not only humans but also pigs, poultry, and wild birds [13,25,26]. IBV and influenza C viruses (ICV) primarily circulate in humans. However, limited instances of spillover to seals and swine have been reported for both types respectively [43-45]. ICV can also cause influenza-like illness and hospitalization in children [46]. Influenza D viruses (IDV) are known to circulate in pigs, cattle, and goats. However, the potential zoonotic threat to humans remains unclear, despite some serological evidence of infection [13,47].

The expression profile of the sialic acid (SA) receptor is a key determinant of influenza virus species specificity. Human-adapted influenza viruses specifically bind SA linked to α2-6, while

HAs of AIV attach to α2-3 SA. However, several AIV subtypes that are not circulating among humans either already possess or can develop affinity to the α2-6 SA [48-50]. This is the case of the HPAI H7N9, which infected more than 1,525 cases and caused over 616 deaths. This strain exhibits binding affinity to the α2-6 SA receptor, which could partially explain the frequent transmission to exposed individuals [51,52]. On the other hand, H5N1 viruses that are responsible for human infection retain preferential binding to the α2-3 SA. They also undergo mutations in the HA surface protein that enable switching of SA specificity to α2-6. These mutations are required for airborne transmission [18,19,49].

# Therapeutic approaches for management of Influenza

## Influenza Vaccines and recent advances

### *Seasonal influenza vaccines*

As an important approach towards influenza virus control, vaccines were used extensively for the protection against influenza virus infections. Although antigenic drift and antigenic shift are recognized problems in vaccine development, vaccine manufacturing techniques remained unchanged for decades [3].

Currently, there are three types of licensed influenza vaccines, live attenuated, inactivated, and recombinant HA vaccines, and each vaccine has advantages and drawbacks [53]. However, the current seasonal human influenza vaccines are not optimal, their effectiveness varies from year to year, and necessitate biannual reformulation to match circulating strains in both the northern and southern hemispheres [3,16,54]. Also, varying vaccine effectiveness has been implicated with poor protection in terms of subtype measurements against the H3N2 subtype [55,56].

The currently approved vaccines focus only on the HA proteins of circulating influenza strains. Vaccine mismatch occurs not only as the most prevalent antigenic strain is missed but also because of the emergence of egg-adaptive strain during the vaccine production process [57,58]. Moreover, the glycosylation of HA may hamper the development of broadly protective influenza vaccines. This was the case of the 2016-2017 seasonal vaccine that lacked the glycosylation site presented in the H3N2 circulating strains which led to alteration of the

vaccine components antigenicity [59-61]. These challenges contribute to the variability in vaccine effectiveness against influenza strains.

## Recent advances in influenza vaccines development

Frequent update of current seasonal human influenza vaccines is a necessity to ensure sufficient coverage and antigenic relatedness between vaccines and circulating virus variants. Therefore, several approaches have been proposed to produce so-called universal influenza vaccines. These approaches focus on different aspects of the virus aiming to provide broad protection against diverse influenza strains. These approaches include targeting the HA stem, the HA RBS, T cell-based vaccine, and utilizing mRNA-based technology [16,53].

### Headless HA vaccines

Although the variable antigenicity of HA domains between influenza virus subtypes, the HA stalk domain remains more conserved among HA group members [62,63]. Also, generating a robust antibody response against the stalk domain presents a challenge due to the immunodominance of the HA head. Therefore, several strategies, such as vaccination with headless HA, have been suggested to elicit anti-HA stem antibodies [64-67].

This concept was initially reported in 1983 and further developments have been made by other researchers [64,67,68]. The Headless HA vaccine approach is seemingly an obvious solution. It involves designing immunogens based on the HA-conserved stalk domain. However, some limitations are associated with this technique, in particular, the inclusion of heterologous elements that give rise to autoimmunity concerns [69]. It is critical for the efficacy of headless HA vaccines that the proteins remain stable and properly folded. Any misfolding or instability could jeopardize their capacity to trigger a protective immune response. Thus, due to the removal of the HA globular head, the folding of headless HA constructs is impacted. Consequently, many stalk-reactive antibodies, that bind specifically to conformational epitopes, encounter troubles in recognizing these constructs very well [70].

### Chimeric HA vaccines

To refocus the immune response from the HA globular head to the stalk domain, a sequential chimeric HA (cHA) vaccine strategy was developed. These cHA vaccines consist of a stalk domain from either HA from H1 (group 1) or H3 (group 2) combined with a head domain

derived from AIV subtypes [71-73]. Repeated exposure to the same stalk domain boosts the immune response related to the stalk response, while divergent globular head domains, typically immunodominant, only trigger a primary immune response. Preclinical studies revealed that sequential vaccination using the cHA vaccine approach provides broad protection against different influenza virus subtypes [72,74-77]. Of note, the protective efficacy of the cHA approach may still be a point of concern relying on the specific chimeric antigen subtypes, and planned antigens selection is required [78]. Additionally, the clinical trials provide a proof of concept and specifically focus only on group 1 IAVs [71,79,80].

### *COBRA approach*

The computationally optimized broadly reactive antigen (COBRA) is another approach that uses a consensus sequence of divergent HA sequences within one IAV subtype to induce antibody response against the HA head domain [81-83]. The immunity induced by this strategy is limited to one subtype or specific clade within the subtype making it less cross-protective compared to the anti-stalk approach [70]. The efficacy of this method could be significantly influenced by the phenomenon of head-specific-imprinting, which may have either beneficial or detrimental impacts on the vaccine effectiveness depending on the imprinting as well as the exposure background of the vaccine recipient [12].

### *mRNA vaccines*

mRNA vaccines are considered a promising universal next-generation influenza vaccine platform. A significant milestone was first achieved by demonstrating the effectiveness of an mRNA vaccine encoding the HA protein from the IAV strain A/Puerto Rico/8/1934 (H1N1). This vaccine successfully induced an increased amount of virus-neutralizing antibodies, marking a breakthrough in the quest for a more broadly protective flu vaccine [84]. Further progress was made by developing an mRNA encoding the HA protein of IAV H7N9 and H10N8 subtypes, which induce potent humoral and cellular immune responses [84]. In a randomized phase I clinical trial, this vaccine underwent further testing and was well-tolerated without showing any vaccine-associated adverse effects. However, significant cell-mediated immune responses were not reported, and high seroconversion rate can only be achieved by higher vaccine doses [85].

A nucleoside-modified mRNA–lipid nanoparticle (mRNA-LNP) vaccine was also developed by encoding the full-length HA protein of the H1N1pdm09 strain, which elicits antibodies against the HA stalk and head domains [86,87]. Unmodified mRNA lipid nanoparticle (LNP) formulations encoding the full-length of either HA or NA protein were further developed. These formulations, whether as monovalent or multivalent administration, elicited a robust antibody as well as cellular immune responses in nonhuman primates. Furthermore, they demonstrated protective efficacy against virus challenge in mice [88].

The modified mRNA-LNP technology was further utilized to deliver a combination of four different proteins from influenza A group 2 viruses: HA, NA, NP, and M2. This innovative approach aims to induce a robust immune response and overcome the limitations of most traditional influenza vaccines that target only a limited number of antigens. This quadrivalent mRNA-LNP vaccine elicited antigen-specific cellular and humoral immune responses and protected mice from all challenge viruses [89]. Furthermore, a broader protective pentavalent nucleoside-modified mRNA-LNP vaccine was developed against IBV. This vaccine encodes HA protein from the B/Yamagata/16/1988-like lineage and HA, NA, M2, and NP from the B/Victoria/2/1987-like lineage. This vaccine showed better protection against morbidity at an impressively lower dose [90].

The nucleoside-modified mRNA-LNP vaccine has been further improved to induce universal immunity by encoding HA antigens that represent each known influenza virus subtype [91]. This advancement offers the potential for a more thorough and efficient strategy in influenza vaccination. However, arguments arose that increasing the number of vaccine targets may increase the evolution of the influenza virus. Additionally, questions persist regarding the regulatory approval of such vaccines that target influenza viruses with pandemic potential but not currently circulating in humans [92].

In general, mRNA vaccines with a rapid production timeline represent a promising alternative to conventional vaccine approaches. However, since this approach still mainly focuses on the HA surface protein or specific influenza virus group or subtype, annual review, and reformulation may be required to cope with the rapid influenza virus evolution. Also, further randomized studies are still required to evaluate the efficacy and safety of the mRNA-based influenza vaccines [88,93,94].

### *T cell-based vaccines*

Cytotoxic T lymphocytes (CTLs) are key players in mediating the cellular arm of the adaptive immune response for influenza and have a crucial role in viral clearance and providing cross-protective immunity. Major Histocompatibility Complex Class I (MHC-I) molecules on the surface of infected cells present influenza peptides that are recognized by virus-specific CD8+ T lymphocytes, leading to the destruction of the infected cells [95-97].

Current seasonal influenza-inactivated vaccines do not induce a cellular immune response and antibodies produced by the seasonal vaccination usually confer strain-specific immunity targeting the variable HA head domain [98,99]. Even though they can offer neutralizing immunity, the persistent antigenic drift of hemagglutinin renders these antibodies inappropriate for cross-protection. In contrast, cytotoxic CD8+ T cells confer heterosubtypic protection against seasonal IAV or IBV as well as pandemic and avian strains [97,100-105].

The primary targets of CTLs are the M1, and NP, polymerase complex subunits that are comparatively conserved. The high conservation of presented peptides facilitates cross-recognition across different influenza virus strains and subtypes. Also, the breadth of epitope-specific CD8+ T cell cross-reactivity among antigenically distinct IAV strains enhanced their potential as targets for universal vaccination [3,106,107].

So far, several peptide-based vaccines targeting the highly conserved internal viral proteins M1, NP, and/or the RNA polymerase subunits have been successfully tested in animal models and are still in clinical development [108-112]. Even though the peptide-based vaccine strategy is a promising approach toward universal influenza vaccine, some challenges such as the sequence variations among influenza virus subtypes still persist [78]. Thus, prior knowledge of conserved peptides and their human leukocyte antigen (HLA) restriction is necessary to facilitate immunogen design and identify antigen-specific CD8+ T cells. This can help to orientate the immune response to protective epitopes and get more information about the composition of T cell-based vaccines [78,107].

## Broadly neutralizing antibodies-based therapeutics

Seasonal vaccination and earlier exposure to influenza viruses can induce antibodies against the recognized strains. However, influenza viruses are able to elude antibody-mediated

immunity by gradual accumulation of mutations in HA and NA proteins, known as antigenic drift. Antigenic drift was also reported in T cell epitopes but not as frequent as antibody-mediated drifts [3,113-115].

Polyclonal antibodies-based therapeutics were considered a therapeutic approach over the past decades in treating individuals with severe infectious diseases when limited therapeutic options were available. In the event of expanding epidemics, convalescent plasma can be quickly used to generate passive immunity against disease [116-118].

## Immune plasma

This approach was implemented during the Spanish flu in 1918 and the avian influenza virus H5N1 outbreaks in 2006 [117,119,120]. A meta-analysis study reported that early administration of convalescent blood products was able to reduce the risk of mortality from 37% to 16% during the H1N1 pandemic in 1918 [119]. Convalescent plasma was also administrated alongside neuraminidase inhibitors (NAI) in H5N1 patients with favorable outcomes [120].

Moreover, this approach regained great interest after the emergence of oseltamivir-resistance strains [121], pandemic H1N1 in 2009 [122], and H7N9 in 2013 [123]. A prospective multicenter case-control study evaluated the use of convalescent plasma for H1N1pdm09 IAV treatment and all participants also received standard NAI treatment. The mortality rate was 20% among the 20 patients who accepted the plasma compared to 54% in those who declined [123]. However, the control arm mortality was significantly higher than anticipated for similar severity of illness [124].

A phase 2 randomized multicenter control trial study in which patients with severe influenza A or B were randomly assigned to receive either standard-of-care (SOC) alone or immune plasma plus SOC and were followed up for 28 days. The study was unable to show definitive benefits in the primary endpoint of normalization of respiratory status [125]. Further reports speculated that the insufficient antibody dose in immune plasma might have been an important factor in the absence of apparent antiviral activity and the marginal clinical efficacy in this trial [116,126]. Another randomized, double-blind, controlled phase 3 trial was conducted in patients with severe IAV infection comparing the clinical efficacy of high-titer

immune plasma to the standard low-titer plasma. The high-titer immune plasma was unable to confer significant benefits over the low-titer plasma. Also, the clinical benefits were insufficient to justify using immune plasma for severe influenza treatment [116,117].

### *Anti-HA monoclonal antibodies*

During the last decade, the development of broad-spectrum mAbs targeting conserved regions in IAV as a potential therapeutic approach was a point of concern. Of note, at least eight antibody candidates were under development and registered for clinical trials [116].

The broadly neutralizing antibodies can provide heterosubtypic protection against IAV group 1 (e.g. H1, H2, H5) CR6261 [63], CT-P27 (previously known as CT149) [127], group 2 (e.g. H3, H7) CR8020 [62], or both HAs groups MEDI8852 [128], VIS410 [129,130], MHAA4549A (originally referred to as 39.29) [131]. Moreover, for certain mAbs, the therapeutic potential was also demonstrated for avian H5N1 and H7N9 [132,133].

Nevertheless, the breadth of HA stem-targeting mAbs antiviral effectiveness varies. Therefore, the required dose of the mAbs may vary depending on the model system and the virus strain [132]. These antibodies could be also useful approaches as pre- or postexposure prophylaxis, but other factors e.g. relatively short protection duration, high cost and limited production capacity could constrain the application of prophylactic use [134].

### *Anti-NA monoclonal antibodies*

The NA surface glycoprotein is also an attractive target for developing therapeutic antibodies due to the highly conserved AAs in the NA active site [135]. Attempts to produce heterosubtypic NA mAbs in rabbits against a conserved, linear peptide yielded mAbs with low neuraminidase-inhibiting (NI) activity and weak protective effect [136,137]. However, further reports suggested that antibodies against NA could contribute to protection [138-140]. To date, a limited number of NA cross-reactive mAbs have been reported. Of note, three human anti-NA mAbs (1G01, 1G04, 1E01) with cross-reactivity against IAV and IBV were isolated from plasmablasts of H3N2-infected individual. Epitope footprints of such NI mAbs revealed that these clones directly targeted the NA active site and mediated strong protection *in vivo* [141]. Another study reported a novel human anti-NA mAb (DA03E17) with heterosubtypic NI activity to NAs from IAV group 1 (N1, N4, N5, N8), group 2 (N2, N3, N6, N7, N9), and IBVs [135].

In addition to their therapeutic potential, these NA cross-protective antibodies can boost the development of NA-based vaccines, nevertheless, there is much work still required [141].

In general, the use of mAbs for passive immunization as a prophylactic measure against seasonal or pandemic influenza virus infections may be highly expensive and unfeasible. Nevertheless, their potential for the treatment of severe influenza virus cases, particularly illnesses caused by zoonotic influenza viruses like H5N1 or H7N9 remains significant. Additionally, they may serve as prophylactic options for vulnerable populations e.g. pregnant women, children, elderly people, and immunocompromised individuals during influenza seasons, or in the event of a pandemic [142].

## Antiviral drugs

### *Direct-acting antiviral drugs*

Currently, there are three classes of influenza direct-acting antiviral drugs licensed for the prophylaxis and treatment of influenza virus infection. These include NAIs, M2 ion channel blocker adamantanes derivatives (amantadine, rimantadine), and polymerase inhibitors (e.g. Baloxavir Marboxil, Favipiravir) [116,143,144].

#### *M2 ion channel inhibitors*

The adamantane derivates, amantadine and rimantadine, were the first-choice antiviral drugs for many years against IAV outbreaks. Adamantanes block the viral replication cycle within the infected cells by inhibiting the M2 ion channel protein of IAV [145]. However, due to the structural difference of IBV M2 protein, IBV were completely insensitive to the M2 blockers and therefore these drugs were inappropriate for IBV treatment [146,147].

During treatment, drug-resistance variants of IAV rapidly emerged. These variants are characterized by single AA substitution within the transmembrane domain of M2 protein at positions 26, 27, 30, 31, or 34 [130,148,149]. IAV-resistant strains commonly exhibit V27A and S31N mutations. Also, variants with dual mutations have been reported [130,150]. The amantadine-resistant H3N2 strains and the pandemic H1N1pdm09 strains were also reported and the level of resistance among circulating strains reached >99% [151-153]. Thus, the adamantanes derivates were no longer recommended since 2004-2005 for prophylaxis or treatment of current circulating IAV strains [154,155].

### Neuraminidase inhibitors

Four NAI (oseltamivir, zanamivir, peramivir, laninamivir) are currently licensed for the treatment of IAV and IBV infections. The first two NAI were globally approved in 1999, laninamivir was licensed only in Japan in 2010 and peramivir gained approval in 2014 in various countries. While these drugs share a certain degree of chemical structure similarities, they differ in the treatment regimen, administration route, and other attributes [156].

Oseltamivir is the most widely used NAI and considered the SOC for the treatment of hospitalized patients or ambulatory patients with underlying conditions associated with higher complications [116,157]. Safety and suitability for the treatment of children and during pregnancy were also demonstrated [158,159]. All four approved NAI drugs display low $IC_{50}$ values in nanomolar and subnanomolar ranges in NA inhibition assays and potentially reduce influenza virus NA activity [160,161].

Despite the potency of NAI, there are some challenges associated with their administration. Of note, the treatment should commence within 48 hours post infection, while clinical symptoms typically manifest within 24 to 36 hours [143].

Furthermore, the effectiveness of the NA inhibitor may be diminished by certain NA substitutions that arise naturally or are acquired during viral replication while the NAI is being administrated [156]. The most common changes conferring oseltamivir resistance are H274Y in the N1 subtype and R292K in the N2 subtype [162]. Moreover, the H274Y mutation showed a significant reduction in sensitivity to peramivir [163]. Although laninamivir and zanamivir retained activity against the oseltamivir-resistant mutation [164], further mutations, E119G and E119A, associated with both zanamivir and laninamivir resistance were reported [165,166]. Noteworthy, substitution at the same residue E119V, exhibits oseltamivir resistance in the IAV N2 subtype while it does not affect the zanamivir binding [166,167]. It is also reported that the D197E substitution in IBV NA protein and the E119G substitution in the IAV N9 subtype led to 50- and 150-fold reduced susceptibility to laninamivir. This reduced susceptibility resulted in faster drug binding and dissociation [165].

## Polymerase inhibitors

The polymerase complex has been proposed as a potential target for antiviral drugs since it is necessary for influenza virus replication. Several polymerase inhibitors that specifically target each polymerase subunit have been recently developed [168]. These include the PA inhibitor baloxavir marboxil [169], the PB1 inhibitor favipiravir [170], and the PB2 inhibitor pimodivir [171]. Baloxavir marboxil is approved for clinical use in multiple countries as a treatment for uncomplicated influenza [172]. Favipiravir is licensed in Japan with an indication limited to patients with novel or reemerging influenza viruses of insufficient response to current drugs. This limitation is due to safety concerns including increasing risk for teratogenicity and embryotoxicity [173].

Like other antiviral drugs, resistance against polymerase inhibitors was also reported. In phase 2 and 3 clinical trials, several mutations conferring resistance in the PA protein against baloxavir marboxil have emerged following treatment. For H1N1 pdm09, these mutations occur at positions E23K, I38T, and I38F. In H3N2, the mutations are E23G/K, A37T, I38T, I38M, and E199G [172,174,175]. These substitutions resulted in a 4.5–57-fold reduction in baloxavir susceptibility [174]. Moreover, The K229R mutation in the PB1 subunit is present across different influenza virus subtypes and confers a 31-fold reduction in favipiravir susceptibility. Although this mutation reduces viral replication fitness, this can be compensated for the fitness cost by another P653L substitution in the PA subunit [176]. Muchmore, various substitutions (i.e., Q306H, S324I, S324N, S324R, F404Y, and N510T) in the PB2 subunit were identified after *in vitro* passaging of H1N1 in the presence of pimodivir. These mutations conferred 63- to 257-fold reduced susceptibility to pimodivir [177]. Also, in phase 2a randomized, double-blind, placebo-controlled clinical trial, the PB2 S324C, K376R, M431L/R/V, and M431I variants were observed in 9.7% of pimodivir-treated volunteers between days 3 and 8 post treatment [178].

## Host-targeted antiviral drugs

Like other viruses, influenza viruses rely on interactions with host cell function to support their replication. These interactions involve a complex of intracellular cellular signaling pathways which offers a feasible alternative strategy to control viral infection instead of targeting the

pathogen itself. Hence, the emergence of resistant viral variants should be an infrequent occurrence [179,180].

Fludase, also known as DAS181, is a novel recombinant fusion protein that exhibits sialidase activity. It functions by enzymatically cleaving the sialic acid receptors on the host epithelial cells, which in turn effectively prevents the attachment and replication of influenza viruses [181,182]. Preclinical investigations have revealed the ability of DAS181 to inhibit the replication of human and avian influenza viruses, including H1N1pdm09 as well as the HPAI H5N1 and H7N9 [181,183,184]. In a randomized, double-blind, placebo-controlled phase 2 study, it was demonstrated that fludase effectively reduced the viral load and viral shedding in humans. Importantly, there were no significant adverse effects observed in patients who received the treatment [185]. However, it was observed that patients developed an immune response against DAS181 when the treatment window extended beyond seven days, resulting in reduced efficacy [186].

Nitazoxanide is primarily licensed for the treatment of intestinal parasite infections [187]. In terms of repurposing, it has also demonstrated antiviral activity against a broad range of viruses including influenza [188]. The active metabolite, tizoxanide, selectively hinders the maturation of influenza viruses by inhibiting the HA intracellular trafficking [189]. In preclinical studies, nitazoxanide has exhibited antiviral activity against various IAV and IBV strains from both human and avian origin [190,191]. In ferrets, administering a combination of oseltamivir and nitazoxanide as prophylaxis two hours before infection resulted in significantly reduced virus shedding and no detectable virus in the lower respiratory tract. This outcome was more favorable compared to using either drug as a standalone treatment [192]. However, in a case study of an immunocompromised child, the combination treatment with nitazoxanide alongside oseltamivir and zanamivir did not successfully clear the infection IBV [193].

### *Targeting the Raf/MEK/ERK Pathway*

Mitogen-activated protein kinase (MAPK) cascades are key signaling pathways that regulate cell proliferation, and differentiation [194,195]. As a part of the MAPK, the Raf/MEK/ERK kinase cascade translates extracellular signals, e.g. cell surface receptors, through sequential phosphorylation steps of the Raf and MEK kinases, which in turn activate the ERK kinase that has different downstream targets in the cell [194,196].

Activation of the Raf/MEK/ERK pathway is essential for efficient influenza virus replication cycle facilitating the vRNPs nuclear export to the cytoplasm. It was reported that MEK inhibition does not affect the viral RNA and protein synthesis, but Inhibition of this cascade leads to nuclear retention of the viral RNPs in the late stage of the viral replication cycle [21,180,197]. Moreover, activation of the cascade at the late stage of the replication cycle is necessary for activation of a downstream kinase (RSK1), a key factor for the viral NP phosphorylation at two distinct sites which in turn provides a signal for the association of the M1 and NP proteins [198,199].

The pivotal role of the Raf/MEK/ERK signaling cascade for influenza viruses sheds light on the possibility of using this pathway as a promising target for novel anti-influenza approaches. Along this line, different kinase inhibitors targeting the MEK kinase, the bottleneck of the signaling pathway, are developed, or licensed for clinical use in cancer treatment and would allow a repurposing approach [180]. These inhibitors, e.g. U0126 [21,200], CI-1040 [201], AZD-6244 and Trametinib [202], were shown to exhibit antiviral activity *in vitro* and/or *in vivo* against different influenza virus strains and subtypes [180,198].

A potential advantage of host-targeted antiviral drugs is their ability to reduce the emergence frequency of resistant viral variants. Moreover, MEK inhibitors showed a prolonged treatment window compared to the SOC and would overcome the major drawbacks of the direct-acting antiviral (DAA) drugs [198,201].

## References

[1] Uyeki TM, Hui DS, Zambon M, Wentworth DE and Monto AS. Influenza. Lancet. **2022**;400(10353):693-706.

[2] Iuliano AD, Roguski KM, Chang HH, Muscatello DJ, Palekar R, Tempia S, Cohen C, Gran JM, Schanzer D, Cowling BJ, Wu P, Kyncl J, Ang LW, Park M, Redlberger-Fritz M, Yu H, Espenhain L, Krishnan A, Emukule G, van Asten L, Pereira da Silva S, Aungkulanon S, Buchholz U, Widdowson MA, Bresee JS and Global Seasonal Influenza-associated Mortality Collaborator N. Estimates of global seasonal influenza-associated respiratory mortality: a modelling study. Lancet. **2018**;391(10127):1285-1300.

[3] Krammer F, Smith GJD, Fouchier RAM, Peiris M, Kedzierska K, Doherty PC, Palese P, Shaw ML, Treanor J, Webster RG and García-Sastre A. Influenza. Nature Reviews Disease Primers. **2018**;4(1):3.

[4] WHO. Influenza (Seasonal) - Fact Sheets. https://www.who.int/news-room/fact-sheets/detail/influenza-(seasonal) . Last accessed: Jan. 18, 2024. **2023**.

[5] Nair H, Brooks WA, Katz M, Roca A, Berkley JA, Madhi SA, Simmerman JM, Gordon A, Sato M, Howie S, Krishnan A, Ope M, Lindblade KA, Carosone-Link P, Lucero M, Ochieng W, Kamimoto L, Dueger E, Bhat N, Vong S, Theodoratou E, Chittaganpitch M, Chimah O, Balmaseda A, Buchy P, Harris E, Evans V, Katayose M, Gaur B, O'Callaghan-Gordo C, Goswami D, Arvelo W, Venter M, Briese T, Tokarz R, Widdowson MA, Mounts AW, Breiman RF, Feikin DR, Klugman KP, Olsen SJ, Gessner BD, Wright PF, Rudan I, Broor S, Simoes EA and Campbell H. Global burden of respiratory infections due to seasonal influenza in young children: a systematic review and meta-analysis. Lancet. **2011**;378(9807):1917-30.

[6] Nayak J, Hoy G and Gordon A. Influenza in Children. Cold Spring Harb Perspect Med. **2021**;11(1).

[7] Palese P. Influenza: old and new threats. Nature medicine. **2004**;10(12 Suppl):S82-7.

[8] Watanabe T, Zhong G, Russell CA, Nakajima N, Hatta M, Hanson A, McBride R, Burke DF, Takahashi K, Fukuyama S, Tomita Y, Maher EA, Watanabe S, Imai M, Neumann G, Hasegawa H, Paulson JC, Smith DJ and Kawaoka Y. Circulating avian influenza viruses closely related to the 1918 virus have pandemic potential. Cell Host Microbe. **2014**;15(6):692-705.

[9] Guan Y, Vijaykrishna D, Bahl J, Zhu H, Wang J and Smith GJ. The emergence of pandemic influenza viruses. Protein Cell. **2010**;1(1):9-13.

[10] Smith GJ, Vijaykrishna D, Bahl J, Lycett SJ, Worobey M, Pybus OG, Ma SK, Cheung CL, Raghwani J, Bhatt S, Peiris JS, Guan Y and Rambaut A. Origins and evolutionary genomics of the 2009 swine-origin H1N1 influenza A epidemic. Nature. **2009**;459(7250):1122-5.

[11] Shinde V, Bridges CB, Uyeki TM, Shu B, Balish A, Xu X, Lindstrom S, Gubareva LV, Deyde V, Garten RJ, Harris M, Gerber S, Vagasky S, Smith F, Pascoe N, Martin K, Dufficy D, Ritger K, Conover C, Quinlisk P, Klimov A, Bresee JS and Finelli L. Triple-reassortant swine influenza A (H1) in humans in the United States, 2005-2009. N Engl J Med. **2009**;360(25):2616-25.

[12] Krammer F. The human antibody response to influenza A virus infection and vaccination. Nat Rev Immunol. **2019**;19(6):383-397.

[13] Long JS, Mistry B, Haslam SM and Barclay WS. Host and viral determinants of influenza A virus species specificity. Nat Rev Microbiol. **2019**;17(2):67-81.

[14] Krammer F and Palese P. Orthomyxoviridae: The Viruses and Their Replication. In: Howley PM, Knipe DM, editors. Fields Virology: Emerging Viruses. Vol. Seventh edition. Philadelphia: Wolters Kluwer Health; 2020. p. 1224-1337.

[15] Wu Y, Wu Y, Tefsen B, Shi Y and Gao GF. Bat-derived influenza-like viruses H17N10 and H18N11. Trends Microbiol. **2014**;22(4):183-91.

[16] Yamayoshi S and Kawaoka Y. Current and future influenza vaccines. Nature medicine. **2019**;25(2):212-220.

[17] Yamayoshi S, Watanabe M, Goto H and Kawaoka Y. Identification of a Novel Viral Protein Expressed from the PB2 Segment of Influenza A Virus. J Virol. **2016**;90(1):444-56.

[18] Herfst S, Schrauwen EJ, Linster M, Chutinimitkul S, de Wit E, Munster VJ, Sorrell EM, Bestebroer TM, Burke DF, Smith DJ, Rimmelzwaan GF, Osterhaus AD and Fouchier RA. Airborne transmission of influenza A/H5N1 virus between ferrets. Science (New York, NY). **2012**;336(6088):1534-41.

[19] Imai M, Watanabe T, Hatta M, Das SC, Ozawa M, Shinya K, Zhong G, Hanson A, Katsura H, Watanabe S, Li C, Kawakami E, Yamada S, Kiso M, Suzuki Y, Maher EA, Neumann G and Kawaoka Y. Experimental adaptation of an influenza H5 HA confers respiratory droplet transmission to a reassortant H5 HA/H1N1 virus in ferrets. Nature. **2012**;486(7403):420-8.

[20] Pflug A, Lukarska M, Resa-Infante P, Reich S and Cusack S. Structural insights into RNA synthesis by the influenza virus transcription-replication machine. Virus Res. **2017**;234:103-117.

[21] Pleschka S, Wolff T, Ehrhardt C, Hobom G, Planz O, Rapp UR and Ludwig S. Influenza virus propagation is impaired by inhibition of the Raf/MEK/ERK signalling cascade. Nature cell biology. **2001**;3(3):301-5.

[22] Fodor E. The RNA polymerase of influenza a virus: mechanisms of viral transcription and replication. Acta virologica. **2013**;57(2):113-22.

[23] Muhlbauer D, Dzieciolowski J, Hardt M, Hocke A, Schierhorn KL, Mostafa A, Muller C, Wisskirchen C, Herold S, Wolff T, Ziebuhr J and Pleschka S. Influenza virus-induced caspase-dependent enlargement of nuclear pores promotes nuclear export of viral ribonucleoprotein complexes. J Virol. **2015**;89(11):6009-21.

[24] Obayashi E, Yoshida H, Kawai F, Shibayama N, Kawaguchi A, Nagata K, Tame JR and Park SY. The structural basis for an essential subunit interaction in influenza virus RNA polymerase. Nature. **2008**;454(7208):1127-31.

[25] Neumann G and Kawaoka Y. Transmission of influenza A viruses. Virology. **2015**;479-480:234-46.

[26] Olsen B, Munster VJ, Wallensten A, Waldenstrom J, Osterhaus AD and Fouchier RA. Global patterns of influenza a virus in wild birds. Science (New York, NY). **2006**;312(5772):384-8.

[27] Lauring AS and Andino R. Quasispecies theory and the behavior of RNA viruses. PLoS pathogens. **2010**;6(7):e1001005.

[28] Medina RA and Garcia-Sastre A. Influenza A viruses: new research developments. Nat Rev Microbiol. **2011**;9(8):590-603.

[29] Trifonov V, Khiabanian H and Rabadan R. Geographic dependence, surveillance, and origins of the 2009 influenza A (H1N1) virus. N Engl J Med. **2009**;361(2):115-9.

[30] Garten RJ, Davis CT, Russell CA, Shu B, Lindstrom S, Balish A, Sessions WM, Xu X, Skepner E, Deyde V, Okomo-Adhiambo M, Gubareva L, Barnes J, Smith CB, Emery SL, Hillman MJ, Rivailler P, Smagala J, de Graaf M, Burke DF, Fouchier RA, Pappas C, Alpuche-Aranda CM, Lopez-Gatell H, Olivera H, Lopez I, Myers CA, Faix D, Blair PJ, Yu C, Keene KM, Dotson PD, Jr., Boxrud D, Sambol AR, Abid SH, St George K, Bannerman T, Moore AL, Stringer DJ, Blevins P, Demmler-Harrison GJ, Ginsberg M, Kriner P, Waterman S, Smole S, Guevara HF, Belongia EA, Clark PA, Beatrice ST, Donis R, Katz J, Finelli L, Bridges CB, Shaw M, Jernigan DB, Uyeki TM, Smith DJ, Klimov AI and Cox NJ. Antigenic and genetic characteristics of swine-origin 2009 A(H1N1) influenza viruses circulating in humans. Science (New York, NY). **2009**;325(5937):197-201.

[31] Lam TT, Wang J, Shen Y, Zhou B, Duan L, Cheung CL, Ma C, Lycett SJ, Leung CY, Chen X, Li L, Hong W, Chai Y, Zhou L, Liang H, Ou Z, Liu Y, Farooqui A, Kelvin DJ, Poon LL, Smith DK, Pybus OG, Leung GM, Shu Y, Webster RG, Webby RJ, Peiris JS, Rambaut A, Zhu H and Guan Y. The genesis and source of the H7N9 influenza viruses causing human infections in China. Nature. **2013**;502(7470):241-4.

[32] Gao R, Cao B, Hu Y, Feng Z, Wang D, Hu W, Chen J, Jie Z, Qiu H, Xu K, Xu X, Lu H, Zhu W, Gao Z, Xiang N, Shen Y, He Z, Gu Y, Zhang Z, Yang Y, Zhao X, Zhou L, Li X, Zou S, Zhang Y, Li X, Yang L, Guo J, Dong J, Li Q, Dong L, Zhu Y, Bai T, Wang S, Hao P, Yang W, Zhang Y, Han J, Yu H, Li D, Gao GF, Wu G, Wang Y, Yuan Z and Shu Y. Human infection with a novel avian-origin influenza A (H7N9) virus. N Engl J Med. **2013**;368(20):1888-97.

[33] Gaymard A, Le Briand N, Frobert E, Lina B and Escuret V. Functional balance between neuraminidase and haemagglutinin in influenza viruses. Clin Microbiol Infect. **2016**;22(12):975-983.

[34] Tumpey TM, Maines TR, Van Hoeven N, Glaser L, Solorzano A, Pappas C, Cox NJ, Swayne DE, Palese P, Katz JM and Garcia-Sastre A. A two-amino acid change in the hemagglutinin of the 1918 influenza virus abolishes transmission. Science (New York, NY). **2007**;315(5812):655-9.

[35] Mitnaul LJ, Matrosovich MN, Castrucci MR, Tuzikov AB, Bovin NV, Kobasa D and Kawaoka Y. Balanced hemagglutinin and neuraminidase activities are critical for efficient replication of influenza A virus. J Virol. **2000**;74(13):6015-20.

[36] Reed ML, Bridges OA, Seiler P, Kim JK, Yen HL, Salomon R, Govorkova EA, Webster RG and Russell CJ. The pH of activation of the hemagglutinin protein regulates H5N1 influenza virus pathogenicity and transmissibility in ducks. J Virol. **2010**;84(3):1527-35.

[37] Andino R and Domingo E. Viral quasispecies. Virology. **2015**;479-480:46-51.

[38] Das SR, Puigbo P, Hensley SE, Hurt DE, Bennink JR and Yewdell JW. Glycosylation focuses sequence variation in the influenza A virus H1 hemagglutinin globular domain. PLoS pathogens. **2010**;6(11):e1001211.

[39] Medina RA, Stertz S, Manicassamy B, Zimmermann P, Sun X, Albrecht RA, Uusi-Kerttula H, Zagordi O, Belshe RB, Frey SE, Tumpey TM and Garcia-Sastre A. Glycosylations in the globular head of the hemagglutinin protein modulate the virulence and antigenic properties of the H1N1 influenza viruses. Sci Transl Med. **2013**;5(187):187ra70.

[40] Das SR, Hensley SE, David A, Schmidt L, Gibbs JS, Puigbo P, Ince WL, Bennink JR and Yewdell JW. Fitness costs limit influenza A virus hemagglutinin glycosylation as an immune evasion strategy. Proceedings of the National Academy of Sciences of the United States of America. **2011**;108(51):E1417-22.

[41] Skehel JJ, Stevens DJ, Daniels RS, Douglas AR, Knossow M, Wilson IA and Wiley DC. A carbohydrate side chain on hemagglutinins of Hong Kong influenza viruses inhibits recognition by a monoclonal antibody. Proceedings of the National Academy of Sciences of the United States of America. **1984**;81(6):1779-83.

[42] Mosterin Hopping A, McElhaney J, Fonville JM, Powers DC, Beyer WEP and Smith DJ. The confounded effects of age and exposure history in response to influenza vaccination. Vaccine. **2016**;34(4):540-546.

[43] Hause BM, Ducatez M, Collin EA, Ran Z, Liu R, Sheng Z, Armien A, Kaplan B, Chakravarty S, Hoppe AD, Webby RJ, Simonson RR and Li F. Isolation of a novel swine influenza virus from Oklahoma in 2011 which is distantly related to human influenza C viruses. PLoS pathogens. **2013**;9(2):e1003176.

[44] Osterhaus AD, Rimmelzwaan GF, Martina BE, Bestebroer TM and Fouchier RA. Influenza B virus in seals. Science (New York, NY). **2000**;288(5468):1051-3.

[45] Bodewes R, Morick D, de Mutsert G, Osinga N, Bestebroer T, van der Vliet S, Smits SL, Kuiken T, Rimmelzwaan GF, Fouchier RA and Osterhaus AD. Recurring influenza B virus infections in seals. Emerg Infect Dis. **2013**;19(3):511-2.

[46] Matsuzaki Y, Katsushima N, Nagai Y, Shoji M, Itagaki T, Sakamoto M, Kitaoka S, Mizuta K and Nishimura H. Clinical features of influenza C virus infection in children. J Infect Dis. **2006**;193(9):1229-35.

[47] Zhai SL, Zhang H, Chen SN, Zhou X, Lin T, Liu R, Lv DH, Wen XH, Wei WK, Wang D and Li F. Influenza D Virus in Animal Species in Guangdong Province, Southern China. Emerg Infect Dis. **2017**;23(8):1392-1396.

[48] Shi Y, Wu Y, Zhang W, Qi J and Gao GF. Enabling the 'host jump': structural determinants of receptor-binding specificity in influenza A viruses. Nat Rev Microbiol. **2014**;12(12):822-31.

[49] Xiong X, Martin SR, Haire LF, Wharton SA, Daniels RS, Bennett MS, McCauley JW, Collins PJ, Walker PA, Skehel JJ and Gamblin SJ. Receptor binding by an H7N9 influenza virus from humans. Nature. **2013**;499(7459):496-9.

[50] Lipsitch M, Barclay W, Raman R, Russell CJ, Belser JA, Cobey S, Kasson PM, Lloyd-Smith JO, Maurer-Stroh S, Riley S, Beauchemin CA, Bedford T, Friedrich TC, Handel A, Herfst S, Murcia PR, Roche B, Wilke CO and Russell CA. Viral factors in influenza pandemic risk assessment. Elife. **2016**;5.

[51] FAO. Avian Influenza A(H7N9) virus situation update. https://www.fao.org/animal-health/situation-updates/avian-influenza-A(H7N9)-virus/en .Last accessed: Jan. 18, 2024. **2022**.

[52] WHO. Avian Influenza Weekly Update 2023. WHO Regional Office for the Western Pacific. https://iris.who.int/handle/10665/365675 . **2023**.

[53] Rajao DS and Perez DR. Universal Vaccines and Vaccine Platforms to Protect against Influenza Viruses in Humans and Agriculture. Frontiers in microbiology. **2018**;9:123.

[54] McLean HQ, Petrie JG, Hanson KE, Meece JK, Rolfes MA, Sylvester GC, Neumann G, Kawaoka Y and Belongia EA. Interim Estimates of 2022-23 Seasonal Influenza Vaccine Effectiveness - Wisconsin, October 2022-February 2023. MMWR Morb Mortal Wkly Rep. **2023**;72(8):201-205.

[55] Belongia EA, Simpson MD, King JP, Sundaram ME, Kelley NS, Osterholm MT and McLean HQ. Variable influenza vaccine effectiveness by subtype: a systematic review and meta-analysis of test-negative design studies. The Lancet Infectious diseases. **2016**;16(8):942-51.

[56] Okoli GN, Racovitan F, Abdulwahid T, Righolt CH and Mahmud SM. Variable seasonal influenza vaccine effectiveness across geographical regions, age groups and levels of vaccine antigenic similarity with circulating virus strains: A systematic review and

meta-analysis of the evidence from test-negative design studies after the 2009/10 influenza pandemic. Vaccine. **2021**;39(8):1225-1240.

[57] Rajaram S, Wojcik R, Moore C, Ortiz de Lejarazu R, de Lusignan S, Montomoli E, Rossi A, Perez-Rubio A, Trilla A, Baldo V, Jandhyala R and Kassianos G. The impact of candidate influenza virus and egg-based manufacture on vaccine effectiveness: Literature review and expert consensus. Vaccine. **2020**;38(38):6047-6056.

[58] Kodihalli S, Justewicz DM, Gubareva LV and Webster RG. Selection of a single amino acid substitution in the hemagglutinin molecule by chicken eggs can render influenza A virus (H3) candidate vaccine ineffective. J Virol. **1995**;69(8):4888-97.

[59] Zost SJ, Parkhouse K, Gumina ME, Kim K, Diaz Perez S, Wilson PC, Treanor JJ, Sant AJ, Cobey S and Hensley SE. Contemporary H3N2 influenza viruses have a glycosylation site that alters binding of antibodies elicited by egg-adapted vaccine strains. Proceedings of the National Academy of Sciences of the United States of America. **2017**;114(47):12578-12583.

[60] Wu NC, Zost SJ, Thompson AJ, Oyen D, Nycholat CM, McBride R, Paulson JC, Hensley SE and Wilson IA. A structural explanation for the low effectiveness of the seasonal influenza H3N2 vaccine. PLoS pathogens. **2017**;13(10):e1006682.

[61] Raymond DD, Stewart SM, Lee J, Ferdman J, Bajic G, Do KT, Ernandes MJ, Suphaphiphat P, Settembre EC, Dormitzer PR, Del Giudice G, Finco O, Kang TH, Ippolito GC, Georgiou G, Kepler TB, Haynes BF, Moody MA, Liao HX, Schmidt AG and Harrison SC. Influenza immunization elicits antibodies specific for an egg-adapted vaccine strain. Nature medicine. **2016**;22(12):1465-1469.

[62] Ekiert DC, Friesen RH, Bhabha G, Kwaks T, Jongeneelen M, Yu W, Ophorst C, Cox F, Korse HJ, Brandenburg B, Vogels R, Brakenhoff JP, Kompier R, Koldijk MH, Cornelissen LA, Poon LL, Peiris M, Koudstaal W, Wilson IA and Goudsmit J. A highly conserved neutralizing epitope on group 2 influenza A viruses. Science (New York, NY). **2011**;333(6044):843-50.

[63] Throsby M, van den Brink E, Jongeneelen M, Poon LL, Alard P, Cornelissen L, Bakker A, Cox F, van Deventer E, Guan Y, Cinatl J, ter Meulen J, Lasters I, Carsetti R, Peiris M, de Kruif J and Goudsmit J. Heterosubtypic neutralizing monoclonal antibodies cross-protective against H5N1 and H1N1 recovered from human IgM+ memory B cells. PloS one. **2008**;3(12):e3942.

[64] Impagliazzo A, Milder F, Kuipers H, Wagner MV, Zhu X, Hoffman RM, van Meersbergen R, Huizingh J, Wanningen P, Verspuij J, de Man M, Ding Z, Apetri A, Kukrer B, Sneekes-Vriese E, Tomkiewicz D, Laursen NS, Lee PS, Zakrzewska A, Dekking L, Tolboom J, Tettero L, van Meerten S, Yu W, Koudstaal W, Goudsmit J, Ward AB, Meijberg W, Wilson IA and Radosevic K. A stable trimeric influenza hemagglutinin stem as a broadly protective immunogen. Science (New York, NY). **2015**;349(6254):1301-6.

[65] Lu Y, Welsh JP and Swartz JR. Production and stabilization of the trimeric influenza hemagglutinin stem domain for potentially broadly protective influenza vaccines.

Proceedings of the National Academy of Sciences of the United States of America. **2014**;111(1):125-30.

[66] Steel J, Lowen AC, Wang TT, Yondola M, Gao Q, Haye K, Garcia-Sastre A and Palese P. Influenza virus vaccine based on the conserved hemagglutinin stalk domain. mBio. **2010**;1(1).

[67] Yassine HM, Boyington JC, McTamney PM, Wei CJ, Kanekiyo M, Kong WP, Gallagher JR, Wang L, Zhang Y, Joyce MG, Lingwood D, Moin SM, Andersen H, Okuno Y, Rao SS, Harris AK, Kwong PD, Mascola JR, Nabel GJ and Graham BS. Hemagglutinin-stem nanoparticles generate heterosubtypic influenza protection. Nature medicine. **2015**;21(9):1065-70.

[68] Graves PN, Schulman JL, Young JF and Palese P. Preparation of influenza virus subviral particles lacking the HA1 subunit of hemagglutinin: unmasking of cross-reactive HA2 determinants. Virology. **1983**;126(1):106-16.

[69] Krammer F. The Quest for a Universal Flu Vaccine: Headless HA 2.0. Cell Host Microbe. **2015**;18(4):395-7.

[70] Krammer F. Emerging influenza viruses and the prospect of a universal influenza virus vaccine. Biotechnol J. **2015**;10(5):690-701.

[71] Nachbagauer R, Feser J, Naficy A, Bernstein DI, Guptill J, Walter EB, Berlanda-Scorza F, Stadlbauer D, Wilson PC, Aydillo T, Behzadi MA, Bhavsar D, Bliss C, Capuano C, Carreno JM, Chromikova V, Claeys C, Coughlan L, Freyn AW, Gast C, Javier A, Jiang K, Mariottini C, McMahon M, McNeal M, Solorzano A, Strohmeier S, Sun W, Van der Wielen M, Innis BL, Garcia-Sastre A, Palese P and Krammer F. A chimeric hemagglutinin-based universal influenza virus vaccine approach induces broad and long-lasting immunity in a randomized, placebo-controlled phase I trial. Nature medicine. **2021**;27(1):106-114.

[72] Krammer F, Pica N, Hai R, Margine I and Palese P. Chimeric hemagglutinin influenza virus vaccine constructs elicit broadly protective stalk-specific antibodies. J Virol. **2013**;87(12):6542-50.

[73] Hai R, Krammer F, Tan GS, Pica N, Eggink D, Maamary J, Margine I, Albrecht RA and Palese P. Influenza viruses expressing chimeric hemagglutinins: globular head and stalk domains derived from different subtypes. J Virol. **2012**;86(10):5774-81.

[74] Choi A, Bouzya B, Cortes Franco KD, Stadlbauer D, Rajabhathor A, Rouxel RN, Mainil R, Van der Wielen M, Palese P, Garcia-Sastre A, Innis BL, Krammer F, Schotsaert M, Mallett CP and Nachbagauer R. Chimeric Hemagglutinin-Based Influenza Virus Vaccines Induce Protective Stalk-Specific Humoral Immunity and Cellular Responses in Mice. Immunohorizons. **2019**;3(4):133-148.

[75] Nachbagauer R, Liu WC, Choi A, Wohlbold TJ, Atlas T, Rajendran M, Solorzano A, Berlanda-Scorza F, Garcia-Sastre A, Palese P, Albrecht RA and Krammer F. A universal influenza virus vaccine candidate confers protection against pandemic H1N1 infection in preclinical ferret studies. NPJ Vaccines. **2017**;2:26.

[76] Nachbagauer R, Kinzler D, Choi A, Hirsh A, Beaulieu E, Lecrenier N, Innis BL, Palese P, Mallett CP and Krammer F. A chimeric haemagglutinin-based influenza split virion vaccine adjuvanted with AS03 induces protective stalk-reactive antibodies in mice. NPJ Vaccines. **2016**;1:16015-.

[77] Margine I, Krammer F, Hai R, Heaton NS, Tan GS, Andrews SA, Runstadler JA, Wilson PC, Albrecht RA, Garcia-Sastre A and Palese P. Hemagglutinin stalk-based universal vaccine constructs protect against group 2 influenza A viruses. J Virol. **2013**;87(19):10435-46.

[78] Nguyen QT and Choi YK. Targeting Antigens for Universal Influenza Vaccine Development. Viruses. **2021**;13(6).

[79] Deviatkin AA, Simonov RA, Trutneva KA, Maznina AA, Khavina EM and Volchkov PY. Universal Flu mRNA Vaccine: Promises, Prospects, and Problems. Vaccines (Basel). **2022**;10(5).

[80] Bernstein DI, Guptill J, Naficy A, Nachbagauer R, Berlanda-Scorza F, Feser J, Wilson PC, Solorzano A, Van der Wielen M, Walter EB, Albrecht RA, Buschle KN, Chen YQ, Claeys C, Dickey M, Dugan HL, Ermler ME, Freeman D, Gao M, Gast C, Guthmiller JJ, Hai R, Henry C, Lan LY, McNeal M, Palm AE, Shaw DG, Stamper CT, Sun W, Sutton V, Tepora ME, Wahid R, Wenzel H, Wohlbold TJ, Innis BL, Garcia-Sastre A, Palese P and Krammer F. Immunogenicity of chimeric haemagglutinin-based, universal influenza virus vaccine candidates: interim results of a randomised, placebo-controlled, phase 1 clinical trial. The Lancet Infectious diseases. **2020**;20(1):80-91.

[81] Wong TM, Allen JD, Bebin-Blackwell AG, Carter DM, Alefantis T, DiNapoli J, Kleanthous H and Ross TM. Computationally Optimized Broadly Reactive Hemagglutinin Elicits Hemagglutination Inhibition Antibodies against a Panel of H3N2 Influenza Virus Cocirculating Variants. J Virol. **2017**;91(24).

[82] Carter DM, Darby CA, Lefoley BC, Crevar CJ, Alefantis T, Oomen R, Anderson SF, Strugnell T, Cortes-Garcia G, Vogel TU, Parrington M, Kleanthous H and Ross TM. Design and Characterization of a Computationally Optimized Broadly Reactive Hemagglutinin Vaccine for H1N1 Influenza Viruses. J Virol. **2016**;90(9):4720-4734.

[83] Giles BM and Ross TM. Computationally optimized antigens to overcome influenza viral diversity. Expert review of vaccines. **2012**;11(3):267-9.

[84] Petsch B, Schnee M, Vogel AB, Lange E, Hoffmann B, Voss D, Schlake T, Thess A, Kallen KJ, Stitz L and Kramps T. Protective efficacy of in vitro synthesized, specific mRNA vaccines against influenza A virus infection. Nature biotechnology. **2012**;30(12):1210-6.

[85] Feldman RA, Fuhr R, Smolenov I, Mick Ribeiro A, Panther L, Watson M, Senn JJ, Smith M, Almarsson Ö, Pujar HS, Laska ME, Thompson J, Zaks T and Ciaramella G. mRNA vaccines against H10N8 and H7N9 influenza viruses of pandemic potential are immunogenic and well tolerated in healthy adults in phase 1 randomized clinical trials. Vaccine. **2019**;37(25):3326-3334.

[86] Willis E, Pardi N, Parkhouse K, Mui BL, Tam YK, Weissman D and Hensley SE. Nucleoside-modified mRNA vaccination partially overcomes maternal antibody inhibition of de novo immune responses in mice. Sci Transl Med. **2020**;12(525).

[87] Pardi N, Parkhouse K, Kirkpatrick E, McMahon M, Zost SJ, Mui BL, Tam YK, Kariko K, Barbosa CJ, Madden TD, Hope MJ, Krammer F, Hensley SE and Weissman D. Nucleoside-modified mRNA immunization elicits influenza virus hemagglutinin stalk-specific antibodies. Nature communications. **2018**;9(1):3361.

[88] Zhang G, Tang T, Chen Y, Huang X and Liang T. mRNA vaccines in disease prevention and treatment. Signal Transduct Target Ther. **2023**;8(1):365.

[89] McMahon M, O'Dell G, Tan J, Sarkozy A, Vadovics M, Carreno JM, Puente-Massaguer E, Muramatsu H, Bajusz C, Rijnink W, Beattie M, Tam YK, Kirkpatrick Roubidoux E, Francisco I, Strohmeier S, Kanekiyo M, Graham BS, Krammer F and Pardi N. Assessment of a quadrivalent nucleoside-modified mRNA vaccine that protects against group 2 influenza viruses. Proceedings of the National Academy of Sciences of the United States of America. **2022**;119(45):e2206333119.

[90] Pardi N, Carreno JM, O'Dell G, Tan J, Bajusz C, Muramatsu H, Rijnink W, Strohmeier S, Loganathan M, Bielak D, Sung MMH, Tam YK, Krammer F and McMahon M. Development of a pentavalent broadly protective nucleoside-modified mRNA vaccine against influenza B viruses. Nature communications. **2022**;13(1):4677.

[91] Arevalo CP, Bolton MJ, Le Sage V, Ye N, Furey C, Muramatsu H, Alameh MG, Pardi N, Drapeau EM, Parkhouse K, Garretson T, Morris JS, Moncla LH, Tam YK, Fan SHY, Lakdawala SS, Weissman D and Hensley SE. A multivalent nucleoside-modified mRNA vaccine against all known influenza virus subtypes. Science (New York, NY). **2022**;378(6622):899-904.

[92] Kelvin AA and Falzarano D. The influenza universe in an mRNA vaccine. Science (New York, NY). **2022**;378(6622):827-828.

[93] Pardi N, Hogan MJ, Porter FW and Weissman D. mRNA vaccines - a new era in vaccinology. Nat Rev Drug Discov. **2018**;17(4):261-279.

[94] Pecetta S and Rappuoli R. mRNA, the beginning of a new influenza vaccine game. Proceedings of the National Academy of Sciences of the United States of America. **2022**;119(50):e2217533119.

[95] Janssens Y, Joye J, Waerlop G, Clement F, Leroux-Roels G and Leroux-Roels I. The role of cell-mediated immunity against influenza and its implications for vaccine evaluation. Frontiers in immunology. **2022**;13:959379.

[96] La Gruta NL and Turner SJ. T cell mediated immunity to influenza: mechanisms of viral control. Trends Immunol. **2014**;35(8):396-402.

[97] Sridhar S, Begom S, Bermingham A, Hoschler K, Adamson W, Carman W, Bean T, Barclay W, Deeks JJ and Lalvani A. Cellular immune correlates of protection against symptomatic pandemic influenza. Nature medicine. **2013**;19(10):1305-12.

[98] Koutsakos M, Wheatley AK, Loh L, Clemens EB, Sant S, Nussing S, Fox A, Chung AW, Laurie KL, Hurt AC, Rockman S, Lappas M, Loudovaris T, Mannering SI, Westall GP, Elliot M, Tangye SG, Wakim LM, Kent SJ, Nguyen THO and Kedzierska K. Circulating T(FH) cells, serological memory, and tissue compartmentalization shape human influenza-specific B cell immunity. Sci Transl Med. **2018**;10(428).

[99] Soema PC, van Riet E, Kersten G and Amorij JP. Development of cross-protective influenza a vaccines based on cellular responses. Frontiers in immunology. **2015**;6:237.

[100] van de Sandt CE, Dou Y, Vogelzang-van Trierum SE, Westgeest KB, Pronk MR, Osterhaus A, Fouchier RAM, Rimmelzwaan GF and Hillaire MLB. Influenza B virus-specific CD8+ T-lymphocytes strongly cross-react with viruses of the opposing influenza B lineage. J Gen Virol. **2015**;96(8):2061-2073.

[101] Hayward AC, Wang L, Goonetilleke N, Fragaszy EB, Bermingham A, Copas A, Dukes O, Millett ER, Nazareth I, Nguyen-Van-Tam JS, Watson JM, Zambon M, Flu Watch G, Johnson AM and McMichael AJ. Natural T Cell-mediated Protection against Seasonal and Pandemic Influenza. Results of the Flu Watch Cohort Study. American journal of respiratory and critical care medicine. **2015**;191(12):1422-31.

[102] Gras S, Kedzierski L, Valkenburg SA, Laurie K, Liu YC, Denholm JT, Richards MJ, Rimmelzwaan GF, Kelso A, Doherty PC, Turner SJ, Rossjohn J and Kedzierska K. Cross-reactive CD8+ T-cell immunity between the pandemic H1N1-2009 and H1N1-1918 influenza A viruses. Proceedings of the National Academy of Sciences of the United States of America. **2010**;107(28):12599-604.

[103] Quinones-Parra SM, Clemens EB, Wang Z, Croom HA, Kedzierski L, McVernon J, Vijaykrishna D and Kedzierska K. A Role of Influenza Virus Exposure History in Determining Pandemic Susceptibility and CD8+ T Cell Responses. J Virol. **2016**;90(15):6936-6947.

[104] Wang Z, Wan Y, Qiu C, Quinones-Parra S, Zhu Z, Loh L, Tian D, Ren Y, Hu Y, Zhang X, Thomas PG, Inouye M, Doherty PC, Kedzierska K and Xu J. Recovery from severe H7N9 disease is associated with diverse response mechanisms dominated by CD8(+) T cells. Nature communications. **2015**;6:6833.

[105] Quinones-Parra S, Grant E, Loh L, Nguyen TH, Campbell KA, Tong SY, Miller A, Doherty PC, Vijaykrishna D, Rossjohn J, Gras S and Kedzierska K. Preexisting CD8+ T-cell immunity to the H7N9 influenza A virus varies across ethnicities. Proceedings of the National Academy of Sciences of the United States of America. **2014**;111(3):1049-54.

[106] Hillaire MLB, Vogelzang-van Trierum SE, Kreijtz J, de Mutsert G, Fouchier RAM, Osterhaus A and Rimmelzwaan GF. Human T-cells directed to seasonal influenza A virus cross-react with 2009 pandemic influenza A (H1N1) and swine-origin triple-reassortant H3N2 influenza viruses. J Gen Virol. **2013**;94(Pt 3):583-592.

[107] Koutsakos M, Illing PT, Nguyen THO, Mifsud NA, Crawford JC, Rizzetto S, Eltahla AA, Clemens EB, Sant S, Chua BY, Wong CY, Allen EK, Teng D, Dash P, Boyd DF, Grzelak L, Zeng W, Hurt AC, Barr I, Rockman S, Jackson DC, Kotsimbos TC, Cheng AC, Richards M, Westall GP, Loudovaris T, Mannering SI, Elliott M, Tangye SG, Wakim LM, Rossjohn J, Vijaykrishna D, Luciani F, Thomas PG, Gras S, Purcell AW and Kedzierska K. Human CD8(+) T cell cross-reactivity across influenza A, B and C viruses. Nat Immunol. **2019**;20(5):613-625.

[108] Pleguezuelos O, Robinson S, Fernandez A, Stoloff GA, Mann A, Gilbert A, Balaratnam G, Wilkinson T, Lambkin-Williams R, Oxford J and Caparros-Wanderley W. A Synthetic Influenza Virus Vaccine Induces a Cellular Immune Response That Correlates with Reduction in Symptomatology and Virus Shedding in a Randomized Phase Ib Live-Virus Challenge in Humans. Clin Vaccine Immunol. **2015**;22(7):828-35.

[109] Francis JN, Bunce CJ, Horlock C, Watson JM, Warrington SJ, Georges B and Brown CB. A novel peptide-based pan-influenza A vaccine: a double blind, randomised clinical trial of immunogenicity and safety. Vaccine. **2015**;33(2):396-402.

[110] Lillie PJ, Berthoud TK, Powell TJ, Lambe T, Mullarkey C, Spencer AJ, Hamill M, Peng Y, Blais ME, Duncan CJ, Sheehy SH, Havelock T, Faust SN, Williams RL, Gilbert A, Oxford J, Dong T, Hill AV and Gilbert SC. Preliminary assessment of the efficacy of a T-cell-based influenza vaccine, MVA-NP+M1, in humans. Clinical infectious diseases : an official publication of the Infectious Diseases Society of America. **2012**;55(1):19-25.

[111] Lanfermeijer J, van de Ven K, van Dijken H, Hendriks M, Talavera Ormeno CMP, de Heij F, Roholl P, Borghans JAM, van Baarle D and de Jonge J. Modified influenza M1(58-66) peptide vaccination induces non-relevant T-cells and may enhance pathology after challenge. NPJ Vaccines. **2023**;8(1):116.

[112] Oftung F, Naess LM, Laake I, Stoloff G and Pleguezuelos O. FLU-v, a Broad-Spectrum Influenza Vaccine, Induces Cross-Reactive Cellular Immune Responses in Humans Measured by Dual IFN-gamma and Granzyme B ELISpot Assay. Vaccines (Basel). **2022**;10(9).

[113] Li ZT, Zarnitsyna VI, Lowen AC, Weissman D, Koelle K, Kohlmeier JE and Antia R. Why Are CD8 T Cell Epitopes of Human Influenza A Virus Conserved? J Virol. **2019**;93(6).

[114] Rimmelzwaan GF, Kreijtz JH, Bodewes R, Fouchier RA and Osterhaus AD. Influenza virus CTL epitopes, remarkably conserved and remarkably variable. Vaccine. **2009**;27(45):6363-5.

[115] Voeten JT, Bestebroer TM, Nieuwkoop NJ, Fouchier RA, Osterhaus AD and Rimmelzwaan GF. Antigenic drift in the influenza A virus (H3N2) nucleoprotein and escape from recognition by cytotoxic T lymphocytes. J Virol. **2000**;74(15):6800-7.

[116] Beigel JH and Hayden FG. Influenza Therapeutics in Clinical Practice-Challenges and Recent Advances. Cold Spring Harb Perspect Med. **2021**;11(4).

[117] Beigel JH, Aga E, Elie-Turenne MC, Cho J, Tebas P, Clark CL, Metcalf JP, Ozment C, Raviprakash K, Beeler J, Holley HP, Jr., Warner S, Chorley C, Lane HC, Hughes MD, Davey RT, Jr. and Team IRCS. Anti-influenza immune plasma for the treatment of patients with severe influenza A: a randomised, double-blind, phase 3 trial. Lancet Respir Med. **2019**;7(11):941-950.

[118] Luke TC, Casadevall A, Watowich SJ, Hoffman SL, Beigel JH and Burgess TH. Hark back: passive immunotherapy for influenza and other serious infections. Crit Care Med. **2010**;38(4 Suppl):e66-73.

[119] Luke TC, Kilbane EM, Jackson JL and Hoffman SL. Meta-analysis: convalescent blood products for Spanish influenza pneumonia: a future H5N1 treatment? Annals of internal medicine. **2006**;145(8):599-609.

[120] Zhou B, Zhong N and Guan Y. Treatment with convalescent plasma for influenza A (H5N1) infection. N Engl J Med. **2007**;357(14):1450-1.

[121] Dharan NJ, Gubareva LV, Meyer JJ, Okomo-Adhiambo M, McClinton RC, Marshall SA, St George K, Epperson S, Brammer L, Klimov AI, Bresee JS, Fry AM and Oseltamivir-Resistance Working G. Infections with oseltamivir-resistant influenza A(H1N1) virus in the United States. The Journal of the American Medical Association. **2009**;301(10):1034-41.

[122] Hung IF, To KK, Lee CK, Lee KL, Chan K, Yan WW, Liu R, Watt CL, Chan WM, Lai KY, Koo CK, Buckley T, Chow FL, Wong KK, Chan HS, Ching CK, Tang BS, Lau CC, Li IW, Liu SH, Chan KH, Lin CK and Yuen KY. Convalescent plasma treatment reduced mortality in patients with severe pandemic influenza A (H1N1) 2009 virus infection. Clinical infectious diseases : an official publication of the Infectious Diseases Society of America. **2011**;52(4):447-56.

[123] Wu XX, Gao HN, Wu HB, Peng XM, Ou HL and Li LJ. Successful treatment of avian-origin influenza A (H7N9) infection using convalescent plasma. Int J Infect Dis. **2015**;41:3-5.

[124] Duggal A, Pinto R, Rubenfeld G and Fowler RA. Global Variability in Reported Mortality for Critical Illness during the 2009-10 Influenza A(H1N1) Pandemic: A Systematic Review and Meta-Regression to Guide Reporting of Outcomes during Disease Outbreaks. PloS one. **2016**;11(5):e0155044.

[125] Beigel JH, Tebas P, Elie-Turenne MC, Bajwa E, Bell TE, Cairns CB, Shoham S, Deville JG, Feucht E, Feinberg J, Luke T, Raviprakash K, Danko J, O'Neil D, Metcalf JA, King K, Burgess TH, Aga E, Lane HC, Hughes MD, Davey RT and Team IRCS. Immune plasma for the treatment of severe influenza: an open-label, multicentre, phase 2 randomised study. Lancet Respir Med. **2017**;5(6):500-511.

[126] Scott D, Epstein JS and Hayden FG. Serotherapy for patients with severe influenza. Lancet Respir Med. **2017**;5(6):462-464.

[127] Wu Y, Cho M, Shore D, Song M, Choi J, Jiang T, Deng YQ, Bourgeois M, Almli L, Yang H, Chen LM, Shi Y, Qi J, Li A, Yi KS, Chang M, Bae JS, Lee H, Shin J, Stevens J, Hong S, Qin

CF, Gao GF, Chang SJ and Donis RO. A potent broad-spectrum protective human monoclonal antibody crosslinking two haemagglutinin monomers of influenza A virus. Nature communications. **2015**;6:7708.

[128] Kallewaard NL, Corti D, Collins PJ, Neu U, McAuliffe JM, Benjamin E, Wachter-Rosati L, Palmer-Hill FJ, Yuan AQ, Walker PA, Vorlaender MK, Bianchi S, Guarino B, De Marco A, Vanzetta F, Agatic G, Foglierini M, Pinna D, Fernandez-Rodriguez B, Fruehwirth A, Silacci C, Ogrodowicz RW, Martin SR, Sallusto F, Suzich JA, Lanzavecchia A, Zhu Q, Gamblin SJ and Skehel JJ. Structure and Function Analysis of an Antibody Recognizing All Influenza A Subtypes. Cell. **2016**;166(3):596-608.

[129] Hershberger E, Sloan S, Narayan K, Hay CA, Smith P, Engler F, Jeeninga R, Smits S, Trevejo J, Shriver Z and Oldach D. Safety and efficacy of monoclonal antibody VIS410 in adults with uncomplicated influenza A infection: Results from a randomized, double-blind, phase-2, placebo-controlled study. EBioMedicine. **2019**;40:574-582.

[130] McKimm-Breschkin JL, Jiang S, Hui DS, Beigel JH, Govorkova EA and Lee N. Prevention and treatment of respiratory viral infections: Presentations on antivirals, traditional therapies and host-directed interventions at the 5th ISIRV Antiviral Group conference. Antiviral research. **2018**;149:118-142.

[131] Nakamura G, Chai N, Park S, Chiang N, Lin Z, Chiu H, Fong R, Yan D, Kim J, Zhang J, Lee WP, Estevez A, Coons M, Xu M, Lupardus P, Balazs M and Swem LR. An in vivo human-plasmablast enrichment technique allows rapid identification of therapeutic influenza A antibodies. Cell Host Microbe. **2013**;14(1):93-103.

[132] Baranovich T, Jones JC, Russier M, Vogel P, Szretter KJ, Sloan SE, Seiler P, Trevejo JM, Webby RJ and Govorkova EA. The Hemagglutinin Stem-Binding Monoclonal Antibody VIS410 Controls Influenza Virus-Induced Acute Respiratory Distress Syndrome. Antimicrobial agents and chemotherapy. **2016**;60(4):2118-31.

[133] Tharakaraman K, Subramanian V, Viswanathan K, Sloan S, Yen HL, Barnard DL, Leung YH, Szretter KJ, Koch TJ, Delaney JC, Babcock GJ, Wogan GN, Sasisekharan R and Shriver Z. A broadly neutralizing human monoclonal antibody is effective against H7N9. Proceedings of the National Academy of Sciences of the United States of America. **2015**;112(35):10890-5.

[134] Sparrow E, Friede M, Sheikh M, Torvaldsen S and Newall AT. Passive immunization for influenza through antibody therapies, a review of the pipeline, challenges and potential applications. Vaccine. **2016**;34(45):5442-5448.

[135] Yasuhara A, Yamayoshi S, Kiso M, Sakai-Tagawa Y, Okuda M and Kawaoka Y. A broadly protective human monoclonal antibody targeting the sialidase activity of influenza A and B virus neuraminidases. Nature communications. **2022**;13(1):6602.

[136] Doyle TM, Li C, Bucher DJ, Hashem AM, Van Domselaar G, Wang J, Farnsworth A, She YM, Cyr T, He R, Brown EG, Hurt AC and Li X. A monoclonal antibody targeting a highly conserved epitope in influenza B neuraminidase provides protection against drug resistant strains. Biochem Biophys Res Commun. **2013**;441(1):226-9.

[137] Doyle TM, Hashem AM, Li C, Van Domselaar G, Larocque L, Wang J, Smith D, Cyr T, Farnsworth A, He R, Hurt AC, Brown EG and Li X. Universal anti-neuraminidase antibody inhibiting all influenza A subtypes. Antiviral research. **2013**;100(2):567-74.

[138] Chen YQ, Wohlbold TJ, Zheng NY, Huang M, Huang Y, Neu KE, Lee J, Wan H, Rojas KT, Kirkpatrick E, Henry C, Palm AE, Stamper CT, Lan LY, Topham DJ, Treanor J, Wrammert J, Ahmed R, Eichelberger MC, Georgiou G, Krammer F and Wilson PC. Influenza Infection in Humans Induces Broadly Cross-Reactive and Protective Neuraminidase-Reactive Antibodies. Cell. **2018**;173(2):417-429 e10.

[139] Wohlbold TJ, Podolsky KA, Chromikova V, Kirkpatrick E, Falconieri V, Meade P, Amanat F, Tan J, tenOever BR, Tan GS, Subramaniam S, Palese P and Krammer F. Broadly protective murine monoclonal antibodies against influenza B virus target highly conserved neuraminidase epitopes. Nature microbiology. **2017**;2(10):1415-1424.

[140] Wilson JR, Guo Z, Reber A, Kamal RP, Music N, Gansebom S, Bai Y, Levine M, Carney P, Tzeng WP, Stevens J and York IA. An influenza A virus (H7N9) anti-neuraminidase monoclonal antibody with prophylactic and therapeutic activity in vivo. Antiviral research. **2016**;135:48-55.

[141] Stadlbauer D, Zhu X, McMahon M, Turner JS, Wohlbold TJ, Schmitz AJ, Strohmeier S, Yu W, Nachbagauer R, Mudd PA, Wilson IA, Ellebedy AH and Krammer F. Broadly protective human antibodies that target the active site of influenza virus neuraminidase. Science (New York, NY). **2019**;366(6464):499-504.

[142] Nachbagauer R and Krammer F. Universal influenza virus vaccines and therapeutic antibodies. Clin Microbiol Infect. **2017**;23(4):222-228.

[143] Planz O. Antiviral Drugs Against Influenza Virus. New Drug Development for Known and Emerging Viruses2022. p. 59-96.

[144] Li Y, Huo S, Yin Z, Tian Z, Huang F, Liu P, Liu Y and Yu F. The current state of research on influenza antiviral drug development: drugs in clinical trial and licensed drugs. mBio. **2023**;14(5):e0127323.

[145] Bright RA, Shay DK, Shu B, Cox NJ and Klimov AI. Adamantane resistance among influenza A viruses isolated early during the 2005-2006 influenza season in the United States. The Journal of the American Medical Association. **2006**;295(8):891-4.

[146] Pielak RM and Chou JJ. Influenza M2 proton channels. Biochimica et biophysica acta. **2011**;1808(2):522-9.

[147] Mould JA, Paterson RG, Takeda M, Ohigashi Y, Venkataraman P, Lamb RA and Pinto LH. Influenza B virus BM2 protein has ion channel activity that conducts protons across membranes. Dev Cell. **2003**;5(1):175-84.

[148] Belshe RB, Smith MH, Hall CB, Betts R and Hay AJ. Genetic basis of resistance to rimantadine emerging during treatment of influenza virus infection. J Virol. **1988**;62(5):1508-12.

[149] Hay AJ, Zambon MC, Wolstenholme AJ, Skehel JJ and Smith MH. Molecular basis of resistance of influenza A viruses to amantadine. J Antimicrob Chemother. **1986**;18 Suppl B:19-29.

[150] Bean WJ, Threlkeld SC and Webster RG. Biologic potential of amantadine-resistant influenza A virus in an avian model. J Infect Dis. **1989**;159(6):1050-6.

[151] Gubareva LV, Trujillo AA, Okomo-Adhiambo M, Mishin VP, Deyde VM, Sleeman K, Nguyen HT, Sheu TG, Garten RJ, Shaw MW, Fry AM and Klimov AI. Comprehensive assessment of 2009 pandemic influenza A (H1N1) virus drug susceptibility in vitro. Antivir Ther. **2010**;15(8):1151-9.

[152] Saito R, Suzuki Y, Li D, Zaraket H, Sato I, Masaki H, Kawashima T, Hibi S, Sano Y, Shobugawa Y, Oguma T and Suzuki H. Increased incidence of adamantane-resistant influenza A(H1N1) and A(H3N2) viruses during the 2006-2007 influenza season in Japan. J Infect Dis. **2008**;197(4):630-2; author reply 632-3.

[153] Bright RA, Medina MJ, Xu X, Perez-Oronoz G, Wallis TR, Davis XM, Povinelli L, Cox NJ and Klimov AI. Incidence of adamantane resistance among influenza A (H3N2) viruses isolated worldwide from 1994 to 2005: a cause for concern. Lancet. **2005**;366(9492):1175-81.

[154] Principi N, Camilloni B, Alunno A, Polinori I, Argentiero A and Esposito S. Drugs for Influenza Treatment: Is There Significant News? Front Med (Lausanne). **2019**;6:109.

[155] Duwe S. Influenza viruses - antiviral therapy and resistance. GMS infectious diseases. **2017**;5:Doc04.

[156] Gubareva L and Mohan T. Antivirals Targeting the Neuraminidase. Cold Spring Harb Perspect Med. **2022**;12(1).

[157] Dobson J, Whitley RJ, Pocock S and Monto AS. Oseltamivir treatment for influenza in adults: a meta-analysis of randomised controlled trials. Lancet. **2015**;385(9979):1729-1737.

[158] Beigi RH, Venkataramanan R and Caritis SN. Oseltamivir for influenza in pregnancy. Semin Perinatol. **2014**;38(8):503-7.

[159] Whitley RJ, Hayden FG, Reisinger KS, Young N, Dutkowski R, Ipe D, Mills RG and Ward P. Oral oseltamivir treatment of influenza in children. The Pediatric infectious disease journal. **2001**;20(2):127-33.

[160] Ikematsu H, Kawai N, Iwaki N and Kashiwagi S. In vitro neuraminidase inhibitory activity of four neuraminidase inhibitors against clinical isolates of influenza virus in the Japanese 2012-2013 season. J Infect Chemother. **2015**;21(1):39-42.

[161] Gubareva LV, Webster RG and Hayden FG. Comparison of the activities of zanamivir, oseltamivir, and RWJ-270201 against clinical isolates of influenza virus and

neuraminidase inhibitor-resistant variants. Antimicrobial agents and chemotherapy. **2001**;45(12):3403-8.

[162] Whitley RJ, Boucher CA, Lina B, Nguyen-Van-Tam JS, Osterhaus A, Schutten M and Monto AS. Global assessment of resistance to neuraminidase inhibitors, 2008-2011: the Influenza Resistance Information Study (IRIS). Clinical infectious diseases : an official publication of the Infectious Diseases Society of America. **2013**;56(9):1197-205.

[163] Memoli MJ, Hrabal RJ, Hassantoufighi A, Eichelberger MC and Taubenberger JK. Rapid selection of oseltamivir- and peramivir-resistant pandemic H1N1 virus during therapy in 2 immunocompromised hosts. Clinical infectious diseases : an official publication of the Infectious Diseases Society of America. **2010**;50(9):1252-5.

[164] Yamashita M. Laninamivir and its prodrug, CS-8958: long-acting neuraminidase inhibitors for the treatment of influenza. Antivir Chem Chemother. **2010**;21(2):71-84.

[165] McKimm-Breschkin JL and Barrett S. Neuraminidase mutations conferring resistance to laninamivir lead to faster drug binding and dissociation. Antiviral research. **2015**;114:62-6.

[166] Zurcher T, Yates PJ, Daly J, Sahasrabudhe A, Walters M, Dash L, Tisdale M and McKimm-Breschkin JL. Mutations conferring zanamivir resistance in human influenza virus N2 neuraminidases compromise virus fitness and are not stably maintained in vitro. J Antimicrob Chemother. **2006**;58(4):723-32.

[167] Gaymard A, Charles-Dufant A, Sabatier M, Cortay JC, Frobert E, Picard C, Casalegno JS, Rosa-Calatrava M, Ferraris O, Valette M, Ottmann M, Lina B and Escuret V. Impact on antiviral resistance of E119V, I222L and R292K substitutions in influenza A viruses bearing a group 2 neuraminidase (N2, N3, N6, N7 and N9). J Antimicrob Chemother. **2016**;71(11):3036-3045.

[168] Takashita E. Influenza Polymerase Inhibitors: Mechanisms of Action and Resistance. Cold Spring Harb Perspect Med. **2021**;11(5).

[169] Noshi T, Kitano M, Taniguchi K, Yamamoto A, Omoto S, Baba K, Hashimoto T, Ishida K, Kushima Y, Hattori K, Kawai M, Yoshida R, Kobayashi M, Yoshinaga T, Sato A, Okamatsu M, Sakoda Y, Kida H, Shishido T and Naito A. In vitro characterization of baloxavir acid, a first-in-class cap-dependent endonuclease inhibitor of the influenza virus polymerase PA subunit. Antiviral research. **2018**;160:109-117.

[170] Furuta Y, Gowen BB, Takahashi K, Shiraki K, Smee DF and Barnard DL. Favipiravir (T-705), a novel viral RNA polymerase inhibitor. Antiviral research. **2013**;100(2):446-54.

[171] Clark MP, Ledeboer MW, Davies I, Byrn RA, Jones SM, Perola E, Tsai A, Jacobs M, Nti-Addae K, Bandarage UK, Boyd MJ, Bethiel RS, Court JJ, Deng H, Duffy JP, Dorsch WA, Farmer LJ, Gao H, Gu W, Jackson K, Jacobs DH, Kennedy JM, Ledford B, Liang J, Maltais F, Murcko M, Wang T, Wannamaker MW, Bennett HB, Leeman JR, McNeil C, Taylor WP, Memmott C, Jiang M, Rijnbrand R, Bral C, Germann U, Nezami A, Zhang Y, Salituro FG, Bennani YL and Charifson PS. Discovery of a novel, first-in-class, orally bioavailable

azaindole inhibitor (VX-787) of influenza PB2. Journal of medicinal chemistry. **2014**;57(15):6668-78.

[172] Hayden FG, Sugaya N, Hirotsu N, Lee N, de Jong MD, Hurt AC, Ishida T, Sekino H, Yamada K, Portsmouth S, Kawaguchi K, Shishido T, Arai M, Tsuchiya K, Uehara T, Watanabe A and Baloxavir Marboxil Investigators G. Baloxavir Marboxil for Uncomplicated Influenza in Adults and Adolescents. N Engl J Med. **2018**;379(10):913-923.

[173] Furuta Y, Komeno T and Nakamura T. Favipiravir (T-705), a broad spectrum inhibitor of viral RNA polymerase. Proc Jpn Acad Ser B Phys Biol Sci. **2017**;93(7):449-463.

[174] Omoto S, Speranzini V, Hashimoto T, Noshi T, Yamaguchi H, Kawai M, Kawaguchi K, Uehara T, Shishido T, Naito A and Cusack S. Characterization of influenza virus variants induced by treatment with the endonuclease inhibitor baloxavir marboxil. Scientific reports. **2018**;8(1):9633.

[175] Hirotsu N, Sakaguchi H, Sato C, Ishibashi T, Baba K, Omoto S, Shishido T, Tsuchiya K, Hayden FG, Uehara T and Watanabe A. Baloxavir Marboxil in Japanese Pediatric Patients With Influenza: Safety and Clinical and Virologic Outcomes. Clinical infectious diseases : an official publication of the Infectious Diseases Society of America. **2020**;71(4):971-981.

[176] Goldhill DH, Te Velthuis AJW, Fletcher RA, Langat P, Zambon M, Lackenby A and Barclay WS. The mechanism of resistance to favipiravir in influenza. Proceedings of the National Academy of Sciences of the United States of America. **2018**;115(45):11613-11618.

[177] Byrn RA, Jones SM, Bennett HB, Bral C, Clark MP, Jacobs MD, Kwong AD, Ledeboer MW, Leeman JR, McNeil CF, Murcko MA, Nezami A, Perola E, Rijnbrand R, Saxena K, Tsai AW, Zhou Y and Charifson PS. Preclinical activity of VX-787, a first-in-class, orally bioavailable inhibitor of the influenza virus polymerase PB2 subunit. Antimicrobial agents and chemotherapy. **2015**;59(3):1569-82.

[178] Trevejo JM, Asmal M, Vingerhoets J, Polo R, Robertson S, Jiang Y, Kieffer TL and Leopold L. Pimodivir treatment in adult volunteers experimentally inoculated with live influenza virus: a Phase IIa, randomized, double-blind, placebo-controlled study. Antivir Ther. **2018**;23(4):335-344.

[179] Ludwig S, Planz O, Pleschka S and Wolff T. Influenza-virus-induced signaling cascades: targets for antiviral therapy? Trends in molecular medicine. **2003**;9(2):46-52.

[180] Planz O. Development of cellular signaling pathway inhibitors as new antivirals against influenza. Antiviral research. **2013**;98(3):457-68.

[181] Marjuki H, Mishin VP, Chesnokov AP, De La Cruz JA, Fry AM, Villanueva J and Gubareva LV. An investigational antiviral drug, DAS181, effectively inhibits replication of zoonotic influenza A virus subtype H7N9 and protects mice from lethality. J Infect Dis. **2014**;210(3):435-40.

[182] Malakhov MP, Aschenbrenner LM, Smee DF, Wandersee MK, Sidwell RW, Gubareva LV, Mishin VP, Hayden FG, Kim DH, Ing A, Campbell ER, Yu M and Fang F. Sialidase fusion protein as a novel broad-spectrum inhibitor of influenza virus infection. Antimicrobial agents and chemotherapy. **2006**;50(4):1470-9.

[183] Triana-Baltzer GB, Gubareva LV, Nicholls JM, Pearce MB, Mishin VP, Belser JA, Chen LM, Chan RW, Chan MC, Hedlund M, Larson JL, Moss RB, Katz JM, Tumpey TM and Fang F. Novel pandemic influenza A(H1N1) viruses are potently inhibited by DAS181, a sialidase fusion protein. PloS one. **2009**;4(11):e7788.

[184] Belser JA, Lu X, Szretter KJ, Jin X, Aschenbrenner LM, Lee A, Hawley S, Kim DH, Malakhov MP, Yu M, Fang F and Katz JM. DAS181, a novel sialidase fusion protein, protects mice from lethal avian influenza H5N1 virus infection. J Infect Dis. **2007**;196(10):1493-9.

[185] Moss RB, Hansen C, Sanders RL, Hawley S, Li T and Steigbigel RT. A phase II study of DAS181, a novel host directed antiviral for the treatment of influenza infection. J Infect Dis. **2012**;206(12):1844-51.

[186] Zenilman JM, Fuchs EJ, Hendrix CW, Radebaugh C, Jurao R, Nayak SU, Hamilton RG and McLeod Griffiss J. Phase 1 clinical trials of DAS181, an inhaled sialidase, in healthy adults. Antiviral research. **2015**;123:114-9.

[187] Fox LM and Saravolatz LD. Nitazoxanide: a new thiazolide antiparasitic agent. Clinical infectious diseases : an official publication of the Infectious Diseases Society of America. **2005**;40(8):1173-80.

[188] Beigel JH, Nam HH, Adams PL, Krafft A, Ince WL, El-Kamary SS and Sims AC. Advances in respiratory virus therapeutics - A meeting report from the 6th isirv Antiviral Group conference. Antiviral research. **2019**;167:45-67.

[189] Rossignol JF, La Frazia S, Chiappa L, Ciucci A and Santoro MG. Thiazolides, a new class of anti-influenza molecules targeting viral hemagglutinin at the post-translational level. J Biol Chem. **2009**;284(43):29798-808.

[190] Sleeman K, Mishin VP, Guo Z, Garten RJ, Balish A, Fry AM, Villanueva J, Stevens J and Gubareva LV. Antiviral susceptibility of variant influenza A(H3N2)v viruses isolated in the United States from 2011 to 2013. Antimicrobial agents and chemotherapy. **2014**;58(4):2045-51.

[191] Rossignol JF. Nitazoxanide: a first-in-class broad-spectrum antiviral agent. Antiviral research. **2014**;110:94-103.

[192] Mifsud EJ, Tilmanis D, Oh DY, Ming-Kay Tai C, Rossignol JF and Hurt AC. Prophylaxis of ferrets with nitazoxanide and oseltamivir combinations is more effective at reducing the impact of influenza a virus infection compared to oseltamivir monotherapy. Antiviral research. **2020**;176:104751.

[193] Lumby CK, Zhao L, Oporto M, Best T, Tutill H, Shah D, Veys P, Williams R, Worth A, Illingworth CJR and Breuer J. Favipiravir and Zanamivir Cleared Infection with Influenza B in a Severely Immunocompromised Child. Clinical infectious diseases : an official publication of the Infectious Diseases Society of America. **2020**;71(7):e191-e194.

[194] Roberts PJ and Der CJ. Targeting the Raf-MEK-ERK mitogen-activated protein kinase cascade for the treatment of cancer. Oncogene. **2007**;26(22):3291-310.

[195] Robinson MJ and Cobb MH. Mitogen-activated protein kinase pathways. Curr Opin Cell Biol. **1997**;9(2):180-6.

[196] Widmann C, Gibson S, Jarpe MB and Johnson GL. Mitogen-activated protein kinase: conservation of a three-kinase module from yeast to human. Physiol Rev. **1999**;79(1):143-80.

[197] Ludwig S, Wolff T, Ehrhardt C, Wurzer WJ, Reinhardt J, Planz O and Pleschka S. MEK inhibition impairs influenza B virus propagation without emergence of resistant variants. FEBS letters. **2004**;561(1-3):37-43.

[198] Ludwig S, Pleschka S and Planz O. MEK inhibitors as novel host-targeted antivirals with a dual-benefit mode of action against hyperinflammatory respiratory viral diseases. Current opinion in virology. **2023**;59:101304.

[199] Schreiber A, Boff L, Anhlan D, Krischuns T, Brunotte L, Schuberth C, Wedlich-Soldner R, Drexler H and Ludwig S. Dissecting the mechanism of signaling-triggered nuclear export of newly synthesized influenza virus ribonucleoprotein complexes. Proceedings of the National Academy of Sciences of the United States of America. **2020**;117(28):16557-16566.

[200] Droebner K, Pleschka S, Ludwig S and Planz O. Antiviral activity of the MEK-inhibitor U0126 against pandemic H1N1v and highly pathogenic avian influenza virus in vitro and in vivo. Antiviral research. **2011**;92(2):195-203.

[201] Haasbach E, Muller C, Ehrhardt C, Schreiber A, Pleschka S, Ludwig S and Planz O. The MEK-inhibitor CI-1040 displays a broad anti-influenza virus activity in vitro and provides a prolonged treatment window compared to standard of care in vivo. Antiviral research. **2017**;142:178-184.

[202] Schrader T, Dudek SE, Schreiber A, Ehrhardt C, Planz O and Ludwig S. The clinically approved MEK inhibitor Trametinib efficiently blocks influenza A virus propagation and cytokine expression. Antiviral research. **2018**;157:80-92.

# Objectives

Influenza poses a substantial global health threat, and efforts to prevent and manage it remain crucial. Influenza viruses exploit a high rate of mutations that significantly attributed to their evolution, resulting in the emergence of a multitude of genetic and antigenic variants. Thus, the development of novel, effective therapeutic approaches remains indispensable. Given that influenza viruses trigger various signaling pathways within the host cell, including the Raf/MEK/ERK kinase cascade, essential for effective replication, blocking such cascade results in compromised virus propagation. In the context of repurposing strategy, the present work aims to address the development of the antiviral potential of MEK-inhibitor zapnometinib (PD0184264, previously known as ATR-002) the active metabolite of CI-1040, against influenza viruses. Also, in terms of improved therapeutic efficacy, this work presents the efficacy of combination treatment with another DAA, the polymerase inhibitor baloxavir marboxil. Moreover, the study investigates the immunomodulatory potential of zapnometinib.

On the other hand, annual reformulation of influenza vaccines is necessary to match the circulating strains. Given that current influenza vaccines have no influence on the CD8+ and innate T cell activation, insights gleaned from past pandemics indicate that individuals with preexisting cellular immune responses are either protected or manifest milder symptoms when exposed to the infection. Thus, broadly reactive vaccines that can harness the potential of CD8+ T cell cross-protective immunity against different influenza virus strains and subtypes would be desirable. The key to developing peptide-based vaccines lies in unveiling factors that impact peptide immunogenicity and the strength of the immune response. From this perspective, by implementing a mass spectrometry-based immunopeptidomics approach, the aims are to identify novel and highly immunogenic naturally presented IAV-derived CD8 T cell epitopes. It also investigates the functional validation and temporal dynamics of the identified IAV-derived ligands. Moreover, assessing the conservation of the identified epitopes among major zoonotic reservoirs is a bottleneck in providing potential heterosubtypic protection.

Ultimately, this project contributes to the development of alternative therapeutic approaches to tackle the threats posed by the rapidly evolving influenza viruses.

# Results

The results section of this thesis is divided into two separate parts.

**Part I** addresses the development of MEK inhibitor, zapnometinib, as a host-targeted antiviral drug against IAV. This part encompasses four Chapters: **Chapter 1 and Chapter 2** investigate the antiviral potential of zapnometinib against different IAV subtypes, including baloxavir-resistant strains, via nuclear retention of influenza vRNP. Moreover, **Chapter 2** extends the investigations by highlighting the synergistic effect of zapnometinib and baloxavir marboxil which substantiate two distinct scenarios for the use of zapnometinib either as standalone monotherapy, or in a combination approach alongside SOC drugs. **Chapter 3** sheds light on the immunomodulatory potential of zapnometinib using acute lung injury (ALI) model. This chapter is finalized and in the process of publication.

**Part II** consists of **Chapter 4** which focuses on implementing a mass spectrometry-based immunopeptidomics approach to identify naturally presented IAV-derived MHC-I restricted epitopes. It also investigates the functional validation and temporal dynamics of the identified IAV-derived ligands. Moreover, this chapter delves into the conservation of the identified epitopes among major zoonotic reservoirs that represent a major challenge in achieving potential heterosubtypic protection.

# Part I

# Chapter 1

# Antiviral Efficacy Against Influenza Virus and Pharmacokinetic Analysis of a Novel MEK-Inhibitor, ATR-002, in Cell Culture and in the Mouse Model

Martin Laure[1,2], Hazem Hamza[1,2,3], Julia Koch-Heier[1,2], Martin Quernheim[4], Christin Müller[5], Andre Schreiber[6], Gerhard Müller[7], Stephan Pleschka[5], Stephan Ludwig[6] and Oliver Planz[1,2]*

[1] Interfaculty Institute for Cell Biology, Department of Immunology, Eberhard Karls University Tübingen, Germany

[2] Atriva Therapeutics GmbH, Christophstr. 32, 72072 Tübingen, Germany

[3] Virology Laboratory, Environmental Research Division, National Research Centre, Cairo, Egypt

[4] Chemcon GmbH, Engesserstr. 4B, 79108 Freiburg i. Brsg., Germany

[5] Institute of Medical Virology, Justus Liebig University Giessen, Germany

[6] Institute of Virology, Westfaelische Wilhelms-University Muenster, Germany

[7] Gotham Therapeutics, New York, U.S.A.

* Corresponding author

*Antiviral Res. 2020 Jun; (178):104806 PMID: 32304723 DOI: 10.1016/j.antiviral.2020.104806*

## *Disclosure of authorship contribution*

HH performed the drug testing experiments *in vitro*. HH involved in all steps of data analysis and visualization. HH was strongly involved in drafting and reviewing the manuscript. Further information is provided in the "Author Contribution" section at the end of this chapter/manuscript.

## Abstract

Antiviral therapies against influenza are required, especially for high-risk patients, severe influenza and in case of highly pathogenic influenza virus (IV) strains. However, currently, licensed drugs that target the virus directly are not very effective and often lead to the development of resistant IV variants. This may be overcome by targeting host cell factors that are required for IV propagation. IV induces a variety of host cell signaling cascades, such as the Raf/MEK/ERK kinase pathway. The activation of this pathway is necessary for IV propagation. MEK inhibitors block the activation of the pathway on the bottleneck of the signaling cascade leading to impaired virus propagation. In the present study, we aimed to compare the antiviral potency and bioavailability of the MEK inhibitor CI-1040 versus its major active metabolite ATR-002, *in vitro* as well as in the mouse model. In cell culture assays, an approximately 10-fold higher concentration of ATR-002 is required to generate the same antiviral activity as for CI-1040. Interestingly, we observed that considerably lower concentrations of ATR-002 were required to achieve a reduction of the viral load *in vivo*. Pharmacokinetic studies with ATR-002 and CI-1040 in mice have found the $C_{max}$ and AUC to be far higher for ATR-002 than for CI-1040. Our results thereby demonstrate the *in vivo* superiority of the active metabolite ATR-002 over CI-1040 as an antiviral agent despite its weaker cell membrane permeability. Therefore, ATR-002 is an attractive candidate for development as an efficient antiviral agent, especially given the fact that a treatment based on cellular pathway inhibition would be far less likely to lead to viral drug resistance.


## Introduction

Despite intensive efforts to fight and prevent influenza, it still remains a worldwide threat. Seasonal outbreaks are estimated to cause 290,000 – 650,000 deaths among adults, and over 100,000 deaths among children under the age of 5 years old, annually [1]. Hospitalization rates range between 3 and 5 million per year [2], and damage to national economies is considerable [3,4]. Vaccination strategies are the core of influenza management [5-8], but reliable and effective drugs for immediate treatment once the disease has manifested are equally important. However, for both the well-known and direct-acting classes of antivirals available for clinical use [neuraminidase inhibitors (e.g. oseltamivir, zanamivir, peramivir and M2) ion-channel inhibitors (e.g. amantadine, rimantadine)], resistance is increasingly reported [9-12].

Even against the recently developed novel anti-influenza drug Baloxavir, an inhibitor of the cap-dependent endonuclease activity within the polymerase subunit PA of influenza A and B viruses, resistance is already occurring at a frightening frequency [13]. For example, insensitive mutant strains that have the same fitness as wild-type strains have been reported, as well as events of human-to-human transmission of resistant variants. This emphasizes the inherent potential of the influenza virus (IV) to adapt quickly when targeted directly and thereby escape current treatment options.

An alternative approach to prevent drug resistance is to target essential cellular pathways on which the virus depends for survival. We were able to demonstrate that the MEK-inhibitor CI-1040, a small-molecule inhibitor of the dual-specificity kinases MEK (mitogen-activated protein kinase kinase) -1 and MEK2, that was previously used in clinical studies against cancer [14,15] showed strong antiviral activity against IV *in vitro* and *in vivo* [16,17]. Infection with IV leads to a bi-phasic activation of the Raf/MEK/ERK signaling pathway and it seems that the late stage of activation is the functionally most relevant. In this phase of the replication cycle the IV needs to drive the export of the viral genome-containing ribonucleoprotein (vRNP)-complexes out of the nucleus and into the cytoplasm. Accordingly, inhibition of the pathway using MEK inhibitors results in impaired virus propagation concomitant with nuclear retention of vRNPs in the nucleus [16-20]. Moreover, activation of the Raf/MEK/ERK pathway is required by the virus for phosphorylation of viral proteins and constant activation strongly supports virus propagation [18,21].

A phase I study reported that maximum CI-1040 plasma concentrations ($C_{max}$) and the area under the curve (AUC) of the plasma concentration are insignificant, even when high doses of CI-1040 were administered and development was therefore abandoned [14]. Interestingly, the same study also observed approximately 5-fold higher plasma concentrations for the active metabolite of CI-1040, PD-0184264 (now designated ATR-002). However, due to its acid group, which is thought to obstruct the ability of a molecule to penetrate cellular membranes, pharmaceutical development of PD-0184264 was not pursued further even though the 50% inhibitory concentration ($IC_{50}$) value of PD-0184264 for MEK inhibition was slightly lower (5.73 nM) when compared to CI-1040 (17.00 nM) [22,23]. Consequently, we were interested in investigating whether this active metabolite would also have antiviral potency against IV.

Here, we demonstrate the *in vitro* and *in vivo* antiviral potential of the MEK-inhibitor PD0184264 (ATR-002, the active metabolite of CI-1040) against IVs. Moreover, we have elucidated the antiviral mode of action against both influenza A and B viruses.

## Materials and methods

**Drugs**

CI-1040 [2-(2-chloro-4-iodophenylamino)-N-(cyclopropylmethoxy)-3,4-difluoro benzamide], (M=478,66g/mol) and ATR-002 (PD0184264) [2-(2-chloro-4-iodophenylamino)-N-3,4-difluoro benzoic acid], (M=409,55g/mol) were synthesized at ChemCon GmbH (Freiburg, Germany). For all cell culture experiments, fresh 10 mM stock solutions of CI-1040 and ATR-002 were prepared in DMSO (Merck-Millipore, Darmstadt, Germany) and further diluted in the respective media or buffer.

Synthesis of CI-1040 was achieved by the coupling of o-cyclopropylmethylhydroxylamin hydrochloride and ATR-002 (Fig. 1), which were prepared by two synthetic routes. The amide bond was formed using 1-propanephosphonic anhydride (T3P) to activate the carboxylic acid. The side chain o-cyclopropylmethylhydroxylamin hydrochloride was prepared in a one-pot reaction starting from ethyl-N-acetohydroxyacetamidate. The active substance ATR-002 was prepared in one step by nucleophilic aromatic substitution. Next, 2,3,4 Trifluorobenzoic acid and 2-chloro-4-iodo aniline were coupled using lithium amide as an efficient base in THF/acetonitrile.

**Cells and viruses**

Human adenocarcinoma type II alveolar lung epithelial cells (A549, ATCC® CCL185™) and Madin-Darby canine kidney cells (MDCK II, ATCC® CRL2936™) were purchased from ATCC and cultured in Iscove's Modified Dulbecco's Medium (IMDM, Thermo Fisher Scientific, Waltham, Massachusetts, USA) supplemented with 10% (v/v) fetal bovine serum (FBS, Sigma-Aldrich, St. Louis, Missouri, U.S.A.), 100 U/mL penicillin, and 100 µg/mL streptomycin (Sigma-Aldrich, St. Louis, Missouri, U.S.A.). Cells were maintained in a 37 °C and 5% $CO_2$ atmosphere. Human PBMCs were provided by healthy donors and purified by standard Ficoll gradient.

Virus inhibition experiments were carried out with influenza A virus (IAV) strain RB1 [A/Regensburg/D6/09 (H1N1pdm09)] with a multiplicity of infection (MOI) of 0.001, IV

A/Fukui/20/2004 (H3N2) with a MOI of 0.001 and influenza B virus (IBV) strain B/Lee/40 with a MOI of 0.001 and B/Münster/341-200/18 with a MOI of 5.

**Mice**

Eight-week-old male NMRI mice (Charles River Laboratories, Germany) with a body weight of 23.9 – 36.5 gr. at administration were used for pharmacokinetic studies. Eight-week-old female C57BL/6 mice (Charles River Laboratories, Germany) with a body weight of 21.0 – 24.0 gr. at administration were used for the antiviral studies. The animals were fed with standard food. Drinking water was available *ad libitum*.

**Drug administration to mice**

Drugs were either administered using single dosing on test day 1 by oral gavage or by intravenous (i.v.) bolus injection into a tail vein. The injection speed was 15 sec/dose with an administration volume of 200 µl.

**Progeny virus inhibition assay**

A549 cells were inoculated with the aforementioned IAV strains at the respective MOI prepared in phosphate-buffered saline (PBS) supplemented with 0.2% (w/v) bovine serum albumin (BSA, Carl Roth, Karlsruhe, Germany), 1 mM $MgCl_2$, 0.5 mM $CaCl_2$, 100 U/mL penicillin, 100 µg/mL streptomycin (Merck, Germany) for 45 minutes at 37°C and 5% $CO_2$. Inocula were removed, cells were rinsed with PBS, and supplemented with 1 mL IV infection media (Dulbecco's Modified Eagle Medium; DMEM; Thermo Fisher Scientific, Waltham, Massachusetts, U.S.A supplemented with 0.2% BSA, 1 mM $MgCl_2$, 0.5 mM $CaCl_2$, 100 U/mL penicillin, 100 µg/mL streptomycin, and 2 µg/mL TPCK-treated Trypsin, containing different concentrations of either CI-1040 or ATR-002 (100 µM, 50 µM, 10 µM, 5 µM, 1 µM, 0.5 µM, and 0.1 µM, final DMSO concentration 1% for 24h at 37 °C in 5% $CO_2$).

**Influenza virus titration (AVICEL® plaque assays)**

All AVICEL® plaque assays were carried out as previously described [24,25]. Briefly, MDCK-II virus-infected cells were immunostained 22 hours post infection (hpi) with mouse anti-IAV nucleoprotein monoclonal antibody (Bio-Rad, Hercules, California, USA) followed by peroxidase-labeled anti-mouse antibody and True Blue™ peroxidase substrate (SeraCare, Life Sciences, Milford, Massachusetts U.S.A.).

**Determination of viral load in lungs**

Mice were sacrificed by $CO_2$ gassing. Lungs were removed, weighed and transferred into a Lysing Matrix D tube (MP Biomedicals, Eschwege, Germany). Next, 500 µl ice-cold PBS was added and the tissue organs were shredded using the FastPrep FP 120 (Savant). The homogenized tissue was centrifuged for 10 min at 18,000 × g at 4 °C. Supernatant was transferred into sterile 1.5 ml safe-lock tubes (Eppendorf, Hamburg, Germany) and kept on ice until further storage at -80 °C. To determine the virus load, supernatant was thawed on ice and an AVICEL® plaque assay using MDCK II cells was performed.

**Cell viability assay (WST-Assay)**

A549 cells, MDCK cells and human PBMCs were seeded in a 96-well flat-bottom tissue plate (Greiner, Bio-One, Frickenhausen, Germany) and were grown overnight as described in section 2.2. Thereafter, cells were treated with different concentrations of ATR-002 (100 µM, 50 µM, 10 µM, 5 µM, 1 µM, 0.5 µM, and 0.1 µM) dissolved in 100 µl IMDM supplemented with 5% FBS with a final DMSO concentration of 1% (v/v). Cells were cultured at 37 °C with 5% $CO_2$ for 24 hrs. Thereafter, 10 µl WST-1 reagent (Roche, Basel, Switzerland) was added to the culture medium and incubated for 4 hrs. Thereafter, the formazan dye formed was quantified on an ELISA plate reader (Molecular Devices, San Jose, California, U.S.A.) at 405 nm.

**Immunofluorescence staining and microscopy**

For immunofluorescence analysis of infected and inhibitor-treated A549 cells, samples were washed with PBS and fixed with ice-cold methanol (-20 °C, Carl Roth, Karlsruhe, Germany) for 10 min at 4 °C. Afterwards cells were washed with PBS and blocked with 3% (w/v) BSA in PBS for 1 h at 21 °C (room temperature). Primary antibodies against influenza B virus (IBV) NP (Bio-Rad, Hercules, California, USA) and IBV-M1 (GeneTex) were diluted 1:1000 in 3 % BSA in PBS (BSA/PBS). Primary antibody incubation was performed for 1 hr at RT. After washing with BSA/PBS, samples were incubated for 45 min in BSA/PBS containing 1:800 diluted anti-mouse Alexa 488 IgY (Thermo Fisher Scientific, Waltham, Massachusetts, U.S.A) and anti-rabbit Alexa 561 IgG (Thermo Fisher Scientific, Waltham, Massachusetts, U.S.A) secondary antibodies and DAPI (5 mg/mL) (4´,6-diamino-2-phenylindole, Thermo Fisher Scientific, Waltham, Massachusetts, U.S.A) diluted 1:10000. After the final PBS wash, samples were mounted onto object slides with Fluorescence Mounting Medium (Dako, Jena, Germany).

Immunofluorescence analysis was performed with an epifluorescence microscope (Axiovert 200M, Carl Zeiss, Jena Germany).

**Determination of $IC_{50}$ values for CI-1040 and ATR-002**

Detailed methods for the cell-free kinase assay and the kinase assays in A549, MDCK cells and human PBMCs were described in the supplementary (Supplementary S1).

**Western blot analysis**

Protein concentration was determined by BCA Protein Assay (Thermo Fisher Scientific, Waltham, Massachusetts, U.S.A.) before the lysates were subjected to sodium dodecyl sulphate-polyacrylamide gel electrophoresis (SDS-PAGE) and transferred onto polyvinylidene fluoride (PVDF) membranes (Bio-Rad, Hercules, California, U.S.A.). Membranes were incubated with a phospho-specific anti pERK mAb (1:500; Santa Cruz, Biotechnology, Dallas, Texas, U.S.A.) diluted in 5% BSA/TBS/T (20 mM Tris–HCl pH 7.6, 140 mM NaCl, 0.05% Tween 20) overnight at 4 °C. After stripping (Merck Millipore, Darmstadt, Germany,) bound antibodies and washing in TBS/Tween buffer, total ERK2 was detected using anti-ERK2 mAb (1:500; Santa Cruz, Biotechnology, Dallas, Texas, U.S.A.) for 1 hr at RT followed by incubation with a peroxidase-coupled, species-specific HRP-conjugated anti-mouse monoclonal secondary antibodies (1:800; Santa Cruz, Biotechnology, Dallas, Texas, U.S.A.) and a standard enhanced chemiluminescence reaction (Santa Cruz, Biotechnology, Dallas, Texas, U.S.A.). Specific bands were quantified on the Fusion software.

**Determination of pERK/ERK2 ratio by Wes™ analysis**

Wes™ capillary electrophoresis by ProteinSimple® was used to identify and quantify pERK/ERK2. Cell lysates were diluted 1:2 with 0.1X Sample Buffer (ProteinSimple, Abingdon, Oxford, UK) and analyzed using specific antibodies. The primary antibodies pERK mouse monoclonal IgG2a and ERK-2 mouse monoclonal IgG2a were purchased from Santa Cruz Biotechnology (Santa Cruz Biotechnology, Dallas, Texas, U.S.A.) and used at 1:25 dilutions in antibody diluent (Protein Simple, Abingdon, Oxford, UK). The anti-rabbit secondary antibody and all used reagents were also purchased from ProteinSimple and were ready to use.

**Preparation of compounds for pharmacokinetic analysis**

For i.v. administration, 30.65 mg CI-1040 was dissolved in 0.075 mL DMSO (Sigma-Aldrich, St. Louis, Missouri, U.S.A.) and further diluted with 0.225 mL Cremophor EL (Merck-Millipore, Darmstadt, Germany) and 2.7 mL PBS (Thermo Fisher Scientific, Waltham, Massachusetts, U.S.A.). Next, 34.88 mg ATR-002 was dissolved in 0.075 mL DMSO and further diluted with 0.225 mL Cremophor EL and 2.7 mL PBS. For oral administration 202.5 mg CI-1040 was dissolved in 0.5 mL DMSO, 1.5 mL Cremophor EL, and 8.0 mL PBS. Accordingly, 81.0 mg ATR-002 was dissolved in 0.2 mL DMSO, 0.6 mL Cremophor EL, and 3.2 mL PBS.

**Blood sampling and preparation of plasma**

Experiments were performed at LPT GmbH (Hamburg, Germany). Whole blood from mice, taken under isoflurane anesthesia, was collected to obtain at least 2 × 100 µL Li-Heparin plasma of 3 animals per group and time-points at the following times: 0 (predose), 15 min, 30 min, 1 h, 2 h, 4 h, 6 h, 8 h, and 24 h (test day 2) after administration. The whole blood samples were instantly cooled using an Iso-Therm-Rack system (Eppendorf AG, Hamburg, Germany) until centrifugation within 0.5 hours after withdrawal. Immediately after centrifugation, the samples were stored at -20°C until further analysis. Plasma analysis was performed using standard procedures at Prolytic GmbH (Frankfurt, Germany).

**Preparation of compounds to investigate virus titer reduction in the lungs of mice**

For oral application of 25 mgATR-002/kg body weight, 10 mg of ATR-002 was dissolved in 50 µl DMSO (Sigma-Aldrich, St. Louis, Missouri, U.S.A.) and further diluted with 0.15 mL Cremophor EL and 0.8 mL PBS. For application of 8.4 mg/kg and 2.8 mg/kg, 3.36 mg or 1.12 mg ATR-002 was dissolved in 50 µl DMSO and further diluted with 0.15 mL Cremophor EL and 0.8 mL PBS. Additionally, 202.5 mg CI-1040 was dissolved in 0.5 mL DMSO, 0.15 mL Cremophor EL, and 0.8 mL PBS.

**Treatment and preparation of MDCK cells for detection of intracellular deposition**

MDCK-II cells were seeded in 3.5 cm dishes of 6-well plates (Greiner, Bio-One, Frickenhausen, Germany) and grown in DMEM supplemented with 10% FBS and 100 U/ml Penicillin and 100U/mL Streptomycin. After washing the cells were incubated with DMEM/BA (DMEM containing 0.2% BA, P/S), which either contained CI-1040 or ATR-002 at a concentration of 10 or 50 µM solved in DMSO, or just DMSO (negative control). At 0.5, 2 and 6 h post inhibitor/DMSO-treatment cells (infected or uninfected) were washed with $PBS^{++}$ scraped off,

collected in a 15 ml tube, and pelleted by centrifugation. The supernatant (SN) was removed, and the cells were resuspended in 10 ml $PBS^{++}$ for washing. After pelleting, the SN was removed, and the cells were transferred into a 1.5 ml reaction tube in 1 ml $PBS^{++}$. After precipitation and removal of the SN the cell pellet was dissolved in 50 µl of 6 M Guanidinium thiocyanate (Sigma-Aldrich, St. Louis, Missouri, U.S.A.) and stored at -70°C for further processing. All experiments were performed in triplicate. Lysed cells were used to determine intracellular deposition of either CI-1040 or ATR-002 with mass spectrometry using the standard procedures at Prolytic GmbH (Frankfurt, Germany).

## Results

**Synthetic scheme for the synthesis of ATR-002 and CI-1040**

One initial aim of the work presented here was the development of an efficient route towards the synthesis of CI-1040. The synthesis was achieved by the coupling of the two building blocks o-cyclopropylmethylhydroxylamin hydrochloride and 2-(2-Chloro-4-iodo-phenylamino)-3,4-difluoro benzoic acid (ATR-002), which were prepared by two separate synthetic routes. ATR-002 was prepared in a one-step reaction with 2,3,4 Triflourobenzoic acid and 2-Chloro-4-iodo aniline by nucleophilic aromatic substitution (Fig. 1). The synthesis of o-cyclopropylmethylhydroxylamin hydrochloride is described in the Materials and methods section.

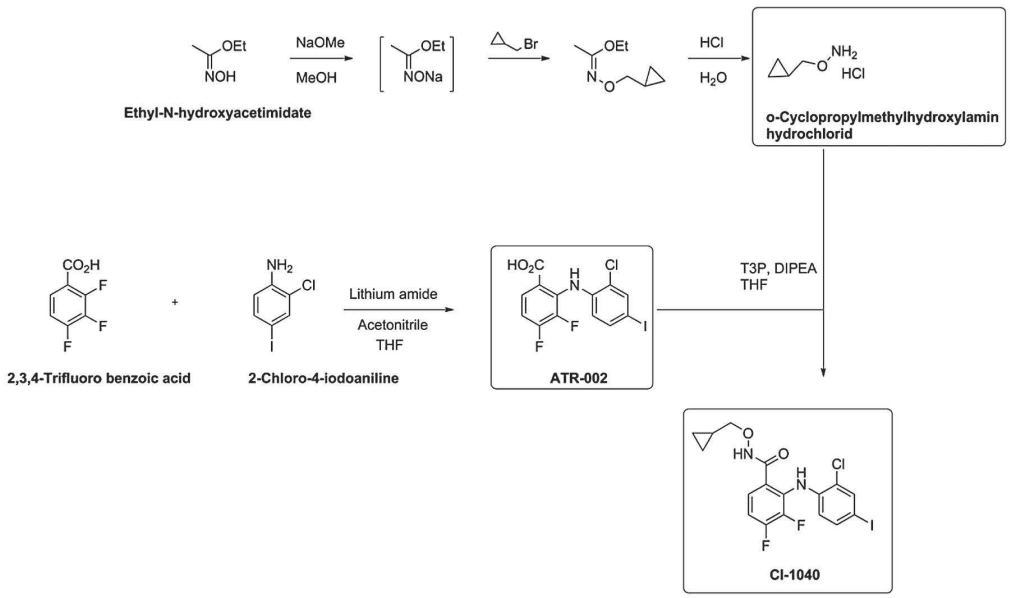

***Figure 1: Synthesis of ATR-002 and CI-1040.*** *The side chain o-cyclopropylmethylhydroxylamin hydrochloride was prepared in a one-pot reaction starting from ethyl-N-acetohydroxacetamidate. ATR-002 was prepared in one step by nucleophilic aromatic substitution. 2,3,4 Triflourobenzoic acid and 2-chloro-4-iodo aniline were coupled by using lithium amide as an efficient base in THF/acetonitrile. The synthesis of CI-1040 was achieved by coupling of the two building blocks o-cyclopropylmethylhydroxylamin hydrochloride and ATR-002. The amide bond was formed using 1-propanephosphonic anhydride (T3P) to activate the carboxylic acid of ATR-002.*

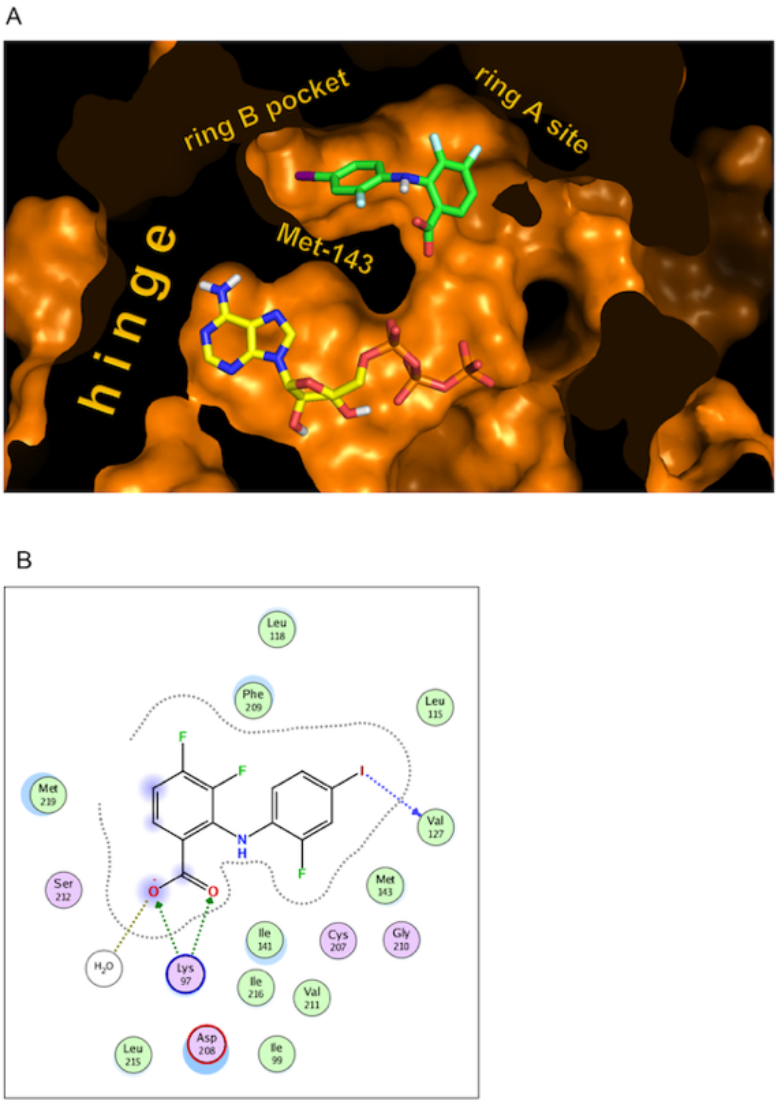


***Figure 2: Modelling of ATR-002 into the MEK binding region. (A)*** *View into the active site of the modeled MEK-1 inhibitor complex structure obtained from the Protein Data Bank (1s9j.pdb). The protein is shown in a solvent-accessible surface representation, while the ATP and inhibitor molecule are depicted in stick mode. The hinge region is shown on the left.* ***(B)*** *Schematic interaction diagram of ATR-002 bound to MEK-1. The halogen bond of the iodine atom in ring-B to Val-127 is shown explicitly.*

**Modeling of CI-1040 and ATR-002 onto MEK**

Based on a thorough visual inspection of the X-ray structure (Protein Data Bank; 1s9j.pdb) of a ternary complex of MEK-1, ATP and a small-molecule inhibitor structurally closely related to ATR-002 and CI-1040 [26], we modified the inhibitor structure to resemble ATR-002 in order to rationalize the binding mode. Energetic relaxation resulted in a model structure in which ATR-002 is docked into the type-III inhibitor-binding pocket of MEK-1 (Fig. 2A). As exemplified in the interaction diagram (Fig. 2B), the B-ring is perfectly accommodated in its original binding pocket delineated by predominately hydrophobic residues. The Iodine atom is within 3.7 Å of the Val-127 backbone carbonyl oxygen atom. The A-ring remains very close to its original position within the parent complex structure. The side chain of Lys-97 slightly changes its position towards the charged carboxylate of ATR-002 and together with the gatekeeper residue Met-143 it physically sequesters the type-III inhibitor pocket from the active site of the enzyme in which ATP is concurrently bound. Given the close structural resemblance of ATR-002 to the first-generation MEK1/2 inhibitors, we strongly believe that the binding mode exemplified in this molecular modeling study reflects the physiologically relevant situation.

**Antiviral activity of ATR-002 against influenza virus**

The antiviral activity of ATR-002 against IAV was investigated in a standard virus inhibition assay (Fig. 3). We demonstrate a reduction in viral titers of the pandemic H1N1 strain A/Regensburg/D6/2009 (RB1, H1N1pdm09) after treatment with 100 µM or 50 µM ATR-002, respectively (Fig. 3A). Moreover, a quite similar pattern of titer reduction was observed for the seasonal H3N2 strain A/Fukui/20/2004 (H3N2) strain, with the two above-mentioned ATR-002 concentrations. Comparing the effect of ATR-002 on these two viruses, 10 µM ATR-002 resulted in a titer reduction of roughly 50% of H1N1pdm09, and a stronger decrease was found for the H3N2 strain (87%). Moreover, 1 µM ATR-002 was insufficient to significantly affect virus titers of both, the H1N1pdm09 and the H3N2 strains (Fig. 3A, D). Thus, in comparison to the virus reduction observed with 10 µM CI-1040 [17] an almost 10-fold higher concentration of ATR-002 is needed to achieve a similar reduction of progeny virus.

As an important step towards developing an effective antiviral drug, the pharmacological parameters, both the half maximal effective concentration ($EC_{50}$) and the 50% cytotoxic concentration ($CC_{50}$) were determined. The $CC_{50}$ value for ATR-002 was 271.8 µM on A549

cells and on MDCK II cells 188.6 µM (Fig 3C, H). Afterwards, the $EC_{50}$, was analyzed using a wide range of ATR-002 concentrations on A549 cells infected with either the H1N1pdm09 or the H3N2 strain and on MDCK II cells infected with B/Lee/40. $EC_{50}$ values for ATR-002 against these three viruses were in the same range (4.190 – 6.356 µM) (Fig. 3B, E, G). Comparison of the $CC_{50}$ and $EC_{50}$ of ATR-002 resulted in a selectivity index (SI) of 42.8 for H1N1pdm09, 60.4 for H3N2, and 45.0 for B/Lee/40.

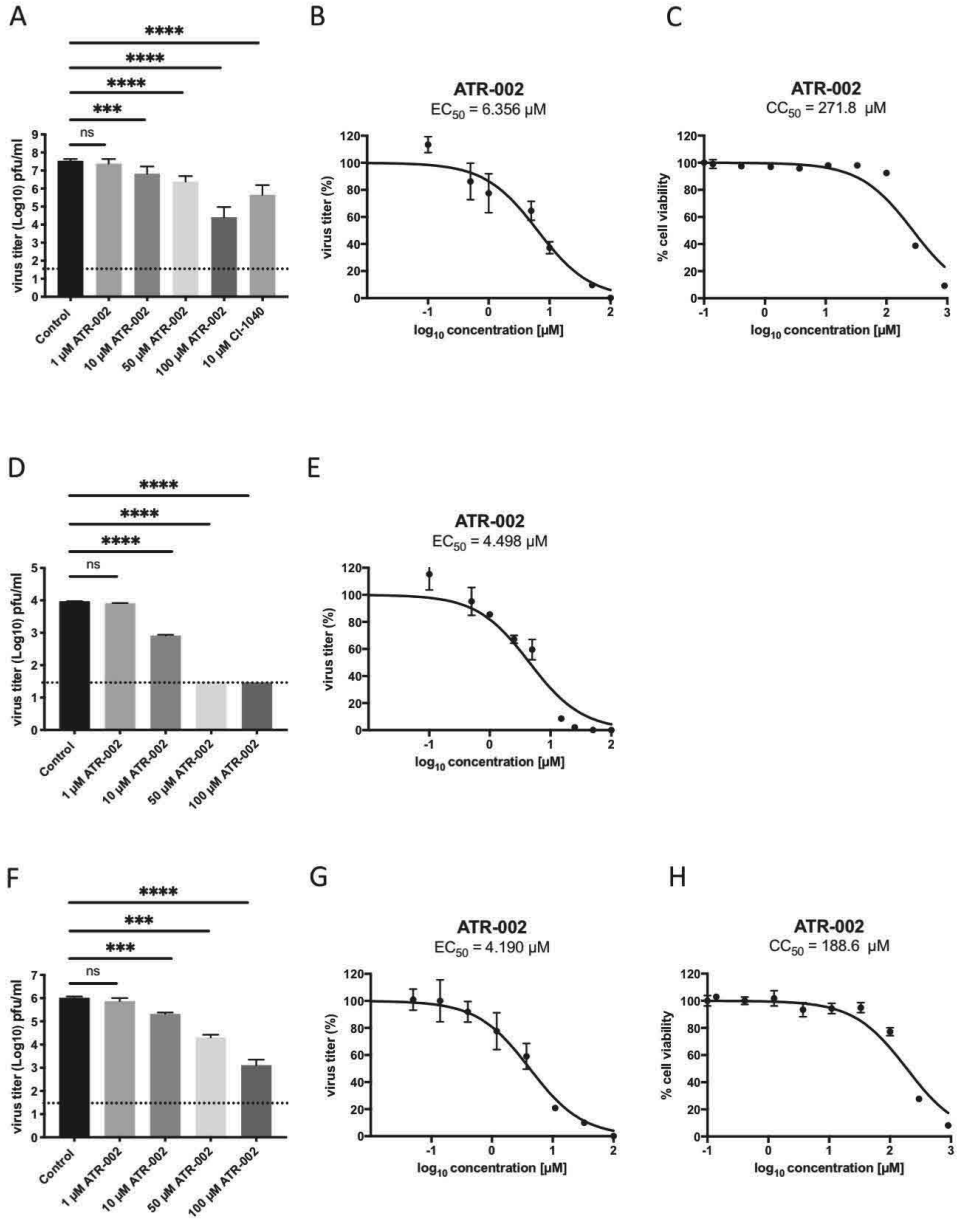


***Figure 3: Antiviral activity of ATR-002 against IV H1N1pdm09, H3N2, and nuclear vRNP-retention of IBV after pathway inhibition. (A)*** *A549 were infected with RBI (MOI=0.001) to determine virus titer reduction. Dose-dependent inhibition was found for ATR-002 compared to solvent control. 100 µM ATR-*

*002 resulted in a 99.87% ± 0.01% reduction of virus titer (Unpaired t-test with Welch's correction P >0.0001). Similar significance was found using 50 µM ATR-002 (Unpaired t-test with Welch's correction P >0.0001) while no significant virus titer reduction was found using 10 µM and 1 µM ATR-002. 10 µM CI-1040 also resulted in a strong reduction of virus titer (Unpaired t-test with Welch's correction P >0.0001). The figure represents the results of three experiments.* ***(B)*** *A549 cells were infected with RBI (MOI=0.001) and treated with different concentrations of ATR-002 to determine the* $EC_{50}$ *value. The data shown here is an average of four independent experiments. A549 cells* ***(C)*** *and MDCK II cells* ***(H)*** *were treated with different concentrations of ATR-002 for 24 hrs followed by 4 hrs WST-staining to determine the* $CC_{50}$ *values.* ***(D)*** *The potency of ATR-002 against H3N2 after 24 hrs (p.i) was tested. Linear regression analysis in order to calculate the* $EC_{50}$ *of ATR-002 against H3N2* ***(E)*** *and B/Lee/40* ***(G)****. Data are shown in* $log_{10}$ *concentration. All statistical tests were performed using GraphPad Prism 8.* ***(F)*** *Antiviral potential of ATR-002 against B/Lee/40. All antiviral data was analyzed using an Unpaired t-test with Welch's correction. Asterisks above bars represent statistical significance.*

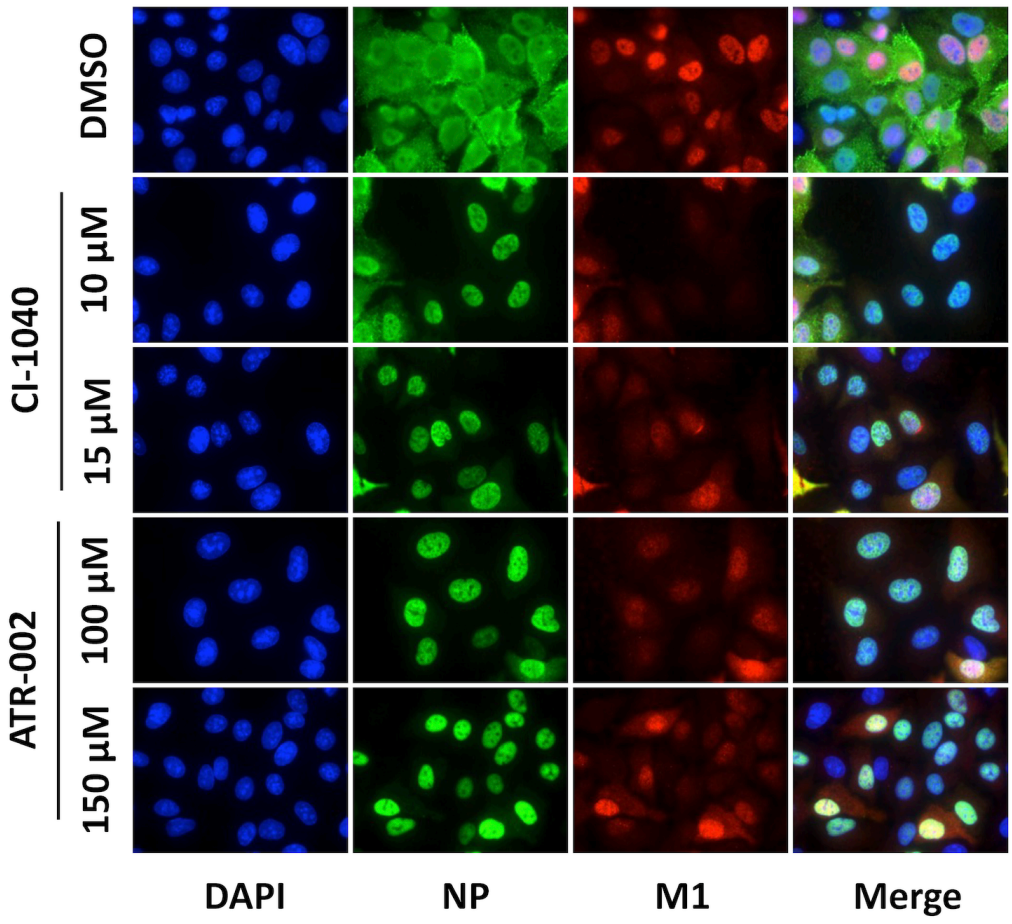


***Figure 4: Nuclear vRNP-retention of IBV after pathway inhibition.*** *Human lung epithelial cells (A549) were infected with Influenza B/Münster/341-200/18 at a multiplicity of infection (MOI) of 5 for 30*

*minutes at 33 °C. Cells were prepared for immunofluorescence staining of the viral nucleoprotein (NP) (green) and matrix protein 1 (M1) (red). Anti-NP (Bio-Rad) and anti-M1 (GeneTex) were used to detect the viral proteins. Nuclei were stained with DAPI (blue).*

On a molecular level, the antiviral action of MEK inhibitors was shown to be due to the nuclear retention of viral vRNPs [18]. However, while MEK inhibitors such as U0126 [27] and CI-1040 [17] also impair IBV replication, it has not yet been shown whether this also occurs via the same mechanism. While vRNPs of B/Münster/341-200/18 are readily translocated to the cytoplasm shown by a predominant cytoplasmic staining of NP 12 hpi (Fig. 4, upper lane), all tested concentrations of both, CI-1040 (Fig. 4, middle lane) and ATR-002 (Fig. 4, lower lane) blocked the export of newly synthesized vRNPs as indicated by the prevalent staining of NP in the nuclei.

**Determination of $IC_{50}$ kinase inhibition values for CI-1040 and ATR-002**

The 10-fold higher concentrations of ATR-002 needed to achieve the same antiviral effect as of CI-1040 is striking, given the fact that similar $IC_{50}$ values towards MEK (CI-1040: 17.0 nM; ATR-002: 5.7 nM) were published for these two compounds [22,23]. Therefore, we re-determined the $IC_{50}$ values for CI-1040 and ATR-002 in a cell-free environment, in two different cell lines (A549; Fig. 5C and MDCK; Fig. 4D), and human PBMCs (Fig. 5E).

The $IC_{50}$ of the MEK-Inhibitors CI-1040 and its acid metabolite ATR-002 on the kinase MEK was assessed using purified recombinant active c-Raf DD, GST-MEK1wt and His-ERK2wt in a cell-free reconstitution assay of the Raf/MEK/ERK kinase cascade. Phosphorylation of ERK was measured in an ELISA assay via activation state-specific phospho-ERK antibodies and was used as an indication of the activity of the *in vitro* reconstituted Raf/MEK/ERK kinase cascade. For ATR-002, an $IC_{50}$ value of 30.96 nM was measured while an $IC_{50}$ of 2.51 nM was determined for CI-1040. Both values are in the low nanomolar range, allowing the conclusion that both, CI-1040 and ATR-002 are very potent MEK inhibiting agents. Nevertheless, the fact that ATR-002 shows a roughly 10-fold higher $IC_{50}$ compared to CI-1040 was in disagreement with published data [22,23]. Therefore, we additionally investigated the $IC_{50}$ values of the two compounds in cell-based assays.

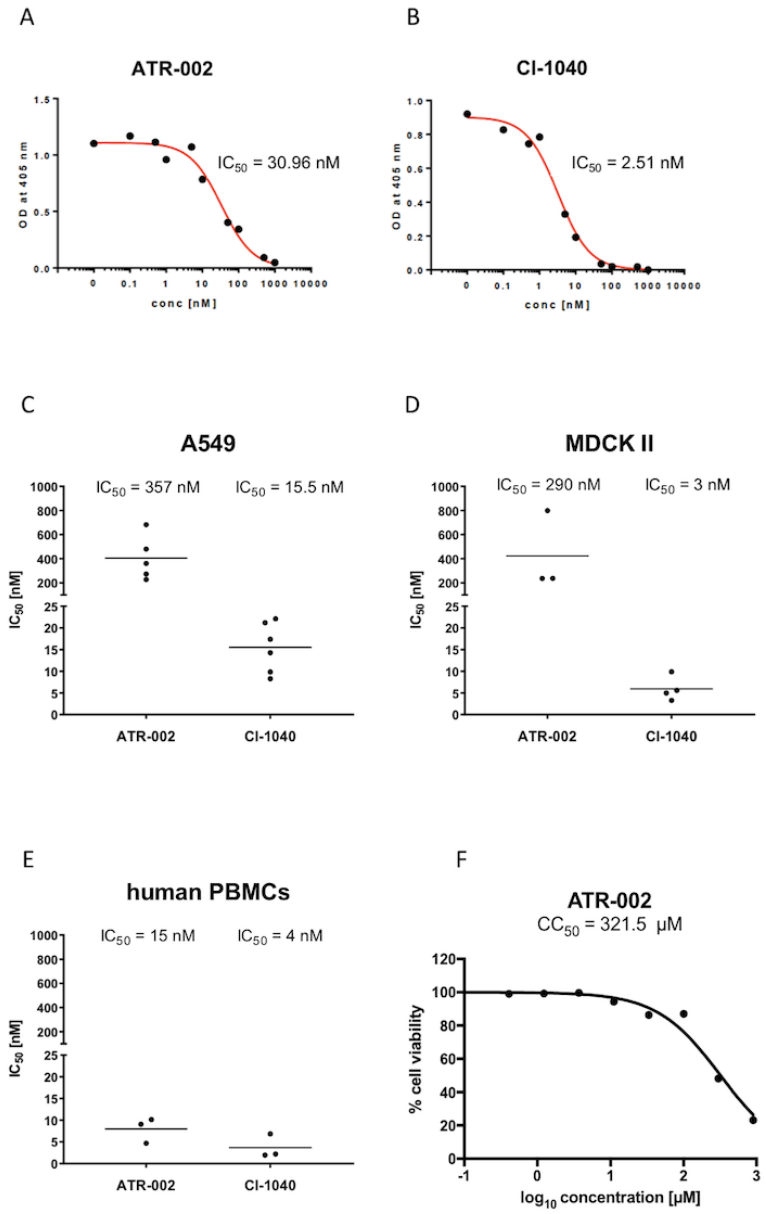


***Figure 5: Determination of $IC_{50}$ values for CI-1040 and ATR-002 in cell-free kinase assay and $IC_{50}$ values for CI-1040 and ATR-002 in A549, MDCK cells, and human PBMCs. (A, B)*** *Cell-free kinase assays. As readout, phosphorylated ERK was measured in an ELISA format as described in Materials and Methods.* ***(C)*** *A549 cells were treated with different concentrations of either CI-1040 or ATR-002 as described in Materials and Methods. Six biological replicates were analyzed. $IC_{50}$ for CI-1040 of MEK derived from A549 cells was 15.5 ± 5 nM. $IC_{50}$ for ATR-002 was 357 ± 198 nM.* ***(D)*** *For the analysis of MDCK cells treatment was identical to A549 cells. Four biological replicates were analyzed. $IC_{50}$ for CI-1040 of MEK derived from MDCK cells was 3.0 ± 1.1 nM. $IC_{50}$ for ATR-002 was 290 ± 168 nM.* ***(E)*** *Analyses of human PBMCs were identical to A549 and MDCK cells. Three biological replicates were analyzed. $IC_{50}$ for CI-1040 of MEK derived from PBMCs was 4.0 ± 0.8 nM. $IC_{50}$ for ATR-002 was 15 ± 1.4 nM.* ***(F)*** *$CC_{50}$ value of ATR-002 on human PBMCs.*

A549 and MDCK cells were used to investigate the $IC_{50}$ values in cellular systems. Both cell lines were treated with different concentrations of either CI-1040 or ATR-002. Western blot analysis was performed, and the level of ERK-phosphorylation was investigated using pERK and ERK-specific antibodies and quantified as described in the Materials and Methods section (Supplementary S1). Quantification was performed by densitometric analysis. As shown in Figure 5C the $IC_{50}$ value of CI-1040 for MEK inhibition in A549 cells was 15.5 nM, while the $IC_{50}$ value of ATR-002 was 23-fold higher at 357 nM (Fig. 5C). The $IC_{50}$ of CI-1040 in MDCK cells was 3 nM and 97-fold lower than the $IC_{50}$ of ATR-002, which was 290 nM (Fig. 5D). While the ATR-002 $IC_{50}$ values are similar in A549 cells and MDCK cells, the $IC_{50}$ value of CI-1040 in MDCK cells is 5-fold lower than in A549 cells. For human PBMCs the $IC_{50}$ value of CI-1040 was determined at 4 nM, while it was 15 nM for ATR-002 (Fig. 5E). Here, we also have provided the $CC_{50}$ value of ATR-002 on human PBMCs (Fig. 5F). Based on the $IC_{50}$ values and the use of the GraphPad Prism software 8, we were able to calculate the $IC_{90}$ values for ATR-002 [A549 (3.213 µM), MDCK (2.610 µM), human PBMCs (0.135 µM)] and for CI-1040 [A549 (0.139 µM), MDCK (0.027 µM), human PBMCs (0.036 µM)]. Altogether, these results demonstrated that ATR-002 is a weaker MEK inhibitor than CI-1040.

**Comparison of ERK-phosphorylation in human PBMCs**

Wes (Simple Western™) uses capillary electrophoresis to identify and quantify a protein of interest and the phosphorylation status of a protein. We have used this method to characterize the phosphorylation/activation status of ERK in human PBMCs. Wes (Simple Western™) detects a chemiluminescence signal in the flow-through and calculates the area under the peak, which is then used for quantification. Figure 6A shows the lane view of the analysis. Detecting a reduced pERK signal demonstrates the inhibitory potential of ATR-002 and CI-1040. The pERK2 intensities were normalized to the loading control (ERK2) by the software. Untreated cells are used as a negative control and PMA/I treated cells show an activated MAPK signaling pathway (positive control). CI-1040 treatment, at a concentration of 10µM, shows almost a complete inhibition of ERK-phosphorylation. A concentration of 100 µM ATR-002, showed the same inhibition of ERK-phosphorylation as 10 µM CI-1040 (Fig. 6A, B) which agrees with our previous data where we show that roughly 10-fold more ATR-002 is needed to inhibit MEK to the same extent as CI-1040.

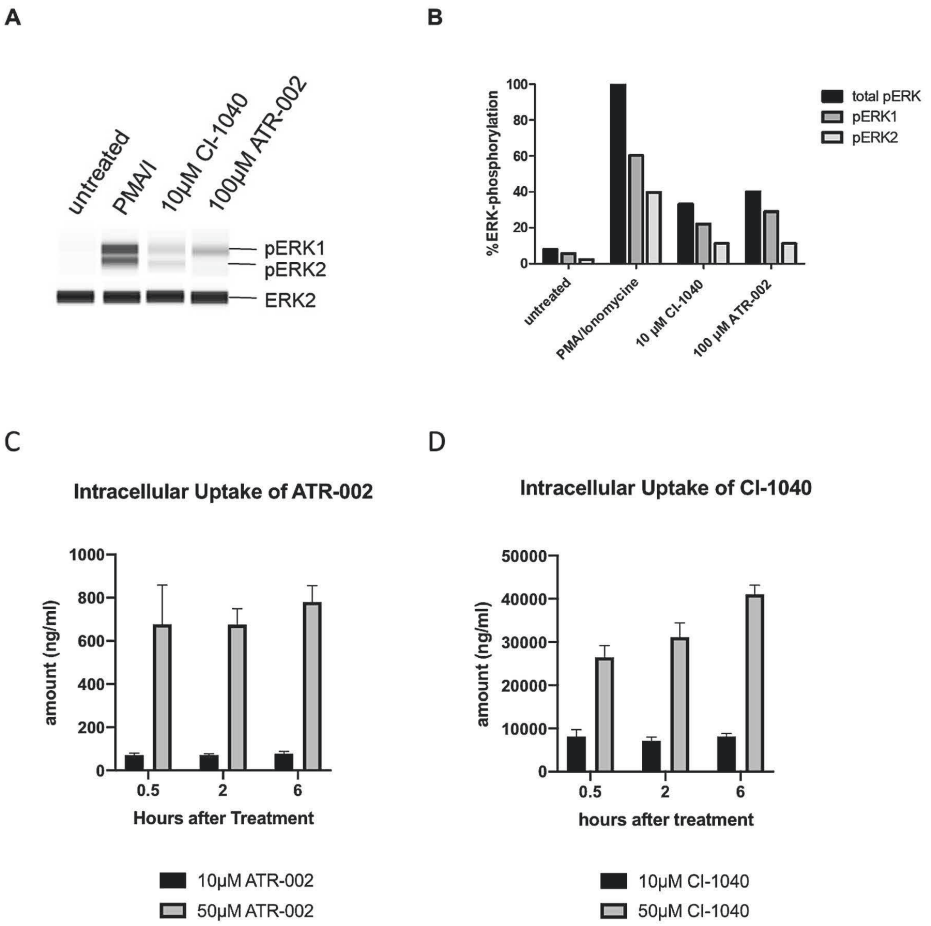


***Figure 6: Comparison of ERK-phosphorylation in human PBMCs and intracellular deposition.*** *Human PBMCs were stimulated with 100 ng/ml PMA and 1 µg/ml Ionomycin (PMA/I) and then treated with 10 µM CI-1040 or 100 µM ATR-002 for 4 hrs. Untreated cells were used as control. The cells were lysed and then analyzed with Wes technology.* ***(A)*** *pERK1/2 and ERK-2 results are shown as gel-like image view.* ***(B)*** *Quantification of MEK inhibition with CI-1040 and ATR-002 and comparison of ERK1 (dark grey area) and ERK2 (light grey area) phosphorylation. pERK1/2 were normalized to ERK2 and PMA/I was set as 100%. In all samples, ERK1 has increased phosphorylation compared to ERK2. Total ERK (dark grey) was set as 100%, ERK1 and ERK2 were then correlated to this value.* ***(C, D)*** *MDCK cells were treated with indicated concentrations of ATR-002 or CI-1040. After extensive washing, cells were harvested, lysed and intracellular deposition was measured using mass spectrometry. 50 to 100-fold more CI-1040 could be detected in MDCKs.*

### Intracellular uptake

To investigate the reason for the reduced activity of ATR-002 compared to CI-1040, the intracellular uptake of either ATR-002 or CI-1040 was determined. MDCK cells were treated with either 10 µM or 50 µM ATR-002 or CI-1040. At different time points after treatment (0.5,

2, 6 hrs) cells were harvested, extensively washed, and prepared for mass-spectrometry analysis as described in the Materials and Methods section. Using a concentration of 10 µM for treatment, an uptake of 73.4 ± 2.6 ng/ml ATR-002 was found (mean of the three time-points). In contrast, 7768.8 ± 492.5 ng/ml of intracellular CI-1040 was detected (mean of the three time-points), which is a 105-fold increase compared to ATR-002 (Fig. 6C, D). By using the 50 µM for treatment, an intracellular increase of CI-1040 over time was found and a mean intracellular amount of 32,872.2 ± 596.7 ng/ml (Fig. 6D, grey bars). For 50 µM ATR-002, a mean intracellular uptake of 710.9 ± 61.7 ng/ml was detected (Fig. 6C, grey bars), a 46-fold decrease compared to CI-1040.

**Comparison of plasma concentrations of ATR-002 vs. CI-1040**

Next, pharmacokinetics and the bioavailability of ATR-002 and CI-1040 were investigated in a mouse model. NMRI mice were treated via the i.v. or oral route with 150mg/kg of either CI-1040 or ATR-002. Blood was collected at different time-points after treatment as indicated in the Materials and Methods section. The amount of either ATR-002 or CI-1040 was determined by mass spectrometry. Pharmacokinetic experiments revealed that after i.v. and oral (Fig. 7A and 7B, respectively) treatment, larger quantities of ATR-002 (AUC values – i.v.: 860.02 µg*h/ml; oral: 1953.68 µg*h/ml) were found in the plasma of mice compared to CI-1040 (AUC values – i.v.: 223.12 µg*h/ml; oral: 156.16 µg*h/ml). Note that at eight hours post i.v. or post oral application of CI-1040 and eight hours post i.v. application of ATR-002, almost no drug was detectable in the plasma. In contrast, after oral application of ATR-002, a large amount of the drug was detected over the whole period, which declined only slightly towards the end of the observation period.

**Reduction of lung virus titers and enhanced survival of CI-1040 and ATR-002-treated mice after lethal H1N1pdm09 infection**

To determine the actual efficacy of both inhibitors *in vivo* we infected C57BL/6 mice with a lethal dose ($3\times10^5$ pfu) of H1N1pdm09. The mice were treated orally either with a total of 8.4, 25, or 75 mg/kg/day (three times a day (TID) 2.8, 8.4 or 25 mg/kg) ATR-002 or with a total of 25, 225 or 450 mg/kg/day (TID 25, 75 or 150 mg/kg) CI-1040. Twenty-four hours later, the mice were sacrificed, the lungs were taken, and the lung virus titer was determined. A significant reduction of virus titer was achieved with a daily dose of 450 mg/kg/day of CI-1040

(*P* = 0.0349; unpaired t-test). In contrast, when mice were treated with ATR-002 a daily dose of either 75 mg/kg/Day (*P* = 0.0159; unpaired t-test) or 25 mg/kg/Day (*P* = 0.0453; unpaired t-test) was sufficient for a significant virus titer reduction (Fig 7C).

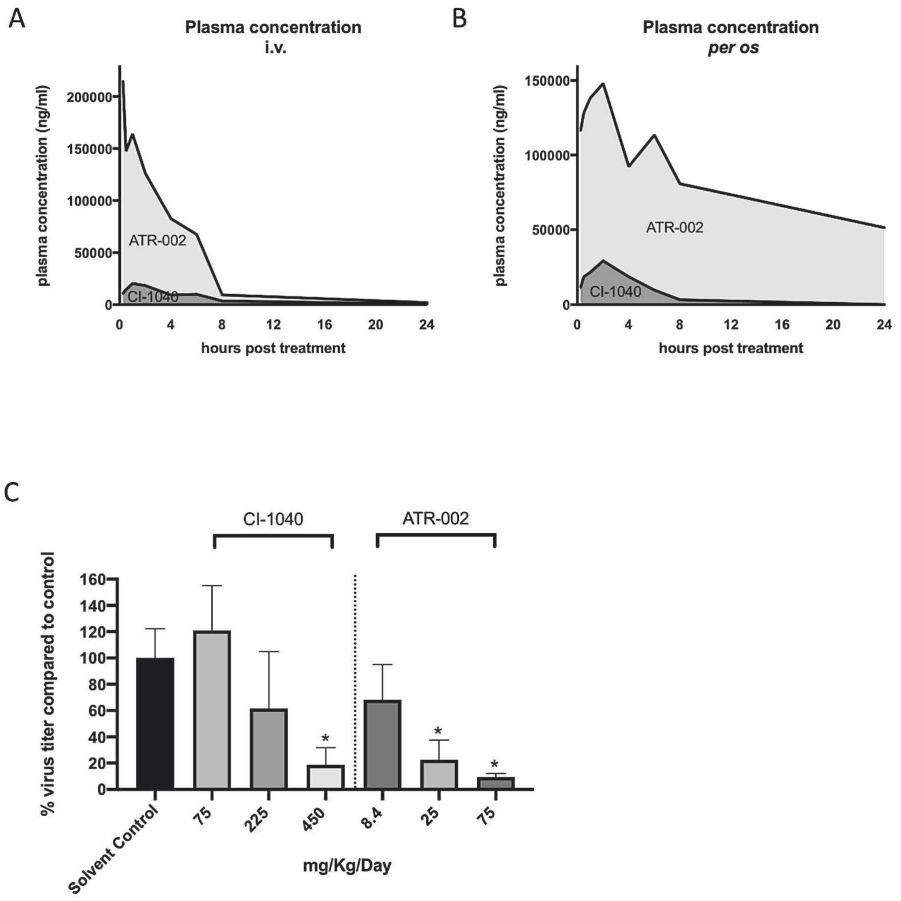


***Figure 7: Comparison of plasma concentration and reduction of virus titer in the lung of mice.*** *Male NMRI mice were either treated with a single dose of either 75 mg/kg CI-1040 (dark grey area) or with 75 mg/kg ATR-002 by the intravenous route* ***(A)*** *or with either 150 mg/kg CI-1040 (dark grey area) or with 150 mg/kg ATR-002 using oral gavage* ***(B)****. Blood was collected at different time-points after administration and plasma was analyzed for the presence of the drug. Each data point represents the mean value of three plasma samples. GraphPad Prism 7 software was used to illustrate both figures.* ***(C)*** *C57BL/6 mice were infected with H1N1pdm09 and treated with different concentrations of either ATR-002 or CI-1040 as indicated. 24 hrs later, mice were sacrificed, lungs were taken, and virus titer was determined. Virus titer from solvent-treated mice was set as 100% and virus titer reduction compared to solvent control was calculated.*

To next investigate the influence of ATR-002 on IAV induced lethality and disease symptoms, when treatment was started at different time points post infection, mice were infected with

H1N1pdm09 and treated twice daily orally (9.00 a.m. and 5.00 p.m.) with 25mg/kg resulting in a total daily dose of 50 mg/kg/day of ATR-002. Treatment started 24, 48 or 72 hrs post infection. All infected mice developed systemic clinical symptoms. None of the animals died spontaneously because of disease symptoms. Most of them had to be sacrificed according to animal protection laws due to bodyweight reduction of >20%. Some of the solvent-treated animals had to be sacrificed because of the development of severe disease symptoms in combination with a reduction of bodyweight. When treatment started at 24 hpi, six out of eight ATR-002-treated mice survived the lethal infection (Fig. 8, blue lines; upper panel).

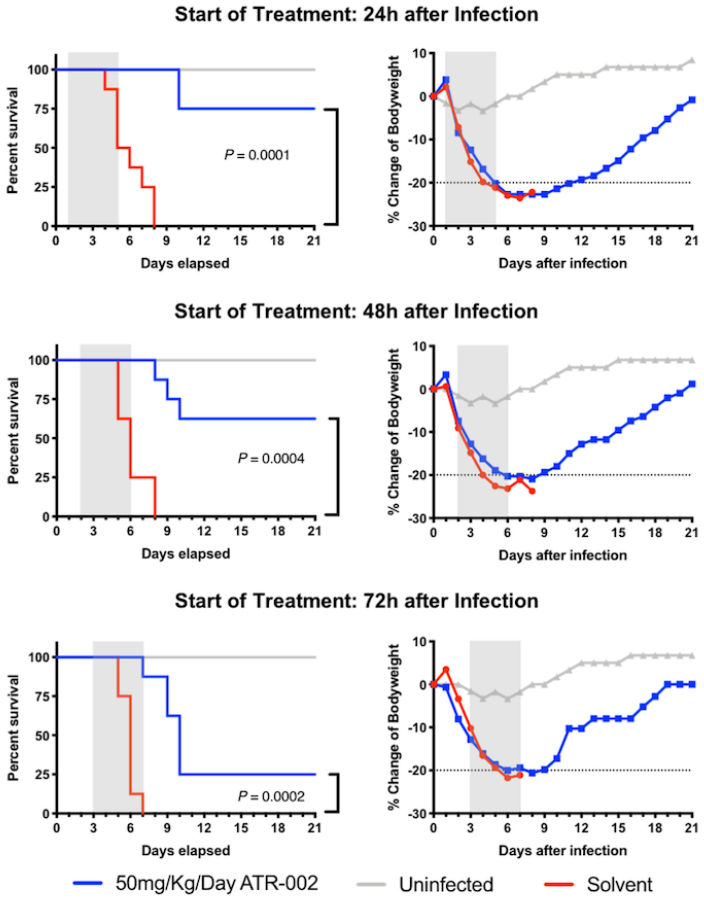


***Figure 8: Survival and bodyweight of IV-infected mice treated with ATR-002.*** *Eight female C57BL/6 mice were infected with H1N1pdm09 infection and treated with 50 mg/kg/day (treated twice daily with 25 mg/kg) ATR-002 (blue line) or with solvent alone (red line) via the oral route. Treatment started at 24, 48 or 72 hpi for five days as indicated in the graphs (grey bar). Mice had to be sacrificed when a bodyweight reduction of 20% was found (grey dotted line). GraphPad Prism 8 software was used to illustrate both figures. P-value was determined using Log-rank (Mantel-Cox) test.*

All animals lost weight and developed mild to moderate disease symptoms. Nevertheless, no disease symptoms were observed 14 days post infection and the mice regained bodyweight until the end of the observation period. The difference in survival compared to solvent-treated control animals was significant [*P* = 0.0001; Log-rank (Mantel-Cox test)]. When treatment started at 48 hpi, three out of eight ATR-002-treated mice (Fig. 8, blue lines; middle panel) survived the lethal infection. Again, all mice lost weight and developed mild to moderate disease symptoms. However, in the surviving animals, no disease symptoms were observed 14 days after infection and the mice regained bodyweight until the end of the observation period. The difference in survival compared to solvent-treated control animals was again significant [*P* = 0.0004; Log-rank (Mantel-Cox test)].

When treatment started 72 hrs after infection, two out of eight ATR-002-treated mice survived the lethal infection (Fig. 8, blue lines; lower panel). All lost weight and developed mild to moderate disease symptoms. Again, the surviving animals showed no disease symptoms and re-gained bodyweight by day 14 after infection. The difference in survival compared to solvent-treated control animals was significant [*P* = 0.0002; Log-rank (Mantel-Cox test)]. Three uninfected mice were treated with 50 mg/kg/day ATR-002 for five days. During treatment, they showed a slight reduction of bodyweight (in all animals less than 5%) (Fig. 8, grey lines). After treatment, they re-gained bodyweight. These results indicate that ATR-002 treatment started as late as 48 hrs after infection still influences disease outcomes in mice infected with a lethal H1N1pdm09 dose.

## Discussion

To date, all licensed influenza drugs and almost all drugs in late-stage clinical development target the virus directly [28-30]. In the past, small molecules have been designed with high specificity against specific viral target proteins, such as the neuraminidase, the viral endonuclease and in a more preliminary stage also against the viral nucleoprotein [30-32]. Even though neuraminidase inhibitors are the standard of care to treat influenza, the strategy of targeting the virus directly has an enormous disadvantage, namely the development of virus variants that are less sensitive or even totally resistant to the respective drug [33-37]. A recent example is Baloxavir, which on one hand demonstrates an impressively fast-acting *in vivo* antiviral activity after only one treatment, but on the other hand, has already led to the

development of resistant virus variants in the course of clinical trial testing [13,38,39]. IV polymerase has no proofreading activity, leading to a high mutation rate and, consequently, to the selection of variants that escape antiviral drugs [40,41]. For this reason, it is hypothesized that whenever a drug targets an IV directly, drug-resistant variants of the virus will inevitably develop.

The solution to this problem would be to develop either a combinational antiviral therapy, similar to the one available against HIV, or target cellular functions that the virus needs in order to ensure its replication. Approaches using host cell-directed targets have already reached the clinical stage. DAS181, a recombinant sialidase fusion protein, cleaves the cellular sialic acids, which are required by influenza virus to attach to the host cell [42]. Nitazoxanide inhibits the trafficking of the HA thus preventing the assembly of viral particles [30]. We have previously shown that IV needs to activate the Raf/MEK/ERK signaling pathway to survive [18]. By inhibiting this pathway, we were able to demonstrate a reduction of virus propagation *in vitro* and *in vivo* [16-18]. Initially, most of our *in vitro* studies were performed with the experimental MEK-inhibitor U0126. While this inhibitor demonstrates excellent MEK-inhibition in cell culture, the bioavailability and stability of this compound *in vivo* is rather weak and the drug does not qualify for further clinical development. Thus, we decided to investigate the MEK inhibitor, CI-1040, for further *in vivo* studies [17]. Unfortunately, the bioavailability for CI-1040 is also not very high [14]. Moreover, during clinical trial testing, data showed that the active metabolite of CI-1040, PD0184264 (ATR-002) is present in similar higher concentrations in the plasma as the parental compound CI-1040 [14]. Therefore, in the present study, we have explored whether ATR-002, similar to CI-1040, would also demonstrate antiviral properties. ATR-002 is the free carboxylate metabolite of CI-1040, lacking the hydroxamic ester part of the parental compound. Based on extensive structure-activity relationships (SAR) findings published for several different MEK inhibitors [43] and the available high-resolution structures of ligand-MEK1/2 complexes [26], it is reasonable to assume that ATR-002 will adopt a binding mode comparable to the vast majority of MEK-inhibitors that are based on the bis-aryl amine chemotype, where Lys-97 might be recognized by the carboxylate moiety of ATR-002. Nevertheless, further investigations need to be performed to finally prove this hypothesis. Interestingly, the kinase exhibits an overall closed conformation similar to the active state of the enzyme, while the activation loop and the helix

C within the N-terminal lobe are significantly rearranged compared to the catalytically competent conformation. Additionally, the highly conserved salt bridge between the sidechains of Gln-114 and Lys-97 is disrupted.

We were able to demonstrate the antiviral activity of ATR-002 against the seasonal IAV (H1N1pdm09; H3N2) and also against IBV, with $EC_{50}$ values that are higher compared to trametinib, a licensed MEK-inhibitor, but this inhibitor showed a very narrow therapeutic index [44]. Interestingly, when compared to the antiviral potential of CI-1040, a comparable reduction of virus titer was only achieved with a 10-fold higher concentration of ATR-002 (100 µM vs. 10 µM; Fig. 3). This was unexpected because similar $IC_{50}$ values for CI-1040 and ATR-002 (PD0184264) were previously published. As Tecle and colleagues mentioned, it is difficult to compare the $IC_{50}$ values because of the different methods used in separate studies [23]. Thus, we have repeated these investigations using a cell-free system (Fig. 5A, B), two different cell lines (Figure 5C, D), and freshly isolated human PBMCs (Fig. 4E). In general, higher $IC_{50}$ values were found in stable cell lines compared to the primary PBMCs. Interestingly, the $IC_{50}$ value for ATR-002 in PBMCs is roughly 2-fold less when compared to the ATR-002 $IC_{50}$ value in the cell-free systems (Fig. 5B). This might support the statement that it is difficult to compare different assays for $IC_{50}$ value determination [23]. In addition, also $IC_{90}$ values were determined, which are in the same range as the $EC_{50}$ value. Regardless of which experimental setup was used, we always found higher $IC_{50}$ values for ATR-002. These findings were also supported by capillary western blot technology (Wes; ProteinSimple®), where we could demonstrate equal inhibition of ERK-phosphorylation, the substrate of MEK, when a 10-fold higher concentration of ATR-002 was used compared to CI-1040. What might be the reason for this apparent difference in $IC_{50}$ values? ATR-002 is a weak acid and these compounds are known to show reduced cell membrane permeability [45]. Thus, we investigated whether this would also be true for ATR-002 by studying the intracellular deposition of ATR-002 in MDCK cells. This cell line represents a very good epithelial model for IAV infection because it is highly polarized and has high transepithelial electrical resistance [46]. When compared to CI-1040, we found a much lower intracellular deposition for ATR-002 (Fig. 6C, D). This may explain the different $IC_{50}$ values for ATR-002 and CI-1040 in cell lines and primary PBMCs, but it does not explain the different $IC_{50}$ values for the two compounds in the cell-free assay (Fig. 5A, B).

Nevertheless, from the modeling (Fig. 2) one might speculate a weaker binding affinity of ATR-002 compared to CI-1040.

At this stage of the project, it was difficult to see an advantage of ATR-002 over CI-1040. However, the fact that ATR-002 was present in higher amounts in the plasma of patients treated with CI-1040 prompted us to compare the pharmacokinetic properties of CI-1040 and ATR-002 in mice. The higher concentration of ATR-002 (Fig. 7B) might be explained because CI-1040 is metabolized into ATR-002, which reduces the amount of the parental compound in the blood. Indeed, we could detect ATR-002 in CI-1040-treated mice. These results support the observations that ATR-002 is a major active metabolite of CI-1040 and available in higher amounts compared to the parent compound [14].

Based on these results, we investigated the antiviral potential of ATR-002 against H1N1pdm09 IV-infected mice. Due to the high plasma levels of ATR-002 in mice, the amount of ATR-002 that needed to be applied to mice to achieve the same titer reduction was 6-fold lower compared to CI-1040. In our view, these results are fully in line with the pharmacokinetic data. Based on the much better bioavailability of ATR-002 a lower concentration is required for *in vivo* treatment compared to CI-1040. We next questioned whether ATR-002 would also be suitable to protect mice against a lethal H1N1pdm09 infection. For CI-1040 we have already shown that treatment up to 48 hpi is sufficient to protect or partially protect mice against lethal IV infection [17]. In this experiment, we started treatment 24, 48 and even 72 hrs after lethal infection and treated the animals for five consecutive days. Since this represented a multiple-dose treatment scheme, we reduced the daily dosage to 50 mg/kg/day. Based on pharmacokinetic data, ATR-002 was still present in the plasma of mice the next day, when treated with 25 mg/kg twice daily. As shown in Figure 8, there is no complete protection, but while all the solvent control animals died, ATR-002 treated animals survived.

In summary, we have demonstrated that ATR-002 has a superior *in viv*o antiviral effect against IV compared to CI-1040. Since treatment of IV-infected mice with oseltamivir starting at 48 hpi is ineffective, ATR-002 is also superior in this effect. A formal toxicology study in rats and dogs was successful (manuscript in preparation). Therefore, the development of ATR-002 as an antiviral was moved to the next stage. A phase I clinical trial is currently underway.

## Acknowledgments

We would like to thank Rebecca Binzberger, Lea Hasen-Palmus, and Magdalena Bauer for their help performing the different $IC_{50}$ assays. This work was supported in part by grants from the Deutsche Forschungsgemeinschaft (Grants Lu477/23-1, SFB1009 B2 and KFO342 to S.L.; SFB 1021 C1 to S.P.), by the German Centre for Infection Research (DZIF), partner site Giessen, Germany (TTU 01.803 Broad-spectrum Antivirals to S.P.). S.L. O.P. and S.P. are members of the German FluResearchNet, a nationwide research network on zoonotic influenza.

## References

[1] Iuliano AD, Roguski KM, Chang HH, Muscatello DJ, Palekar R, Tempia S, Cohen C, Gran JM, Schanzer D, Cowling BJ, Wu P, Kyncl J, Ang LW, Park M, Redlberger-Fritz M, Yu H, Espenhain L, Krishnan A, Emukule G, van Asten L, Pereira da Silva S, Aungkulanon S, Buchholz U, Widdowson MA, Bresee JS and Global Seasonal Influenza-associated Mortality Collaborator N. Estimates of global seasonal influenza-associated respiratory mortality: a modelling study. Lancet. **2018**;391(10127):1285-1300.

[2] Lambert LC and Fauci AS. Influenza vaccines for the future. N Engl J Med. **2010**;363(21):2036-44.

[3] Putri W, Muscatello DJ, Stockwell MS and Newall AT. Economic burden of seasonal influenza in the United States. Vaccine. **2018**;36(27):3960-3966.

[4] Tempia S, Moyes J, Cohen AL, Walaza S, Edoka I, McMorrow ML, Treurnicht FK, Hellferscee O, Wolter N, von Gottberg A, Nguweneza A, McAnerney JM, Dawood H, Variava E and Cohen C. Health and economic burden of influenza-associated illness in South Africa, 2013-2015. Influenza Other Respir Viruses. **2019**(13):484-495.

[5] Nichol KL, Lind A, Margolis KL, Murdoch M, McFadden R, Hauge M, Magnan S and Drake M. The effectiveness of vaccination against influenza in healthy, working adults. N Engl J Med. **1995**;333(14):889-93.

[6] Nichol KL and Treanor JJ. Vaccines for seasonal and pandemic influenza. J Infect Dis. **2006**;194 Suppl 2:S111-8.

[7] Belshe RB, Edwards KM, Vesikari T, Black SV, Walker RE, Hultquist M, Kemble G, Connor EM and Group C-TCES. Live attenuated versus inactivated influenza vaccine in infants and young children. N Engl J Med. **2007**;356(7):685-96.

[8] Radin JM, Hawksworth AW, Myers CA, Ricketts MN, Hansen EA and Brice GT. Influenza vaccine effectiveness: Maintained protection throughout the duration of influenza seasons 2010-2011 through 2013-2014. Vaccine. **2016**;34(33):3907-12.

[9] Kiso M, Mitamura K, Sakai-Tagawa Y, Shiraishi K, Kawakami C, Kimura K, Hayden FG, Sugaya N and Kawaoka Y. Resistant influenza A viruses in children treated with oseltamivir: descriptive study. Lancet. **2004**;364(9436):759-65.

[10] Baranovich T, Saito R, Suzuki Y, Zaraket H, Dapat C, Caperig-Dapat I, Oguma T, Shabana, II, Saito T, Suzuki H and Japanese Influenza Collaborative Study G. Emergence of H274Y oseltamivir-resistant A(H1N1) influenza viruses in Japan during the 2008-2009 season. J Clin Virol. **2010**;47(1):23-8.

[11] Dong G, Peng C, Luo J, Wang C, Han L, Wu B, Ji G and He H. Adamantane-resistant influenza a viruses in the world (1902-2013): frequency and distribution of M2 gene mutations. PloS one. **2015**;10(3):e0119115.

[12] Correia V, Santos LA, Giria M, Almeida-Santos MM and Rebelo-de-Andrade H. Influenza A(H1N1)pdm09 resistance and cross-decreased susceptibility to oseltamivir and zanamivir antiviral drugs. J Med Virol. **2015**;87(1):45-56.

[13] Omoto S, Speranzini V, Hashimoto T, Noshi T, Yamaguchi H, Kawai M, Kawaguchi K, Uehara T, Shishido T, Naito A and Cusack S. Characterization of influenza virus variants induced by treatment with the endonuclease inhibitor baloxavir marboxil. Scientific reports. **2018**;8(1):9633.

[14] Lorusso PM, Adjei AA, Varterasian M, Gadgeel S, Reid J, Mitchell DY, Hanson L, DeLuca P, Bruzek L, Piens J, Asbury P, Van Becelaere K, Herrera R, Sebolt-Leopold J and Meyer MB. Phase I and pharmacodynamic study of the oral MEK inhibitor CI-1040 in patients with advanced malignancies. Journal of clinical oncology : official journal of the American Society of Clinical Oncology. **2005**;23(23):5281-93.

[15] Sebolt-Leopold JS. MEK inhibitors: a therapeutic approach to targeting the Ras-MAP kinase pathway in tumors [Review]. Curr Pharm Des. **2004**;10(16):1907-14.

[16] Droebner K, Pleschka S, Ludwig S and Planz O. Antiviral activity of the MEK-inhibitor U0126 against pandemic H1N1v and highly pathogenic avian influenza virus in vitro and in vivo [Research Support, Non-U.S. Gov't]. Antiviral Res. **2011**;92(2):195-203.

[17] Haasbach E, Muller C, Ehrhardt C, Schreiber A, Pleschka S, Ludwig S and Planz O. The MEK-inhibitor CI-1040 displays a broad anti-influenza virus activity in vitro and provides a prolonged treatment window compared to standard of care in vivo. Antiviral research. **2017**;142:178-184.

[18] Pleschka S, Wolff T, Ehrhardt C, Hobom G, Planz O, Rapp UR and Ludwig S. Influenza virus propagation is impaired by inhibition of the Raf/MEK/ERK signalling cascade [Research Support, Non-U.S. Gov't]. Nat Cell Biol. **2001**;3(3):301-5.

[19] Planz O. Development of cellular signaling pathway inhibitors as new antivirals against influenza. Antiviral Res. **2013**;98(3):457-68.

[20] Ludwig S, Pleschka S, Planz O and Wolff T. Ringing the alarm bells: signalling and apoptosis in influenza virus infected cells. Cellular microbiology. **2006**;8(3):375-86.

[21] Olschlager V, Pleschka S, Fischer T, Rziha HJ, Wurzer W, Stitz L, Rapp UR, Ludwig S and Planz O. Lung-specific expression of active Raf kinase results in increased mortality of influenza A virus-infected mice [Research Support, Non-U.S. Gov't]. Oncogene. **2004**;23(39):6639-46.

[22] Sebolt-Leopold JS, Dudley DT, Herrera R, Van Becelaere K, Wiland A, Gowan RC, Tecle H, Barrett SD, Bridges A, Przybranowski S, Leopold WR and Saltiel AR. Blockade of the MAP kinase pathway suppresses growth of colon tumors in vivo. Nature medicine. **1999**;5(7):810-6.

[23] Tecle H, Shao JX, Li YH, Kothe M, Kazmirski S, Penzotti J, Ding YH, Ohren J, Moshinsky D, Coli R, Jhawar N, Bora E, Jacques-O'Hagan S and Wua J. Beyond the MEK-pocket: Can current MEK kinase inhibitors be utilized to synthesize novel type III NCKIs? Does the MEK-pocket exist in kinases other than MEK? Bioorg Med Chem Lett. **2009**;19(1):226-229.

[24] Haasbach E, Pauli EK, Spranger R, Mitzner D, Schubert U, Kircheis R and Planz O. Antiviral activity of the proteasome inhibitor VL-01 against influenza A viruses [Research Support, Non-U.S. Gov't]. Antiviral Res. **2011**;91(3):304-13.

[25] Matrosovich M, Matrosovich T, Garten W and Klenk HD. New low-viscosity overlay medium for viral plaque assays [Research Support, Non-U.S. Gov't]. Virol J. **2006**;3:63.

[26] Ohren JF, Chen H, Pavlovsky A, Whitehead C, Zhang E, Kuffa P, Yan C, McConnell P, Spessard C, Banotai C, Mueller WT, Delaney A, Omer C, Sebolt-Leopold J, Dudley DT, Leung IK, Flamme C, Warmus J, Kaufman M, Barrett S, Tecle H and Hasemann CA. Structures of human MAP kinase kinase 1 (MEK1) and MEK2 describe novel noncompetitive kinase inhibition. Nat Struct Mol Biol. **2004**;11(12):1192-7.

[27] Ludwig S, Wolff T, Ehrhardt C, Wurzer WJ, Reinhardt J, Planz O and Pleschka S. MEK inhibition impairs influenza B virus propagation without emergence of resistant variants [Research Support, Non-U.S. Gov't]. FEBS Lett. **2004**;561(1-3):37-43.

[28] McKimm-Breschkin JL, Jiang SB, Hui DS, Beigel JH, Govorkova EA and Lee N. Prevention and treatment of respiratory viral infections: Presentations on antivirals, traditional therapies and host-directed interventions at the 5th ISIRV Antiviral Group conference. Antiviral Res. **2018**;149:118-142.

[29] Mifsud EJ, Hayden FG and Hurt AC. Antivirals targeting the polymerase complex of influenza viruses. Antiviral Res. **2019**;169:104545.

[30] Koszalka P, Tilmanis D and Hurt AC. Influenza antivirals currently in late-phase clinical trial. Influenza Other Respir Viruses. **2017**;11(3):240-246.

[31] Kao RY, Yang D, Lau LS, Tsui WH, Hu L, Dai J, Chan MP, Chan CM, Wang P, Zheng BJ, Sun J, Huang JD, Madar J, Chen G, Chen H, Guan Y and Yuen KY. Identification of influenza A nucleoprotein as an antiviral target. Nature biotechnology. **2010**;28(6):600-5.

[32] Ison MG. Clinical use of approved influenza antivirals: therapy and prophylaxis. Influenza Other Respir Viruses. **2013**;7 Suppl 1:7-13.

[33] van der Vries E, Schutten M, Fraaij P, Boucher C and Osterhaus A. Influenza virus resistance to antiviral therapy. Adv Pharmacol. **2013**;67:217-46.

[34] Lina B, Boucher C, Osterhaus A, Monto AS, Schutten M, Whitley RJ and Nguyen-Van-Tam JS. Five years of monitoring for the emergence of oseltamivir resistance in patients with influenza A infections in the Influenza Resistance Information Study. Influenza Other Respir Viruses. **2018**;12(2):267-278.

[35] de Jong MD, Tran TT, Truong HK, Vo MH, Smith GJ, Nguyen VC, Bach VC, Phan TQ, Do QH, Guan Y, Peiris JS, Tran TH and Farrar J. Oseltamivir resistance during treatment of influenza A (H5N1) infection. N Engl J Med. **2005**;353(25):2667-72.

[36] Cheng PK, Leung TW, Ho EC, Leung PC, Ng AY, Lai MY and Lim WW. Oseltamivir- and amantadine-resistant influenza viruses A (H1N1). Emerg Infect Dis. **2009**;15(6):966-8.

[37] Goldhill DH, Te Velthuis AJW, Fletcher RA, Langat P, Zambon M, Lackenby A and Barclay WS. The mechanism of resistance to favipiravir in influenza. Proceedings of the National Academy of Sciences of the United States of America. **2018**;115(45):11613-11618.

[38] Gubareva LV, Mishin VP, Patel MC, Chesnokov A, Nguyen HT, De La Cruz J, Spencer S, Campbell AP, Sinner M, Reid H, Garten R, Katz JM, Fry AM, Barnes J and Wentworth DE. Assessing baloxavir susceptibility of influenza viruses circulating in the United States during the 2016/17 and 2017/18 seasons. Euro Surveill. **2019**;24(3):1-5.

[39] Yang T. Baloxavir Marboxil: The First Cap-Dependent Endonuclease Inhibitor for the Treatment of Influenza. Ann Pharmacother. **2019**;53(7):754-759.

[40] Boivin S, Cusack S, Ruigrok RW and Hart DJ. Influenza A virus polymerase: structural insights into replication and host adaptation mechanisms. J Biol Chem. **2010**;285(37):28411-7.

[41] Drake JW. Rates of spontaneous mutation among RNA viruses. Proc Natl Acad Sci U S A. **1993**;90(9):4171-5.

[42] Behzadi MA and Leyva-Grado VH. Overview of Current Therapeutics and Novel Candidates Against Influenza, Respiratory Syncytial Virus, and Middle East Respiratory Syndrome Coronavirus Infections. Front Microbiol. **2019**;10:1327.

[43] Cheng Y and Tian H. Current Development Status of MEK Inhibitors. Molecules. **2017**;22(10):1-20.

[44] Schrader T, Dudek SE, Schreiber A, Ehrhardt C, Planz O and Ludwig S. The clinically approved MEK inhibitor Trametinib efficiently blocks influenza A virus propagation and cytokine expression. Antiviral research. **2018**;157:80-92.

[45] Saparov SM, Antonenko YN and Pohl P. A new model of weak acid permeation through membranes revisited: does Overton still rule? Biophys J. **2006**;90(11):L86-8.

[46] von Bonsdorff CH, Fuller SD and Simons K. Apical and basolateral endocytosis in Madin-Darby canine kidney (MDCK) cells grown on nitrocellulose filters. Embo J. **1985**;4(11):2781-92.

## Supplementary materials

**Determination of IC50 values for CI-1040 and ATR-002**

**Cell free kinase assay**

A 96-well microtiter plate was coated overnight with the monoclonal anti-ERK (extracellular signal-regulated kinase) antibody (Cell Signaling Technologies) in a dilution 1:1000 (100 µl/well) in TBST (50 mM Tris-HCl, 0.9% NaCl, 0.05% Tween 20). After washing (3 × 5 min) with 100 µl/well TBST, wells were blocked with 100 µl/well of 1% BSA in PBS for 60 min at RT. Prior to the addition of the kinase reaction sample (see below), the plates were washed again. To determine the $IC_{50}$ value of the inhibitors, the final test concentrations (1 µM, 500 nM, 100 nM, 50 nM, 10 nM, 5 nM, 1 nM, 0.5 nM, and 0.1 nM in DMSO) were prepared. Active GST c-Raf1-DD was expressed in Baculovirus-infected SF9 cells, while GST-MEK1 and His-ERK2 were expressed in *Escherichia coli.* GST-tagged proteins were purified via binding to glutathione sepharose beads and His-tagged ERK2 was purified on a Ni-chelate column. The three purified recombinant kinases were mixed in a 3:2:3 ratio in kinase buffer (10 mM $MgCl_2$, 25 mM beta-glycerophosphate, 25 mM HEPES; pH 7.5, 5 mM benzamidine, 0.5 mM dithiothreitol, 1 mM sodium vanadate) and DMSO/inhibitor and was pre-incubated in a dark at RT followed by the addition of 10 mM ATP and further incubation for 30 min. To stop the kinase reaction, a 20% SDS solution was added for 10 min at 50°C and further diluted with blocking buffer (1% BSA in TBST). Next, 100 µl of each sample was added to the anti-ERK coated 96-well microtiter plate. The kinase reaction samples were incubated for 60 min at RT in the anti-ERK coated 96-well microtiter plate blocked with BSA. For the detection of phosphorylated ERK, the samples were incubated overnight at 4°C with an anti-phospho ERK (p44/p42) antibody followed by Horseradish Peroxidase anti-mouse IgG specific antibody diluted in TBST buffer for 60 min at RT. Afterward, the plate was washed and incubated for 30 min with ABTS substrate solution (Roche, Mannheim, Germany). The reaction was terminated with a 20% SDS solution followed by measurement of the Optical Density at 405 nm with an ELISA reader.

**Kinase assays in A549, MDCK cells and human PBMCs**

A549 and MDCK II cells were cultured in IMDM (Sigma Aldrich, St. Louis, Missouri, US) containing 10% FBS (Thermo Fisher Scientific, Waltham, Massachusetts, U.S.A.), 100U/mL Penicillin, 100 µl/mL Streptomycin and 1% L-Glutamine (Lonza, Basel, Switzerland). Next,

$4\times10^5$ A549 or MDCK II cells were seeded in a 24-well plate overnight and then starved for 24 hrs in IMDM containing 0% FBS (Sigma Aldrich, St. Louis, Missouri, U.S.A.). After starvation, the cells were stimulated with 20 ng/ml tumor necrosis factor $\alpha$ (TNF-$\alpha$, Sigma Aldrich, St. Louis, Missouri, U.S.A.) for 30 minutes and then treated with different concentrations of either CI-1040 or ATR-002 (ChemCon, Freiburg, Germany) dissolved in DMSO, for 1 h. To determine the $IC_{50}$ value for CI-1040 and ATR-002 on MDCK II cells, 12 test concentrations in two-fold dilution steps were used (CI-1040: 6.25 µM, to 3 nM; ATR-002: 25 µM to 12 nM. To determine the $IC_{50}$ value for CI-1040 and ATR-002 on A549 cells, 12 test concentrations in two-fold dilution steps were prepared (CI-1040: 3.07 µM to 1.5 nM; ATR-002: 30.72 µM to 15 nM). Treatments were stopped immediately after the incubation time by washing the cells twice with ice-cold PBS. Cells were lysed on ice in ice-cold modified-RIPA buffer (50 mM Tris-HCl, pH 7.4; 1% NP-40; 0.25% sodium deoxycholate; 150 mM NaCl) supplemented with Complete Protease Inhibitor Cocktails (Roche Diagnostics) and Phosphatase Inhibitor Cocktails (Roche Diagnostics, Mannheim, Germany). The lysates were sonicated briefly and centrifuged at 18,000 × g for 5 minutes at 4°C.

Human peripheral blood mononuclear cells (PBMCs) were isolated from fresh blood by Ficoll density gradient separation and then cultured in RPMI 1640-medium (Thermo Fisher Scientific, Waltham, Massachusetts, U.S.A.) containing 10% autologous serum, 100 U/mL Penicillin, 100 µg/mL Streptomycin and 1% L-Glutamine (Lonza, Basel, Switzerland). Then $5x10^6$ of the cultured PBMCs were seeded in a 24-well plate and stimulated with 100 ng/mL Phorbol 12-myristate 13-acetate (PMA) and 1 µg/mL ionomycin (I) (Sigma Aldrich, St. Louis, Missouri, U.S.A.) for 4 hrs. To determine the $IC_{50}$ value for CI-1040 and ATR-002 on human PBMCs, 12 test concentrations in two-fold dilution steps were prepared (CI-1040: 200 nM to 0.097 nM; ATR-002: 780 nM to 0.38 nM). Treatments were stopped and the procedure was continued as described for A549/MDCK cells. All samples were kept for western blot analysis.

# Chapter 2

# Improved *in vitro* Efficacy of Baloxavir Marboxil Against Influenza A Virus Infection by Combination Treatment with the MEK Inhibitor ATR-002

Hazem Hamza[1, 2], Mahmoud M. Shehata[2, 3], Ahmed Mostafa[2, 3, 4], Stephan Pleschka[4, 5* §], Oliver Planz[1* §]

[1] Department of Immunology, Institute for Cell Biology, Eberhard Karls University of Tübingen, Tübingen, Germany

[2] Virology Laboratory, Environmental Research Division, National Research Centre, Giza, Egypt

[3] Center of Scientific Excellence for Influenza Viruses, National Research Centre, Giza, Egypt

[4] Institute of Medical Virology, Justus Liebig University Giessen, Giessen, Germany

[5] German Center for Infection Research (DZIF), Partner Site Giessen, Giessen, Germany

* Corresponding authors

§ These authors contributed equally to this work.

***Front Microbiol. 2021 Feb 12; (12):611958 PMID: 33679636 DOI: 10.3389/fmicb.2021.611958***

## *Disclosure of authorship contribution*

HH performed all experimental drug testing and cytotoxicity experiments and analyzed the respective data. MMS and AM conducted the recombinant virus experiments. HH performed drug combination treatment experiments and analyzed the respective data. HH and MMS analyzed the data. HH carried out the data visualization and drafted the manuscript. Further information is provided in the "Author Contribution" section at the end of this chapter/manuscript.

## Abstract

Currently, all available antiviral drugs against influenza virus (IV) that target the virus proteins directly, like Baloxavir acid (BXA), lead to viral resistance. Therefore, cellular mechanisms and factors essential for IV replication are promising antiviral targets. As IV strongly depends on the virus-induced Raf/MEK/ERK signal pathway for efficient generation of infectious progeny virions, this pathway represents an important target. We aimed to determine whether the MEK inhibitor ATR-002 (PD0184264) can impair the replication of BXA-resistant influenza A viruses (IAV) and whether a treatment combining BXA and ATR-002 improves the therapeutic efficiency in vitro. A549 cells infected with different IAV strains including BXA-resistant variants were treated with ATR-002 or BXA and the effect on virus titer reduction was determined. The synergistic effect of ATR-002 and BXA was also analyzed using different evaluation methods. The data demonstrated that ATR-002 has a significant and dose-dependent inhibitory effect on IAV replication across different strains and subtypes. IAV with the PA-I38T mutation shows resistance against BXA but is still susceptible to ATR-002. The combination of ATR-002 and BXA exhibited a synergistic potency reflected by low combination index values. In conclusion, we show that ATR-002 permits to counteract the limitations of BXA against BXA-resistant IAV. Moreover, the results support the use of ATR-002 (i) in a monotherapy, as well as (ii) in a combined approach together with BXA. These findings might also apply to the treatment of infections with IAV, resistant to other direct-acting antiviral compounds.


## Introduction

Influenza virus (IV) drug resistance represents a significant health threat. The hetero-trimeric RNA-dependent RNA polymerase (RdRp) complex of IV is comprised of three subunits: PB2, PB1, and PA, each with specific functions [1,2]. The PA subunit contains the endonuclease that cleaves the CAP structure (cap-snatching) from cellular mRNAs, which is then used by the RdRp to generate capped primers for viral mRNA synthesis [3-5]. Together with the viral RNA (vRNA) and the nucleocapsid protein (NP), the RdRp forms the biologically active viral ribonucleoprotein complex (vRNP), which transcribes and replicates the viral genome within the nucleus of the infected cell. The virus can escape selective pressures as the RdRp lacks a proofreading function. Accumulating point mutations constantly alter the genome sequence,

allowing the virus to generate a multitude of genetic and antigenic variants. Furthermore, the segmented genome permits the exchange of vRNA segments between different viruses upon co-infection, leading to new viruses with altered characteristics [6].

Currently, three classes of FDA-approved antiviral drugs are worldwide available, M2 channel ion blockers (Adamantanes), neuraminidase inhibitors (NAIs), and polymerase inhibitors. Due to the widespread resistance of circulating viruses, adamantanes are not recommended presently for clinical use and NAIs are the only effective antivirals used in most countries. However, the global circulation of NAIs-resistant IV variants remains a threat [7,8]. Several new antiviral drugs that target RdRp functions are in clinical development; these include Pimodivir®, a PB2 inhibitor [9], and Favipiravir®, a PB1 inhibitor [10]. Recently, the cap-dependent endonuclease inhibitor Baloxavir acid (BXA) has been licensed in Japan and the USA for the treatment of uncomplicated influenza and high-risk patients [11-13]. Unfortunately, already during clinical trials, BXA-resistant variants were detected in the post-treatment monitoring. The PA-I38T substitution strongly reduced PA susceptibility to BXA [13-15]. Even though these mutants showed impaired replicative fitness, other studies have well demonstrated that endonuclease-resistant variants with only modest effects on viral fitness can emerge *in vitro* and *in vivo* [16].

However, all IVs also depend on essential host factors including cellular signaling cascades. Importantly, these are not virus-encoded and are therefore not prone to mutations caused by the RdRp. Therefore, such essential host factors are promising antiviral targets. Several studies demonstrate that blocking specific signaling pathways not only reduced viral titers but also led to immunomodulation regulating an uncontrolled host response without the occurrence of viral resistance [17-20]. The mitogen-activated protein kinase (MAPK) cascade is closely associated with cell proliferation and its inhibition is a cornerstone in different cancer therapies [21-23]. Upon infection, the virus induces the activation of the Raf/MEK/ERK signaling pathway, which is pivotal for efficient influenza A virus (IAV) replication leading to enhanced RdRp activity [24] and temporal/spatial coordination of the nuclear vRNP export essential for efficient production of infectious progeny virions [25]. Therefore, blockade of this pathway by specific MEK-inhibitors leads to nuclear vRNP retention [26,27] and different MEK-inhibitors, which are already approved for cancer treatment (Trametinib®) or used earlier in clinical trials (CI-1040), have shown a high anti-IV activity [28,29]. However, despite the

antiviral activity of CI-1040, phase I and pharmacodynamics studies reported that the CI-1040 plasma concentrations are increased in less than a proportional manner and appear to plateau even when administrated at high doses. Yet, it was observed that the active metabolite ATR-002 (PD0184264) was present in the plasma at higher concentrations than the parent compound [22]. However, the pharmaceutical development of ATR-002 was not further promoted as an antitumor agent [30,31]. Nevertheless, we previously explored the antiviral potential of ATR-002 compared to CI-1040 and could demonstrate the *in vivo* superiority of ATR-002 over CI-1040 as an antiviral compound, despite its weaker membrane permeability [32].

In addition to monotherapies, combinatorial therapies with drugs that either have similar or different activities, targeting various viral proteins or host factors, might further reduce the emergence of drug-resistant strains [33,34]. Therefore, not only the simultaneous application of two drugs, both *in vivo* and *in vitro* [35-37], but also triple combinations have been investigated [38,39].

Given the frequency of viral resistance to BXA, we here evaluated the anti-IAV potential of the MEK inhibitor ATR-002 compared to BXA against wild-type and BXA-resistant strains. In terms of improved therapeutic efficacy, treatment applying ATR-002 together with BXA was also conducted to investigate whether the combined agents would reduce the replication of different IAV synergistically, additively, or antagonistically.

## *Materials and methods*

### Drugs

ATR-002 (PD0184264) [2-(2-chloro-4-iodophenylamino)-N-3,4-difluoro benzoic acid], the active metabolite of CI-1040, was synthesized at ChemCon GmbH (Freiburg, Germany). Baloxavir acid (BXA) was purchased from Hycultec GmbH (Cat: HY-109025) and prepared at a stock concentration of 1 mM according to the manufacturer's instructions.

### Cells and viruses

Human lung adenocarcinoma cells (A549, ATCC® CCL185™) and Madin-Darby canine kidney cells (MDCK II, ATCC® CRL2936™) were cultured in IMDM medium. Human embryonic kidney cells expressing the SV40 large T-antigen (HEK 293T, ATCC® CRL-3216™) were maintained in

DMEM Medium. Following wild type IAV strains were used: A/Mississippi/3/2001 (H1N1), A/Perth/265/2009 (H1N1pdm09), A/Puerto Rico/8/34 (H1N1), and A/Victoria/03/75 (H3N2).

**Generation of recombinant viruses**

Two recombinant wild-type IAV rgA/Giessen/6/2009 (H1N1-WT) and rgA/Victoria/3/75 (H3N2-WT) and their variants rgA/Giessen/6/2009 (H1N1-PA-I38T), rgA/Victoria/3/75 (H3N2-PA-I38T) harboring the BXA-resistance mutation PA-I38T were generated using a reverse genetic system as previously described by [40]. Briefly, a complete set of pMP plasmids encoding the eight viral segments of A/Giessen/6/2009 (H1N1) and A/Victoria/3/75 (H3N2) were constructed. Relevant primer pairs (**Table 1**, **supplementary materials**) were used for site-directed mutagenesis to introduce PA segment I38T mutation into the pMP-PA-Gi/-Vic plasmid. PA I38T mutation in pMP-PA-Gi /-Vic and absence of PCR introduced errors in purified plasmid DNA was confirmed by sequencing using gene-specific primers and vector-specific primers (**Table 2**, **supplementary materials**).

**Rescue of recombinant viruses**

Rescue was performed as previously described [40]. Briefly, the complete set of eight vectors encoding the vRNA of wild type and variant rgA/Victoria/3/75 (rgH3N2-WT, rgH3N2-PA-I38T) and rgA/Giessen/6/2009 (rgH1N1-WT, rgH1N1-PA-I38T) were co-transfected into a co-culture of 293T/MDCK-II cells. At 72 h post transfection, a 500 µl aliquot of each supernatant was used to inoculate MDCK-II cells, which were then incubated for 72 h in the presence of 2 µg/ml TPCK-treated trypsin. Rescued viruses from these cells were stored at −80 °C. After viral RNA extraction, RT-PCR targeting the full PA segment was performed for each recombinant virus. The amplified PA segments were purified and subject to sequencing using specific primers (**Table 3**, **supplementary materials**).

***In vitro* replication kinetics of recombinant viruses**

Confluent MDCK-II monolayers were infected in triplicate with each of the recombinant viruses (MOI: 0.001). After 1 h incubation at 37 °C, the inocula were removed, cell monolayers washed with $PBS^{++}$, and overlaid with infection media (1X DMEM supplemented with Penicillin/Streptomycin (P/S), 0.3% BSA, and 2 µg/ml TPCK-treated trypsin). Aliquots, 200 µl each, of supernatant were collected at 6, 24 and 48 hours post infection (hpi). The virus titer was subsequently determined via focus assay [41,42].

**Virus yield reduction (VYR) assay**

IAV susceptibility to either ATR-002 or BXA was determined by measuring the titer reduction in the presence of the drugs. Different concentrations of each drug were prepared in DMEM infection media. Confluent monolayers of A549 cells in 24-well plates were infected in triplicates with A/Mississippi/3/2001 (H1N1), A/Perth/265/2009 (H1N1pdm09), A/Puerto Rico/8/34 (H1N1), or A/Victoria/03/75 (H3N2) at an MOI of 0.005, 0.005, 0.001 and 0.001, respectively. After 1h incubation, the inocula were removed, the infection media containing both drugs combinations were added and subjected to focus assay after 24 hpi.

**Virus titration (Focus Assay)**

Virus titers were determined using focus assay as described earlier [41,42]. Briefly, MDCK II cells were seeded in 96-well plates and incubated overnight. MDCK II plates were washed with PBS and infected in triplicates with virus-containing supernatants in a 10-fold dilution in PBS/BA (PBS++ containing 0.3% BSA, P/S). After 1 hpi, the inocula were removed and the Avicel® overlay was added to each well. At 24 hpi, the cells were fixed and permeabilized with PBS containing 4% paraformaldehyde and 1% triton-X 100. Afterward, cells were immunostained with mouse anti-IAV nucleoprotein monoclonal antibody (Bio-Rad) followed by goat anti-mouse IgG-HRP (Jackson ImmunoResearch Laboratories). After extensive washing, True Blue™ peroxidase substrate (SeraCare, USA) was added to detect foci and the stained plates were scanned and analyzed. The virus titers in the focus-forming unit (FFU/ml) were calculated by multiplying the average FFU for each treatment, the dilution factor, and by the inoculum volume normalization factor. The reduction in virus titers was expressed as (%) by dividing the average FFU for each treatment by the average FFU of the infected non-drug-treated control.

**Analysis of synergy/antagonism from combination studies**

Different concentrations (0.4 – 50 μM) of ATR-002 and (0.008 – 1 nM) BXA were prepared by making 5-fold serial dilution in infection media. Combinations between both drugs were tested in a 4 × 4 matrix and all values normalized to Mock-infected control (DMSO). A549 cells were infected with A/Puerto Rico/8/34 (MOI: 0.001). After incubation, the inocula were removed, the confluent monolayers were supplemented with DMEM infection medium containing the tested inhibitor combinations and subjected to focus assay after 24 hpi.

To determine the possible additive and synergistic effects when using combinations of ATR-002 with BXA, the data from VYR assay were analyzed according to the Chou–Talalay model[43,44] using CompuSyn software[45]. The software calculates the combination index (CI) for each drug combination, where a CI value < 1 indicates synergy, CI=1 is additive and CI > 1 indicates antagonism. The data were also analyzed using the Combenefit software [46] which simultaneously assesses synergy/antagonism based on the assumption of non-interaction using three published models (Highest single agent (HSA), Bliss, and Loewe). Dose-response curves were also included for each drug to generate a dose-response surface for the reference models, from which the experimental surface and modelled surface were then compared. At each combination, deviations in the experimental surface from the modelled surface were attributed to a percentage score indicating the degree of either synergy (increased effect) or antagonism (decreased effect). The "Contour" and "surface" plots were selected as graphical outputs for the synergy distribution.

**Cytotoxicity of drug combinations (WST-1 assay)**

The cytotoxic effect of the drug combinations was monitored by the colorimetric WST-1 assay according to the manufacturer's instructions (Roche Diagnostic, Mannheim, Germany). Briefly, A549 cells were seeded in 96-well plates and incubated for 24 h at 37 °C. Thereafter, the cells were treated with ATR-002 and BXA combinations at the indicated concentrations. The cells were further incubated for 24 h followed by the addition of WST-1 reagent. The quantification of the formazan dye produced by metabolically active cells was measured using a scanning multi-well spectrophotometer at 450 nm and 650 nm for the reference wavelength after 4 h incubation.

**Statistical analysis**

Statistical analysis was performed using GraphPad Prism ver. 6 software. Data from three independent experiments are presented as the mean ± standard error (SEM). Dose-response as well as nonlinear regression analysis for $EC_{50}$ were calculated. Statistical differences were determined using unpaired *t*-test with Welch's correction. *P* values of ≤ 0.05 were considered statistically significant.

## Results

**Antiviral activity of ATR-002 against different IAV strains and subtypes**

To explore the antiviral potential of ATR-002 we determined virus titer reduction of different IAV strains and subtypes in the presence of defined ATR-002 concentrations (1, 10, 50, 100 µM), which are below the cytotoxic concentration 50% ($CC_{50}$) for ATR-002 on A549 cells (271.8 µM)[32]. At 100 µM ATR-002, we could not detect progeny virions of all investigated IAV strains (**Figure 1 A-D**) and 50 µM ATR-002 still significantly (P > 0.0001) reduced the titer of the three H1N1-type IAV strains tested by 97.11 ± 0.72 % for A/Mississippi/3/2001 (H1N1), 82 ± 1.49 % for A/Perth/265/2009 (H1N1pdm09), and 85.5 ± 3.04 % for A/Puerto Rico/8/34 (H1N1) **(Figure 1 A-C**). A quite similar titer reduction by 76.4 ± 2.04 % was observed for the H3N2-type A/Victoria/03/75 (H3N2) (**Figure 1D**). At 10 µM ATR-002 is also still able to reduce the titer by 71.81 ± 3.49, 61.14 ± 6.7, 63.21 ± 2.96 % for the tested H1N1 strains respectively and by 64.29 ± 4.24 % for an H3N2-type IAV. In contrast, 1 µM ATR-002 was insufficient to affect the titers of all examined strains significantly. Collectively, we demonstrate that ATR-002 has the capacity to block IAV replication across different strains and subtypes.

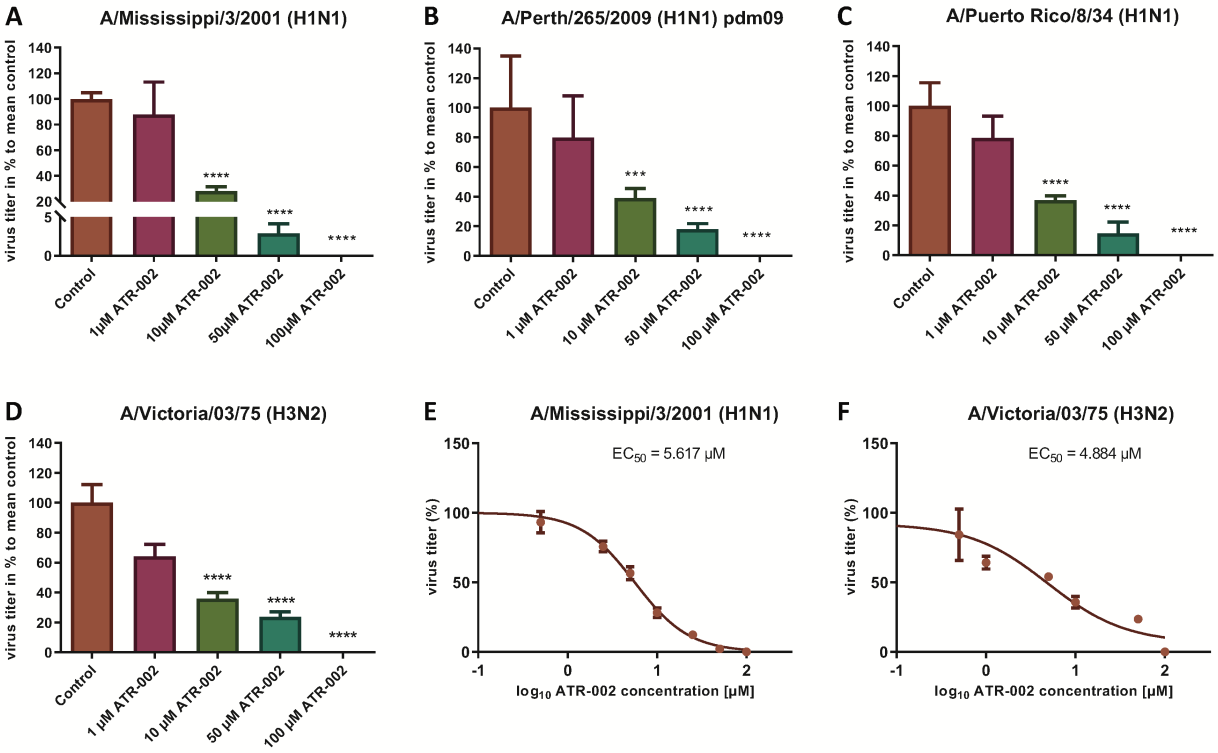


***Figure 1: Antiviral potential of ATR-002 against different IAV strains and subtypes**. (**A-D**) dose-dependent inhibition was compared to control. Data are presented as mean ± SEM analyzed using unpaired t-test with Welch's correction. Asterisks above columns represent the statistical significance ($p < 0.05$); (**E-F**) nonlinear regression analysis to evaluate the $EC_{50}$ values. Data are shown in $log_{10}$ concentrations. All statistical tests were performed using GraphPad Prism 6.0 software (La Jolla California, USA).*

Next, the effective concentration 50% ($EC_{50}$) for ATR-002 at which IAV progeny is reduced by 50%, was determined for two different IAV subtypes to be 5.62 µM for A/Mississippi/3/2001 (H1N1) and 4.884 µM for A/Victoria/03/75 (H3N2) (**Figure 1E-F**). These $EC_{50}$ values are in line with our previous *in vitro* results for ATR-002 against an H1N1 (6.36 µM) and an H3N2 (4.84 µM) IAV strain [32]. Equally, the corresponding selectivity index (SI = $CC_{50}$ / $EC_{50}$) of 281 and 323 for A/Mississippi/3/2001 (H1N1) and A/Victoria/03/75 (H3N2), respectively, is comparable to the previously determined SI for a H1N1 subtype (SI: 248) and a H3N2 subtype (SI: 326) [32]. These results indicate that ATR-002 can impair the replication of different IAV subtypes and strains with comparable efficiency.

**Growth kinetics of recombinant viruses**

To determine the replication kinetics of the recombinant viruses (rgH1N1-PA-I38T, rgH3N2-PA-I38T) carrying the PA-I38T mutation in comparison to their respective recombinant wild type (rgH1N1-WT, rgH3N2-WT), we analyzed the increase in virus titer in the supernatant of cells infected with the different viruses at 6, 24 and 48 hpi. For both pairs of recombinant viruses (PA-mutant, WT) we found similar replication dynamics even though the titer for the PA mutants (rgH1N1-/rgH3N2-PA-I38T) was always below the titer of the WT viruses by 0.28 – 0.62 $log_{10}$ (**Figure 2A, B**). This is in agreement with published data indicating that the fitness of viruses isolated from BXA-treated persons, carrying the PA-I38T mutation, is reduced to a similar extent [14]. Taken together, the kinetics and the efficiencies in replication of the rgWT and the rgPA-mutants generated by reverse genetics reflect the data obtained from naturally occurring virus variants. Therefore, the recombinant viruses should possess the biological properties needed for further analysis.

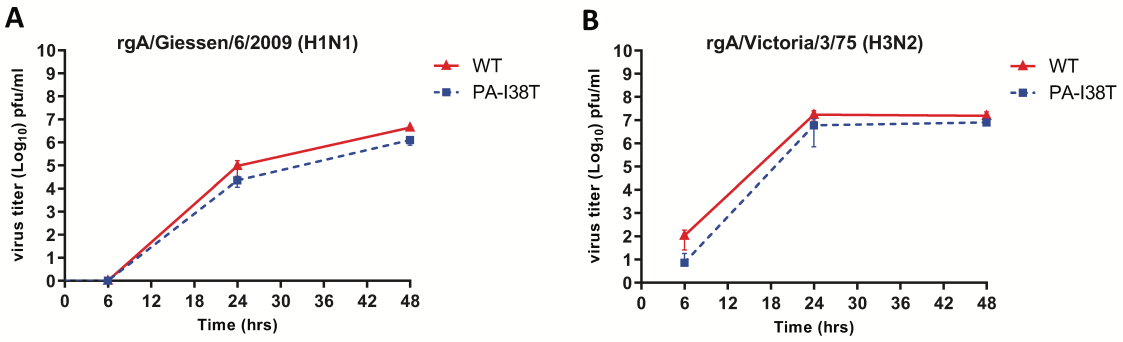


***Figure 2: Replication curves of wild-type viruses compared to the variant viruses with the indicated amino acid substitution in the PA protein.*** *MDCK cells were infected (MOI = 0.001) with either wild-*

*type or PA-I38T mutant influenza virus (A) rgA/Giessen/6/2009 (H1N1) or (B) rgA/Victoria/3/75 (H3N2). The virus titers were determined in the supernatants at the respective time points. The data represent the mean values of three independent experiments. The statistical significance was evaluated using paired student's t-test ($p < 0.05$) and it was not significant.*

**Antiviral activity of ATR-002 against BXA-susceptible and resistant IAV**

To confirm (i) reduced susceptibility towards BXA of the two recombinant PA-mutants (rgH1N1-PA-I38T, rgH3N2-PA-I38T) compared to the respective recombinant wild type viruses (rgH1N1-WT, rgH3N2-WT) and (ii) to further validate the antiviral activity of ATR-002 against the recombinant PA-mutants and WT viruses, we investigated the effect of ATR-002 versus BXA on the virus titer of the recombinant WT- and PA-mutant viruses 24 hpi compared to the untreated controls set to 100% (**Figure 3 A, B)**. The results demonstrate that BXA (0.9 nM) very efficiently inhibits rgH1N1-WT and rgH3N2-WT by 99.95 ± 0.02 % and 99.2 ± 0.08 %, respectively, while ATR-002 (100 µM) reduced the titers by 86.4 ± 2.24 % and 98.4 ± 0.30 %, respectively. In contrast, BXA reduced the titer of the PA-mutants rgH1N1-PA-I38T and rgH3N2-PA-I38T only by 63 ± 3.23 % and 60 ± 2.70 %, whereas ATR-002 still achieved a reduction by 87.80 ± 2.20 % and 99.70 ± 0.10 %, respectively. This corroborates that the PA-I38T mutation confers resistance towards BXA and clearly indicates that BXA-resistant viruses are still highly sensitive towards MEK inhibition by ATR-002.

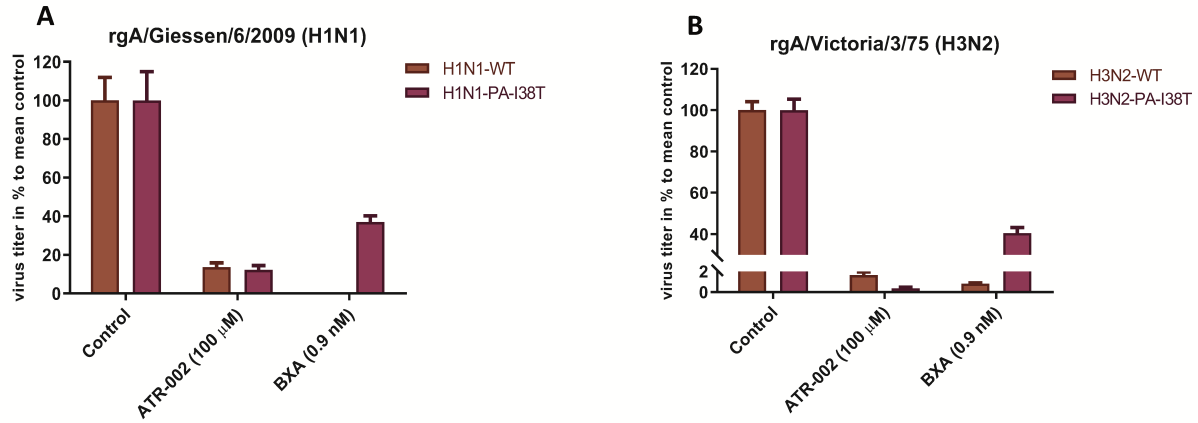


***Figure 3: Antiviral activity of BXA or ATR-002 against both recombinant wild-type and BXA-resistant influenza virus strains.*** *(A) rgA/Giessen/06/2009 (H1N1), (B) rgA/Victoria/3/75 (H3N2). Confluent monolayers of MDCK-II cells were infected with the respective virus strains (MOI = 0.001) and incubated for 1 h. Subsequently, cells were treated by adding infection media containing either BXA or ATR-002 at the indicated concentrations. After 24 h, the virus titers were determined by focus assay. The data*

*represent the mean ±SD values (n=6) and were analyzed using GraphPad Prism 6.0 software (La Jolla California, USA).*

**Synergy results at lower ATR-002 and BXA dose combinations**

Based on the above-mentioned results we next investigated the synergistic potential of the combined treatment with BXA and ATR-002, as this would not only allow to impair BXA-resistant strains, but also to profit from possibly augmented virus inhibition due to the different modes of action simultaneously exerted by the two compounds. Hence, we designed a 4 × 4 matrix for the single/combined use of both compounds applying concentrations related to the determined $EC_{50}$ values, against the model IAV strain A/Puerto Rico/8/34. Compared to the individual treatment with each drug virus titers indicated enhanced antiviral activity upon combining ATR-002 (0.4, 2, and 10 µM) with BXA (0.008 and 1.0 nM) (**Figure 4**). Moreover, there was no cytotoxicity associated with any of the drug combinations (no reduction in cell numbers by a companion assay of cells alone exposed to the same drug combinations) (**Figure S1**, **supplementary materials**).

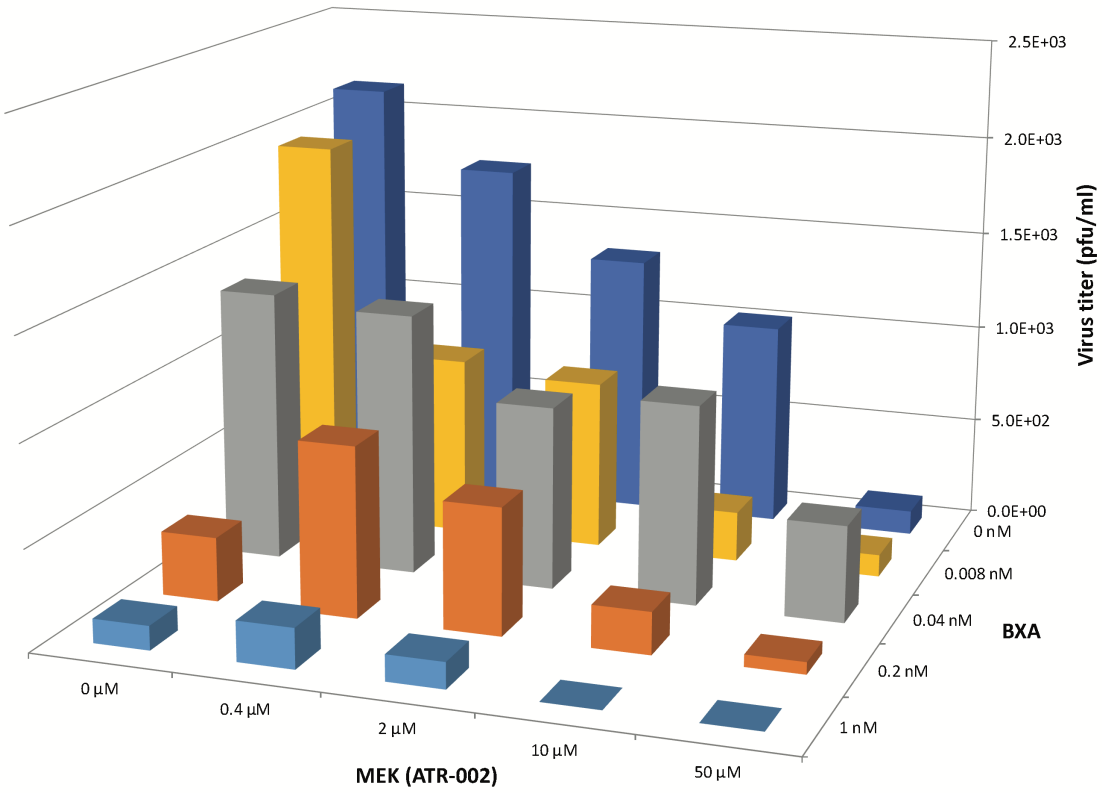


***Figure 4: Antiviral effect of BXA/ATR-002 combinations.*** *A549 cells were infected with A/Puerto Rico/8/34 (H1N1) (MOI = 0.001) and subsequently treated with the two inhibitors alone or in*

*combination at the indicated concentrations. After 24 h, the virus titers in the supernatant from the infected cells were determined by focus assay. The plotted viral titers represent the mean values (n=3) and indicate the increased or reduced antiviral activity.*

To assess whether this observation was due to synergistic or additive effects of the two compounds, "CompuSyn" software was applied, which uses the "Combination Index" model (CI) that defines synergism or antagonism by referring to a quantitative degree of drug interaction to analyze the above-mentioned data.

Firstly, a "Median-Effect" plot (ME-plot) was generated for both drugs (**Figure 5A**) to determine the quality of the obtained data by plotting the log values of the dose (D) versus the fraction affected/fraction unaffected ($f_a/f_u$) and the "Median Effect Dose" ($D_m$) was calculated according to the median-effect plot equation "log ($f_a/f_u$) = m log (D) – m log ($D_m$)". Primarily, as a step towards evaluating the conformity and the fidelity of the experimental data, the linear correlation coefficient (r) of the ME-plot was calculated for both drugs BXA (r=0.99) and ATR-002 (r=0.95), which reflects the validity of the obtained combination data. Moreover, $D_m$, which under the described conditions determines the "Inhibitory Concentration 50" ($IC_{50}$) value, was determined from the x-intercept of the ME-plot. The $D_m$ values were found to be 0.0613 nM and 3.4884 µM for BXA and ATR-002, respectively.

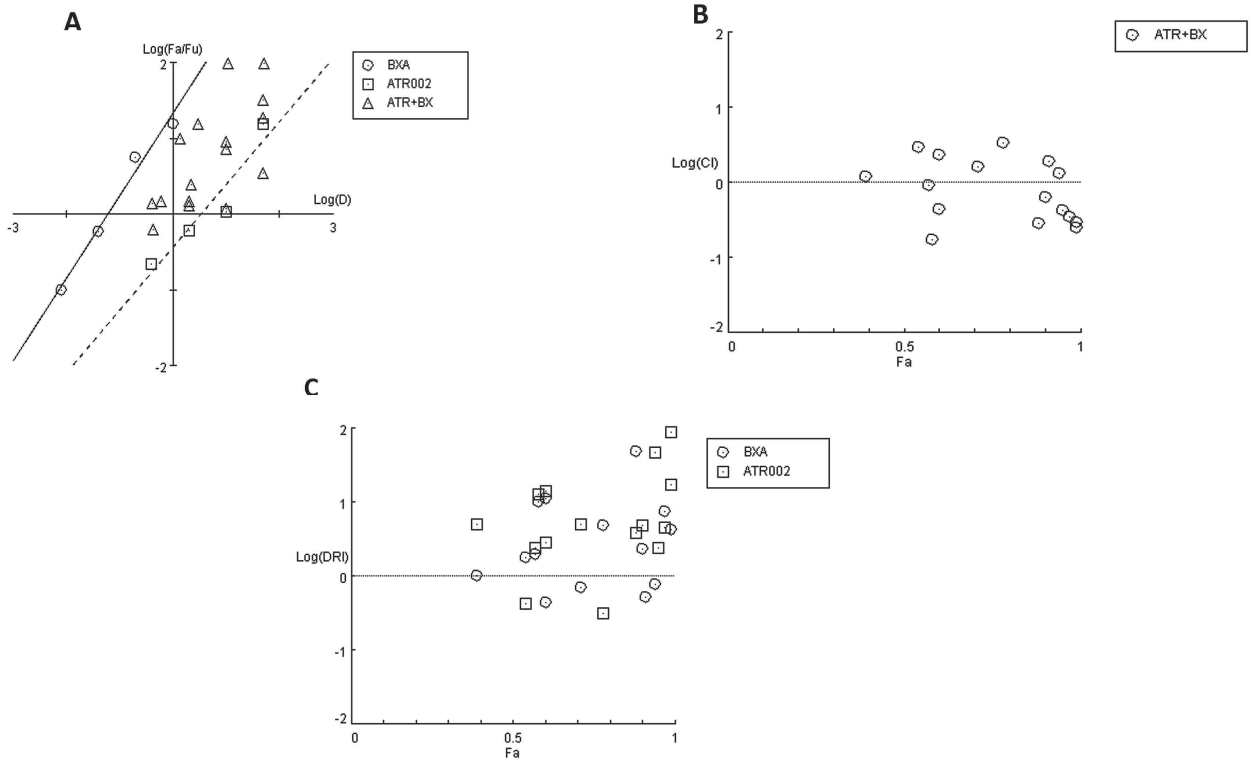

***Figure 5: Analysis of BXA/ATR-002 combinations (Supplementary Table 4) with CompuSyn software.*** *(**A**) median-effect plot (ME-plot) for BXA and ATR-002. This plot was generated by plotting the log values of x= D (dose) versus y=$f_a/f_u$ (fraction affected/fraction unaffected) and the $D_m$ was calculated according to the median-effect plot equation. (**B**) Logarithmic Combination Index Plot. Synergism/antagonism was plotted as the Log (CI) on the y-axis versus the Fraction affected ($F_a$) on the x-axis. Combinations with CI value CI=1 are additive and plotted on, or near the horizontal line, combinations with CI<1 are synergistic and plotted below the horizontal line, and combinations with CI>1 indicate antagonism and plotted above the horizontal line; (**C**) Fa-DRI plot of BXA and ATR-002 against influenza virus. DRI values above 1 (log (DRI) =0) represent favorable drug dose reduction for each drug, DRI =1 and <1 indicate neutral, and negative dose reduction, respectively (Supplementary Table 5).*

Next, by applying a logarithmic "Combination Index" (CI) plot synergistic effects were determined (**Figure 5B**). As shown, there are 8 data points for specific drug combinations out of 16 that fall below the additive line (< 1), revealing a synergistic effect with CI values ranging between 0.17 and 0.63 (**Table 4**, **supplementary materials**). Otherwise, data points of two combinations are near the additive line with a CI score of 0.91 – 1.18, indicating an additive effect and 6 further combinations are well above the additive line with CI scores of 1.31-3.32. These data indicate that the combination of ATR-002 and BXA results in a strong synergistic effect reflected by low CI values compared to the single-use concentration. Finally, using "CompuSyn" software, the potentially beneficial effect of combined treatment was further analyzed by calculating the drug synergism as the "Dose-Reduction Index" (DRI) from a "Fa-DRI" plot (Chou-Martin plot) (**Figure 5C**). This method delineates how many folds the dose of each drug can be reduced when used in combination. DRI values above 1 describe a favorable "Dose Reduction" (DR). Explicitly, to achieve virus titer reduction by 57%, either 0.079 nM of BXA or 4.89 µM of ATR-002 are required in a single-use (**Table 5**, **supplementary materials**). However, in combination about 1.98 fold less BXA and 2.44 fold less ATR002 is required to achieve the same inhibition, which corresponds to 0.039 nM BXA and 2.004 µM ATR-002. Nevertheless, it should be noted that despite the advantage of overcoming the toxic effects of a single drug application, DRI prediction can overestimate the doses predicted, as indicated by the shift from their empirical estimation. As such DRI would predict that either 4.23 nM BXA or 879.68 µM ATR-002 are needed in a single-use to achieve 99% virus titer reduction, but this prediction is not in line with our experimental data since this level of virus reduction

could already be achieved with 1 nM BXA or 100 µM ATR-002 (**Table 5**, **supplementary materials**).

These data were confirmed using "Combenefit" software, allowing to compare the results of three different mathematical models (HSA, Bliss, and Loewe). These models evaluate the combinatory effect as scores, which reflect the distribution of synergism/antagonism and facilitate the comparison between the assigned models. Synergy levels were depicted as surface and contour plots, revealing that these models confirm the overall evaluation of the synergistic activity of both compounds against IAV at lower concentrations of each drug when compared to higher concentrations (**Figure 6**). Differences in the synergistic scores between the "HAS" model and the "Bliss" and "Loewe" models can be explained by the different hypotheses of each model and the corresponding equations. Taken together, compared to the individual doses of both compounds, lower drug dose combinations result in considerable synergy, as well as decreased additive effects in contrast to higher dose combinations.

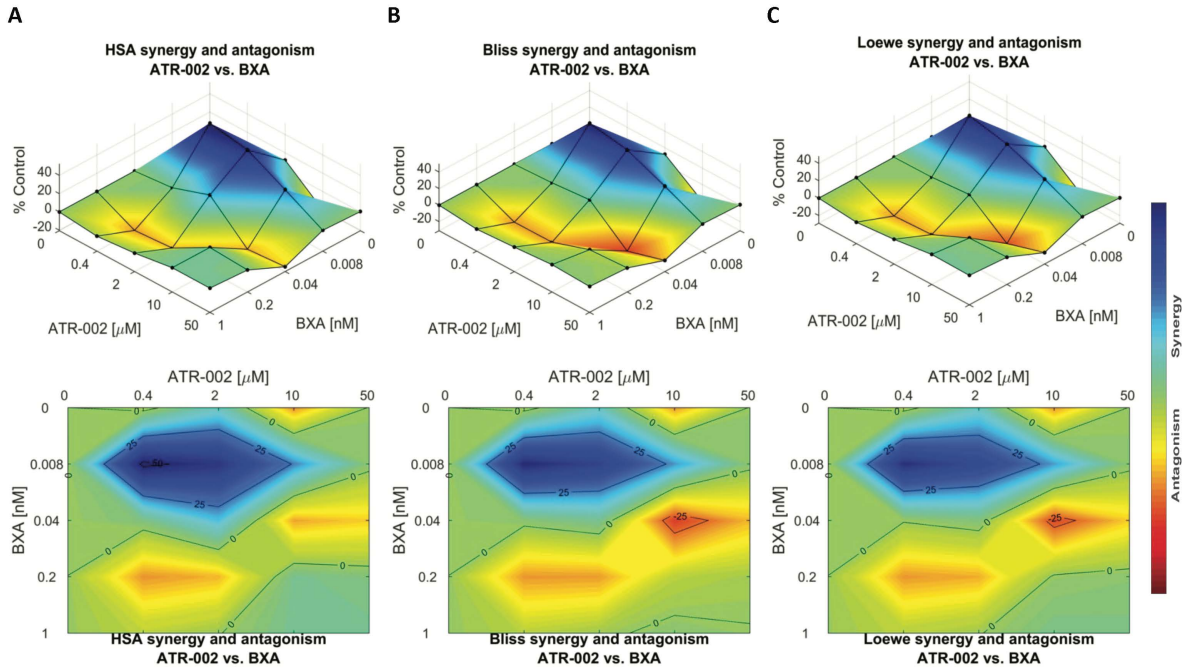


***Figure 6: Data obtained from combinations of BXA/ATR-002 were tested in a 4 × 4 matrix and all values normalized to Mock-infected control (DMSO).*** *Contour and surface plots were generated by Combenefit software upon processing data using three different synergy models: (A) HSA; (B) Bliss; (C) Loewe. The level of synergism or antagonism is represented with a color scale bar. Synergy is denoted by dark blue surface area and the antagonism effect is indicated by red surface area.*

## Discussion

Efforts to control IAV infection and the emergence of new strains are based on the development of vaccines and antiviral drugs. Of the currently worldwide available classes of antiviral drugs, the NAIs are used as the standard-of-care (SOC) treatment. Nevertheless, despite the low frequency of viruses with reduced susceptibility to NAI, the necessity of early initiation of treatment together with the emergence of drug-resistant strains are considered a major challenge for the use of these antivirals [7,47]. Furthermore, it was reported that the activity of oseltamivir carboxylate, the active metabolite of oseltamivir, is associated with delayed antiviral effects and clinical resolution during the treatment of Influenza B viruses (IBV) infections when compared to the treatment of IAV infections [34,48,49]. Among different antiviral approaches, BXA is not only effective against human IAV and IBV but also avian and porcine subtypes and has been approved in Japan and USA [12,14,50-52]. Despite the robustness of BXA as a single-dose antiviral drug, BXA treatment has resulted in a high level of viral resistance with 76- to 120-fold reduced BXA susceptibility in Japan [51] and 4- to 10-fold in the USA [53]. Moreover, another study reported that even though the $IC_{50}$ of BXA against a wide type pandemic H1N1-type IAV (WT/H1N1 pdm09) was 0.42 ± 0.37 nM, its $IC_{50}$ against the I38T variant was 41.96 ± 9.42 nM; and the $IC_{50}$ value for WT H3N2 virus was 0.66 ± 0.17 nM, but 139.73 ± 24.97 nM for the I38t mutant [54]. Altogether, the above-mentioned limitations highlight the urgent need for alternative approaches.

In response to an influenza virus infection, several intracellular signal transduction pathways are triggered and play a key role in the viral replication cycle. Earlier *in vitro* studies reported the applicability of MEK inhibitors as promising antiviral compounds showing that inhibiting MEK leads to nuclear retention of vRNPs, thereby suppressing viral replication [27]. Furthermore, MEK inhibition exhibited a high antiviral potential against diverse IAV/IBV strains including H5N1-type highly pathogenic avian influenza viruses (HPAIV) [26,28,55]. Adverse effects are often considered the main concern upon inhibition of cellular signaling in the treatment of seasonal influenza. As suggested earlier, these concerns could be minimized by either the short-term treatment of IV-infected patients compared to the long-term and repeated treatment of cancer patients or by reducing the dose while maintaining a strong antiviral activity through the combination of the signaling inhibitor with other direct-acting

antiviral compounds [17]. Along this line, we extended our investigations of the antiviral activity of ATR-002.

Herein, we report that ATR-002 (50 µM) is able to diminish IAV replication reducing the viral titer by 82 ± 1.49 % to 97.8 % for different H1N1 subtypes and by 76.4 ± 2.04 % for H3N2 subtype (**Figure 1**) with similar $EC_{50}$ values from 5.617 µM to 4.884 µM for H1N1- and H3N2-type IAV strains, respectively. These results demonstrate that ATR-002 efficiently blocks IAV replication across different strains and subtypes and corroborate our previously published data [32] demonstrating the *in vitro* and *in vivo* efficacy of ATR-002 or CI-1040, against IAV.

To evaluate whether the indirectly antiviral-acting host-targeting MEK inhibitor could overcome viral resistance of IAV carrying substitutions mounted against the directly acting antiviral BXA, the inhibitory activity of ATR-002 was validated against two recombinant IAVs, a H1N1- and a H3N2-strain, both either wild type and carrying the BXA resistance-associated PA-I38T mutation. In regard to comparability and to exclude unwanted additional mutations/differences, we generated these viruses as recombinant wild-type and mutant variants (rgH1N1-WT/- PA-I38T, rgH3N2-WT/- PA-I38T) allowing us to perform unbiased comparison of the activities exerted by BXA or ATR-002. Notably, both mutant strains replicate with a lower efficiency compared to their wild type counterpart, as described for isolates obtained from BXA-treated individuals [14] (**Figure 2**), indicating that the recombinant viruses reflect the biological properties of the natural isolates. On the contrary, in a growth-competition experiment, the growth-kinetics analysis revealed that the I38T substitution impairs the replication fitness of A/H1N1pdm viruses, while this mutation does not alter the fitness of A/H3N2 viruses *in vitro*. Moreover, the A/H1N1pdm viral replication fitness of the original clinical isolates may be restored by a concomitant compensatory mutation(s) [56]. The same study also showed no substantial change in the replication fitness between the mutant and wild-type viruses of both IAV subtypes *in vivo*.

The PA-I38T mutation was described to be associated with reduced IAV susceptibility to BXA [14,53] and IAV variants harboring an I38T, I38F or I38M substitution showed reduced BXA susceptibility during phase 2 and phase 3 trials, respectively [12]. Furthermore, IAV circulating during the 2016/2017 and 2017/2018 seasons in the USA gained amino acid substitutions in the PA-I38 position conferring a 4-10-fold reduction in BXA susceptibility [53]. Here we

demonstrate that, despite the potent effect of BXA against both WT strains, its antiviral effect was significantly reduced by ~40% against the mutant strains, while ATR-002 still impaired the PA-I38T mutants to a similar extent as the respective wild-type strains (**Figure 3**). Based on our previous findings, these results underline that targeting cellular MEK can overcome viral resistance mounted against directly acting antiviral compounds.

Notwithstanding the single use of antiviral compounds, combination therapy may be useful, not only to increase the antiviral potential of the therapy but also to counteract the limitations of SOC mono-therapy, such as rapid viral resistance against direct-acting antiviral compounds, and may enhance the clinical benefits by minimizing the dose-related toxicity [33]. Additionally, with regard to more severe scenarios e.g. severe infection or immunocompromised individuals, the combination treatment presumably provides meaningful benefits beyond those attained with current agents in many other situations like the delayed treatment with SOC antivirals following symptom onset that the SOC inefficient to reduce severity, illness duration, or duration of virus detection. We addressed a combination therapy approach by simultaneously employing two different antiviral mechanisms, e.g. inhibition of nuclear vRNP export and the PA endonuclease activity. Compared to monotherapy, this combination regimen reduced the IAV titer more efficiently. Importantly, the combined BXA/ATR-002 treatment achieved a synergistic effect with CI values ranging from 0.17 to 0.63, especially when both compounds were combined in concentrations below their single-use concentration. The most commonly used approaches to estimate synergism can be divided into effect-based approaches and dose-effect-based approaches. Each approach has practical advantages and limitations. Yet, in the absence of a reference methodology suitable for all biomedical situations, the analysis of drug combinations should benefit from a collective, appropriate, and rigorous application of the concepts and methods [57]. Along this line, we have chosen the most commonly used methods as representative analysis models and synergy was then further validated by three different models, which confirmed that our estimation of synergism is in line with the interpretation of the CI model.

Previously, another example of a combinatorial drug treatment approach based on cell-culture assays showed that nitazoxanide (blocking viral hemagglutinin maturation) exerts a synergistic effect when combined with oseltamivir or zanamivir (targeting the viral

neuraminidase) [35]. Also, in a triple combination antiviral regime, the activity of oseltamivir, amantadine (targeting the viral M2 protein), and ribavirin (targeting the RdRp) was evaluated against oseltamivir- and amantadine-resistant seasonal IAV strains and exhibited a higher synergistic effect than double combinations [38]. In support of such studies that employ combinations of divergent antiviral mechanisms, we have previously investigated the effect of oseltamivir combined with different MEK inhibitors and could additionally demonstrate a synergistic effect [36].

## Conclusion

In regard to our earlier studies, it is tempting to speculate that repurposing the MEK- inhibitor ATR-002, may represent an attractive approach to counteract the limitations of currently approved drugs against influenza viruses, that all target a viral function, to successfully address viral resistance. Moreover, these results substantiate both scenarios for the use of ATR-002 (i) in a monotherapy, as well as (ii) in a combination approach (together with SOC drugs) targeting different viral and host factors. To address the safety of cell signaling inhibitors as antivirals, it should be noted that ATR-002 was successfully tested in phase I clinical trial demonstrating no considerable adverse effects and is now in progress for further development.

## Acknowledgments

HH received a Ph.D. fellowship from the German Academic Exchange Service (DAAD) and the Egyptian Ministry of Higher Education and Scientific Research.

## Author contributions

HH, MMS, AM, SP, and OP participated in the conceptualization and design of the study. HH and MMS performed experimental drug testing experiments. HH performed drug combination treatment experiments. MMS and AM conducted the recombinant virus experiments. HH, MMS, AM, SP, and OP analyzed and interpreted the data. HH drafted the article. AM, SP, and OP administered the project and supervised the study. All authors revised and approved the submitted manuscript.

## Funding

This work was supported in part by the DFG-funded Collaborative Research Centre 1021 ‘RNA viruses: RNA metabolism, host response and pathogenesis’ (SFB1021; project C01 to Co-PI SP),

the BMBF-funded German Centre for Infection Research, partner site Giessen (DZIF, TTU 01.806 to Co-PI SP), a postdoctoral fellowship of the Justus-Liebig University, Giessen, Germany and the NRC-internal project (TT110801 to AM). This study was also supported by Atriva Therapeutics GmbH (Tübingen, Germany), manufacturer/licensee of ATR-002.

### *Transparency declarations*

The funders had no role in study design, data collection and analysis, decision to publish, or preparation of the manuscript. SP and OP are members of the German FluResearchNet, a nationwide research network on zoonotic influenza and are consultants for Atriva Therapeutics GmbH.

## *References*

[1] Muhlbauer D, Dzieciolowski J, Hardt M, Hocke A, Schierhorn KL, Mostafa A, Muller C, Wisskirchen C, Herold S, Wolff T, Ziebuhr J and Pleschka S. Influenza virus-induced caspase-dependent enlargement of nuclear pores promotes nuclear export of viral ribonucleoprotein complexes. J Virol. **2015**;89(11):6009-21.

[2] Obayashi E, Yoshida H, Kawai F, Shibayama N, Kawaguchi A, Nagata K, Tame JR and Park SY. The structural basis for an essential subunit interaction in influenza virus RNA polymerase. Nature. **2008**;454(7208):1127-31.

[3] Pleschka S. Overview of influenza viruses. Current topics in microbiology and immunology. **2013**;370:1-20.

[4] Fodor E. The RNA polymerase of influenza a virus: mechanisms of viral transcription and replication. Acta virologica. **2013**;57(2):113-22.

[5] Pflug A, Lukarska M, Resa-Infante P, Reich S and Cusack S. Structural insights into RNA synthesis by the influenza virus transcription-replication machine. Virus Res. **2017**;234:103-117.

[6] Lauring AS and Andino R. Quasispecies theory and the behavior of RNA viruses. PLoS pathogens. **2010**;6(7):e1001005.

[7] Hayden FG and Shindo N. Influenza virus polymerase inhibitors in clinical development. Current opinion in infectious diseases. **2019**;32(2):176-186.

[8] Duwe S. Influenza viruses - antiviral therapy and resistance. GMS infectious diseases. **2017**;5:Doc04.

[9] Clark MP, Ledeboer MW, Davies I, Byrn RA, Jones SM, Perola E, Tsai A, Jacobs M, Nti-Addae K, Bandarage UK, Boyd MJ, Bethiel RS, Court JJ, Deng H, Duffy JP, Dorsch WA, Farmer LJ, Gao H, Gu W, Jackson K, Jacobs DH, Kennedy JM, Ledford B, Liang J, Maltais F, Murcko M, Wang T, Wannamaker MW, Bennett HB, Leeman JR, McNeil C, Taylor

WP, Memmott C, Jiang M, Rijnbrand R, Bral C, Germann U, Nezami A, Zhang Y, Salituro FG, Bennani YL and Charifson PS. Discovery of a novel, first-in-class, orally bioavailable azaindole inhibitor (VX-787) of influenza PB2. Journal of medicinal chemistry. **2014**;57(15):6668-78.

[10] Vanderlinden E, Vrancken B, Van Houdt J, Rajwanshi VK, Gillemot S, Andrei G, Lemey P and Naesens L. Distinct Effects of T-705 (Favipiravir) and Ribavirin on Influenza Virus Replication and Viral RNA Synthesis. Antimicrobial agents and chemotherapy. **2016**;60(11):6679-6691.

[11] Noshi T, Kitano M, Taniguchi K, Yamamoto A, Omoto S, Baba K, Hashimoto T, Ishida K, Kushima Y, Hattori K, Kawai M, Yoshida R, Kobayashi M, Yoshinaga T, Sato A, Okamatsu M, Sakoda Y, Kida H, Shishido T and Naito A. In vitro characterization of baloxavir acid, a first-in-class cap-dependent endonuclease inhibitor of the influenza virus polymerase PA subunit. Antiviral research. **2018**;160:109-117.

[12] Hayden FG, Sugaya N, Hirotsu N, Lee N, de Jong MD, Hurt AC, Ishida T, Sekino H, Yamada K, Portsmouth S, Kawaguchi K, Shishido T, Arai M, Tsuchiya K, Uehara T, Watanabe A and Baloxavir Marboxil Investigators G. Baloxavir Marboxil for Uncomplicated Influenza in Adults and Adolescents. N Engl J Med. **2018**;379(10):913-923.

[13] Hirotsu N, Sakaguchi H, Sato C, Ishibashi T, Baba K, Omoto S, Shishido T, Tsuchiya K, Hayden FG, Uehara T and Watanabe A. Baloxavir marboxil in Japanese pediatric patients with influenza: safety and clinical and virologic outcomes. Clinical infectious diseases : an official publication of the Infectious Diseases Society of America. **2019**.

[14] Omoto S, Speranzini V, Hashimoto T, Noshi T, Yamaguchi H, Kawai M, Kawaguchi K, Uehara T, Shishido T, Naito A and Cusack S. Characterization of influenza virus variants induced by treatment with the endonuclease inhibitor baloxavir marboxil. Scientific reports. **2018**;8(1):9633.

[15] Jones JC, Kumar G, Barman S, Najera I, White SW, Webby RJ and Govorkova EA. Identification of the I38T PA Substitution as a Resistance Marker for Next-Generation Influenza Virus Endonuclease Inhibitors. mBio. **2018**;9(2).

[16] Song MS, Kumar G, Shadrick WR, Zhou W, Jeevan T, Li Z, Slavish PJ, Fabrizio TP, Yoon SW, Webb TR, Webby RJ and White SW. Identification and characterization of influenza variants resistant to a viral endonuclease inhibitor. Proceedings of the National Academy of Sciences of the United States of America. **2016**;113(13):3669-74.

[17] Planz O. Development of cellular signaling pathway inhibitors as new antivirals against influenza. Antiviral research. **2013**;98(3):457-468.

[18] Ludwig S. Disruption of virus-host cell interactions and cell signaling pathways as an anti-viral approach against influenza virus infections. Biological chemistry. **2011**;392(10):837-47.

[19] Lee SM and Yen HL. Targeting the host or the virus: current and novel concepts for antiviral approaches against influenza virus infection. Antiviral research. **2012**;96(3):391-404.

[20] Pinto R, Herold S, Cakarova L, Hoegner K, Lohmeyer J, Planz O and Pleschka S. Inhibition of influenza virus-induced NF-kappaB and Raf/MEK/ERK activation can reduce both virus titers and cytokine expression simultaneously in vitro and in vivo. Antiviral research. **2011**;92(1):45-56.

[21] Fremin C and Meloche S. From basic research to clinical development of MEK1/2 inhibitors for cancer therapy. Journal of hematology & oncology. **2010**;3:8.

[22] Lorusso PM, Adjei AA, Varterasian M, Gadgeel S, Reid J, Mitchell DY, Hanson L, DeLuca P, Bruzek L, Piens J, Asbury P, Van Becelaere K, Herrera R, Sebolt-Leopold J and Meyer MB. Phase I and pharmacodynamic study of the oral MEK inhibitor CI-1040 in patients with advanced malignancies. Journal of clinical oncology : official journal of the American Society of Clinical Oncology. **2005**;23(23):5281-93.

[23] Sebolt-Leopold JS. MEK inhibitors: a therapeutic approach to targeting the Ras-MAP kinase pathway in tumors. Current pharmaceutical design. **2004**;10(16):1907-14.

[24] Marjuki H, Yen HL, Franks J, Webster RG, Pleschka S and Hoffmann E. Higher polymerase activity of a human influenza virus enhances activation of the hemagglutinin-induced Raf/MEK/ERK signal cascade. Virol J. **2007**;4:134.

[25] Marjuki H, Alam MI, Ehrhardt C, Wagner R, Planz O, Klenk HD, Ludwig S and Pleschka S. Membrane accumulation of influenza A virus hemagglutinin triggers nuclear export of the viral genome via protein kinase Calpha-mediated activation of ERK signaling. J Biol Chem. **2006**;281(24):16707-15.

[26] Droebner K, Pleschka S, Ludwig S and Planz O. Antiviral activity of the MEK-inhibitor U0126 against pandemic H1N1v and highly pathogenic avian influenza virus in vitro and in vivo. Antiviral research. **2011**;92(2):195-203.

[27] Pleschka S, Wolff T, Ehrhardt C, Hobom G, Planz O, Rapp UR and Ludwig S. Influenza virus propagation is impaired by inhibition of the Raf/MEK/ERK signalling cascade. Nature cell biology. **2001**;3(3):301-5.

[28] Haasbach E, Muller C, Ehrhardt C, Schreiber A, Pleschka S, Ludwig S and Planz O. The MEK-inhibitor CI-1040 displays a broad anti-influenza virus activity in vitro and provides a prolonged treatment window compared to standard of care in vivo. Antiviral research. **2017**;142:178-184.

[29] Schrader T, Dudek SE, Schreiber A, Ehrhardt C, Planz O and Ludwig S. The clinically approved MEK inhibitor Trametinib efficiently blocks influenza A virus propagation and cytokine expression. Antiviral research. **2018**;157:80-92.

[30] Sebolt-Leopold JS, Dudley DT, Herrera R, Van Becelaere K, Wiland A, Gowan RC, Tecle H, Barrett SD, Bridges A, Przybranowski S, Leopold WR and Saltiel AR. Blockade of the

MAP kinase pathway suppresses growth of colon tumors in vivo. Nature medicine. **1999**;5(7):810-6.

[31] Tecle H, Shao J, Li Y, Kothe M, Kazmirski S, Penzotti J, Ding YH, Ohren J, Moshinsky D, Coli R, Jhawar N, Bora E, Jacques-O'Hagan S and Wu J. Beyond the MEK-pocket: can current MEK kinase inhibitors be utilized to synthesize novel type III NCKIs? Does the MEK-pocket exist in kinases other than MEK? Bioorganic & medicinal chemistry letters. **2009**;19(1):226-9.

[32] Laure M, Hamza H, Koch-Heier J, Quernheim M, Muller C, Schreiber A, Muller G, Pleschka S, Ludwig S and Planz O. Antiviral efficacy against influenza virus and pharmacokinetic analysis of a novel MEK-inhibitor, ATR-002, in cell culture and in the mouse model. Antiviral research. **2020**;178:104806.

[33] Govorkova EA and Webster RG. Combination chemotherapy for influenza. Viruses. **2010**;2(8):1510-29.

[34] Hayden F. Developing new antiviral agents for influenza treatment: what does the future hold? Clinical infectious diseases : an official publication of the Infectious Diseases Society of America. **2009**;48 Suppl 1:S3-13.

[35] Belardo G, Cenciarelli O, La Frazia S, Rossignol JF and Santoro MG. Synergistic effect of nitazoxanide with neuraminidase inhibitors against influenza A viruses in vitro. Antimicrobial agents and chemotherapy. **2015**;59(2):1061-9.

[36] Haasbach E, Hartmayer C and Planz O. Combination of MEK inhibitors and oseltamivir leads to synergistic antiviral effects after influenza A virus infection in vitro. Antiviral Res. **2013**;98(2):319-24.

[37] Pires de Mello CP, Drusano GL, Adams JR, Shudt M, Kulawy R and Brown AN. Oseltamivir-zanamivir combination therapy suppresses drug-resistant H1N1 influenza A viruses in the hollow fiber infection model (HFIM) system. European journal of pharmaceutical sciences : official journal of the European Federation for Pharmaceutical Sciences. **2018**;111:443-449.

[38] Nguyen JT, Hoopes JD, Le MH, Smee DF, Patick AK, Faix DJ, Blair PJ, de Jong MD, Prichard MN and Went GT. Triple combination of amantadine, ribavirin, and oseltamivir is highly active and synergistic against drug resistant influenza virus strains in vitro. PloS one. **2010**;5(2):e9332.

[39] Kim WY, Young Suh G, Huh JW, Kim SH, Kim MJ, Kim YS, Kim HR, Ryu YJ, Han MS, Ko YG, Chon GR, Lee KH, Choi SH, Hong SB and Korean Society of Critical Care Medicine HNC. Triple-combination antiviral drug for pandemic H1N1 influenza virus infection in critically ill patients on mechanical ventilation. Antimicrobial agents and chemotherapy. **2011**;55(12):5703-9.

[40] Mostafa A, Kanrai P, Ziebuhr J and Pleschka S. Improved dual promotor-driven reverse genetics system for influenza viruses. Journal of Virological Methods. **2013**;193(2):603-610.

[41] Ma W, Brenner D, Wang Z, Dauber B, Ehrhardt C, Högner K, Herold S, Ludwig S, Wolff T, Yu K, Richt JA, Planz O and Pleschka S. The NS Segment of an H5N1 Highly Pathogenic Avian Influenza Virus (HPAIV) Is Sufficient To Alter Replication Efficiency, Cell Tropism, and Host Range of an H7N1 HPAIV. Journal of Virology. **2010**;84(4):2122.

[42] Matrosovich M, Matrosovich T, Garten W and Klenk H-D. New low-viscosity overlay medium for viral plaque assays. Virology journal. **2006**;3(1):63.

[43] Chou TC and Talalay P. Quantitative analysis of dose-effect relationships: the combined effects of multiple drugs or enzyme inhibitors. Advances in enzyme regulation. **1984**;22:27-55.

[44] Chou TC. Drug combination studies and their synergy quantification using the Chou-Talalay method. Cancer research. **2010**;70(2):440-6.

[45] Chou T and Martin N. CompuSyn for drug combinations: PC software and user's guide: a computer program for quantitation of synergism and antagonism in drug combinations, and the determination of IC50 and ED50 and LD50 values. ComboSyn, Paramus, NJ. **2005**.

[46] Di Veroli GY, Fornari C, Wang D, Mollard S, Bramhall JL, Richards FM and Jodrell DI. Combenefit: an interactive platform for the analysis and visualization of drug combinations. Bioinformatics (Oxford, England). **2016**;32(18):2866-8.

[47] Takashita E, Daniels RS, Fujisaki S, Gregory V, Gubareva LV, Huang W, Hurt AC, Lackenby A, Nguyen HT, Pereyaslov D, Roe M, Samaan M, Subbarao K, Tse H, Wang D, Yen H-L, Zhang W and Meijer A. Global update on the susceptibilities of human influenza viruses to neuraminidase inhibitors and the cap-dependent endonuclease inhibitor baloxavir, 2017–2018. Antiviral research. **2020**;175:104718.

[48] Sugaya N, Mitamura K, Yamazaki M, Tamura D, Ichikawa M, Kimura K, Kawakami C, Kiso M, Ito M, Hatakeyama S and Kawaoka Y. Lower clinical effectiveness of oseltamivir against influenza B contrasted with influenza A infection in children. Clinical infectious diseases : an official publication of the Infectious Diseases Society of America. **2007**;44(2):197-202.

[49] Kawai N, Ikematsu H, Iwaki N, Maeda T, Satoh I, Hirotsu N and Kashiwagi S. A comparison of the effectiveness of oseltamivir for the treatment of influenza A and influenza B: a Japanese multicenter study of the 2003-2004 and 2004-2005 influenza seasons. Clinical infectious diseases : an official publication of the Infectious Diseases Society of America. **2006**;43(4):439-44.

[50] Mishin VP, Patel MC, Chesnokov A, De La Cruz J, Nguyen HT, Lollis L, Hodges E, Jang Y, Barnes J, Uyeki T, Davis CT, Wentworth DE and Gubareva LV. Susceptibility of Influenza A, B, C, and D Viruses to Baloxavir. Emerg Infect Dis. **2019**;25(10):1969-1972.

[51] Takashita E, Kawakami C, Morita H, Ogawa R, Fujisaki S, Shirakura M, Miura H, Nakamura K, Kishida N, Kuwahara T, Mitamura K, Abe T, Ichikawa M, Yamazaki M, Watanabe S, Odagiri T and On Behalf Of The Influenza Virus Surveillance Group Of J.

Detection of influenza A(H3N2) viruses exhibiting reduced susceptibility to the novel cap-dependent endonuclease inhibitor baloxavir in Japan, December 2018. Euro Surveill. **2019**;24(3).

[52] Heo YA. Baloxavir: First Global Approval. Drugs. **2018**;78(6):693-697.

[53] Gubareva LV, Mishin VP, Patel MC, Chesnokov A, Nguyen HT, De La Cruz J, Spencer S, Campbell AP, Sinner M, Reid H, Garten R, Katz JM, Fry AM, Barnes J and Wentworth DE. Assessing baloxavir susceptibility of influenza viruses circulating in the United States during the 2016/17 and 2017/18 seasons. Euro Surveill. **2019**;24(3).

[54] Checkmahomed L, M'Hamdi Z, Carbonneau J, Venable MC, Baz M, Abed Y and Boivin G. Impact of the Baloxavir-Resistant Polymerase Acid I38T Substitution on the Fitness of Contemporary Influenza A(H1N1)pdm09 and A(H3N2) Strains. J Infect Dis. **2020**;221(1):63-70.

[55] Ludwig S, Wolff T, Ehrhardt C, Wurzer WJ, Reinhardt J, Planz O and Pleschka S. MEK inhibition impairs influenza B virus propagation without emergence of resistant variants. FEBS letters. **2004**;561(1-3):37-43.

[56] Imai M, Yamashita M, Sakai-Tagawa Y, Iwatsuki-Horimoto K, Kiso M, Murakami J, Yasuhara A, Takada K, Ito M, Nakajima N, Takahashi K, Lopes TJS, Dutta J, Khan Z, Kriti D, van Bakel H, Tokita A, Hagiwara H, Izumida N, Kuroki H, Nishino T, Wada N, Koga M, Adachi E, Jubishi D, Hasegawa H and Kawaoka Y. Influenza A variants with reduced susceptibility to baloxavir isolated from Japanese patients are fit and transmit through respiratory droplets. Nature microbiology. **2020**;5(1):27-33.

[57] Foucquier J and Guedj M. Analysis of drug combinations: current methodological landscape. Pharmacology research & perspectives. **2015**;3(3):e00149.

## Supplementary materials

**Supplementary Table 1: Primers used to generate the PA-I38T mutation via site direct mutagenesis.**

| Primer name | Sequence (5` to 3`) |
|---|---|
| PA-H1-09-I38T-F | CTAACAAGTTTGCTGCAACATGCACACATTTGGAAG |
| PA-H1-09-I38T-R | CTTCCAAATGTGTGCATGTTGCAGCAAACTTGTTAG |
| PA-H3Vic-I38T-F | CAAACAAATTTGCAGCAACATGCACTCACTTGGAGG |
| PA-H3Vic-I38T-R | CCTCCAAGTGAGTGCATGTTGCTGCAAATTTGTTTG |

**Supplementary Table 2: Sequencing primers used for complete sequencing of pMP-PA plasmids.**

| Primer name | Sequence (5` to 3`) |
|---|---|
| SPA-1198R | GCTCTGGCTCATCACTGTCATACT |
| SPA-558F | TCTATGGGATTCCTTTCGTCAGTC |
| SPA-1982R | TCAGCCGAAAACCCCTCAAGT |
| SPA-1117F | AATATGGCACCAGAAAAAGTAGAC |
| PA-H3N2Vict-1892R | TCCCCAATGGGCCATGTTTC |
| PA-H3N2Vict-990F | CGTCAAACCACACGAAAGGG |
| PA-H3N2Vict-491F | CCACAAAGGCCGACTACACT |
| PA-H3N2Vict-1154R | TCTGGTGCCATGTTCTCACC |
| pHW2000R | GCTCCGTGTGTGGCTGCGAT |
| pHW2000F | GGTAAATGGCCCGCCTGGCA |

**Table (3): Primers used in RT-PCR and sequencing.**

| Primer name | Sequence (5` to 3`) |
|---|---|
| Primers used for RT-PCR | |
| Bm-PA-1F | TATTCGTCTCAGGGAGCGAAAGCAGGTAC |
| Bm-PA-2233R | ATATCGTCTCGTATTAGTAGAAACAAGGTACTT |
| Primers used for sequencing | |
| Bm-PA-1F | TATTCGTCTCAGGGAGCGAAAGCAGGTAC |
| SPA-1198R | GCTCTGGCTCATCACTGTCATACT |
| PA-H3N2Vict-1154R | TCTGGTGCCATGTTCTCACC |

**Supplementary Table 4: Combination Index (CI) values for drug combos.**

| Dose BXM | Dose ATR-002 | Effect* | CI |
|---|---|---|---|
| 0.0080 | 0.4 | 0.58 | 0.17469 |
| 1.0 | 10.0 | 0.99 | 0.24757 |
| 0.0080 | 10.0 | 0.88 | 0.28142 |
| 1.0 | 50.0 | 0.99 | 0.29305 |
| 0.2 | 50.0 | 0.97 | 0.35104 |
| 0.0080 | 50.0 | 0.95 | 0.42303 |
| 0.0080 | 2.0 | 0.6 | 0.44177 |
| 0.2 | 10.0 | 0.9 | 0.63435 |
| 0.04 | 2.0 | 0.57 | 0.91172 |
| 0.04 | 0.4 | 0.39 | 1.18204 |
| 1.0 | 2.0 | 0.94 | 1.31281 |
| 0.2 | 2.0 | 0.71 | 1.62481 |
| 1.0 | 0.4 | 0.91 | 1.94132 |
| 0.2 | 0.4 | 0.6 | 2.31597 |
| 0.04 | 10.0 | 0.54 | 2.92652 |
| 0.04 | 50.0 | 0.78 | 3.32808 |

*% reduction in virus titer

**Supplementary Table 5: Drug dose reduction (DRI) data example of BXM and ATR-002 prediction combo**

| Fa* | Dose BXM (nM) | Dose ATR-002 (μM) | DRI BXM | DRI AT-R002 |
|---|---|---|---|---|
| 0.99 | 4.23358[a] | 879.684[a] | 4.23358 | 17.5937 |
| 0.97 | 1.50936 | 228.8[a] | 7.54681 | 4.57599 |
| 0.95 | 0.92466 | 120.664[a] | 115.583 | 2.41327 |
| 0.94 | 0.77405 | 95.6649 | 0.77405 | 47.8325 |
| 0.91 | 0.517 | 56.4779 | 0.517 | 141.195 |
| 0.9 | 0.4644 | 49.0947 | 2.32201 | 4.90947 |
| 0.88 | 0.38452 | 38.3704 | 48.0652 | 3.83704 |
| 0.78 | 0.1968 | 16.0009 | 4.91991 | 0.32002 |
| 0.71 | 0.1399 | 10.2473 | 0.69948 | 5.12367 |
| 0.6 | 0.08906 | 5.68262 | 11.133 | 2.84131 |

| Fa* | Dose BXM (nM) | Dose ATR-002 (µM) | DRI BXM | DRI AT-R002 |
|---|---|---|---|---|
| 0.58 | 0.08253 | 5.14432 | 10.316 | 12.8608 |
| 0.57 | 0.07947 | 4.89711 | 1.98684 | 2.44855 |
| 0.54 | 0.07105 | 4.23089 | 1.77634 | 0.42309 |

*% reduction in virus titer

[a] Predicted dose that shifts from its empirical estimation

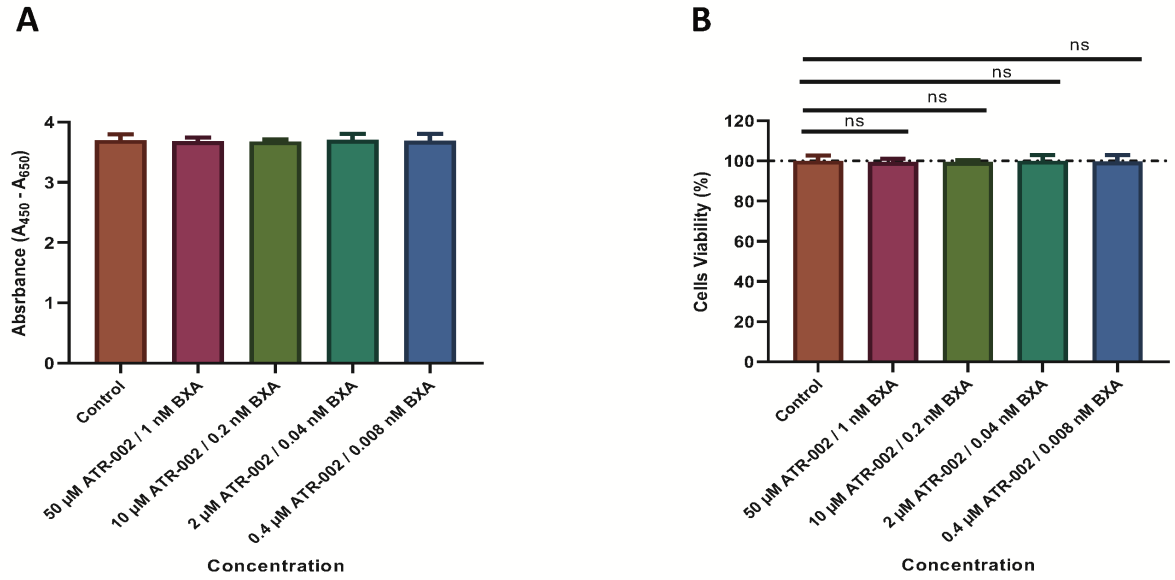


***Supplementary Figure 1: Evaluation of the cytotoxic effect of BXA and ATR-002 combinations.*** *The bar graphs depict the cytotoxicity data determined by the WST-1 assay. A549 cells were treated with the highest relevant combinations of both tested drugs (ATR-002/BXA) (50 µM / 1 nM; 10 µM / 0.2 nM; 2 µM/0.04 nM; 0.4 µM / 0.008 nM) and the viability was tested as indicated in the material and methods section. Values of the WST-1 assay are presented as (A) normalized absorbance values to the reference wavelength and (B) the viability percentage with control as 100 %. The data represent the mean ±SD (n=3) and the statistical significance was evaluated using unpaired t-test with Welch's correction compared to the control (ns: not significant). The data were analyzed using GraphPad Prism 6.0 software (La Jolla California, USA).*

# Chapter 3

# Antiviral and Immunomodulatory Effect of Zapnometinib in Animal Models and Hospitalized COVID-19 Patients

Yvonne Füll[1,2], Lara M. Schüssele[1,2], Hazem Hamza[1,2,3], Helen Hoffmann[1,2], Martin Bauer[2], Stephan Stenglein[2], Oliver Pötz[4], Andreas Steinhilber[4], Viktoria Anselm[4], Mark W. Delany[5], Judith M.A. van den Brand[5], Geert van Amerongen[6], Leon de Waal[6], Stephan Pleschka[7], Stephan Ludwig[8] and Oliver Planz[1]*

[1] Interfaculty Institute for Cell Biology, Department of Immunology, Eberhard Karls University Tübingen, Germany

[2] Atriva Therapeutics GmbH, Christophstr. 32, 72072 Tübingen, Germany

[3] Virology Laboratory, Environmental Research Division, National Research Centre, Cairo, Egypt

[4] SIGNATOPE GmbH, Reutlingen, Germany

[5] Division of Pathology, Faculty of Veterinary Medicine Utrecht, University Utrecht, the Netherlands

[6] Viroclinics-DDL, Cerba Research Company, Schaijk, the Netherlands

[7] Institute of Medical Virology, Justus Liebig University, Giessen, Germany

[8] Institute of Virology (IVM), Centre for Molecular Biology of Inflammation, University of Muenster, Muenster, Nordrhein-Westfalen, Germany

* Corresponding author

***Unpublished, manuscript under review.***

## *Disclosure of authorship contribution*

In this chapter, only the acute lung injury (ALI) mouse model belongs to the thesis. HH designed and performed the ALI model experiment. HH generated all figures involved in this part. HH performed the relative gene expression analysis and generated all respective figures. HH established, performed, and analyzed all RT-qPCR experiments. HH was strongly involved in data visualization, drafting, and reviewing the manuscript. Further information and contributions to other parts are provided in the “Author Contribution” section at the end of this chapter/manuscript.

## Abstract

**Background:** In severe COVID-19, direct-acting antiviral drugs were not effective in hyperinflammatory stages and steroid treatment may weaken host immunity. The MEK inhibitor zapnometinib, as a host-targeting drug, has demonstrated promising efficacy against severe acute viral infections. Proof-of-concept for the innovative approach was presented in a clinical Phase 2 trial with hospitalized COVID-19 patients.

**Methods:** The antiviral and immunomodulatory potential of zapnometinib was investigated in samples obtained from COVID-19 patients enrolled in a Phase 2 clinical trial (RESPIRE), as well as in a SARS-CoV-2 Syrian hamster model, an acute lung injury mouse model, and in cell culture. The antiviral activity of zapnometinib was assessed using viral load reduction assays and RT-qPCR. Cytokines and chemokines were analyzed via ELISA and RT-qPCR. Alterations in T and B cells from COVID-19 patients were analyzed using flow cytometry. Biomarker analysis in hamster serum was conducted to monitor potential toxic effects.

**Findings:** Zapnometinib reduced SARS-CoV-2 viral load in hospitalized COVID-19 patients, in the hamster model, and in various highly pathogenic coronaviruses *in vitro*. Pro-inflammatory cytokines and chemokines decreased in COVID-19 patients, in a lung injury mouse model, and *in vitro* in primary human blood cells treated with zapnometinib. In the hamster model, zapnometinib alleviated SARS-CoV-2-mediated lung pathology. In patients with COVID-19, zapnometinib increased T and plasma B cells.

**Interpretation:** Unlike direct-acting antivirals, zapnometinib's dual effect highlights its therapeutic potential in the treatment of severe acute viral infections, with favorable antiviral and immunomodulatory properties.

## *Research in context*

### Evidence before this study

Several studies suggest that a novel therapeutic approach against various viral diseases may involve interfering with host cell factors that viruses utilize for their replication, rather than directly targeting the virus itself. The small molecule drug zapnometinib has demonstrated potential antiviral effects against both influenza virus and SARS-CoV-2, and on top of that, it exhibits immunomodulating properties that aid in combating viral infections. Currently, it is undergoing development for the treatment of severe viral infections, and a phase 2 trial in COVID-19 patients has shown promising results in terms of both safety and clinical efficacy.

### Added value of this study

In this study, we were able to provide further evidence substantiating that the MEK inhibitor zapnometinib exhibits a broad antiviral effect and, additionally, possesses positive immunomodulating properties that aid in combating diseases and alleviating symptoms. From studies in cell-based systems to animal models and actual patients in a clinical trial, the dual effect of the drug has been demonstrated. This further supports the characterization of a new therapeutic approach and its treatment options.

### Implications of all the available evidence

Our study contributes to the essential knowledge required for further development of the drug zapnometinib, offering a promising therapeutic strategy for the treatment of severe respiratory infections. The results also aid in enhancing our understanding of the dual effect of zapnometinib, which includes viral load reduction and modulation of the immune response.

## Introduction

In late 2019, severe acute respiratory syndrome coronavirus 2 (SARS-CoV-2), which causes coronavirus disease 2019 (COVID-19), emerged in humans. The World Health Organization (WHO) declared COVID-19 a pandemic due to the rapid person-to-person transmission of SARS-CoV-2 and the significant morbidity and mortality it caused worldwide [1-3]. The severity of COVID-19 varies widely from asymptomatic infection to severe disease, with the latter being associated with lower respiratory tract symptoms and pathological hyperinflammation [4-6] which may lead to multiorgan dysfunction, including acute respiratory distress syndrome (ARDS), neurological symptoms, cardiovascular events, and coagulopathies [7-9]. While the viral load is high at onset and in the early stages of COVID-19, the hyperinflammatory response plays a more important role in determining disease severity in later stages [10]. Hyperinflammation is evidenced by significantly elevated levels of certain proinflammatory cytokines and chemokines observed in the majority of COVID-19 patients, particularly in those with severe disease requiring intensive care [11].

Currently available treatments can be categorized into therapeutic antibodies, repurposed direct-acting antivirals (DAA) like nirmatrelvir, remdesivir, or molnupiravir, and immunomodulating drugs, such as dexamethasone or anti-IL-6 antibodies [12-16]. They all have their limitations. Therapeutic antibodies have become less effective due to the emergence of new SARS-CoV-2 variants, underscoring the issue of viral escape leading to resistance. Direct-acting antivirals must be administered very early in the onset of infection and have not proven to be highly effective in treating severely ill patients. Various immunomodulatory approaches, some with promising results, were employed for treating lung inflammation in COVID-19 patients. Examples of these include the intake of probiotics, prebiotics, vitamins, or zinc - with dosage and timing of intake still to be evaluated, and the benefits should outweigh the risks [17-19]. Approved immunomodulating drugs such as dexamethasone have demonstrated significant efficacy in advanced stages of infection. Nevertheless, administering them too early could potentially impede the initiation of an antiviral immune response. Thus, a drug that is effective throughout the full course of the disease is still missing. Targeting cellular factors presents a promising avenue for addressing this therapeutic gap. The cellular Raf/MEK/ERK signaling pathway is mainly involved in cell proliferation and regulation of cytokine and chemokine expression [20]. Furthermore, the

inhibition of this signaling pathway induces a shift in the adaptive immune response towards an effector immune reaction [21-23]. Severe cases of COVID-19 are characterized by aberrant adaptive immunity, specifically evidenced by lymphopenia, and especially impaired $CD8^+$ T cell functionality [24,25]. Consequently, targeting this signaling pathway may ameliorate hyperactive innate and adaptive immune responses.

MEK inhibitors prevent the phosphorylation of ERK in cells where the signaling pathway is activated, such as in cancer cells or cells attacked by certain viruses. In most of our somatic cells, the signaling pathway is not highly activated. Several MEK inhibitors are already in development or approved for the treatment of various cancers [26]. We previously demonstrated that targeting the cellular Raf/MEK/ERK signaling pathway leads to a reduction in viral load and protects mice from lethal infection with another health-relevant respiratory virus, the influenza A virus (IAV) [27-29]. Additionally, apart from IAV, various RNA viruses, like Respiratory Syncytial virus (RSV), Zika virus (ZIKV), Dengue virus (DENV), Yellow fever virus (YFV), Borna disease virus (BDV) or Mouse hepatitis virus (MHV), require activation of the Raf/MEK/ERK signaling pathway to ensure their propagation. Inhibition of this pathway disrupts various stages of their viral life cycle [27,30-33]. There are also certain viruses that are not sensitive to MEK inhibition [34,35]. This prompted us to analyze whether inhibition of the pathway would also result in inhibition of SARS-CoV-2 replication. Indeed, we were able to demonstrate that zapnometinib (ATR-002, PD 0184264), an oral MEK inhibitor, not only exhibits antiviral activity against the influenza virus in both *in vitro* and *in vivo* settings, [28,29] but also against SARS-CoV-2 *in vitro* in cell lines as well as in primary air-liquid-interphase epithelial cell cultures, with a safe and selective treatment window [36]. Furthermore, the *in vitro* synergistic effect of zapnometinib was demonstrated in combination with baloxavir marboxil against IAV, [29] and also with various direct-acting SARS-CoV-2 drugs [37]. In the life cycle of IAV, the transport of viral ribonucleoprotein complexes relies on active MEK [27]. Despite SARS-CoV-2 lacking a nuclear phase in its replication cycle, MEK activation assumes a crucial function in the initial phases of infection [36]. It is noteworthy from the aforementioned study that the immunomodulatory impact of zapnometinib operates autonomously from its antiviral properties. It could be shown that MEK inhibition leads to reduced expression of pro-inflammatory cytokines and chemokines without interfering with the interferon-induced antiviral response [38,39]. In the subsequent stages of drug development, it was possible to

demonstrate that zapnometinib showed no toxicity and was well tolerated in humans in two phase 1 studies in healthy volunteers (NCT04385420; EudraCT 2021-005225-25). The correlation between pharmacokinetics, pharmacodynamics and antiviral efficacy could be demonstrated in various animal models and in humans, confirming both safety and efficacy and highlighting the drug's significant therapeutic potential [40]. Moreover, an ADME study in rats showed a favorable distribution and metabolism of the drug [41]. In the phase 2 clinical trial of hospitalized COVID-19 patients (RESPIRE; NCT04776044), zapnometinib treatment was found to be safe and well-tolerated. Consistent trends toward better outcomes were observed with zapnometinib, especially among patients with severe disease [42].

Here, we aim to evaluate the therapeutic potential of zapnometinib against various coronaviruses, demonstrating its dual effect in a phase 2 clinical trial with hospitalized COVID-19 patients as well as through different pre-clinical approaches. Zapnometinib treatment leads to a reduction in viral load and favorable immunomodulatory effects on top of the standard of care. These results are supported by preclinical data from a Syrian hamster SARS-CoV-2 infection model, wherein zapnometinib significantly reduces viral load and lung pathology without causing toxic effects. Furthermore, our findings demonstrate that zapnometinib can significantly alleviate hyperinflammation induced by cytokines and chemokines associated with severe COVID-19 in an acute lung injury (ALI) mouse model and in primary human blood cells.

These findings support the potential of zapnometinib as a promising broad-spectrum antiviral therapeutic with a dual effect, particularly in severe respiratory viral infections leading to hyperinflammation such as COVID-19 or influenza.

## *Materials and methods*

### Ethics

The hamster experiments were carried out in the Central Animal Facilities of Viroclinics-DDL, Cerba Research Company, Schaijk, the Netherlands, in accordance with the standards of the Dutch law for animal experimentation (2010/63/EU). Ethical approval for the present study was obtained from the institutional Animal Welfare Body under the number AVD277002015283-WP24.

The mouse experiments for the ALI mouse model were conducted following review and approval by the Regional Council Tuebingen (35/9185.81-2/ IM 1/17) and in compliance with the institutional Principles of Animal Welfare and Animal Research.

Human sputum and nasopharyngeal swabs were taken from samples collected for the RESPIRE trial (NCT04776044) in 18 hospitals from 5 countries that was approved by respective regulatory authorities and by the Ethics Committees concerned (for details, please see the clinical trial protocol provided in [42].

**Animals**

Seven- to nine-week-old male Syrian hamsters (Janvier, France) with a body weight ranging from 102 to 134 g at the time of drug administration were utilized for the pharmacokinetic study. The same animals, aged 11 to 13 weeks and a body weight ranging from 113 to 148 g, were employed for the efficacy study. The animals were housed in elongated type 2 IVC group cages with two animals per cage under BSL-II conditions during acclimatization and in elongated type 2 group cages under BSL-III conditions (isolators) during challenge, with sawdust as bedding. Daily checks were conducted for overt signs of disease, standard food was provided, and drinking water was available ad libitum. All biotechnical procedures were performed under 3% isoflurane anesthesia.

Six- to eight-week-old female C57BL/6J mice weighing 20-27 g from the Mouse Facility of the University of Tuebingen (Interfaculty Institute for Cell Biology) were utilized to establish an inflammatory ALI model. The animals were maintained in elongated type 2 IVC cages housing four mice each under BSL-II conditions and provided with standard food and drinking water ad libitum.

**Virus and cells**

SARS-CoV-2 (BetaCoV/Munich/BavPat1/2020, containing the D614G substitution in the S1 fragment, kindly provided by Dr. C. Drosten, Berlin, Germany) was passaged once in Vero-TMPRSS2 cells and three times in Vero E6 cells and titered in a $TCID_{50}$ assay as described in the section “Determination of replication-competent virus ($TCID_{50}$ assay)”. SARS-CoV-2 “Omicron” (B.1.1.592) (kindly provided by Prof. Dr. M. Schindler, Institute of Medical Virology and Epidemiology, University Hospital Tübingen) was passaged on Calu-3 cells and titrated by plaque assay, as previously described in Koch-Heier et al. 2021[43]. Briefly, Vero E6 cells were

infected with a 6-fold serial dilution of the virus stock, overlayed with Avicel medium, and incubated for 72h at 37°C, 5% $CO_2$. After fixation and staining of the cell layer with crystal violet solution, the virus titer was determined based on the number of plaques counted per well and the respective dilution factor. Vero E6 (Cat# CRL-1586), Vero cells (Cat# CCL-81), MRC-5 (Cat# CCL-171), and Calu-3 cells (Cat# HTB-55) used for *in vitro* assays were obtained from ATCC (Manassas, Virginia, USA). The virus strains used for *in vitro* studies at a MOI of 0.001 were the following: SARS-CoV-1: SARS-CoV-HKU-39849; SARS-CoV-2 BavPat1: Human 2019-nCoV Isolate, EVAg Ref-SKU:026V-03883; SARS-CoV-2 "Omicron" B.1.1.592 (described in [44]); HCoV-229E (Cat# VR-740; ATCC). HCoV-OC43 (Cat# VR-1558; ATCC) was used at MOI 0.1.

Human peripheral blood mononuclear cells (PBMCs) were isolated from healthy volunteers registered with the Biobank of the Department of Immunology at the University of Tuebingen, after informed consent documented in writing. Ethical approval was obtained upon review by the Ethics Board of the Medical Faculty of the Eberhard Karls University Tuebingen and the University Hospital Tuebingen (887/2020BO2). Briefly, 50 ml whole blood (roughly $5x10^7$ PBMCs) of two donors were taken in 50 ml syringes (BD Biosciences, Franklin Lakes, New Jersey, USA) supplied with heparin-natrium (100.000 I.E./ml; Braun, Melsungen, Germany). The whole blood was mixed with PBS (Gibco, Carlsbad, California, USA) in a 1:1 ratio in 50 ml tubes (Greiner Bio-One, Frickenhausen, Germany), and PBMCs were subsequently isolated from the whole blood by density gradient centrifugation using Histopaque®-1077 (Sigma-Aldrich, St. Louis, Missouri, USA) as density gradient medium. Five milliliters of plasma per donor were preserved for cell culture medium preparation. The PBMCs were then purified by washing them twice with PBS.

**Antiviral activity assays**

The virus yield reduction assay was conducted at Viroclinics Biosciences BV (Rotterdam, the Netherlands) following the company's standard operating procedures (SOPs). In brief, Vero E6 cells (for SARS-CoV-2) or Vero cells (for SARS-CoV-1) were seeded at a density of $1.5x10^4$ cells in 96-well plates the day before infection and inoculated with 0.001 MOI of the appropriate virus in the absence (virus control wells) and presence of 100, 75, 50, 25, 12.5, 6.25, 3.125, 1.5625, 0.78125, 0.390625 or 0 µM zapnometinib. The 96-well plates were incubated for 24 and 48 h at 37 °C. The supernatants were harvested after the incubation, and the viral titer was determined in four replicates by TrueBlue Immunostaining and spot counting using a CTL

Immunospot Image Analyzer. The viral titer measured in the presence of each concentration of zapnometinib was utilized to determine the 50% effective concentration ($EC_{50}$) using a previously described method [45]. A cytotoxicity run was conducted concurrently using an LDH release assay as described in the supplementary.

For the virus yield reduction assay of SARS-CoV-2 Omicron (B.1.1.592), Calu-3 cells were seeded at a density of $3x10^5$ cells in 24-well plates two days before infection and inoculated with 0.001 MOI of SARS-CoV-2 Omicron (B.1.1.592) for 1 h. Subsequently, the inoculum was completely removed, and the cells were treated with 100, 75, 62.5, 50, 25, 12.5, or 0 µM zapnometinib. Plates were incubated for 24 h at 37 °C. The supernatants were harvested after the incubation, and the viral titer was determined using a real-time one-step multiplex RT-qPCR method. Briefly, viral nucleic acid extraction was performed using a QIAamp Viral RNA Mini Kit (QIAGEN, Hilden, Germany) following the manufacturer's instructions. A TaqMan-based RT-qPCR assay was carried out using QuantiNova Pathogen kit (QIAGEN, Hilden, Germany) with specific primers targeting the SARS-CoV-2 N gene (Supplementary Table 1). The viral genome copies were determined based on a standard curve prepared with tenfold serial dilutions of the target gene. For QC, nuclease-free water was included in each set of extractions as a negative control to monitor any possible cross-contamination. Moreover, an artificial exogenous QuantiNova RNA internal control (QIAGEN, Hilden, Germany) was included during the nucleic acid purification to monitor the RNA purification efficiency and the RT-PCR amplification. $EC_{50}$ values were calculated based on the measured viral titers normalized to the solvent control (1 % DMSO).

The virus yield reduction assay of HCoV-229E and HCoV-OC43 was performed on MRC-5 cells seeded at $1.5x10^5$ cells per well in 24-well plates 24 h prior infection with HCoV-229E (MOI 0.001) or HCoV-OC43 (MOI 0.1) for 1 h. The inoculum was completely removed, and the cells were treated with different concentrations of zapnometinib (50 µM to 0.006 µM) and a solvent control in IMDM containing 2 % FBS, 1 % Penicillin/Streptomycin at 34°C, 5% $CO_2$ for 24 h (HCoV-OC43) or 48 h (HCoV-229E). Supernatants were harvested and the viral titer was determined by a real-time one-step multiplex RT-qPCR using specific primers targeting the N and NS2 genes for HCoV-229E and HCoV-OC43 respectively (Supplementary Table 1) $EC_{50}$ values were calculated based on the measured viral titers normalized to the solvent control

(1 % DMSO) and using the "log(inhibitor) vs. response - Variable slope (four parameters)" analysis in GraphPad Prism v9.

**Drug administration in hamsters**

Zapnometinib was synthesized by Chemcon GmbH (Freiburg, Germany). Before administration to Syrian hamsters, it was freshly dissolved in dimethyl sulfoxide (DMSO) (Carl Roth GmbH, Karlsruhe, Germany) and then further dissolved in 15% Kolliphor EL (Sigma-Aldrich, Germany) and 80% phosphate-buffered saline (PBS) (Gibco, Life Technology Europe B.V., Bleiswijk, the Netherlands). Kolliphor EL is used to emulsify and solubilize oils and other water-in-soluble substances, it has been used as a pharmaceutical solvent for numerous drugs and has proven in previous *in vivo* studies with zapnometinib. Zapnometinib was administered orally at the indicated doses in a volume of 500 µL/150 g body weight using a gavage needle.

**Pharmacokinetics**

Drug administration and blood sampling in Syrian hamsters were performed by Viroclinics Xplore (Schaijk, the Netherlands) and are described in the sections "Drug administration" and "Sampling after inoculation". Specifically, at different time points (0, 0.5, 1, 2, 4, 8, 12, and 24 h) after the administration of a single dose of zapnometinib (15, 30, or 60 mg/kg per oral (p.o.)), ~200 µL blood was collected retro-orbitally from three animals per time point per dose and alternating animals between time points (except at 24 h, n = 6 per group) under isoflurane anesthesia using a heparinized capillary tube containing a clot activator (Microvette 500 Z-Gel, Sarstedt). Serum was collected by centrifuging the tubes at 4000 xg for 10 min, aliquoted, and stored at < -70 °C until pharmacokinetic analysis. Daily clinical observations included monitoring of signs such as ruffled fur, hunched back posture, accelerated breathing, and lethargy, and the body weight was monitored before and 24 h post administration.

Bioanalysis and pharmacokinetic evaluation were performed at Prolytic GmbH (Frankfurt, Germany). High-affinity liquid chromatography-tandem mass spectrometry (HPLC-MS/MS) was employed to determine the concentration of zapnometinib in hamster serum in accordance with the company's SOPs. During the analytical phase, two batches were evaluated. The acceptance criteria for the calibration standards and quality control (QC) samples were fulfilled for both batches as per the company's SOPs. The calibration curve was in the range of 10-10000 ng/mL for zapnometinib and showed acceptable linearity over the

calibration range. In total, 81 study test samples were analyzed. The validity of the method during the analysis of the test samples was ensured by assaying QC samples with known concentrations of zapnometinib; zapnometinib 13C6 was used as the internal standard. The lower limit of quantification (LLOQ) of the method was determined to be 10 ng/mL for zapnometinib in undiluted serum. All serum concentrations falling below LLOQ were assigned a value of 0. ANALYST software was used to calculate the concentrations of the test and QC samples based on the corresponding calibration curves. The obtained mean serum concentrations were used for noncompartmental pharmacokinetic evaluation with Phoenix® WinNonLin software (Pharsight Corporation, Mountain View, CA, USA; version 8.1).

**Efficacy study in the Syrian hamster infection model**

On day 0, all animals (n=6 per group) were infected intranasally with SARS-CoV-2 ($1x10^3$ median tissue culture infectious dose ($TCID_{50}$) BetaCoV/Munich/BavPat1/2020 (grown and titered at Viroclinics) in a total volume of 0.1 mL diluted in PBS (Gibco, Paisley, UK) and divided between the nostrils. Zapnometinib (100 mg/kg) was administered p.o. at either +4 h or +24 h post-infection (p.i.). Subsequently, all animals in both groups received a daily dose of 75 mg/kg zapnometinib. The animals in the control group received vehicle +4 h p.i. and once daily thereafter. All animals were euthanized by exsanguination under 3% isoflurane anesthesia on day 4 post-infection (dpi). All individuals conducting clinical observations and laboratory analyses requiring data interpretation were blinded before the conclusion of the study.

**Sampling after inoculation**

Respiratory tract samples were collected daily during the study from Syrian hamsters infected and treated as described in the section “Efficacy study in the Syrian hamster infection model”. Briefly, throat swabs were collected in virus transport medium (Eagles minimal essential medium containing HEPES buffer, Na bicarbonate solution, L-Glutamine, Penicillin, Streptomycin, BSA fraction V and Amphotericin B), and the samples were aliquoted and stored at < -70 °C. Serum was also collected as described for pharmacokinetics at 0 dpi and 4 dpi and frozen at < -70 °C until further analysis.

Additionally, upon necropsy, lung, nasal turbinate, and trachea samples were collected and stored in 10% formalin for histopathology or frozen at < -70 °C for virological analysis. For

virological analysis, the tissue samples were weighed, homogenized in infection medium and centrifuged at 3000 xg for 10 min at room temperature before titration.

**Determination of viral load**

**Detection of replication-competent virus ($TCID_{50}$ assay):** Quadruplicate 10-fold serial dilutions of throat swabs and tissue homogenate samples were used to determine the viral titers in confluent layers of Vero E6 cells. Briefly, serial dilutions of samples were prepared and incubated on Vero E6 monolayers for 1 h at 37 °C. Then, the Vero E6 monolayers were washed once with infection medium (DMEM containing L-Glutamine, Penicillin, Streptomycin, Amphotericin B and Fetal Bovine serum) and incubated for 4-6 days at 37 °C, after which the plates were scored using WST8 (colorimetric assessment). The optical density (OD) of the wells was read at 450 nm ($OD_{450}$) using a microplate reader and compared to the OD of the positive control wells (non-treated, infected cells), which showed a cytopathic effect (CPE). The viral titer ($TCID_{50}$) per mL or g was calculated using the Spearman-Karber method.

**Detection of viral RNA:** The viral titer in throat swabs and homogenized tissue samples was determined using an RT-qPCR method. Briefly, RNA was isolated with a Roche MagNA Pure 96 instrument using a MagNA Pure 96 DNA and Viral NA Small Volume Kit, and a TaqMan-based RT-qPCR assay was performed with specific primers (Supplementary Table 1), as described by Corman et al [46]. The number of viral copies (CP per mL or g) per sample was calculated by using the resulting Ct value of the sample and the slope, intercept, and upper and lower limits of detection of a $log_{10}$ dilution series of a viral stock for which the number of copies per dilution was known.

**Gross pathology**

At the time of necropsy, gross pathology was performed for each animal. All lung lobes were inspected, and the percentage of affected lung tissue was estimated from the dorsal view. In addition, any other abnormalities observed in other organs during full-body gross pathology were documented. Then, the left lung lobes, trachea, and nasal turbinates were preserved in 10% neutral buffered formalin for histopathology, while the right lung lobes and nasal turbinates were subsequently homogenized for TaqMan-based RT-qPCR and virus titration.

**Histopathology**

Histopathological analysis of the left lung, trachea and left nasal turbinate was performed for all animals. After fixation with 10% formalin for at least 2 weeks, tissue sections were embedded in paraffin, micro-sectioned to 3 µm on glass slides and stained with hematoxylin and eosin (H&E) for histological examination. The H&E-stained tissue sections were examined by light microscopy, using an Olympus BX45 light microscope with magnification steps of 40x, 100x, 200x, and 1000x, for histopathology scoring, as well as for the presence of any other lesions. SARS-CoV-2-associated lesions in the lungs were semi-quantitatively assessed as follows: presence of alveolar oedema, alveolar hemorrhage, and type II pneumocyte hyperplasia: 0 = no, and 1 = yes as described previously [47].

**Candidate biomarker analysis**

Serum samples from hamsters collected at pre-infection (0 dpi) and post-infection (4 dpi) and treatment time points were analyzed to evaluate the levels of various candidate safety biomarkers. Serum proteins were enzymatically fragmented through proteolysis, and protein-specific peptides were targeted for quantification of the corresponding protein biomarker levels by immunoaffinity liquid chromatography-tandem mass spectrometry (IA-LC-MS/MS) performed as described previously [48,49]. For further details, see supplementary methods.

**Inflammatory ALI mouse model**

Mice were anesthetized by intraperitoneal (i.p.) injection of ketamine solution (10 mg/kg). Both the treatment and control groups (n = 4 each) received 5 mg/kg LPS (O55:B5, Sigma-Aldrich) in PBS (100 µL per mouse) via i.p. injection. At 1 h post-stimulation, the treatment group received 25 mg/kg zapnometinib via oral gavage, while the control group received vehicle (15% Kolliphor, 5% DMSO in PBS). The mice were euthanized at 6 h post-zapnometinib treatment, and the lungs were preserved in RNAlater (Qiagen, Hilden, Germany).

Lungs were homogenized by a bead-beating system (FastPrep™, MP Biomedicals) the RNA was isolated using RNeasy Plus Universal Midi Kit (Qiagen) according to the manufacturer's instructions. RNA quality (A260/A280 ratio ≥1.8 and A260/A230 in the range of 2.0-2.2) was determined using a NanoDrop spectrophotometer (Thermo Fisher Scientific), and the isolated RNA was reverse transcribed using an RT² First Strand Kit (Qiagen). Afterward, the generated cDNA was subjected to a real-time RT² Profiler PCR Array using RT² SYBR® Green qPCR Mastermix. For optimal performance, the RT² Profiler™ Mouse Cytokines & Chemokines

arrays (PAMM-150ZR, Qiagen) were customized to include 84 genes and 5 housekeeping genes for data normalization (see Supplementary Table 4). For QC, a mouse genomic DNA contamination test, 3 reverse transcription efficiency tests, and 3 PCR array reproducibility tests were included. The data were analyzed using the GeneGlobe portal (Qiagen) according to the ΔΔCt method. The fold change/regulation was calculated, and the threshold value was 2.

**Analysis of cytokine and chemokine levels in human PBMCs**

$2x10^6$ human PBMCs from two donors each were suspended in 1 mL RPMI 1640 medium (Gibco) containing 5% autologous plasma, 1% penicillin/streptomycin (Sigma-Aldrich), and 1% L-glutamine (Sigma-Aldrich) and were treated with 1 µg/mL LPS from *E. coli* O55:B5 (prepared in PBS) and 10 µg/mL zapnometinib (prepared in DMSO and diluted in cell culture medium to a final concentration of 0.1% DMSO) for 6 h at 37 °C and 5% $CO_2$. The supernatants (cell culture medium) were collected and stored at -20 °C until analysis by ELISA. Ready-to-use ELISA kits (Invitrogen, Waltham, Massachusetts, USA) were used according to the manufacturer's instructions to determine the levels of the following cytokines: IL-1β, IL-6, IL-8, IP-10, MCP-1, MIP-1α, and TNF-α. Briefly, the samples and standards were applied to ELISA plates pre-coated with specific antibodies targeting the cytokines of interest. Biotinylated detection antibodies binding to the cytokines of interest were added to the wells followed by a horseradish peroxidase (HRP)-streptavidin conjugate, which binds to the biotinylated detection antibodies. Unbound cytokines, detection antibodies, and HRP-streptavidin conjugate were removed by washing. Tetramethylbenzidine (TMB) substrate was added, and the color change in the wells served as the readout for the ELISA. Optical density (OD) at 450 nm was measured using a SpectraMAX Plus 384 microplate reader. For IL-1β, IL-8, MCP-1, and TNF-α the OD was also read at a reference wavelength of 620 nm, and for IL-6 at a reference wavelength of 550 nm. For IP-10 and MIP-1α no reference wavelength was used. Cytokine and chemokine concentrations were calculated following the manufacturer's instructions for interpolating unknown concentrations from a standard curve.

**Virology and Immunology from the RESPIRE trial**

RESPIRE was a global randomized, double-blind, placebo-controlled proof-of-concept Phase 2 trial in adults with moderate-to-severe COVID-19 requiring hospitalization (clinical severity status (CSS) 3 or 4, measured on a 7-point ordinal scale). The study details are described in

Rohde et al. 2023 [42]. Briefly, patients were randomized 1:1 to oral zapnometinib (900 mg on Day 1 (D1); 600 mg daily on Day 2-6) or matching placebo, on top of standard of care according to local guidelines. Patients, investigators, the study team, and the Sponsor remained blinded to treatment allocation throughout the study.

Viral load: Nasopharyngeal swabs and sputum were collected at time points D1, D3, D5, D8, D11, D15 and D30 after treatment start and the viral load was quantified via RT-qPCR at CheckImmune GmbH, Berlin. Cytokine/chemokine: Parameters from 24 (12 zapnometinib, 12 placebo) study participants at time points D1, D3, D5, D8, D11, D15 and D30 were analyzed using MesoScale V-Plex Proinflammatory Panel I and Chemokine Panel and whole Blood IL-8 (MSD, Rockville, USA). For standard of care treatment see supplementary Table 5.

Adaptive immune cell parameters from 12 (6 zapnometinib, 6 placebo) study participants at time points D1, D3, D5, D8, D11, D15, and D30 were analysed using the following panels: activated/exhausted T cells (Duraclone; Beckman Coulter, Krefeld Germany), activated T cells/Tregs (Duraclone; Beckman Coulter, Krefeld Germany), B cell panel (Duraclone; Beckman Coulter, Krefeld Germany). Patients receiving glucocorticoids as standard of care treatment were excluded from the analyses. Experiments were performed by CheckImmune GmbH according to the companies' SOPs. In short, presence of lymphocytes, T cells and B cells were determined using Flow cytometry analysis. Fresh whole blood from hospitalized SARS-CoV-2 infected patients was stained with the aforementioned DuraClone antibody panels for 15 min at room-temperature and lysed for 15 min at room temperature following the standard staining protocol. Sample acquisition was carried out using the Navios Flow Cytometer (Beckman Coulter). Data analysis was conducted using Kaluza software before being sent to the LIMS system. This procedure is fit for purpose validated under ISO and GCP guidelines.

**Statistical analysis**

Unless otherwise noted, data were collected in MS Excel, and statistical analyses were performed using GraphPad Prism software v8 or v9 (La Jolla, CA, USA). Statistical details for each experiment are described in the corresponding figure legends. Differences in viral titer, lung injury severity or body weight were analyzed by one-way ANOVA. Differences in the mRNA expression of cytokines were assessed by analyzing replicate data using one-way ANOVA with the Kruskal-Wallis test or using Student's t-test (unpaired t-test with Welch's

correction). Differences in cytokine expression at the protein level were analyzed using an unpaired t-test with Welch's correction for normally distributed data; otherwise, the Mann-Whitney test was applied. Differences in biomarkers were evaluated using Brown-Forsythe ANOVA with the Dunnett T3 correction. *P* values < 0.05 were considered statistically significant.

## Results

### Zapnometinib inhibits propagation of coronaviruses *in vitro*

We started out with an *in vitro* analysis of the antiviral efficacy of zapnometinib against the SARS-CoV-2 variant "omicron" and other pathogenic human coronaviruses (HCoV OC43, 229E and SARS-CoV-1) using a Virospot or virus yield reduction assay. The viral titer of all tested coronaviruses could be reduced (Fig. 1a-d). The half-maximal effective concentration ($EC_{50}$) values were in a comparable range, with minor variations attributed to virus-specific assay adjustments, from 16.1 µM (HCoV-OC43) to 37.9 µM (SARS-CoV-2 omicron) for all the viruses tested (Table 1). No cytotoxicity was observed in the *in vitro* antiviral assays, as measured by LDH release (Supplementary Table 2) and calculated by assessing the 50% cytotoxic concentration ($CC_{50}$) (Supplementary Fig. 1; Table 1). These results confirm and extend the data from our recent findings, demonstrating the antiviral efficacy of zapnometinib against the alpha, beta and delta variants of SARS-CoV-2 in cell culture without inducing cytotoxic effects [36]. In summary, the *in vitro* antiviral efficacy of zapnometinib against various coronaviruses has been demonstrated, affirming its broad antiviral therapeutic potential. Moreover, as a host-cell targeting drug, zapnometinib is likely to remain effective against upcoming novel variants or newly emerging zoonotic strains, which is a critical characteristic particularly considering new variants of SARS-CoV-2.

**Table 1:** In vitro data. EC50 values of zapnometinib for different viruses calculated with a Virospot or virus yield reduction assay; CC50 values determined on Calu-3 cells with a LDH cytotoxicity assay after 24 or 48 h zapnometinib treatment.

| | $EC_{50}$ (µM) / (µg/mL) | 95% CI (µM) |
|---|---|---|
| **SARS-CoV-1** | 33.6 / 13.8 | 25.5 - 43.1 |
| **SARS-CoV-2 Omicron B1.1.592** | 37.9 / 15.5 | 27.9 - 57.9 |
| **HCoV OC43** | 16.1 / 6.6 | 13.6 - 18.6 |
| **HCoV 229E** | 26.6 / 10.9 | 25.5 - 27.7 |

| | $CC_{50}$ (µM) / (µg/mL) | 95% CI (µM) |
|---|---|---|
| **24 h** | 532.1 / 217.9 | 422.7 - n/a |
| **48 h** | 471.0 / 192.9 | 439.5 - 496.6 |

*Abbreviations: $EC_{50}$, half maximal effective concentration; CI, confidence interval; SARS-CoV, severe acute respiratory syndrome coronavirus; HCoV, human coronavirus; $CC_{50}$, 50% toxic concentration*

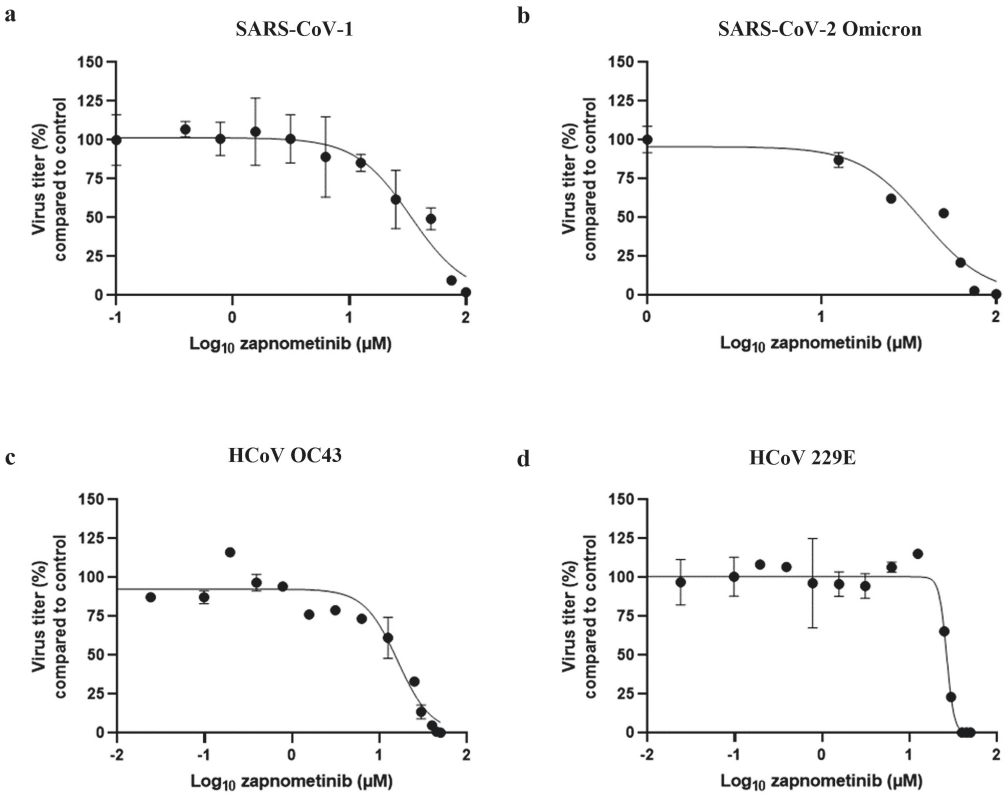


***Figure 1: Zapnometinib inhibits various coronaviruses.*** *The antiviral activity of zapnometinib against different Coronaviruses was assessed using a virus yield reduction assay (SARS-CoV-2 Omicron, HCoV OC43 and 229E) or virospot reduction assay (SARS-CoV-1) and the half-maximal effective concentration ($EC_{50}$) was calculated by plotting the viral titer (compared to control) vs. the zapnometinib concentration. The data is shown as mean with standard deviation. $n_{(SARS\text{-}CoV\text{-}1)} = 4$; $n_{(SARS\text{-}CoV\text{-}2\ Omicron)} = 3$; $n_{(HCoV\ OC43)} \geq 3$ ($n_{(control)} = 9$; $n_{(12.5,\ 25,\ 50\ \mu M)} = 6$; $n_{(0.006,\ 0.024,\ 0.098,\ 0.195,\ 0.391,\ 0.781,\ 1.563,\ 3.125,\ 6.25,\ 30,\ 40,\ 45\ \mu M)} = 3$); $n_{(HCoV\ 229E)} = 3$ or 9 (n = 9 for the control). The $EC_{50}$ values are shown in Table 1.*

### Pharmacokinetics of zapnometinib in Syrian hamsters

Next to the *in vitro* efficacy of a drug, we aimed to confirm the therapeutic potential and efficacy in *in vivo* studies. Prior to the *in vivo* efficacy study, we investigated the pharmacokinetics of zapnometinib in Syrian hamsters, a favorable animal model for SARS-CoV-2 infections, to better understand the metabolism of zapnometinib in this animal and to

determine an appropriate dose for the subsequent efficacy study. In addition, the tolerability of zapnometinib was assessed by monitoring clinical parameters such as ruffled fur, hunched back posture or lethargy. To investigate dose proportionality, clearance, and safety of zapnometinib in hamsters, single doses of 15, 30 or 60 mg/kg zapnometinib were administered p.o. to groups of 6 animals. Blood samples were collected for analysis after 30 min and after 1, 2, 4, 8, 12, and 24 h from 3 alternating animals per group. The serum concentration-time curves for all doses showed a monophasic progression following oral administration. A proportional increase was observed until the maximum observed plasma concentration ($C_{max}$) which was reached after 2 h for the 15 and 30 mg/kg doses and after 4 h for the 60 mg/kg dose (Fig. 2). Moreover, the area under the concentration-time curve (AUC) and the $C_{max}$ values increased proportionally with the dose. The apparent terminal half-life was comparable for all dose groups, ranging from 2 to 3 h (Table 2). Notably, at the highest dose (60 mg/kg), the concentration of zapnometinib after 24 h was 5.32 µg/mL (13 µM) (Table 2; Fig. 2). Based on previous work in our laboratory, 10 µg/mL (24.4 µM) is required for 50% MEK inhibition [40]. Thus, higher doses are required to attain a serum concentration exceeding 10 µg/mL at 24 h, ensuring effective and consistent MEK inhibition. Additionally, all doses were well tolerated, and no adverse events were reported following zapnometinib treatment. Therefore, based on the current data, a loading dose of 100 mg/kg followed by a daily dose of 75 mg/kg was employed for the efficacy study in the Syrian hamster infection model. This regimen was equivalent to the human dosing used in the phase 2 clinical trial, which involved a higher initial loading dose of 900 mg on day 1, followed by daily dosing with 600 mg zapnometinib. This dosing regimen ensures that the drug concentration remains above 10 µg/mL (24.4 µM) throughout the entire treatment period [40,42].

**Table 2**: Summary of pharmacokinetic parameters per dose group for zapnometinib in Syrian hamsters

| Group | Dose (mg/kg) | $C_{max}$ (ng/mL)/(µM) | $T_{max}$ (h) | AUC (h*ng/mL) | T1/2 (h) | $C_{(24\ h)}$ (ng/µL)/(µM) |
|---|---|---|---|---|---|---|
| **1 (n = 6)** | 60 | 242434 / 99.2 | 4 | 2970884 | 3.07 | 5319.1 / 2.18 |
| **2 (n = 6)** | 30 | 131720 / 53.9 | 2 | 1231900 | 2.75 | 1347.23 / 0.55 |
| **3 (n = 6)** | 15 | 85109 / 34.8 | 2 | 672365 | 2.74 | 636.91 / 0.26 |

*Abbreviations: Cmax, maximum observed plasma concentration; Tmax, time to maximum observed plasma concentration; AUC, area under the concentration-time curve; T1/2, terminal half-life; C(24 h), mean concentration at 24 h*

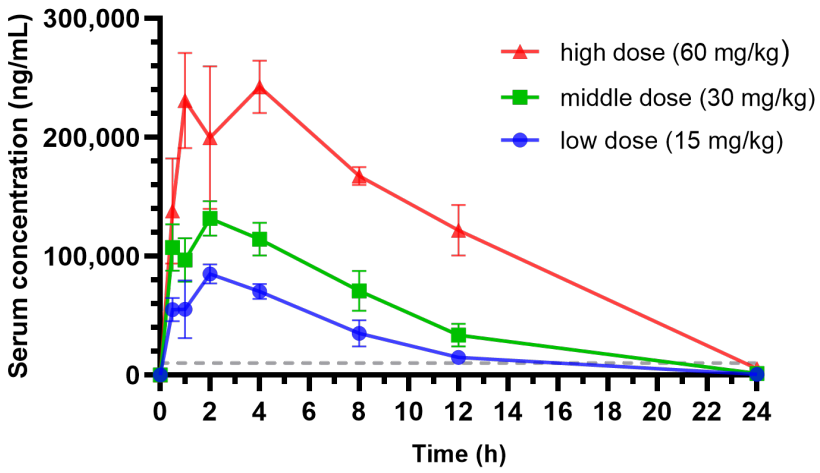


***Figure 2: Pharmacokinetic analysis of zapnometinib in Syrian hamsters.*** *Three different doses (15, 30 and 60 mg/kg) of zapnometinib were administered orally to Syrian hamsters (n = 6 per group), and serum was collected 0.5, 1, 2, 4, 8, 12 and 24 h later (alternately from 3 animals per group). The zapnometinib concentration in the serum was determined by HPLC-MS/MS. The data are presented as mean serum concentration ± SD vs. time profiles. The dashed line shows the critical plasma level for MEK inhibition (approx. 10 µg/mL = 24.4 µM).*

**Efficacy of zapnometinib in the Syrian hamster infection model**

An *in vivo* study was designed to investigate the efficacy of zapnometinib administered p.o. in SARS-CoV-2-infected hamsters. In this efficacy study, all animals were challenged with $1x10^3$ $TCID_{50}$ SARS-CoV-2 via intranasal administration, which induces both high levels of viral replication in the respiratory tract and significant histopathological changes in the lungs [50]. Control animals were treated with vehicle (5% DMSO, 15% Kolliphor in PBS) beginning at +4 h p.i., while the experimental animals were treated with the following regimen: one loading dose of 100 mg/kg zapnometinib (+4 or +24 h p.i.) followed by 75 mg/kg zapnometinib once per day until the day of sacrifice (4 dpi). During the challenge phase, the animals were weighed, clinical observations were monitored following treatment and infection, and throat swabs were taken daily (Fig. 3a). At 4 dpi, all animals were euthanized for virological and pathological analyses.

For the analysis of viral titers, throat swabs were subjected to titration to detect replication-competent virus. Additionally, they were analyzed using TaqMan-based RT-qPCR to detect viral RNA and determine the viral copy number. At 2 dpi, the viral load in the throat swabs was

comparable among all three treatment groups (Fig. 3b). At 3 dpi, the $TCID_{50}$ assay indicated that zapnometinib treatment in both treatment groups resulted in a significant reduction in the amount of replication-competent virus in the throat swabs, with reductions of 1.1 $log_{10}$ (*p = 0.0134*) and 1.3 $log_{10}$ (*p = 0.0191*) noted in the groups treated at +4 h p.i. and +24 h p.i., respectively. These results were supported by the RT-qPCR data, which demonstrated viral titer reductions (number of viral copies) of 1.1 $log_{10}$ (*p = 0.0089*) and 1.2-$log_{10}$ (*p = 0.0090*) in animals treated at +4 h p.i. and +24 h p.i., respectively, compared to control animals (Supplementary Fig. 2a). At 4 dpi, the mean viral titer was still lower in the throat swabs of drug-treated animals, although no statistically significant differences were discernible (Fig. 3b). Nevertheless, in the drug-treated animals, a clear decrease in titer over time (2 dpi, 3 dpi, 4 dpi) was observed, more pronounced than in the control animals.

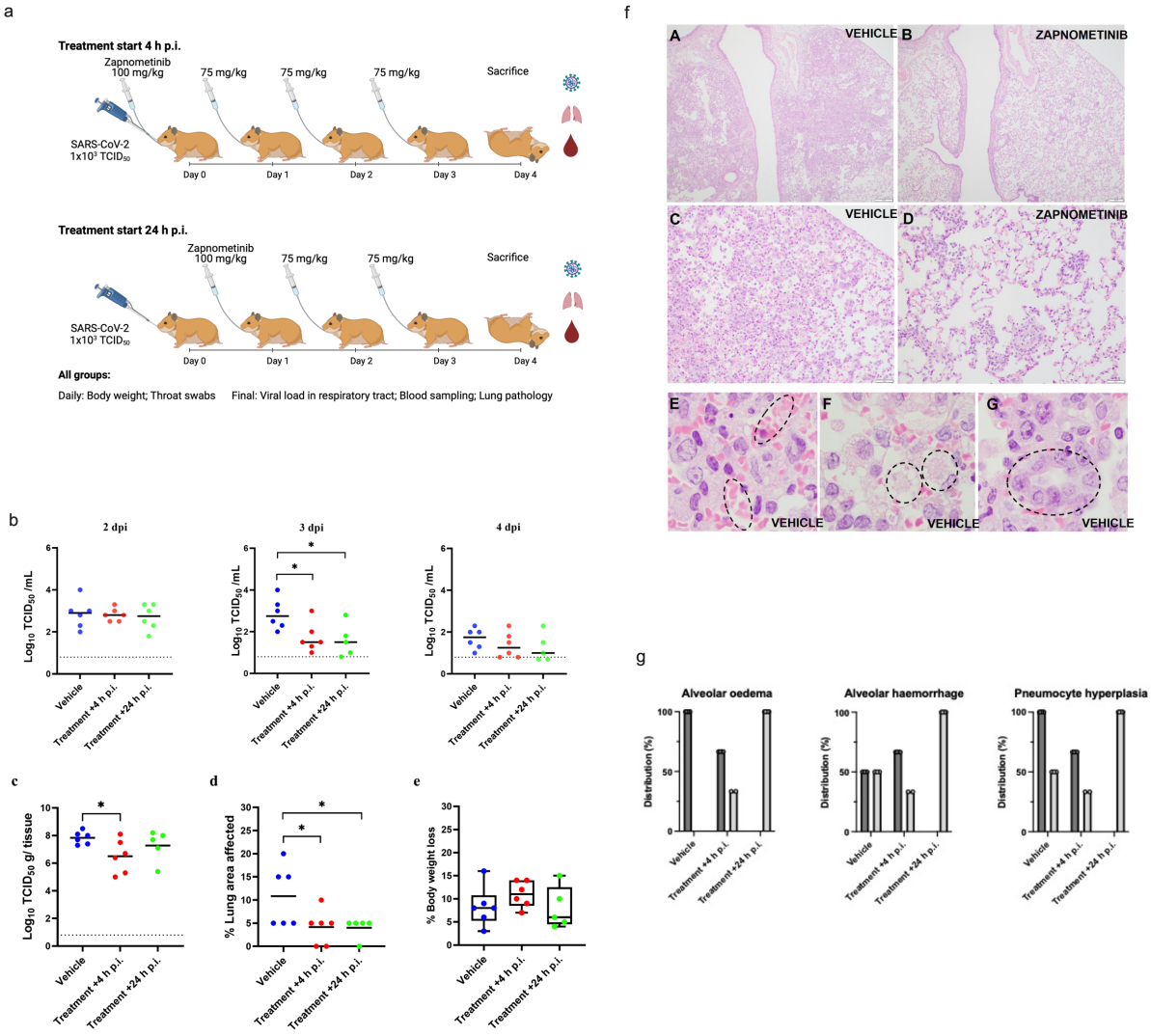

***Figure 3: Study of the efficacy of zapnometinib against SARS-CoV-2 in a Syrian hamster infection model. (a)*** *Study schedule. On day 0, all animals were infected intranasally with 1x10$^3$ $TCID_{50}$ SARS-CoV-2. Zapnometinib (100 mg/kg) was given beginning +4 h p.i. (+ control group that received vehicle) or +24 h p.i. Thereafter, both groups were treated with 75 mg/kg zapnometinib once daily and body weight was measured, and throat swabs were taken daily until sacrifice at 4 dpi. Nasal turbinate tissues were subsequently homogenized and subjected to virus titration. Blood was collected for further analysis, the lungs were inspected, and collected for histopathological examination. The study schedule was created on biorender.com.* ***(b)*** *Infectious viral titers in throat swabs collected at 2, 3 and 4 dpi expressed as $log_{10}$ $TCID_{50}$ of control (vehicle-treated) and zapnometinib-treated SARS-CoV-2-infected hamsters.* ***(c)*** *Infectious viral loads in nasal turbinates collected from control (vehicle-treated) and zapnometinib-treated SARS-CoV-2-infected hamsters at 4 dpi expressed as $log_{10}$ $TCID_{50}$ per g nasal turbinate tissue analyzed via $TCID_{50}$ assay. The dashed line represents the lower limit of detection (0.8 $log_{10}$ $TCID_{50}$/mL).* ***(d)*** *Percentage of lung area with pathological signs in control (vehicle-treated) and zapnometinib-treated SARS-CoV-2-infected hamsters at 4 dpi.* ***(e)*** *Weight loss at 4 dpi as a percentage of the body weight measured at the time of infection. Individual data (dots) and median values (horizontal lines) are presented. The whiskers represent the min. and max. values.* ***(f)*** *Representative histopathologic changes at 4 dpi in the lungs of hamsters infected with SARS-CoV-2 and treated with zapnometinib beginning at +24 h p.i. (B and D) or treated with the vehicle only (A, C, E, F, G). Hemorrhage (E), oedema (F) and type II pneumocyte hyperplasia (G) were observed in the vehicle only animals (shown in dashed circles). Hematoxylin and eosin staining; 40x magnification (A and B), 200x magnification (C and D) and 1000x (E, F, G).* ***(g)*** *Lung slides were examined and scored for the presence of alveolar hemorrhage, oedema, and type II pneumocyte hyperplasia (with: dark grey bars; without: light grey bars). Mean values are presented as percent distribution. All data are from a single experiment. The number of animals per group was as follows: $n_{(Vehicle)} = 6$; $n_{(Treatment +4 h p.i.)} = 6$; $n_{(Treatment +24 h p.i.)} = 5$. The data were analyzed by one-way ANOVA. * $p < 0.05$.*

A similar pattern was observed for the infectious viral load in the nasal turbinates at 4 dpi. Treatment starting at +4 h p.i. significantly reduced the infectious viral titer by 1.3 $log_{10}$ (*p = 0.0335*) (Fig. 3c). These data were further confirmed by RT-qPCR, which showed a reduction of 1.1 $log_{10}$ (*p = 0.0145*) when treatment was started at +4 h p.i. (Supplementary Fig. 2b). Similar results were obtained when treatment was started at +24 h p.i. resulting in a lower mean viral titer but differences were not statistically significant.

To gain further insight into how treatment affects disease progression besides its influence on viral load, the lung lesions of the infected animals were evaluated by gross pathology at 4 dpi, and the percentage of affected lung area was estimated. The percentage of lung injury in lung tissue was significantly reduced in both treated groups (*p = 0.0282* for treatment beginning at +4 h p.i., *p = 0.0314* for treatment beginning at +24 h p.i.) compared to the vehicle-treated group, indicating a beneficial effect of zapnometinib treatment (Fig. 3d). Histopathological evaluation of the lungs revealed that pulmonary changes were mostly mild in all treatment groups. However, inflammation, as indicated by the number of inflammatory cells infiltrating the tissue, consolidation of the tissue, and decreased air containing space in the tissue, was less severe in the zapnometinib-treated groups than in the vehicle-treated control group (Fig. 3f). Hamsters treated with the vehicle showed alveolitis characterized by numerous inflammatory cells, including macrophages and neutrophils in the alveolar septa and lumina, hemorrhage and oedema in the alveolar lumina and type II pneumocyte hyperplasia. In contrast, hamsters treated with zapnometinib exhibited reduced alveolitis with less cellular inflammatory infiltrate containing fewer macrophages and neutrophils and no hemorrhage, oedema, or type II pneumocyte hyperplasia (Fig. 3f). Comparing the lungs of all treatment groups revealed that alveolar oedema, seen as intraluminal proteinaceous fluid, was less frequent in animals treated beginning at +4 h p.i. than in control animals and absent in animals treated beginning at +24 h p.i. Additionally, intra-alveolar hemorrhage, suggestive of epithelial damage and observed as extravasated erythrocytes, was comparable between animals treated beginning at +4 h p.i. and vehicle-treated animals, whereas it was absent in animals treated beginning at +24 h p.i. (Fig. 3g). The alveolar epithelium showed variable scoring of hyperplasia among the different treatment groups (type II hyperplasia), which is related to regeneration and is seen as plump cuboidal epithelium in the place of the usual flatter alveolar epithelium. Animals treated beginning at +4 h p.i. were less affected, and no hyperplasia was observed in animals treated beginning at +24 h p.i. (Fig. 3g).

Significant disparities in outcomes between the two treatment regimens were not observed; however, initiating treatment earlier (+4 h p.i.) seemed to enhance the antiviral efficacy of zapnometinib in the nasal turbinates (Fig. 3c). Conversely, commencing treatment later (+24 h p.i.) exhibited slightly superior effects on certain markers of inflammation in the lungs (Fig. 3g).

In general, treatment was well tolerated in both groups, as no significant differences in weight were observed among all groups; mean body weight loss was higher than 5% and comparable among all groups (ranging from 8-11%) (Fig. 3e). In addition, no treatment-related adverse effects were observed in the zapnometinib-treated groups compared to the vehicle-treated group. Taken together, these results demonstrate that zapnometinib treatment could significantly reduce viral load in the respiratory tract and alleviate lung pathology while being well-tolerated in the Syrian hamster model.

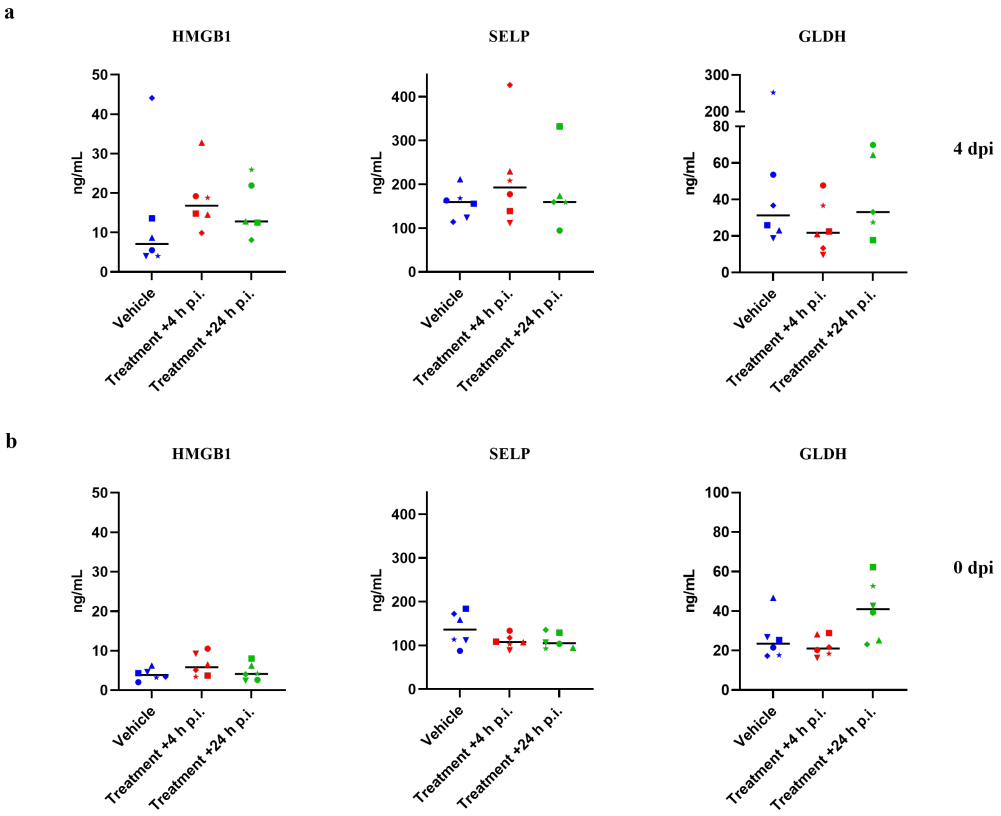


***Figure 4: Candidate safety biomarker analysis.*** *The levels of candidate biomarkers in serum samples from hamsters collected* ***a,*** *at 4 dpi after infection and zapnometinib treatment and* ***b,*** *before infection with SARS-CoV-2 (0 dpi, prior to infection and zapnometinib treatment) and were analysed by IA-LC-MS/MS. High mobility group box 1 protein (HMGB1, an indicator of necrosis), glutamate dehydrogenase (GLDH, an indicator of liver damage), and p-selectin (SELP, an indicator of endothelial damage) levels in the zapnometinib-treated and vehicle-treated groups are shown. The treatment conditions described below the graphs refer to the treatment that the animals received after infection. Individual data and median values are presented. The number of animals per group was as follows:* $n_{(Vehicle)} = 6$; $n_{(Treatment\ +4\ h\ p.i.)} = 6$; $n_{(Treatment\ +24\ h\ p.i.)} = 5$.. *The data were analysed by one-way ANOVA. P values < 0.05 were considered statistically significant.*

**Levels of drug safety biomarkers**

To further evaluate drug safety, serum samples collected pre- (0 dpi) and post-infection (4 dpi) and zapnometinib or vehicle treatment were used to assess candidate protein biomarkers indicative of organ injury. Various candidate biomarkers were analyzed to evaluate drug-induced vascular injury (DIVI) [51] and drug-induced liver injury (DILI) [51,52]. The levels of high mobility group box 1 (HMGB1; an indicator of necrosis)[53,54] and glutamate dehydrogenase (GLDH; an indicator of liver damage)[55] were measured to assess liver injury (DILI), and p-selectin (SELP) was used as an early indicator of endothelial damage to blood vessels (DIVI). There were no prominent changes in the levels of the examined biomarkers before and after infection and treatment of the animals, and the levels always remained comparable among all groups (Fig. 4). When comparing the values from day 0 to day 4, it can also be observed that there was no significant increase in the biomarkers due to the infection. Collectively, these results provide further evidence that the selected treatment regimen (100 mg/kg zapnometinib followed by 75 mg/kg beginning at +4 or +24 h p.i.) was not toxic to hamsters.

**Effect on cytokines and chemokines in preclinical models**

Besides demonstrating the antiviral efficacy, we also examined the potential immunomodulatory properties of zapnometinib. However, in the SARS-CoV-2-challenged Syrian hamster model, the levels of cytokines and chemokines increase only marginally. Therefore, the model is inappropriate for assessing alterations in cytokine and chemokine levels [56]. We confirmed this observation in serum samples from the hamsters obtained from the efficacy study using ELISA, with no major differences between the groups after infection and treatment at 4 dpi (Supplementary Fig. 3a) and in lung tissue samples analyzed by RT-qPCR from the same animals at 4 dpi (Supplementary Fig. 3b). As the effects investigated in the hamster model do not clearly show the immunomodulatory component of zapnometinib, we aimed to demonstrate a direct anti-inflammatory effect in the absence of a dynamic stimulus such as virus infection. We used an LPS-induced acute lung injury (ALI) mouse model to simulate a pathogen-induced hyperinflammatory disease with high severity. Using this virus-independent model, we could demonstrate the direct effect of zapnometinib on cytokine and chemokine expression. Mice were challenged by i.p. injection of 5 mg/kg LPS and then treated with 25 mg/kg zapnometinib 1 h post-stimulation. Alterations in cytokine and chemokine gene expression patterns were evaluated by comparing them with untreated

control mice using an $RT^2$ profiler PCR array. As depicted in the volcano plot, the expression of most of the 84 genes encoding key secreted proteins central to inflammation, such as IL-1β (*Il1b*), IL-6, MCP-1 (*ccl2*), IL-8 (*cxcl1*), IP-10 (*cxcl10*) and MIP-1α (*ccl3*), was downregulated after zapnometinib treatment compared to control treatment (Fig. 5a). Importantly, the levels of the *Ifna2* gene, encoding for IFN-α, a key regulator of the innate antiviral immune response, were not significantly downregulated (*p = 0.118*). The expression of various important genes known to be elevated in COVID-19, such as *Il6*, *Cxcl1* and *Tnf* [57] was significantly reduced in the lung tissues of zapnometinib-treated mice (Fig. 5b). These data represent the first *in vivo* confirmation of previous *in vitro* findings that zapnometinib affects the proinflammatory gene expression response while genes of the antiviral type I IFN response remain largely unaffected [36].

In addition to the animal model, we aimed to demonstrate the immunomodulatory properties of zapnometinib in a primary human cell type, specifically freshly isolated human PBMCs. PBMCs obtained from two healthy donors were challenged with 1 µg/mL LPS from *E. coli* O55:B5 (prepared in PBS) and treated with 10 µg/mL zapnometinib (prepared in 0.1% DMSO) for 6 h. Cytokine and chemokine expression analysis by ELISA confirmed the anti-inflammatory properties of zapnometinib in human PBMCs. Expression levels of IL-1β, IL-6, IL-8, IP-10, MCP-1, MIP-1α, and TNF-α were significantly reduced upon treatment with zapnometinib for 6 h compared to the untreated control group (Fig. 5c, Supplementary Fig. 4). Taken together, these experiments collectively validate the anti-inflammatory properties of zapnometinib both *in vivo* and in primary human blood cells, demonstrating a significant reduction of cytokines and chemokines known to be elevated in COVID-19.

**Effect on cytokines and chemokines in the clinical trial**

To determine whether the reduction in cytokine and chemokine levels following zapnometinib treatment was also observed in hospitalized COVID-19 patients, serum samples from six patients in each group of a randomized, double-blind, placebo-controlled proof-of-concept Phase 2 trial in adults with moderate-to-severe COVID-19 symptoms (clinical severity status CSS 3 or 4; RESPIRE; NCT04776044) were analyzed. Samples were collected at various time points from day 1 to day 30 (D1, D3, D5, D8, D11, D15 and D30) after treatment initiation using a multiplex ELISA system. Despite the absence of a pronounced inflammatory response suggestive of a cytokine storm in the patients, as reflected by their clinical severity scores

(CSS3/4), a significant reduction was observed in MCP-1 (*p = <0.0001*), MIP-1a (*p = <0.0001*), and IFNg (*p = <0.0001*) levels among individuals treated with zapnometinib compared to those in the placebo cohort throughout the study period (up to day 30). IL-6 levels were also reduced (*p = 0.0017*), while TNF-a and IL-8/CXCL-8 were not affected with a statistical significance (Fig. 6a). These results further support the findings from the pre-clinical investigations that zapnometinib treatment leads to a reduction of various pro-inflammatory cytokines and chemokines.

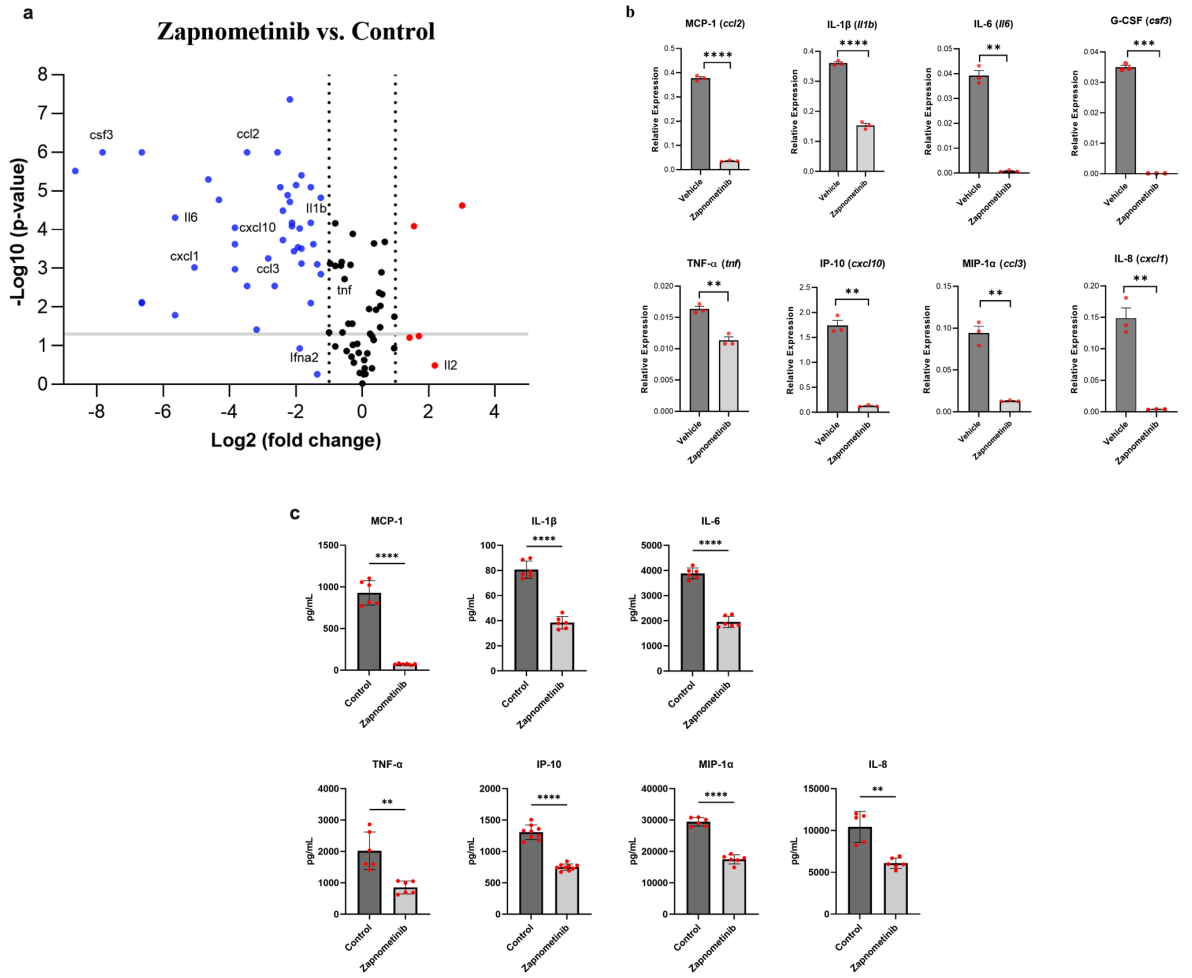


***Figure 5: The levels of cytokines and chemokines associated with COVID-19 are reduced after treatment with zapnometinib (a, b)*** *mRNA expression of different cytokines and chemokines in acute lung injury (ALI) model mice after LPS stimulation and zapnometinib treatment 1h post stimulation (control group received vehicle =1% DMSO in PBS). The mRNA levels were determined at 6 h post treatment by an RT² profiler PCR array.* ***(a)*** *The volcano plot shows gene expression changes. Representative genes mainly associated with COVID-19 are highlighted. Red: upregulation, blue: downregulation, black: no change in gene expression (regardless of statistical significance). The log₂ of*

*the fold change in gene expression is plotted on the x-axis, and statistical significance is plotted on the y-axis. The two dashed vertical lines indicate the fold change threshold, while the horizontal line indicates the p value threshold. Genes represented by data points in the far upper left (downregulated) and far upper right (upregulated) sections met the fold change and p value thresholds, while the genes represented by the data points between the two vertical lines showed no change in gene expression.* ***(b)*** *Representative expression. Mean + SD and individual values of n = 3 technical replicates are shown, gene names in brackets. The data were analyzed using the ΔΔCt method and normalized to the mean expression levels of 5 housekeeping genes. The P values for the difference in replicate (-DeltaCt) expression data for each gene between the control and treatment groups were calculated by unpaired t-test with Welch's correction. ** p < 0.01, *** p < 0.001, **** p < 0.0001.* ***(c)*** *Reduction in cytokine expression after zapnometinib treatment in LPS-stimulated human PBMCs from one healthy donor. Cells were simultaneously stimulated with 1 µg/mL LPS and treated with 10 µg/mL zapnometinib for 6 h. The expression of cytokines in the supernatants was analyzed by ELISA. The data are presented as the mean ± SD of technical replicates.* $n_{(IL\text{-}1ß;\ IL\text{-}6;\ MCP\text{-}1;\ MIP\text{-}1α;\ TNF\text{-}α)} = 6$; $n_{(IP\text{-}10)} = 9$; $n_{(IL\text{-}8\ control)} = 5$; $n_{(IL\text{-}8\ zapnometinib\text{-}treated)} = 6$. *The differences in the levels of all cytokines of interest between the control and zapnometinib-treated groups were analysed with unpaired t-test with Welch's correction. ** p < 0.01; **** p < 0.0001. Results from the second donor are shown in supplementary Figure 4.*

**Modulation of adaptive immune response in the clinical trial**

In addition to the cytokine storm observed in the hyperinflammatory stage in moderate to severe cases of COVID-19, there is also a decrease in the adaptive immune response. Therefore, we also investigated the impact of zapnometinib on the overall number of lymphocytes, as well as T and B cells, which were quantified in the blood using FACS analysis at the same time points as the cytokine analysis. Elevated levels of lymphocytes, plasma B cells, and T cells were observed in individuals undergoing treatment with zapnometinib (Fig. 6b), indicating a beneficial immune enhancement that augments the antiviral response following zapnometinib administration. Notably, a substantial 44.5% increase in lymphocyte count was documented during the 30-day observation period post zapnometinib treatment. For T cells, the increase was even more pronounced (73.7%; $p = 0.0409$). As for Plasma B cells, there was also an increase of 61.8% in favor of zapnometinib, while a reduction was found for memory B cells (-37.4%; $p = 0.0377$) (Fig. 6b). The difference in favor of zapnometinib was consistent across all observation days. Thus, we demonstrate here a positive

immunomodulatory effect of zapnometinib on both the innate and adaptive immune responses.

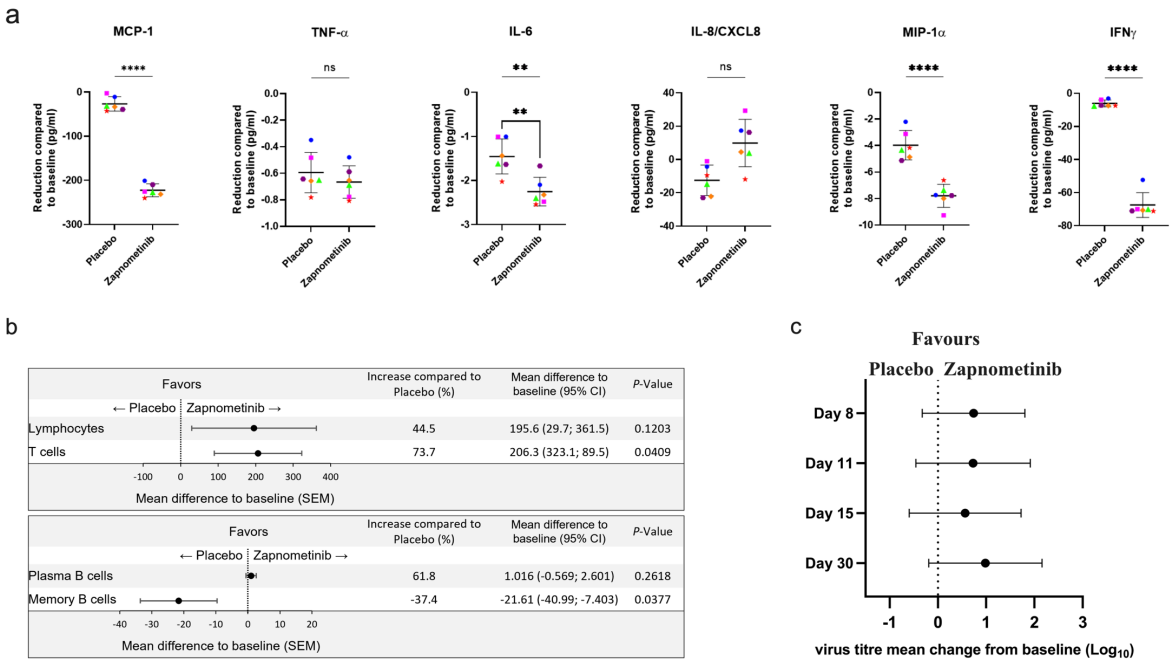


***Figure 6: Immunomodulating effects and viral load analysis of patients hospitalized with COVID-19 and treated with either zapnometinib or placebo for 6 days.*** ***(a)*** *Reduction of cytokine and chemokine expression compared to baseline values. Analysis was performed with blood from 6 patients from each group using Meso Scale V-Plex. All of them received either no standard of care treatment or antiviral treatment. Patients who received glucocorticoids as standard of care were excluded. Analysis was performed with values from the complete observation period (until day 30), horizontal line showing the mean value ± SEM of all days. Color and symbols represent the mean values of n = 6 patients on different days: blue circle = day 3, pink square = day 5; green triangle = day 8; orange rhombus = day 11, aubergine-colored hexagon = day 15, red star = day 30¨. Analysis was performed using a one-tailed t-test. ** p < 0.01; **** p < 0.0001.* ***(b)*** *Mean difference ± SEM of the number of lymphocytes, T cells, Plasma B cells, and Memory B cells compared to baseline in zapnometinib (n = 34), and placebo treated (n = 34) patients. The graphics represent values from the entire study period (D1, D3, D5, D8, D11, D15 and D30). The data were analyzed by one-tailed t-test.* ***(c)*** *RNA virus titer mean change from baseline over time in SARS-CoV-2 sputum samples from hospitalized COVID-19 patients on D8, D11, D15 and D30. The analysis only includes patients with baseline sputum SARS-CoV-2 RNA titer ≥ 500 copies/ml. Difference of mean change from zapnometinib vs. placebo treatment was given as $Log_{10}$ copies/ml ± SEM, analyzed with unpaired t-test with Welch's correction. For further details of analysis see Supplementary Table 3.*

**Antiviral effect of zapnometinib in the clinical trial**

Besides the immunomodulatory effect, the antiviral effect of zapnometinib was also investigated in patients participating in the above-mentioned clinical trial. Therefore, sputum and nasopharyngeal swabs were collected at time points D1, D3, D5, D8, D11, D15, and D30 after treatment initiation, and the viral load was quantified via RT-qPCR. In the modified intention-to-treat population, 62 out of 103 patients (60.2%) had quantifiable RNA above 500 copies/ml confirmed in nasopharyngeal samples at baseline, and 74 out of 103 patients (71.8%) had RNA above 500 copies/ml confirmed in sputum samples (Supplementary Table 3). Patients in the study received either antiviral, glucocorticoid, or no standard of care treatment, with the presence of alpha, beta, gamma, delta and omicron strains. Zapnometinib treatment was associated with greater reductions from baseline in mean viral load than placebo in sputum samples at days 8, 11, 15, and 30 (Fig. 6c and Supplementary Table 3). However, on days 3 and 5, there was only a slight reduction in favor of zapnometinib (Supplementary Table 3). In nasopharyngeal samples, greater reductions from baseline in mean viral load in favor of zapnometinib were also found, albeit to a lesser extent (Supplementary Table 3).

In summary, the positive immunomodulatory properties, and the antiviral effect of zapnometinib demonstrated in various preclinical studies were confirmed in hospitalized patients with a severe viral infection.

## Discussion

Recent cell culture studies have provided initial evidence that the MEK inhibitor zapnometinib exhibits anti-SARS-CoV-2 activity *in vitro* and downregulates the expression of candidate cytokines, suggesting a potential dual benefit in COVID-19 treatment. The present study aimed to substantiate this dual effect through extended preclinical work and further confirm it with clinical data. We evaluated whether these *in vitro* activities translate into efficacy in an infected organism, thereby assessing whether zapnometinib displays a dual therapeutic effect *in vivo*. Therefore, we analyzed the antiviral efficacy and immunomodulatory impact of zapnometinib using a well-established Syrian hamster SARS-CoV-2 infection model and in other models of hyperinflammatory infectious diseases. This study was the first attempt to demonstrate the efficacy of zapnometinib against SARS-CoV-2 *in vivo*. Further details, such as

an optimized treatment regimen, need to be clarified in further studies. Given that *in vitro* activities of antiviral compounds are not always reflected *in vivo,* it is very important that a dual effect of zapnometinib could also be demonstrated *in vivo*. This is evidenced by reduced levels of both viral RNA and infectious particles in hamster throat swabs and nasal turbinates, an ameliorative effect on lung pathology as well as the results of a clinical phase 2 trial with hospitalized COVID-19 patients. The results emphasize the therapeutic potential of zapnometinib against coronavirus infections correlated with hyperinflammatory symptoms.

Zapnometinib, a host-targeted antiviral (HTA) inhibits the cellular Raf/MEK/ERK signaling pathway that is pivotal for the replication of various viruses [58]. As of February 2024, the direct-acting antivirals (DAA) nirmatrelvir, molnupiravir and remdesivir were considered for treatment against COVID-19 [16,59-61]. In the Syrian hamster model of SARS-CoV-2 infection, zapnometinib showed a significant effect on viral load reduction at 3 dpi (Fig. 3b) comparable to that of the direct-acting nucleoside analogue molnupiravir [59]. Furthermore, zapnometinib treatment resulted in a reduction in lung pathology. Based on the data, there is no clear indication of which start of treatment (+4 h p.i. or +24 h p.i.) is ultimately more beneficial. The assessment of the precise contribution of the immunomodulatory component of zapnometinib versus the reduction in viral load to the observed positive impact on lung pathology in the hamster model remains indeterminate. Notably, an in-depth analysis of the effects on the adaptive immune response was omitted in this model. Future investigations are warranted to systematically explore and elucidate the specific mode of action of zapnometinib in this context. Nevertheless, the data from the hamster study could also substantiate the therapeutic success observed in the RESPIRE study [42]. We do not anticipate zapnometinib, being a host-targeted antiviral agent, to induce mutagenic effects on the virus. In contrast, concerns have been raised regarding the mutagenic potential of nucleoside analogue antivirals like molnupiravir and, less frequently, remdesivir, which could potentially enhance viral evolution in treating viral diseases [62-64]. This concern is not applicable to host-targeted antivirals, as they do not interfere with viral RNA replication. Another major advantage of host-targeted antivirals is their high barrier against the emergence of antiviral resistance. This is because the virus faces difficulty in compensating for the absence of cellular functions targeted by the drug. This was evidenced in a resistance study with zapnometinib compared to various direct-acting SARS-CoV-2 drugs [65]. Drug resistance to current DAAs has already

been documented, presenting a challenging problem that could potentially be mitigated by HTAs [66,67]. Given the stable nature of viral dependence on cellular factors, zapnometinib's antiviral activity is likely to remain effective against new and emerging variants. Notably, zapnometinib demonstrated efficacy against a spectrum of coronaviruses, including SARS-CoV-1, SARS-CoV-2 Omicron variant, HCoV-OC43, and HCoV-229E (Fig. 1), underscoring its broad-spectrum potential. In the phase 2 RESPIRE study, various SARS-CoV-2 variants were identified in the patients (alpha, beta, gamma, delta and omicron). The reduction in propagation observed in both omicron and non-omicron strains after zapnometinib treatment underscores the strong correlation between pre-clinical and clinical data. It is important to note that the clinical trial RESPIRE was prematurely terminated, with only 104 out of the intended 220 patients enrolled. Nevertheless, discernible trends and certain significant alterations favoring zapnometinib were evident [42]. Interestingly, no viral load reduction was observed after molnupiravir treatment in hospitalized COVID-19 patients with a similar CSS as in RESPIRE [68]. In a clinical trial involving nirmatrelvir/ritonavir (Paxlovid™) administered to hospitalized patients, no statistically significant variance was observed in the duration of SARS-CoV-2 RNA clearance or mortality rates [69]. For high-risk patients, a favorable impact on the severity of COVID-19 is delineated [70]. However, even if the two approved medications effectively reduce the incidence of hospitalizations and fatalities in non-hospitalized adults with mild-to-moderate COVID-19 in clinical trials, there remains an absence of a viable treatment option for severely ill patients, the specific patient population for which zapnometinib is intended [71-73]. The efficacy of molnupiravir and Paxlovid™ in hospitalized patients appears to be constrained. This represents a critical gap in available treatments that could potentially be addressed by the introduction of zapnometinib.

Understanding cytokine pathways is crucial for developing effective treatments, with ongoing trials exploring anti-inflammatory and antiviral drugs' potential in combating cytokine storms. Additionally, dietary interventions, such as zinc or vitamins, are being studied to regulate cytokine levels and alleviate COVID-19 symptoms. Zinc's anti-inflammatory properties are being evaluated in clinical trials to assess its impact on the immune response and disease prognosis. However, careful risk assessment is necessary for immunomodulatory approaches due to the risk of secondary infections or impairment of viral clearance [17-19].

A major emphasis of the study was to explore the immunomodulatory effects of zapnometinib *in vivo*, as a second beneficial activity alongside its antiviral action. As anticipated, no significant difference in cytokine and chemokine expression was observed at 4 dpi in the SARS-CoV-2 infected Syrian hamster, indicating its unsuitability for infection-related cytokine studies [56]. Therefore, we opted for an *in vivo* ALI model which represents a fulminant hyperinflammatory condition independent of pathogen infection dynamics. The latter model feature is crucial for distinguishing between direct anti-inflammatory actions and indirect effects primarily resulting from pathogen titers reduction. ALI is an inflammatory condition caused by pathogen infection, sepsis, trauma, ischemia, or reperfusion. The most severe form of ALI is ARDS, a clinical feature in severe COVID-19 [74]. In the ALI model, excessive inflammatory response was induced by bacterial LPS stimulation. Zapnometinib treatment led to a massive reduction in hyperinflammatory cytokine responses, highlighting its immunomodulatory potency *in vivo*. In addition, we assessed zapnometinib's effectiveness in a primary human cell model, namely freshly isolated PBMCs, where a similar cytokine reduction was observed, confirming its immunomodulatory effect.

These pre-clinical findings were confirmed in the RESPIRE study, showing significant reductions in MCP-1, MIP-1a and IFNg levels. However, the implications for IFN-γ remain uncertain as it has dual roles as both an inducer and a regulator of inflammation [75]. Notably, IL-8/CXCL8 levels increased slightly with zapnometinib treatment. CXCL8, along with CXCR1/2, triggers neutrophil activity to combat inflammation during bacterial infections [76,77]. This suggests a potentially beneficial role for increased CXCL8 levels in viral-induced inflammation. Overall, these findings highlight zapnometinib's significant anti-inflammatory potential.

In recent years, many studies have highlighted the great potential of MEK inhibitors as immunomodulators [23,78,79]. These inhibitors not only reduce excessive cytokine responses but also modulate the adaptive immune response for improved antiviral efficacy. Severe and moderate stages of COVID-19 are associated with lymphocyte depletion [80]. In the RESPIRE study, we demonstrated that treatment with zapnometinib resulted in an increase in the number of lymphocytes, including T cells and antibody-producing plasma B cells, while the quantity of memory B cells was reduced. This may serve as an initial indication that the overall count of plasma and memory cells remains unchanged following zapnometinib treatment. However, there appears to be an augmented availability of plasma cells, consequently

resulting in a diminished presence of memory B cells [81]. In summary, the positive effect on the adaptive immune response also shows the great potential of treating respiratory viral infections with a MEK inhibitor.

In some patients in the RESPIRE study, glucocorticoids were administered as part of the standard of care. Dexamethasone, a glucocorticoid commonly used to treat severe COVID-19, suppresses cytokine production by mainly targeting NF-κB signaling, as shown in animal models of LPS-induced ALI and in human PBMCs [82,83]. Additionally, dexamethasone down-regulates type I interferons (IFNs), which are crucial in the initial defense against severe viral respiratory infections [74,84,85]. A drawback of glucocorticoids is their immunosuppressive nature, which can compromise host immunity and prolong viral clearance. In addition, tocilizumab and baricitinib, two immunomodulatory agents recommended for severe COVID-19 treatment, have shown effectiveness in attenuating multiple cytokines and chemokines in animal models of ALI and in human PBMCs [86]. The study did not conclusively show a direct impact on interference with type I interferon (IFN). However, as baricitinib inhibits NF-κB, it is presumed that it may influence type I IFN expression since NF-κB plays a crucial role in their regulation [87,88]. In contrast to the NF-κB cascade, inhibiting the Raf/MEK/ERK signaling pathway, as demonstrated in this and previous studies, does not attenuate type I IFNs and downstream IFN-regulated genes [36]. This suggests that zapnometinib treatment has a notable advantage over dexamethasone, tocilizumab, and baricitinib, as it does not diminish the type I IFN response. The potential to modulate an excessive proinflammatory cytokine and chemokine response remains comparable.

Overall, the study underscores the noteworthy therapeutic potential of zapnometinib as a novel and broadly effective approach. In recent years, there have been emerging strategies employing HTAs as broad-spectrum antiviral agents, with particular emphasis on repurposing kinase inhibitors. However, most substances have only been tested in proof-of-concept studies so far [89,90]. Our dual effect represents a distinct advantage over current therapies, which typically target either the virus itself or the hyperinflammatory response. In contrast, by inhibiting the Raf/MEK/ERK signaling pathway, zapnometinib exhibits both a reduction in viral load and a modulation rather than complete suppression of the immune response [39,91]. This sets the drug apart from most, if not all, COVID-19 treatments currently licensed or in development.

The findings presented here align with our earlier studies, [36] emphasizing the potential value of zapnometinib as a standalone treatment or in combination with other drugs targeting various stages of viral infection and disease progression, a promising strategy for COVID-19 control. Furthermore, zapnometinib's implications extend beyond COVID-19, as evidenced by its recent orphan drug designation by the FDA for hantavirus infections and the initiation of a phase 2 clinical trial for influenza. The robust correlation between preclinical and clinical data for SARS-CoV-2 and COVID-19 suggests a potential treatment benefit for influenza [28,29,92]. Collectively, these findings underscore the broad-spectrum anti-infective potential of zapnometinib against acute viral infections.

## *Contributors*

Conceptualization: Y.F., SL, S.P., M.B., St.S. and O.P.; methodology: G.A., Ha.Ha., He.H., L.S., L.dW.; formal analysis: Y.F., O.P., L.dW., Ha.Ha., He.H., L.S., A.S., S.S.; investigation: Ha.Ha., He.H., L.S., L.dW.; histology: JvdB., M.D. resources: O.P.; writing – original draft: Y.F. and O.P.; writing – review & editing: Ha.Ha., L.S., He.H., O.Poe., V.A., A.S., L.dW., JvdB., Y.F., S.L., S.P. and O.P.; visualization: Ha.Ha., He.H, L.S., M.D, Y.F., O.P.; supervision: Y.F. and O.P.; project administration: Y.F., M.B., St.S. and O.P.; funding acquisition: O.P., S.L., M.B. and St.S. O.P. and Y.F. had full access to and verified all study data. All authors were given the opportunity to comment on the draft report and reviewed and approved the final version.

## *Declaration of interests*

O. Planz, S. Ludwig, S. Pleschka and M. Bauer are shareholders of Atriva Therapeutics GmbH and act as consultants for Atriva Therapeutics GmbH. Y. Füll, and S. Stenglein are employees of Atriva Therapeutics GmbH. L. Schüssele and H. Hoffmann are former employees of Atriva Therapeutics GmbH. O. Pötz is the chief executive officer and V. Anselm and A. Steinhilber are former employees of Signatope GmbH. L. de Waal and G. Amerongen are employees of Viroclinics-DDL, Cerba Research Company.

## *Acknowledgements*

The authors thank Annika Schönsiegel for coordinating the shipment of the compound and Eugenia Steinhilber for help with the manuscript.

## *Data sharing statement*

The data that support the findings of this study are available upon reasonable request from the corresponding author.

### Funding

Atriva Therapeutics GmbH, the Federal Ministry of Education and Research, Germany, DFG grants SFB1009B13 and CRU342-P6.

## References

[1] Khan M, Adil SF, Alkhathlan HZ, Tahir MN, Saif S, Khan M and Khan ST. COVID-19: A Global Challenge with Old History, Epidemiology and Progress So Far. Molecules. **2020**;26(1).

[2] O'Driscoll M, Ribeiro Dos Santos G, Wang L, Cummings DAT, Azman AS, Paireau J, Fontanet A, Cauchemez S and Salje H. Age-specific mortality and immunity patterns of SARS-CoV-2. Nature. **2021**;590(7844):140-145.

[3] Alwani M, Yassin A, Al-Zoubi RM, Aboumarzouk OM, Nettleship J, Kelly D, Al-Qudimat AR and Shabsigh R. Sex-based differences in severity and mortality in COVID-19. Rev Med Virol. **2021**;31(6):e2223.

[4] Burkert FR, Lanser L, Bellmann-Weiler R and Weiss G. Coronavirus Disease 2019: Clinics, Treatment, and Prevention. Front Microbiol. **2021**;12:761887.

[5] Wang LL, Yang JW and Xu JF. Coronavirus (SARS-CoV-2) causes lung inflammation and injury. Clin Microbiol Infect. **2021**.

[6] Leisman DE, Ronner L, Pinotti R, Taylor MD, Sinha P, Calfee CS, Hirayama AV, Mastroiani F, Turtle CJ, Harhay MO, Legrand M and Deutschman CS. Cytokine elevation in severe and critical COVID-19: a rapid systematic review, meta-analysis, and comparison with other inflammatory syndromes. Lancet Respir Med. **2020**;8(12):1233-1244.

[7] Fan S, Xiao M, Han F, Xia P, Bai X, Chen H, Zhang H, Ding X, Zhao H, Zhao J, Sun X, Jiang W, Wang C, Cao W, Guo F, Tian R, Gao P, Wu W, Ma J, Wu D, Liu Z, Zhou X, Wang J, Guan T, Qin Y, Li T, Xu Y, Zhang D, Chen Y, Xie J, Li Y, Yan X, Zhu Y, Peng B, Cui L, Zhang S and Guan H. Neurological Manifestations in Critically Ill Patients With COVID-19: A Retrospective Study. Front Neurol. **2020**;11:806.

[8] Aggarwal G, Cheruiyot I, Aggarwal S, Wong J, Lippi G, Lavie CJ, Henry BM and Sanchis-Gomar F. Association of Cardiovascular Disease With Coronavirus Disease 2019 (COVID-19) Severity: A Meta-Analysis. Curr Probl Cardiol. **2020**;45(8):100617.

[9] Shi W, Lv J and Lin L. Coagulopathy in COVID-19: Focus on vascular thrombotic events. J Mol Cell Cardiol. **2020**;146:32-40.

[10] Gustine JN and Jones D. Immunopathology of Hyperinflammation in COVID-19. Am J Pathol. **2021**;191(1):4-17.

[11] Costela-Ruiz VJ, Illescas-Montes R, Puerta-Puerta JM, Ruiz C and Melguizo-Rodriguez L. SARS-CoV-2 infection: The role of cytokines in COVID-19 disease. Cytokine Growth Factor Rev. **2020**;54:62-75.

[12] Group RC, Horby P, Lim WS, Emberson JR, Mafham M, Bell JL, Linsell L, Staplin N, Brightling C, Ustianowski A, Elmahi E, Prudon B, Green C, Felton T, Chadwick D, Rege K, Fegan C, Chappell LC, Faust SN, Jaki T, Jeffery K, Montgomery A, Rowan K, Juszczak E, Baillie JK, Haynes R and Landray MJ. Dexamethasone in Hospitalized Patients with Covid-19. N Engl J Med. **2021**;384(8):693-704.

[13] Goletti D and Cantini F. Baricitinib Therapy in Covid-19 Pneumonia - An Unmet Need Fulfilled. N Engl J Med. **2021**;384(9):867-869.

[14] Stone JH, Frigault MJ, Serling-Boyd NJ, Fernandes AD, Harvey L, Foulkes AS, Horick NK, Healy BC, Shah R, Bensaci AM, Woolley AE, Nikiforow S, Lin N, Sagar M, Schrager H, Huckins DS, Axelrod M, Pincus MD, Fleisher J, Sacks CA, Dougan M, North CM, Halvorsen YD, Thurber TK, Dagher Z, Scherer A, Wallwork RS, Kim AY, Schoenfeld S, Sen P, Neilan TG, Perugino CA, Unizony SH, Collier DS, Matza MA, Yinh JM, Bowman KA, Meyerowitz E, Zafar A, Drobni ZD, Bolster MB, Kohler M, D'Silva KM, Dau J, Lockwood MM, Cubbison C, Weber BN, Mansour MK and Investigators BBTT. Efficacy of Tocilizumab in Patients Hospitalized with Covid-19. N Engl J Med. **2020**;383(24):2333-2344.

[15] Yoon JJ, Toots M, Lee S, Lee ME, Ludeke B, Luczo JM, Ganti K, Cox RM, Sticher ZM, Edpuganti V, Mitchell DG, Lockwood MA, Kolykhalov AA, Greninger AL, Moore ML, Painter GR, Lowen AC, Tompkins SM, Fearns R, Natchus MG and Plemper RK. Orally Efficacious Broad-Spectrum Ribonucleoside Analog Inhibitor of Influenza and Respiratory Syncytial Viruses. Antimicrob Agents Chemother. **2018**;62(8).

[16] Owen DR, Allerton CMN, Anderson AS, Aschenbrenner L, Avery M, Berritt S, Boras B, Cardin RD, Carlo A, Coffman KJ, Dantonio A, Di L, Eng H, Ferre R, Gajiwala KS, Gibson SA, Greasley SE, Hurst BL, Kadar EP, Kalgutkar AS, Lee JC, Lee J, Liu W, Mason SW, Noell S, Novak JJ, Obach RS, Ogilvie K, Patel NC, Pettersson M, Rai DK, Reese MR, Sammons MF, Sathish JG, Singh RSP, Steppan CM, Stewart AE, Tuttle JB, Updyke L, Verhoest PR, Wei L, Yang Q and Zhu Y. An oral SARS-CoV-2 M(pro) inhibitor clinical candidate for the treatment of COVID-19. Science. **2021**:eabl4784.

[17] Verma G, Dhawan M, Saied AA, Kaur G, Kumar R and Emran TB. Immunomodulatory approaches in managing lung inflammation in COVID-19: A double-edge sword. Immun Inflamm Dis. **2023**;11(9):e1020.

[18] Rabaan AA, Al-Ahmed SH, Muhammad J, Khan A, Sule AA, Tirupathi R, Mutair AA, Alhumaid S, Al-Omari A, Dhawan M, Tiwari R, Sharun K, Mohapatra RK, Mitra S, Bilal M, Alyami SA, Emran TB, Moni MA and Dhama K. Role of Inflammatory Cytokines in COVID-19 Patients: A Review on Molecular Mechanisms, Immune Functions,

Immunopathology and Immunomodulatory Drugs to Counter Cytokine Storm. Vaccines (Basel). **2021**;9(5).

[19] Dhawan M, Emran TB, Priyanaka and Choudhary OP. Immunomodulatory effects of zinc and its impact on COVID-19 severity. Ann Med Surg (Lond). **2022**;77:103638.

[20] Chang F, Steelman LS, Lee JT, Shelton JG, Navolanic PM, Blalock WL, Franklin RA and McCubrey JA. Signal transduction mediated by the Ras/Raf/MEK/ERK pathway from cytokine receptors to transcription factors: potential targeting for therapeutic intervention. Leukemia. **2003**;17(7):1263-93.

[21] Lieske NV, Tonby K, Kvale D, Dyrhol-Riise AM and Tasken K. Targeting Tuberculosis and HIV Infection-Specific Regulatory T Cells with MEK/ERK Signaling Pathway Inhibitors. PLoS One. **2015**;10(11):e0141903.

[22] Nakayama T and Yamashita M. The TCR-mediated signaling pathways that control the direction of helper T cell differentiation. Seminars in immunology. **2010**;22(5):303-9.

[23] Verma V, Jafarzadeh N, Boi S, Kundu S, Jiang Z, Fan Y, Lopez J, Nandre R, Zeng P, Alolaqi F, Ahmad S, Gaur P, Barry ST, Valge-Archer VE, Smith PD, Banchereau J, Mkrtichyan M, Youngblood B, Rodriguez PC, Gupta S and Khleif SN. MEK inhibition reprograms CD8(+) T lymphocytes into memory stem cells with potent antitumor effects. Nat Immunol. **2021**;22(1):53-66.

[24] Moss P. The T cell immune response against SARS-CoV-2. Nat Immunol. **2022**;23(2):186-193.

[25] Zhu Q, Xu Y, Wang T and Xie F. Innate and adaptive immune response in SARS-CoV-2 infection-Current perspectives. Front Immunol. **2022**;13:1053437.

[26] Ram T, Singh AK, Kumar A, Singh H, Pathak P, Grishina M, Khalilullah H, Jaremko M, Emwas A-H, Verma A and Kumar P. MEK inhibitors in cancer treatment: structural insights, regulation, recent advances and future perspectives [10.1039/D3MD00145H]. RSC Medicinal Chemistry. **2023**.

[27] Pleschka S, Wolff T, Ehrhardt C, Hobom G, Planz O, Rapp UR and Ludwig S. Influenza virus propagation is impaired by inhibition of the Raf/MEK/ERK signalling cascade [Research Support, Non-U.S. Gov't]. Nat Cell Biol. **2001**;3(3):301-5.

[28] Laure M, Hamza H, Koch-Heier J, Quernheim M, Muller C, Schreiber A, Muller G, Pleschka S, Ludwig S and Planz O. Antiviral efficacy against influenza virus and pharmacokinetic analysis of a novel MEK-inhibitor, ATR-002, in cell culture and in the mouse model. Antiviral research. **2020**;178:104806.

[29] Hamza H, Shehata MM, Mostafa A, Pleschka S and Planz O. Improved in vitro Efficacy of Baloxavir Marboxil Against Influenza A Virus Infection by Combination Treatment With the MEK Inhibitor ATR-002. Front Microbiol. **2021**;12:611958.

[30] Planz O, Pleschka S and Ludwig S. MEK-specific inhibitor U0126 blocks spread of Borna disease virus in cultured cells [Research Support, Non-U.S. Gov't]. J Virol. **2001**;75(10):4871-7.

[31] Preugschas HF, Hrincius ER, Mewis C, Tran GVQ, Ludwig S and Ehrhardt C. Late activation of the Raf/MEK/ERK pathway is required for translocation of the respiratory syncytial virus F protein to the plasma membrane and efficient viral replication. Cell Microbiol. **2019**;21(1):e12955.

[32] Cai Y, Liu Y and Zhang X. Suppression of coronavirus replication by inhibition of the MEK signaling pathway. J Virol. **2007**;81(2):446-56.

[33] Valencia HJ, de Aguiar M, Costa MA, Mendonca DC, Reis EV, Arias NEC, Drumond BP and Bonjardim CA. Evaluation of kinase inhibitors as potential therapeutics for flavivirus infections. Arch Virol. **2021**;166(5):1433-1438.

[34] Lee S, Yang W, Kim DK, Kim H, Shin M, Choi KU, Suh DS, Kim YH, Hwang TH and Kim JH. Inhibition of MEK-ERK pathway enhances oncolytic vaccinia virus replication in doxorubicin-resistant ovarian cancer. Mol Ther Oncolytics. **2022**;25:211-224.

[35] Ndjomou J, Park IW, Liu Y, Mayo LD and He JJ. Up-regulation of hepatitis C virus replication and production by inhibition of MEK/ERK signaling. PLoS One. **2009**;4(10):e7498.

[36] Schreiber A, Viemann D, Schöning J, Schloer S, Mecate Zambrano A, Brunotte L, Faist A, Schöfbänker M, Hrincius E, Hoffmann H, Hoffmann M, Pöhlmann S, Rescher U, Planz O and Ludwig S. The MEK1/2-inhibitor ATR-002 efficiently blocks SARS-CoV-2 propagation and alleviates pro-inflammatory cytokine/chemokine responses. Cell Mol Life Sci. **2022**;79(1):65.

[37] Schreiber A, Ambrosy B, Planz O, Schloer S, Rescher U and Ludwig S. The MEK1/2 Inhibitor ATR-002 (Zapnometinib) Synergistically Potentiates the Antiviral Effect of Direct-Acting Anti-SARS-CoV-2 Drugs. Pharmaceutics. **2022**;14(9).

[38] Schrader T, Dudek SE, Schreiber A, Ehrhardt C, Planz O and Ludwig S. The clinically approved MEK inhibitor Trametinib efficiently blocks influenza A virus propagation and cytokine expression. Antiviral research. **2018**;157:80-92.

[39] Pinto R, Herold S, Cakarova L, Hoegner K, Lohmeyer J, Planz O and Pleschka S. Inhibition of influenza virus-induced NF-kappaB and Raf/MEK/ERK activation can reduce both virus titers and cytokine expression simultaneously in vitro and in vivo. Antiviral Res. **2011**;92(1):45-56.

[40] Koch-Heier J, Schonsiegel A, Waidele LM, Volk J, Full Y, Wallasch C, Canisius S, Burnet M and Planz O. Pharmacokinetics, Pharmacodynamics and Antiviral Efficacy of the MEK Inhibitor Zapnometinib in Animal Models and in Humans. Front Pharmacol. **2022**;13:893635.

[41] Full Y, Wallasch C, Hilton A and Planz O. Pharmacokinetics, absorption, distribution, metabolism and excretion of the MEK inhibitor zapnometinib in rats. Front Pharmacol. **2022**;13:1050193.

[42] Rohde G, Stenglein S, Prozesky H, Manudhane G, Sandulescu O, Bauer M, Overend T, Koch W, Neuschwander D, Planz O, Torres A and Witzenrath M. Efficacy and safety of zapnometinib in hospitalised adult patients with COVID-19 (RESPIRE): a randomised, double-blind, placebo-controlled, multicentre, proof-of-concept, phase 2 trial. eClinicalMedicine. **2023**:102237.

[43] Koch-Heier J, Hoffmann H, Schindler M, Lussi A and Planz O. Inactivation of SARS-CoV-2 through Treatment with the Mouth Rinsing Solutions ViruProX((R)) and BacterX((R)) Pro. Microorganisms. **2021**;9(3).

[44] Zekri L, Ruetalo N, Christie M, Walker C, Manz T, Rammensee HG, Salih HR, Schindler M and Jung G. Novel ACE2 fusion protein with adapting activity against SARS-CoV-2 variants in vitro. Front Immunol. **2023**;14:1112505.

[45] Zielinska E, Liu D, Wu HY, Quiroz J, Rappaport R and Yang DP. Development of an improved microneutralization assay for respiratory syncytial virus by automated plaque counting using imaging analysis. Virol J. **2005**;2:84.

[46] Corman VM, Landt O, Kaiser M, Molenkamp R, Meijer A, Chu DK, Bleicker T, Brunink S, Schneider J, Schmidt ML, Mulders DG, Haagmans BL, van der Veer B, van den Brink S, Wijsman L, Goderski G, Romette JL, Ellis J, Zambon M, Peiris M, Goossens H, Reusken C, Koopmans MP and Drosten C. Detection of 2019 novel coronavirus (2019-nCoV) by real-time RT-PCR. Euro Surveill. **2020**;25(3).

[47] Watterson D, Wijesundara DK, Modhiran N, Mordant FL, Li Z, Avumegah MS, McMillan CL, Lackenby J, Guilfoyle K, van Amerongen G, Stittelaar K, Cheung ST, Bibby S, Daleris M, Hoger K, Gillard M, Radunz E, Jones ML, Hughes K, Hughes B, Goh J, Edwards D, Scoble J, Pearce L, Kowalczyk L, Phan T, La M, Lu L, Pham T, Zhou Q, Brockman DA, Morgan SJ, Lau C, Tran MH, Tapley P, Villalon-Letelier F, Barnes J, Young A, Jaberolansar N, Scott CA, Isaacs A, Amarilla AA, Khromykh AA, van den Brand JM, Reading PC, Ranasinghe C, Subbarao K, Munro TP, Young PR and Chappell KJ. Preclinical development of a molecular clamp-stabilised subunit vaccine for severe acute respiratory syndrome coronavirus 2. Clin Transl Immunology. **2021**;10(4):e1269.

[48] Steinhilber AE, Schmidt FF, Naboulsi W, Planatscher H, Niedzwiecka A, Zagon J, Braeuning A, Lampen A, Joos TO and Poetz O. Mass Spectrometry-Based Immunoassay for the Quantification of Banned Ruminant Processed Animal Proteins in Vegetal Feeds. Anal Chem. **2018**;90(6):4135-4143.

[49] Anselm V, Sommersdorf C, Carrasco-Triguero M, Katavolos P, Planatscher H, Steinhilber A, Joos T and Poetz O. Matrix and Sampling Effects on Quantification of Protein Biomarkers of Drug-Induced Liver Injury. J Proteome Res. **2021**;20(11):4985-4994.

[50] Munoz-Fontela C, Dowling WE, Funnell SGP, Gsell PS, Riveros-Balta AX, Albrecht RA, Andersen H, Baric RS, Carroll MW, Cavaleri M, Qin C, Crozier I, Dallmeier K, de Waal L, de Wit E, Delang L, Dohm E, Duprex WP, Falzarano D, Finch CL, Frieman MB, Graham BS, Gralinski LE, Guilfoyle K, Haagmans BL, Hamilton GA, Hartman AL, Herfst S, Kaptein SJF, Klimstra WB, Knezevic I, Krause PR, Kuhn JH, Le Grand R, Lewis MG, Liu WC, Maisonnasse P, McElroy AK, Munster V, Oreshkova N, Rasmussen AL, Rocha-Pereira J, Rockx B, Rodriguez E, Rogers TF, Salguero FJ, Schotsaert M, Stittelaar KJ, Thibaut HJ, Tseng CT, Vergara-Alert J, Beer M, Brasel T, Chan JFW, Garcia-Sastre A, Neyts J, Perlman S, Reed DS, Richt JA, Roy CJ, Segales J, Vasan SS, Henao-Restrepo AM and Barouch DH. Animal models for COVID-19. Nature. **2020**;586(7830):509-515.

[51] Bendjama K, Guionaud S, Aras G, Arber N, Badimon L, Bamberger U, Bratfalean D, Brott D, David M, Doessegger L, Firat H, Gallas JF, Gautier JC, Hoffmann P, Kraus S, Padro T, Saadoun D, Szczesny P, Thomann P, Vilahur G, Lawton M and Cacoub P. Translation strategy for the qualification of drug-induced vascular injury biomarkers. Toxicol Pathol. **2014**;42(4):658-71.

[52] Church RJ, Kullak-Ublick GA, Aubrecht J, Bonkovsky HL, Chalasani N, Fontana RJ, Goepfert JC, Hackman F, King NMP, Kirby S, Kirby P, Marcinak J, Ormarsdottir S, Schomaker SJ, Schuppe-Koistinen I, Wolenski F, Arber N, Merz M, Sauer JM, Andrade RJ, van Bommel F, Poynard T and Watkins PB. Candidate biomarkers for the diagnosis and prognosis of drug-induced liver injury: An international collaborative effort. Hepatology. **2019**;69(2):760-773.

[53] Scaffidi P, Misteli T and Bianchi ME. Release of chromatin protein HMGB1 by necrotic cells triggers inflammation. Nature. **2002**;418(6894):191-5.

[54] Zemskova M, McClain N, Niihori M, Varghese MV, James J, Rafikov R and Rafikova O. Necrosis-Released HMGB1 (High Mobility Group Box 1) in the Progressive Pulmonary Arterial Hypertension Associated With Male Sex. Hypertension. **2020**;76(6):1787-1799.

[55] Schomaker S, Potter D, Warner R, Larkindale J, King N, Porter AC, Owens J, Tomlinson L, Sauer JM, Johnson K and Aubrecht J. Serum glutamate dehydrogenase activity enables early detection of liver injury in subjects with underlying muscle impairments. PLoS One. **2020**;15(5):e0229753.

[56] Nouailles G, Wyler E, Pennitz P, Postmus D, Vladimirova D, Kazmierski J, Pott F, Dietert K, Muelleder M, Farztdinov V, Obermayer B, Wienhold SM, Andreotti S, Hoefler T, Sawitzki B, Drosten C, Sander LE, Suttorp N, Ralser M, Beule D, Gruber AD, Goffinet C, Landthaler M, Trimpert J and Witzenrath M. Temporal omics analysis in Syrian hamsters unravel cellular effector responses to moderate COVID-19. Nat Commun. **2021**;12(1):4869.

[57] Del Valle DM, Kim-Schulze S, Huang HH, Beckmann ND, Nirenberg S, Wang B, Lavin Y, Swartz TH, Madduri D, Stock A, Marron TU, Xie H, Patel M, Tuballes K, Van Oekelen O, Rahman A, Kovatch P, Aberg JA, Schadt E, Jagannath S, Mazumdar M, Charney AW, Firpo-Betancourt A, Mendu DR, Jhang J, Reich D, Sigel K, Cordon-Cardo C, Feldmann

M, Parekh S, Merad M and Gnjatic S. An inflammatory cytokine signature predicts COVID-19 severity and survival. Nat Med. **2020**;26(10):1636-1643.

[58] Pleschka S. RNA viruses and the mitogenic Raf/MEK/ERK signal transduction cascade. Biological chemistry. **2008**;389(10):1273-82.

[59] Rosenke K, Hansen F, Schwarz B, Feldmann F, Haddock E, Rosenke R, Barbian K, Meade-White K, Okumura A, Leventhal S, Hawman DW, Ricotta E, Bosio CM, Martens C, Saturday G, Feldmann H and Jarvis MA. Orally delivered MK-4482 inhibits SARS-CoV-2 replication in the Syrian hamster model. Nat Commun. **2021**;12(1):2295.

[60] Abdelnabi R, Boudewijns R, Foo CS, Seldeslachts L, Sanchez-Felipe L, Zhang X, Delang L, Maes P, Kaptein SJF, Weynand B, Vande Velde G, Neyts J and Dallmeier K. Comparing infectivity and virulence of emerging SARS-CoV-2 variants in Syrian hamsters. Ebiomedicine. **2021**;68:103403.

[61] Ye ZW, Yuan S, Chan JF, Zhang AJ, Yu CY, Ong CP, Yang D, Chan CC, Tang K, Cao J, Poon VK, Chan CC, Cai JP, Chu H, Yuen KY and Jin DY. Beneficial effect of combinational methylprednisolone and remdesivir in hamster model of SARS-CoV-2 infection. Emerg Microbes Infect. **2021**;10(1):291-304.

[62] Kosakovsky Pond SL and Martin D. Anti-COVID drug accelerates viral evolution. Nature. **2023**;623(7987):486-487.

[63] Gandhi S, Klein J, Robertson AJ, Pena-Hernandez MA, Lin MJ, Roychoudhury P, Lu P, Fournier J, Ferguson D, Mohamed Bakhash SAK, Catherine Muenker M, Srivathsan A, Wunder EA, Jr., Kerantzas N, Wang W, Lindenbach B, Pyle A, Wilen CB, Ogbuagu O, Greninger AL, Iwasaki A, Schulz WL and Ko AI. De novo emergence of a remdesivir resistance mutation during treatment of persistent SARS-CoV-2 infection in an immunocompromised patient: a case report. Nat Commun. **2022**;13(1):1547.

[64] Standing JF, Buggiotti L, Guerra-Assuncao JA, Woodall M, Ellis S, Agyeman AA, Miller C, Okechukwu M, Kirkpatrick E, Jacobs AI, Williams CA, Roy S, Martin-Bernal LM, Williams R, Smith CM, Sanderson T, Ashford FB, Emmanuel B, Afzal ZM, Shields A, Richter AG, Dorward J, Gbinigie O, Van Hecke O, Lown M, Francis N, Jani B, Richards DB, Rahman NM, Yu LM, Thomas NPB, Hart ND, Evans P, Andersson M, Hayward G, Hood K, Nguyen-Van-Tam JS, Little P, Hobbs FDR, Khoo S, Butler C, Lowe DM, Breuer J and Group PV. Randomized controlled trial of molnupiravir SARS-CoV-2 viral and antibody response in at-risk adult outpatients. Nat Commun. **2024**;15(1):1652.

[65] Schreiber A, Rodner F, Oberberg N, Anhlan D, Bletz S, Mellmann A, Planz O and Ludwig S. The host-targeted antiviral drug Zapnometinib exhibits a high barrier to the development of SARS-CoV-2 resistance. Antiviral Res. **2024**;225:105840.

[66] Ip JD, Wing-Ho Chu A, Chan WM, Cheuk-Ying Leung R, Umer Abdullah SM, Sun Y and Kai-Wang To K. Global prevalence of SARS-CoV-2 3CL protease mutations associated with nirmatrelvir or ensitrelvir resistance. Ebiomedicine. **2023**;91:104559.

[67] Hu Y, Lewandowski EM, Tan H, Zhang X, Morgan RT, Zhang X, Jacobs LMC, Butler SG, Gongora MV, Choy J, Deng X, Chen Y and Wang J. Naturally Occurring Mutations of SARS-CoV-2 Main Protease Confer Drug Resistance to Nirmatrelvir. ACS Cent Sci. **2023**;9(8):1658-1669.

[68] Arribas JR, Bhagani S, Lobo SM, Khaertynova I, Mateu L, Fishchuk R, Park WY, Hussein K, Kim SW, Ghosn J, Brown ML, Zhang Y, Gao W, Assaid C, Grobler JA, Strizki J, Vesnesky M, Paschke A, Butterton JR and Anda CD. Randomized Trial of Molnupiravir or Placebo in Patients Hospitalized with Covid-19. NEJM Evidence. **2022**;1(2):EVIDoa2100044.

[69] Liu J, Pan X, Zhang S, Li M, Ma K, Fan C, Lv Y, Guan X, Yang Y, Ye X, Deng X, Wang Y, Qin L, Xia Z, Ge Z, Zhou Q, Zhang X, Ling Y, Qi T, Wen Z, Huang S, Zhang L, Wang T, Liu Y, Huang Y, Li W, Du H, Chen Y, Xu Y, Zhao Q, Zhao R, Annane D, Qu J and Chen D. Efficacy and safety of Paxlovid in severe adult patients with SARS-Cov-2 infection: a multicenter randomized controlled study. Lancet Reg Health West Pac. **2023**;33:100694.

[70] Najjar-Debbiny R, Gronich N, Weber G, Khoury J, Amar M, Stein N, Goldstein LH and Saliba W. Effectiveness of Paxlovid in Reducing Severe Coronavirus Disease 2019 and Mortality in High-Risk Patients. Clin Infect Dis. **2023**;76(3):e342-e349.

[71] Wan EYF, Yan VKC, Wong ZCT, Chui CSL, Lai FTT, Li X, Wong CKH, Hung IFN, Lau CS, Wong ICK and Chan EWY. Effectiveness of molnupiravir vs nirmatrelvir-ritonavir in non-hospitalised and hospitalised patients with COVID-19: a target trial emulation study. EClinicalMedicine. **2023**;64:102225.

[72] Brown AN, Lang Y, Zhou J, Franco EJ, Hanrahan KC, Bulitta JB and Drusano GL. Why Molnupiravir Fails in Hospitalized Patients. mBio. **2022**;13(6):e0291622.

[73] Jayk Bernal A, Gomes da Silva MM, Musungaie DB, Kovalchuk E, Gonzalez A, Delos Reyes V, Martin-Quiros A, Caraco Y, Williams-Diaz A, Brown ML, Du J, Pedley A, Assaid C, Strizki J, Grobler JA, Shamsuddin HH, Tipping R, Wan H, Paschke A, Butterton JR, Johnson MG, De Anda C and Group MO-OS. Molnupiravir for Oral Treatment of Covid-19 in Nonhospitalized Patients. N Engl J Med. **2022**;386(6):509-520.

[74] Sinha S, Rosin NL, Arora R, Labit E, Jaffer A, Cao L, Farias R, Nguyen AP, de Almeida LGN, Dufour A, Bromley A, McDonald B, Gillrie MR, Fritzler MJ, Yipp BG and Biernaskie J. Dexamethasone modulates immature neutrophils and interferon programming in severe COVID-19. Nat Med. **2022**;28(1):201-211.

[75] Zhang J. Yin and yang interplay of IFN-gamma in inflammation and autoimmune disease. J Clin Invest. **2007**;117(4):871-3.

[76] Hartl D, Latzin P, Hordijk P, Marcos V, Rudolph C, Woischnik M, Krauss-Etschmann S, Koller B, Reinhardt D, Roscher AA, Roos D and Griese M. Cleavage of CXCR1 on neutrophils disables bacterial killing in cystic fibrosis lung disease. Nat Med. **2007**;13(12):1423-30.

[77] Ha H, Debnath B and Neamati N. Role of the CXCL8-CXCR1/2 Axis in Cancer and Inflammatory Diseases. Theranostics. **2017**;7(6):1543-1588.

[78] Li D, March ME, Gutierrez-Uzquiza A, Kao C, Seiler C, Pinto E, Matsuoka LS, Battig MR, Bhoj EJ, Wenger TL, Tian L, Robinson N, Wang T, Liu Y, Weinstein BM, Swift M, Jung HM, Kaminski CN, Chiavacci R, Perkins JA, Levine MA, Sleiman PMA, Hicks PJ, Strausbaugh JT, Belasco JB, Dori Y and Hakonarson H. ARAF recurrent mutation causes central conducting lymphatic anomaly treatable with a MEK inhibitor. Nature medicine. **2019**;25(7):1116-1122.

[79] Houde N, Beuret L, Bonaud A, Fortier-Beaulieu SP, Truchon-Landry K, Aoidi R, Pic E, Alouche N, Rondeau V, Schlecht-Louf G, Balabanian K, Espeli M and Charron J. Fine-tuning of MEK signaling is pivotal for limiting B and T cell activation. Cell Rep. **2022**;38(2):110223.

[80] Silva MJA, Ribeiro LR, Lima KVB and Lima L. Adaptive immunity to SARS-CoV-2 infection: A systematic review. Front Immunol. **2022**;13:1001198.

[81] Khodadadi L, Cheng Q, Radbruch A and Hiepe F. The Maintenance of Memory Plasma Cells. Front Immunol. **2019**;10:721.

[82] Mokra D, Mikolka P, Kosutova P and Mokry J. Corticosteroids in Acute Lung Injury: The Dilemma Continues. Int J Mol Sci. **2019**;20(19).

[83] Held HD, Boettcher S, Hamann L and Uhlig S. Ventilation-induced chemokine and cytokine release is associated with activation of nuclear factor-kappaB and is blocked by steroids. Am J Respir Crit Care Med. **2001**;163(3 Pt 1):711-6.

[84] Gessani S, McCandless S and Baglioni C. The glucocorticoid dexamethasone inhibits synthesis of interferon by decreasing the level of its mRNA. J Biol Chem. **1988**;263(16):7454-7.

[85] McCoy CE, Carpenter S, Palsson-McDermott EM, Gearing LJ and O'Neill LA. Glucocorticoids inhibit IRF3 phosphorylation in response to Toll-like receptor-3 and -4 by targeting TBK1 activation. J Biol Chem. **2008**;283(21):14277-85.

[86] Ibrahim YF, Moussa RA, Bayoumi AMA and Ahmed AF. Tocilizumab attenuates acute lung and kidney injuries and improves survival in a rat model of sepsis via down-regulation of NF-kappaB/JNK: a possible role of P-glycoprotein. Inflammopharmacology. **2020**;28(1):215-230.

[87] Marconi VC, Ramanan AV, de Bono S, Kartman CE, Krishnan V, Liao R, Piruzeli MLB, Goldman JD, Alatorre-Alexander J, de Cassia Pellegrini R, Estrada V, Som M, Cardoso A, Chakladar S, Crowe B, Reis P, Zhang X, Adams DH, Ely EW and Group C-BS. Efficacy and safety of baricitinib for the treatment of hospitalised adults with COVID-19 (COV-BARRIER): a randomised, double-blind, parallel-group, placebo-controlled phase 3 trial. Lancet Respir Med. **2021**;9(12):1407-1418.

[88] Zhou Q, Zhang L, Dong Y, Wang Y, Zhang B, Zhou S, Huang Q, Wu T and Chen G. The role of SARS-CoV-2-mediated NF-kappaB activation in COVID-19 patients. Hypertens Res. **2024**;47(2):375-384.

[89] Schor S and Einav S. Repurposing of Kinase Inhibitors as Broad-Spectrum Antiviral Drugs. DNA Cell Biol. **2018**;37(2):63-69.

[90] Kumar N, Sharma S, Kumar R, Tripathi BN, Barua S, Ly H and Rouse BT. Host-Directed Antiviral Therapy. Clin Microbiol Rev. **2020**;33(3).

[91] Wang ZQ, Wu DC, Huang FP and Yang GY. Inhibition of MEK/ERK 1/2 pathway reduces pro-inflammatory cytokine interleukin-1 expression in focal cerebral ischemia. Brain Res. **2004**;996(1):55-66.

[92] Hoffmann H, Ebensperger M, Schönsiegel A, Hamza H, Koch-Heier J, Schreiber A, Ludwig S, Schindler M and Planz O. Influenza A virus replication has a stronger dependency on Raf/MEK/ERK signaling pathway activity than SARS-CoV-2 [Original Research]. Frontiers in Cellular and Infection Microbiology. **2023**;13.

## *Supplementary material*

### Supplementary Materials and Methods

#### Cytotoxicity assessment and $CC_{50}$ determination

In parallel to the *in vitro* antiviral assays, cytotoxicity was analyzed for the corresponding assay conditions using LDH release assay (CyQUANT™ LDH cytotoxicity assay Kit, # 16270972, Fisher Scientific) according to the manufacturer´s protocol. Briefly, 3 µL of cell culture medium supernatant after compound treatment on Vero cells or Vero E6 cells (as described in section "Virospot reduction assay") were diluted in 297 µL LDH storage buffer. The samples were transferred to a 96-well plate, mixed and incubated with the reaction mix for 30 minutes and analyzed by colorimetric read-out in a microplate reader at 490 nm. Maximum LDH release control was cells treated with lysis buffer as described in the manufacturer´s protocol.

The concentrations used in the assays (up to 100 µM) did not reach 50% cytotoxicity, so $CC_{50}$ values were further determined in another experiment using the CyQUANT™ LDH Cytotoxicity Kit (Cat# C20301, Fisher Scientific) following the manufacturer's instructions. In short, $2x10^4$ Calu-3 cells were seeded per well in 96-well cell culture plates in IMDM medium containing 10% FBS, 100 units/mL penicillin, and 100 µg/mL streptomycin two days before treatment. Prior to the treatment, the medium was removed, and the cells were washed once with PBS. The cells were subsequently treated in quadruplicates with 600, 500, 400, 350, 300, 250, 200, 150, or 100 µM zapnometinib dissolved in DMSO and diluted in IMDM medium containing 5% FBS, 100 units/mL penicillin, and 100 µg/mL streptomycin. The DMSO concentration upon treatment was 1%. A DMSO control was supplied with 1% DMSO (without zapnometinib). An untreated control (spontaneous LDH release control) was supplied with cell culture medium (5% FBS). Viability assessment with LDH assay was performed after 24 and 48 h treatment. Therefore, 10 µL 10X Lysis Buffer were added to one well of each quadruplicate treatment set (maximum LDH release control) and the plates were incubated for 45 min at 37 °C and 5% $CO_2$. 50 µL reaction mix were added to the wells of a fresh 96-well plate, and 50 µL cell culture supernatant was transferred from the treated cells to the wells containing Reaction Mix. After 30 min incubation in the dark at RT, 50 µL stop solution were added to the wells and the absorbance was read at 490 nm and 680 nm. The absorbance measured at 680 nm was

subtracted from the absorbance at 490 nm and the %Viability was calculated using the following formula:

%Viability = 100-((compound-treated LDH release - spontaneous LDH release)/(Maximum LDH release - spontaneous LDH release))*100.

The $CC_{50}$ was determined by plotting the viability values (on the y-axis) against the corresponding $log_{10}$ transformed zapnometinib concentrations (on the x-axis) and interpolating the zapnometinib concentration at 50 % viability using the "interpolate a standard curve (Sigmoidal, 4PL, X is log(concentration)" function of the GraphPad Prism software v9.

**Cytokine and chemokine analysis**

Eleven- to thirteen-week-old male Syrian hamsters (Janvier, France) with a body weight of 113-148 g were infected on day 0 intranasally with SARS-CoV-2 ($1x10^3$ median tissue culture infectious dose ($TCID_{50}$) BetaCoV/Munich/BavPat1/2020) in a total volume of 0.1 mL PBS divided between the nostrils. Zapnometinib (100 mg/kg) was administered p.o. at 4 or 24 h p.i. and the animals in both groups were treated thereafter with 75 mg/kg zapnometinib once daily. The animals in the control group received vehicle (5% DMSO, 15% Kolliphor, 80% PBS) 4 h p.i. and thereafter once daily. Serum samples were collected from hamsters before infection (0 dpi) and at 4 dpi, and the levels of different cytokines and chemokines (IL1-β, TNF-α, IL-6, and IP-10) were analyzed by ELISA (Assay Genie, Ireland). ELISA was performed according to the manufacturer's instructions. Briefly, the serum samples and standards were added to ELISA plates precoated with specific antibodies against the cytokines of interest. Biotinylated detection antibodies binding to the cytokines of interest were added to the wells followed by a horseradish peroxidase (HRP)-streptavidin conjugate binding to the biotinylated detection antibodies. Unbound cytokines, detection antibodies, and HRP-streptavidin conjugate were removed by washing. Tetramethylbenzidine (TMB) substrate was added and the color change in the wells was used as a readout for the ELISA. The optical density (OD) at 450 nm was read. Cytokine and chemokine concentrations were calculated following the manufacturer's instructions for interpolating unknown concentrations from a standard curve.

RNA samples derived from hamster lung tissue at 4 dpi from the efficacy study (animals were infected and treated as described above) provided by Viroclinics Xplore were subjected to

gDNA digestion using RNase-free DNase I set (Qiagen, Hilden, Germany) and cleaned with RNeasy Mini kit (Qiagen) according to the manufacturer's instruction. Five primer sets for the TNF-α, IL-6, IL-1β, IP-10, and RPL-18 genes were designed according to the sequences available in GenBank. After evaluating the specificity of the primers by melting curve analysis, in one-step RT-qPCR SYBR Green assay, and agarose gel electrophoresis, real-time one-step multiplex RT-qPCR was carried out using an ultrafast QuantiNova multiplex RT-qPCR kit according to the manufacturer's instructions to evaluate alterations in gene expression. The data were analyzed according to the ΔΔCq method, and relative expression was calculated based on the formula "relative expression = $2^{Cq(ref) - Cq(target)}$".

Statistical analyses were performed using GraphPad Prism software (version 8) (GraphPad Software, San Diego, California, USA). Differences in cytokine and chemokine expression were analyzed using ANOVA, details are described in the corresponding figure legends. P values < 0.05 were considered statistically significant.

**Candidate biomarker analysis**

The candidate protein biomarkers were quantified via specific peptides analyzed by immunoaffinity liquid chromatography-tandem mass spectrometry (IA-LC-MS/MS) assays. For proteolysis, 10 µL of each serum sample was mixed with 50 µL of digestion buffer (100 mM triethanolamine and 0.5% (w/v) n-octylglucoside (NOG)), and proteolysis reagents were added to achieve a final sample volume of 100 µL. The proteolysis procedure included denaturation at 99 °C for 5 minutes, reduction in 5 mM tris(2-carboxyethyl)-phosphine at 22 °C for 5 minutes, alkylation in 10 mM iodoacetamide at 22 °C for 20 minutes and an overnight enzymatic fragmentation at 37 °C with a trypsin-to-protein ratio of 1:20 (assuming a concentration of 60 mg/mL protein in serum). The proteolysis was inactivated by heating at 99 °C for 5 minutes and addition of phenylmethanesulfonylfluoride to a final concentration of 10 mM. For subsequent peptide-targeted immunoaffinity enrichment, a mixture of stable isotope-labeled standard (SIS) peptides with known concentrations was added to the proteolyzed samples as internal standards (Intavis AG, Tuebingen, Germany). Peptide-specific antibodies were generated as described previously [1] and added to the proteolyzed samples for immunoaffinity enrichment. Semiautomated immunoprecipitation was performed with a magnetic particle processor (KingFisher 96, Thermo Fisher Scientific, Waltham, USA) as

described previously [2]. Chromatography and mass spectrometry were performed as previously described [3].

The following peptide transitions were monitored in the mass spectrometer: HGGTIPVVPTAEFQDR (GLDH), endogenous 575.30 (p+++) ® 482.23 (y8+) and SIS 578.63 (p+++) ® 487.23 (y8+), collision energy (CE) 19.6 V; GEHPGLSIGDVAK (HMGB1), endogenous 640.34 (p++) ® 956.54 (y10+), SIS 644.34 (p++) ® 964.56 (y10+), CE 33.4 V; and HFTDLVAIQNK (SELP), endogenous 643.35 (p++) ®573.34 (y5+), SIS 647.36 (p++) ® 581.45 (y5+), CE 36.5 V.

Subsequently, the acquired MRM data files were imported into Skyline software version 19.1 [4]. The peak areas of endogenous and SIS peptides were extracted. The unknown analyte concentration was calculated by referencing the peak area of endogenous signal to the spiked internal standard with a known concentration. Protein concentrations were calculated by converting the quantified peptide concentration (fmol/µL) into a mass concentration (ng/mL) considering the molecular weight of the corresponding protein. The molecular weight of each protein was calculated according to the amino acid sequence, which was inferred from UniProt release 2019_04 (FASTA sequence), and the theoretical molecular weight was calculated using the corresponding amino acid sequence with the online tool ProtParam [5].

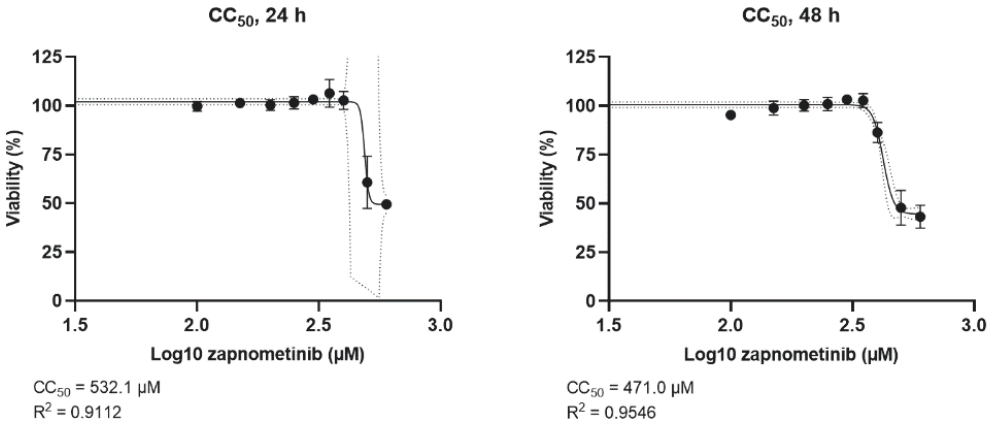


***Supplementary Figure 1. In vitro $CC_{50}$ assessment of zapnometinib.*** *The 50% cytotoxic concentration ($CC_{50}$) was determined on Calu-3 cells in a LDH cytotoxicity assay. The cells were treated with 100-600 µM zapnometinib or were left untreated (control). Viability assessment with LDH assay was performed after 24 and 48 h treatment. The %Viability was calculated and the $CC_{50}$ was determined by plotting the viability vs. the zapnometinib concentration. The data is shown as mean with standard deviation. $n_{(24\ h,\ 200\text{-}500\ \mu M\ and\ control)} = 9$; $n_{(24\ h,\ 100,\ 150,\ and\ 600\ \mu M)} = 6$; $n_{(48\ h,\ 200\text{-}600\ \mu M\ and\ control)} = 9$; $n_{(48\ h,\ 100\ and\ 150\ \mu M)} = 6$.*

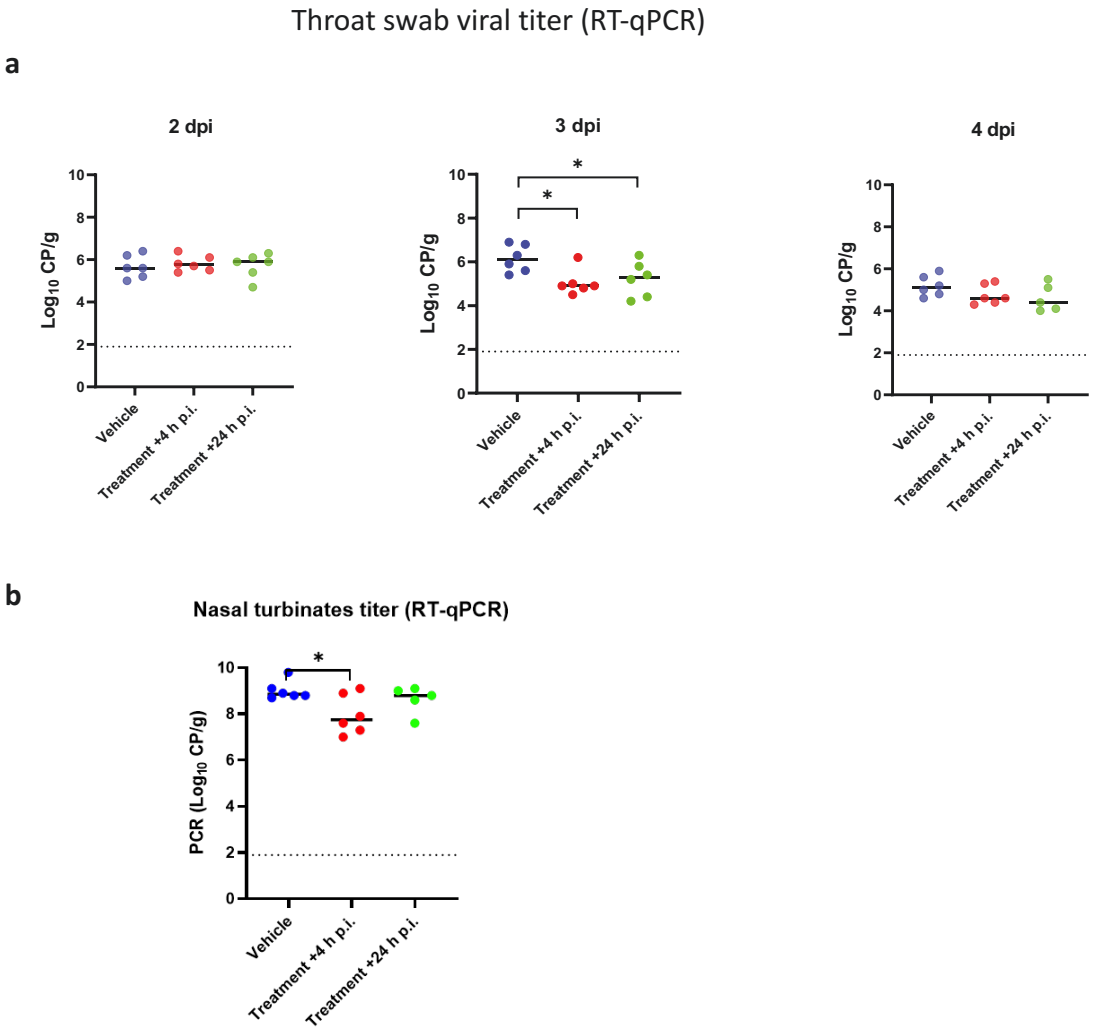


***Supplementary Figure 2. Viral titers analyzed by RT-qPCR in samples of Syrian hamsters infected with SARS-Cov-2 and treated with zapnometinib. (a)*** *Infectious viral titers in throat swabs collected at 2, 3 and 4 dpi of control (vehicle-treated) and zapnometinib-treated SARS-CoV-2-infected hamsters expressed as $Log_{10}$ genome copies per g determined by RT-qPCR.* ***(b)*** *Infectious viral loads in nasal turbinates collected from control (vehicle-treated) and zapnometinib-treated SARS-CoV-2-infected hamsters at 4 dpi expressed as $Log_{10}$ copies per g determined by RT-qPCR. The dashed lines represent the lower limit of detection (1.9 $log_{10}$ CP/mL). Mean and individual values are shown. The data were analyzed by one-way ANOVA. * $p < 0.05$.*

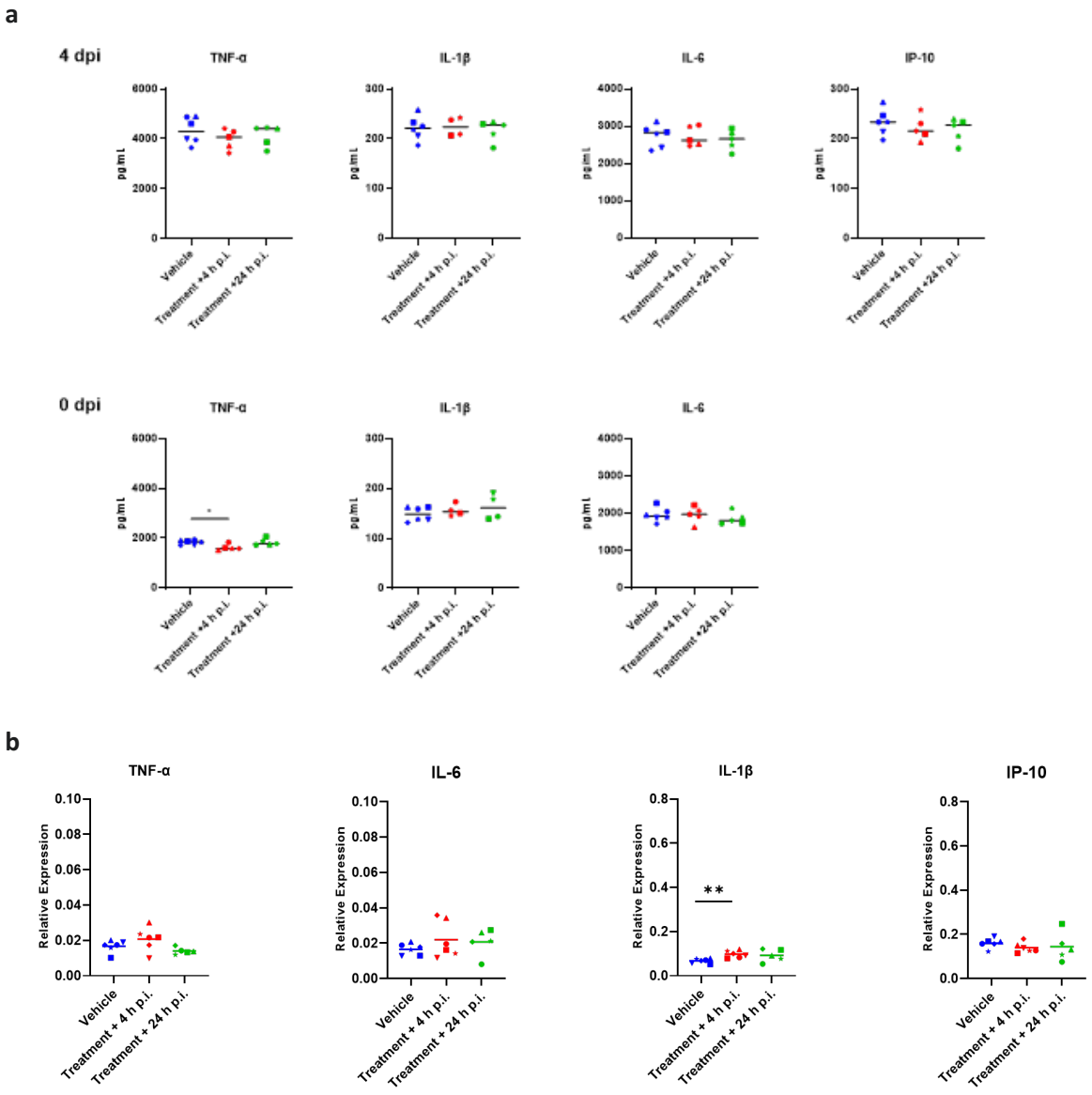


***Supplementary Figure 3. Cytokine and chemokine levels in Syrian hamsters before and after SARS-CoV-2 infection and zapnometinib treatment.*** *Animals were infected on day 0 (0 dpi) with SARS-CoV-2. Zapnometinib (100 mg/kg) was administered p.o. at 4 or 24 h p.i. and the animals in both groups were treated thereafter with 75 mg/kg zapnometinib once daily, control group received vehicle (5% DMSO, 15% Kolliphor, 80% PBS) 4 h p.i. and thereafter once daily.* ***(a)*** *Cytokine levels in serum samples collected at 0 dpi (before infection and treatment, bottom row) and 4 dpi (top row) from vehicle-treated and zapnometinib-treated Syrian hamsters from the efficacy study analyzed by ELISA are shown. The treatment conditions described below the graphs refer to the treatment that the animals received after infection. The cytokine level of each animal and the mean values of each treatment group are presented (horizontal line).* $n_{(vehicle)} = 6$; $n_{(Treatment +4 h p.i.)} = 5$ *or* $4$ *(n = 4 for analysis of IL-1β levels at 4 dpi and 0 dpi);* $n_{(Treatment +24 h p.i.)} = 5$ *or* $4$ *(n = 4 for analysis of IL-1β levels at 0 dpi). Differences between the vehicle and*

*treatment groups were not statistically significant at 4 dpi (Brown-Forsythe ANOVA with the Dunnett T3 correction). Only the TNF-α level at 0 dpi was significantly different between the group that would later be treated with vehicle and the group that would later be treated with zapnometinib at 4 h p.i. (adjusted p value = 0.0415; Brown-Forsythe ANOVA with the Dunnett T3 correction).* ***(b)*** *Relative mRNA expression of different cytokines and chemokines in lung tissue of Syrian hamsters after SARS-CoV-2 infection and zapnometinib treatment**.** mRNA levels were determined using one-step multiplex RT-qPCR in lung samples collected after sacrifice at 4 dpi. The data were analyzed based on the ΔΔCt method, and gene expression was normalized to the expression of the RPL-18 gene as a housekeeping gene. The data are presented as individual values with the mean values of the 6 (Vehicle and Treatment +4 h p.i.) or 5 animals (Treatment +24 h p.i.) per group (n = 3 technical replicates). P values of replicate 2^(-ΔCt) expression values for each gene between the control and treatment groups were calculated by one-way ANOVA and the Kruskal-Wallis test. ** p < 0.01.*

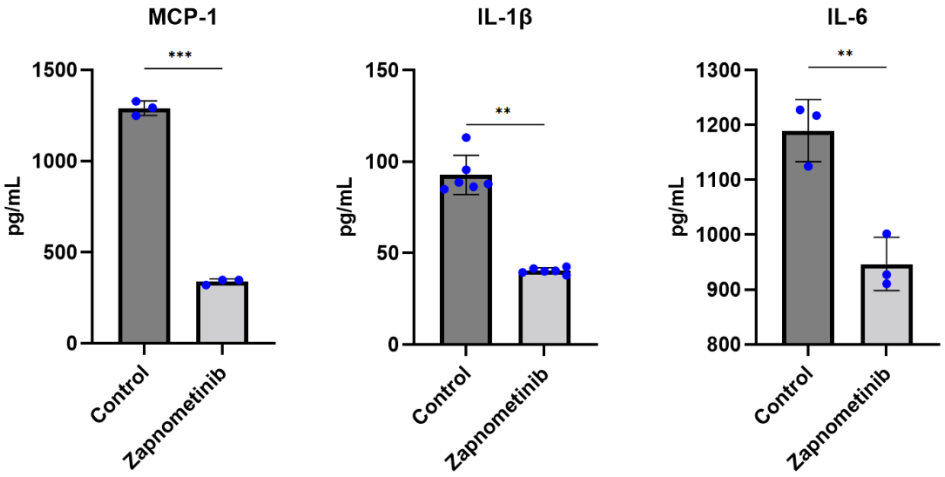


***Supplementary Figure 4. The levels of cytokines and chemokines associated with COVID-19 are reduced after treatment with zapnometinib in human PBMCs.*** *Reduction in cytokine expression after zapnometinib treatment in LPS-stimulated human PBMCs from a second healthy donor. Cells were simultaneously stimulated with 1 µg/mL LPS from E. coli O55:B5 and treated with 10 µg/mL zapnometinib for 6 h. The expression of cytokines in the supernatants was analyzed by ELISA. The data are presented as individual values (dots) and the mean ± SD of technical replicates. $n_{(MCP-1,\ IL-6)}$ = 3; $n_{(IL-1\beta)}$ = 6. The differences in the levels of all cytokines of interest between the control and zapnometinib-treated groups were analyzed with unpaired t-test with Welch's correction if data were normally distributed, otherwise with Mann-Whitney test. ** p > 0.01; *** p > 0.001.*

**Supplementary Table 1**: Oligonucleotide sequences of primers and probes used for the RT–qPCR assays.

| Target gene | Primer/Probe | Sequence (5`-3`) | Reference |
|---|---|---|---|
| TNF | ha_TNF-F | CCCACGTTGTAGCAAACCAC | This study (Hamster) |
| | ha_TNF-R | TTTGAGAGACATGCCGTTGG | |
| | ha_TNF-P | [6FAM] AGCCATCGTGCCAATGCCCT [BHQ1] | |
| IL-6 | ha_IL-6-F | TCAGAGCACCATCAAAACCC | |
| | ha_IL-6-R | TTGGCCACTCCTTTTGTGAC | |
| | ha_IL-6-P | [6FAM] AGCCCAACCTCCAAGGCCAT [BHQ1] | |
| IL-1b | ha_IL-1b-F | TCATCTTTGAAGAAGAGCCCATC | |
| | ha_IL-1b-R | TGTTCTGTCCGTTGAGATGGAG | |
| | ha_IL-1b-P | [6FAM] TCGTGCTGTCTGACCCCTGTGA [BHQ1] | |
| IP-10 | ha_IP-10-F | ATGGTCACATCAGCTGCTATCC | |
| | ha_IP-10-R | AGTTGGGGACTCTTGTCACTG | |
| | ha_IP-10-P | [6FAM] TTCTCCAGGACGATGGGCAGCT [BHQ1] | |
| RPL-18 | ha_RPL-18-F | CAAGATCCTCACCTTTGACCAG | |
| | ha_RPL-18-R | GAGCGGACATAGGGTTTGGTA | |
| | ha_RPL-18-P | [CY5] TGGCACTGTGCTCCTGTCTGGT [BHQ2] | |
| E gene | E_Sarbeco_F<br>E_Sarbeco_R<br>E_Sarbeco_P1 | ACAGGTACGTTAATAGTTAATAGCGT<br>ATATTGCAGCAGTACGCACACA<br>ACACTAGCCATCCTTACTGCGCTTCG | Corman et al. 2020 |
| **SARS-CoV-2 2019 & Omicron variant** | | | |
| N gene | 2019-CoV2-N1F | AACACAAGCTTTCGGCAGAC | This study |
| | 2019-CoV2-N1R | ATTCCGAAGAACGCTGAAGC | |
| | 2019-CoV2-N1P | [6FAM] ACATTGGCCGCAAATTGCACAA [BHQ1] | |
| **HCoV-229E** | | | |
| N gene | HCoV229E-N1F | AAAGCCACGGTGGAAAAGAC | This study |
| | HCoV229E-N1R | AACACCATTGGCCACAACAC | |
| | HCoV229E-N1P | [6FAM] TGGCCCCAGAGACCTTGACCA [BHQ1] | |
| **HCoV-OC43** | | | |
| NS2 gene | HCoVOC43-NS2F | ATTGGCCATTGCACCATAGC | This study |
| | HCoVOC43-NS2R | TTCAAGTCTAGCCGGTGATGAG | |
| | HCoVOC43-NS2P | [6FAM] TCACGGATGCAGCACTGTCCA [BHQ1] | |

**Supplementary Table 2:** Cytotoxicity run (LDH release assay) in parallel to *in vitro* antiviral assay (Virospot reduction assay).

| Cells\Conc.(µM) | 100.00 | 75.00 | 50.00 | 25.00 | 12.50 | 6.25 | 3.13 | 1.56 | 0.78 | 0.39 |
|---|---|---|---|---|---|---|---|---|---|---|
| Vero 24 h 5% FBS | 1.44 | 0.83 | 0.49 | 0.12 | 0.31 | 0.02 | -0.37 | 0.41 | 0.41 | 0.35 |
| Vero E6 24 h 5% FBS | 0.26 | 0.24 | 0.02 | -0.04 | 0.09 | 0.13 | 0.39 | 0.15 | 0.17 | 0.22 |

Data is presented as %LDH release compared to maximum LDH release (cells treated with lysis buffer) set as 100%, each compound concentration was tested in duplicate per cell line.

**Supplementary Table 3**: Mean viral titer and mean change from baseline (Day 0) over time (Day 3 – Day 30) in SARS-CoV-2 RNA titer from nasopharyngeal and sputum samples (all randomized MITT population) from patients of the RESPIRE clinical trial treated either with zapnometinib or placebo D1 - D6.

**Nasopharyngeal**

| Visit | Zapnometinib | | | Placebo | | | Zapnometinib - Placebo | | |
|---|---|---|---|---|---|---|---|---|---|
| | n | Baseline Mean | Mean Change[a] (SD) | n | Baseline Mean | Mean Change[a] (SD) | Diff. | (95% CI) | p-value |
| **SARS-CoV-2 RNA titer (log10 copies/ml) in participants overall** | | | | | | | | | |
| Baseline | 31 | 5.55 | | 30 | 5.02 | | | | |
| Day 3 | 31 | 4.78 | 0.77 (1.51) | 30 | 3.88 | 1.14 (1.37) | -0.36 | -1.104 to 0.375 | 0.1639 |
| Day 5 | 27 | 3.78 | 1.79 (1.64) | 29 | 3.27 | 1.68 (1.48) | 0.11 | -0.728 to 0.950 | 0.3960 |
| Day 8 | 24 | 2.78 | 2.84 (1.59) | 28 | 2.70 | 2.32 (1.59) | 0.53 | -0.349 to 1.404 | 0.1162 |
| Day 11 | 22 | 2.42 | 3.16 (1.82) | 22 | 2.18 | 2.87 (1.39) | 0.29 | -0.700 to 1.273 | 0.2803 |
| Day 15 | 25 | 2.16 | 3.55 (1.79) | 28 | 1.89 | 3.06 (1.57) | 0.49 | -0.443 to 1.428 | 0.1477 |
| Day 30 | 24 | 1.93 | 3.89 (1.60) | 23 | 1.76 | 3.14 (1.61) | 0.75 | -0.195 to 1.687 | 0.0586 |
| **SARS-CoV-2 RNA titer non omicron (log10 copies/ml) in participants overall** | | | | | | | | | |
| Baseline | 17 | 4.72 | | 17 | 4.62 | | | | |
| Day 3 | 17 | 3.67 | 1.05 (1.42) | 17 | 3.43 | 1.19 (1.46) | -0.14 | -1.148 to 0.863 | 0.3874 |
| Day 5 | 15 | 2.85 | 1.72 (1.58) | 16 | 2.85 | 1.62 (1.48) | 0.10 | -1.025 to 1.226 | 0.4280 |
| Day 8 | 13 | 2.21 | 2.50 (1.52) | 15 | 2.14 | 2.43 (1.38) | 0.07 | -1.065 to 1.210 | 0.4482 |
| Day 11 | 11 | 2.43 | 2.03 (1.64) | 12 | 2.16 | 2.74 (1.17) | -0.71 | -1.968 to 0.551 | 0.1263 |
| Day 15 | 13 | 2.24 | 2.45 (1.65) | 15 | 2.08 | 2.35 (1.14) | 0.10 | -1.031 to 1.234 | 0.4269 |
| Day 30 | 12 | 2.00 | 2.83 (1.27) | 12 | 1.90 | 2.55 (1.12) | 0.29 | -0.736 to 1.292 | 0.2874 |
| **SARS-CoV-2 RNA titer omicron (log10 copies/ml) in participants overall** | | | | | | | | | |
| Baseline | 14 | 7.10 | | 13 | 5.54 | | | | |
| Day 3 | 14 | 6.65 | 0.44 (1.60) | 13 | 4.47 | 1.07 (1.31) | -0.63 | -1.786 to 0.528 | 0.1366 |
| Day 5 | 12 | 5.51 | 1.87 (1.78) | 13 | 3.79 | 1.75 (1.54) | 0.12 | -1.261 to 1.510 | 0.4269 |
| Day 8 | 11 | 4.09 | 3.25 (1.64) | 13 | 3.35 | 2.19 (1.77) | 1.06 | -0.382 to 2.505 | 0.0707 |
| Day 11 | 11 | 3.07 | 4.29 (1.18) | 10 | 2.19 | 3.04 (1.68) | 1.25 | -0.100 to 2.608 | **0.0336** |

| | | | | | | | | | | | |
|---|---|---|---|---|---|---|---|---|---|---|---|
| Day 15 | 12 | 2.86 | 4.74 | (1.02) | 13 | 1.66 | 3.88 | (1.64) | 0.87 | -0.264 to 1.995 | 0.0628 |
| Day 30 | 12 | 2.60 | 4.94 | (1.13) | 11 | 1.61 | 3.78 | (1.85) | 1.16 | -0.209 to 2.530 | **0.0457** |

**Sputum**

| Visit | Zapnometinib | | | | Placebo | | | | Zapnometinib - Placebo | | |
|---|---|---|---|---|---|---|---|---|---|---|---|
| | n | Baseline Mean | Mean Change[a] | (SD) | n | Baseline Mean | Mean Change[a] | (SD) | Difference | (95% CI) | p-value |
| **SARS-CoV-2 RNA titer (log10 copies/ml) in participants overall** | | | | | | | | | | | |
| Baseline | 37 | 6.85 | | | 34 | 6.46 | | | | | |
| Day 3 | 36 | 5.79 | 1.08 | (2.08) | 34 | 5.51 | 0.94 | (1.98) | 0.14 | -0.827 to 1.112 | 0.3854 |
| Day 5 | 34 | 5.40 | 1.48 | (1.98) | 31 | 5.01 | 1.38 | (1.56) | 0.10 | -0.785 to 0.977 | 0.4145 |
| Day 8 | 31 | 4.04 | 2.81 | (1.98) | 27 | 4.35 | 2.07 | (1.99) | 0.74 | -0.308 to 1.785 | 0.0814 |
| Day 11 | 28 | 3.39 | 3.68 | (2.18) | 25 | 3.39 | 2.95 | (2.00) | 0.73 | -0.426 to 1.883 | 0.1054 |
| Day 15 | 30 | 2.98 | 3.93 | (2.19) | 4 | 3.74 | 3.36 | (2.11) | 0.56 | -0.570 to 1,697 | 0.1619 |
| Day 30 | 27 | 2.26 | 4.74 | (1.81) | 24 | 2.47 | 3.75 | (2.23) | 0.97 | -0.175 to 2.102 | **0.0476** |
| **SARS-CoV-2 RNA titer non omicron (log10 copies/ml) in participants overall** | | | | | | | | | | | |
| Baseline | 24 | 6.75 | | | 21 | 6.42 | | | | | |
| Day 3 | 23 | 5.80 | 1.16 | (2.25) | 21 | 5.47 | 0.96 | (1.90) | 0.21 | -1.057 to 1.472 | 0.3709 |
| Day 5 | 23 | 5.60 | 1.28 | (2.09) | 18 | 5.24 | 1.07 | (1.28) | 0.21 | -0.867 to 1.278 | 0.3501 |
| Day 8 | 20 | 4.24 | 2.63 | (2.26) | 15 | 5.26 | 1.06 | (1.55) | 1.57 | 0.261 to 2.883 | **0.0101** |
| Day 11 | 17 | 3.61 | 3.62 | (2.62) | 14 | 4.05 | 2.20 | (2.17) | 1,42 | -0.341 to 3.174 | 0.0551 |
| Day 15 | 19 | 3.43 | 3.59 | (2.47) | 16 | 3.74 | 2.40 | (2.08) | 1.18 | -0.385 to 2.744 | 0.0672 |
| Day 30 | 16 | 2.52 | 4.61 | (1.92) | 14 | 2.61 | 3.37 | (2.16) | 1.24 | -0.311 to 2.797 | 0.0561 |
| **SARS-CoV-2 RNA titer omicron (log10 copies/ml) in participants overall** | | | | | | | | | | | |
| Baseline | 13 | 7.02 | | | 13 | 6.51 | | | | | |
| Day 3 | 13 | 5.78 | 0.94 | (1.82) | 13 | 5.59 | 0.92 | (2.19) | 0.02 | -1.608 to 1.656 | 0.4881 |
| Day 5 | 11 | 5.04 | 1.91 | (1.75) | 13 | 4.69 | 1.82 | (1.86) | 0.09 | -1.442 to 1.618 | 0.4532 |
| Day 8 | 11 | 3.73 | 3.12 | (1.36) | 12 | 3.21 | 3.32 | (3.32) | -0.20 | -1.579 to 1.171 | 0.3801 |
| Day 11 | 11 | 3.10 | 3.77 | (1.38) | 11 | 2.57 | 3.90 | (1.31) | -0.13 | -1.326 to 1.066 | 0.4115 |
| Day 15 | 11 | 2.31 | 4.52 | (1.56) | 12 | 1.90 | 4.64 | (1.39) | -0.13 | -1.410 to 1.162 | 0.4216 |
| Day 30 | 11 | 1.95 | 4.92 | (1.71) | 10 | 2.28 | 4.34 | (2.15) | 0.58 | -1.222 to 2.380 | 0.2534 |

Analysis only includes patients with baseline nasopharyngeal or sputum SARS-CoV-2 RNA titer ≥ 500 copies/ml. Baseline results below this limit were excluded from the analysis.

[a]Mean change from baseline values are based on the measurements from patients with values at both baseline and at the time point assessed.

**Supplementary Table 4**: List of genes from the RT² Profiler™ Mouse Cytokines & Chemokines array (PAMM-150ZR, Qiagen) analyzed in the ALI mouse model and presented in the volcano plot (Fig. 5a).

| Position | Refseq | Symbol | Description | RT2 Catalog |
|---|---|---|---|---|
| A01 | NM_009605 | Adipoq | Adiponectin, C1Q and collagen domain containing | **PPM05260A** |
| A02 | NM_007553 | Bmp2 | Bone morphogenetic protein 2 | **PPM03753A** |
| A03 | NM_007554 | Bmp4 | Bone morphogenetic protein 4 | **PPM02998F** |
| A04 | NM_007556 | Bmp6 | Bone morphogenetic protein 6 | **PPM04429F** |
| A05 | NM_007557 | Bmp7 | Bone morphogenetic protein 7 | **PPM03001C** |
| A06 | NM_011329 | Ccl1 | Chemokine (C-C motif) ligand 1 | **PPM03138C** |
| A07 | NM_011330 | Ccl11 | Chemokine (C-C motif) ligand 11 | **PPM02967G** |
| A08 | NM_011331 | Ccl12 | Chemokine (C-C motif) ligand 12 | **PPM02977E** |
| A09 | NM_011332 | Ccl17 | Chemokine (C-C motif) ligand 17 | **PPM02963B** |
| A10 | NM_011888 | Ccl19 | Chemokine (C-C motif) ligand 19 | **PPM03157C** |
| A11 | NM_011333 | Ccl2 | Chemokine (C-C motif) ligand 2 | **PPM03151G** |
| A12 | NM_016960 | Ccl20 | Chemokine (C-C motif) ligand 20 | **PPM03142B** |
| B01 | NM_009137 | Ccl22 | Chemokine (C-C motif) ligand 22 | **PPM02950B** |
| B02 | NM_019577 | Ccl24 | Chemokine (C-C motif) ligand 24 | **PPM03159F** |
| B03 | NM_011337 | Ccl3 | Chemokine (C-C motif) ligand 3 | **PPM02949F** |
| B04 | NM_013652 | Ccl4 | Chemokine (C-C motif) ligand 4 | **PPM02948F** |
| B05 | NM_013653 | Ccl5 | Chemokine (C-C motif) ligand 5 | **PPM02960F** |
| B06 | NM_013654 | Ccl7 | Chemokine (C-C motif) ligand 7 | **PPM02955B** |
| B07 | NM_011616 | Cd40lg | CD40 ligand | **PPM03226C** |
| B08 | NM_011617 | Cd70 | CD70 antigen | **PPM03552E** |
| B09 | NM_170786 | Cntf | Ciliary neurotrophic factor | **PPM68695B** |
| B10 | NM_007778 | Csf1 | Colony stimulating factor 1 (macrophage) | **PPM03116C** |
| B11 | NM_009969 | Csf2 | Colony stimulating factor 2 (granulocyte-macrophage) | **PPM02990F** |
| B12 | NM_009971 | Csf3 | Colony stimulating factor 3 (granulocyte) | **PPM02989B** |
| C01 | NM_007795 | Ctf1 | Cardiotrophin 1 | **PPM05017D** |
| C02 | NM_009142 | Cx3cl1 | Chemokine (C-X3-C motif) ligand 1 | **PPM02959F** |
| C03 | NM_008176 | Cxcl1 | Chemokine (C-X-C motif) ligand 1 | **PPM03058C** |
| C04 | NM_021274 | Cxcl10 | Chemokine (C-X-C motif) ligand 10 | **PPM02978E** |
| C05 | NM_019494 | Cxcl11 | Chemokine (C-X-C motif) ligand 11 | **PPM03192C** |
| C06 | NM_021704 | Cxcl12 | Chemokine (C-X-C motif) ligand 12 | **PPM02965E** |
| C07 | NM_018866 | Cxcl13 | Chemokine (C-X-C motif) ligand 13 | **PPM02947G** |
| C08 | NM_023158 | Cxcl16 | Chemokine (C-X-C motif) ligand 16 | **PPM03775A** |
| C09 | NM_203320 | Cxcl3 | Chemokine (C-X-C motif) ligand 3 | **PPM34590C** |
| C10 | NM_009141 | Cxcl5 | Chemokine (C-X-C motif) ligand 5 | **PPM02966F** |
| C11 | NM_008599 | Cxcl9 | Chemokine (C-X-C motif) ligand 9 | **PPM02973B** |
| C12 | NM_010177 | Fasl | Fas ligand (TNF superfamily, member 6) | **PPM02926E** |
| D01 | NM_008155 | Gpi1 | Glucose phosphate isomerase 1 | **PPM03345C** |
| D02 | NM_010406 | Hc | Hemolytic complement | **PPM24764C** |
| D03 | NM_010503 | Ifna2 | Interferon alpha 2 | **PPM03543A** |
| D04 | NM_008337 | Ifng | Interferon gamma | **PPM03121A** |

| Position | Refseq | Symbol | Description | RT2 Catalog |
|---|---|---|---|---|
| D05 | NM_010548 | Il10 | Interleukin 10 | PPM03017C |
| D06 | NM_008350 | Il11 | Interleukin 11 | PPM03018E |
| D07 | NM_008351 | Il12a | Interleukin 12A | PPM03019A |
| D08 | NM_001303244 | Il12b | Interleukin 12b | PPM03020E |
| D09 | NM_008355 | Il13 | Interleukin 13 | PPM03021B |
| D10 | NM_008357 | Il15 | Interleukin 15 | PPM03022C |
| D11 | NM_010551 | Il16 | Interleukin 16 | PPM03111E |
| D12 | NM_010552 | Il17a | Interleukin 17A | PPM03023A |
| E01 | NM_145856 | Il17f | Interleukin 17F | PPM05398E |
| E02 | NM_008360 | Il18 | Interleukin 18 | PPM03112B |
| E03 | NM_010554 | Il1a | Interleukin 1 alpha | PPM03010F |
| E04 | NM_008361 | Il1b | Interleukin 1 beta | PPM03109F |
| E05 | NM_031167 | Il1rn | Interleukin 1 receptor antagonist | PPM03547B |
| E06 | NM_008366 | Il2 | Interleukin 2 | PPM02937C |
| E07 | NM_021782 | Il21 | Interleukin 21 | PPM03761F |
| E08 | NM_016971 | Il22 | Interleukin 22 | PPM05481A |
| E09 | NM_031252 | Il23a | Interleukin 23, alpha subunit p19 | PPM03763F |
| E10 | NM_053095 | Il24 | Interleukin 24 | PPM04205C |
| E11 | NM_145636 | Il27 | Interleukin 27 | PPM33809A |
| E12 | NM_010556 | Il3 | Interleukin 3 | PPM03012F |
| F01 | NM_021283 | Il4 | Interleukin 4 | PPM03013F |
| F02 | NM_010558 | Il5 | Interleukin 5 | PPM03014F |
| F03 | NM_001314054 | Il6 | Interleukin 6 | PPM03015A |
| F04 | NM_008371 | Il7 | Interleukin 7 | PPM03016C |
| F05 | NM_008373 | Il9 | Interleukin 9 | PPM03110A |
| F06 | NM_008501 | Lif | Leukemia inhibitory factor | PPM02988F |
| F07 | NM_010735 | Lta | Lymphotoxin A | PPM03114A |
| F08 | NM_008518 | Ltb | Lymphotoxin B | PPM03119A |
| F09 | NM_010798 | Mif | Macrophage migration inhibitory factor | PPM02985H |
| F10 | NM_010834 | Mstn | Myostatin | PPM04441F |
| F11 | NM_013611 | Nodal | Nodal | PPM04458A |
| F12 | NM_001013365 | Osm | Oncostatin M | PPM05385B |
| G01 | NM_019932 | Pf4 | Platelet factor 4 | PPM02986C |
| G02 | NM_023785 | Ppbp | Pro-platelet basic protein | PPM03773A |
| G03 | NM_009263 | Spp1 | Secreted phosphoprotein 1 | PPM03648C |
| G04 | NM_009367 | Tgfb2 | Transforming growth factor, beta 2 | PPM02992A |
| G05 | NM_009379 | Thpo | Thrombopoietin | PPM02984B |
| G06 | NM_013693 | Tnf | Tumor necrosis factor | PPM03113G |
| G07 | NM_008764 | Tnfrsf11b | Tumor necrosis factor receptor superfamily, member 11b (osteoprotegerin) | PPM03404F |
| G08 | NM_009425 | Tnfsf10 | Tumor necrosis factor (ligand) superfamily, member 10 | PPM02925B |
| G09 | NM_011613 | Tnfsf11 | Tumor necrosis factor (ligand) superfamily, member 11 | PPM03047F |

| Position | Refseq | Symbol | Description | RT2 Catalog |
|---|---|---|---|---|
| G10 | NM_033622 | Tnfsf13b | Tumor necrosis factor (ligand) superfamily, member 13b | **PPM03751B** |
| G11 | NM_009505 | Vegfa | Vascular endothelial growth factor A | **PPM03041F** |
| G12 | NM_008510 | Xcl1 | Chemokine (C motif) ligand 1 | **PPM02956C** |
| H01 | NM_007393 | Actb | Actin, beta | **PPM02945B** |
| H02 | NM_009735 | B2m | Beta-2 microglobulin | **PPM03562A** |
| H03 | NM_008084 | Gapdh | Glyceraldehyde-3-phosphate dehydrogenase | **PPM02946E** |
| H04 | NM_010368 | Gusb | Glucuronidase, beta | **PPM05490C** |
| H05 | NM_008302 | Hsp90ab1 | Heat shock protein 90 alpha (cytosolic), class B member 1 | **PPM04803F** |
| H06 | SA_00106 | MGDC | Mouse Genomic DNA Contamination | |
| H07 | SA_00104 | RTC | Reverse Transcription Control | **PPX63340A** |
| H08 | SA_00104 | RTC | Reverse Transcription Control | **PPX63340A** |
| H09 | SA_00104 | RTC | Reverse Transcription Control | **PPX63340A** |
| H10 | SA_00103 | PPC | Positive PCR Control | |
| H11 | SA_00103 | PPC | Positive PCR Control | |
| H12 | SA_00103 | PPC | Positive PCR Control | |

**Supplementary Table 5**: Standard of care (SOC) treatment of patients from the RESPIRE clinical trial used for the analysis of virological or immunological parameters

| SOC | SOC-Type | Treatment |
|---|---|---|
| None | Other | Zapnometinb |
| None | Other | Zapnometinb |
| None | Other | Zapnometinb |
| CASIRIVIMAB+IMDEVIMAB | Other | Zapnometinb |
| CASIRIVIMAB+IMDEVIMAB | Other | Zapnometinb |
| CASIRIVIMAB+IMDEVIMAB | Other | Zapnometinb |
| None | Other | Zapnometinb |
| DEXA | Steriode | Zapnometinb |
| DEXA, TLZ | Steriode | Zapnometinb |
| RDV, MPRED | Steriode | Zapnometinb |
| MPRED | Steriode | Zapnometinb |
| BUDE | Steriode | Zapnometinb |
| | | |
| CASIRIVIMAB+IMDEVIMAB | Other | Placebo |
| CASIRIVIMAB+IMDEVIMAB | Other | Placebo |
| CASIRIVIMAB+IMDEVIMAB | Other | Placebo |
| CASIRIVIMAB+IMDEVIMAB | Other | Placebo |
| CASIRIVIMAB+IMDEVIMAB | Other | Placebo |
| CASIRIVIMAB+IMDEVIMAB | Other | Placebo |
| RDV, DEXA, MPRED | Steriode | Placebo |
| PRED | Steriode | Placebo |
| DEXA, BUDE | Steriode | Placebo |
| PRED | Steriode | Placebo |
| DEXA, TLZ | Steriode | Placebo |

| SOC | SOC-Type | Treatment |
|---|---|---|
| DEXA | Steriode | Placebo |

DEXA = Dexamethasone; TLZ = Tocilizumab; RDV = Remdesivir; MPRED = Methylprednisolone; BUDE = Budesonid; PRED = Prednisolone

**Supplementary References**

[1] Hoeppe S, Schreiber TD, Planatscher H, Zell A, Templin MF, Stoll D, Joos TO and Poetz O. Targeting peptide termini, a novel immunoaffinity approach to reduce complexity in mass spectrometric protein identification. Mol Cell Proteomics. **2011**;10(2):M110 002857.

[2] Steinhilber AE, Schmidt FF, Naboulsi W, Planatscher H, Niedzwiecka A, Zagon J, Braeuning A, Lampen A, Joos TO and Poetz O. Mass Spectrometry-Based Immunoassay for the Quantification of Banned Ruminant Processed Animal Proteins in Vegetal Feeds. Anal Chem. **2018**;90(6):4135-4143.

[3] Belghit I, Varunjikar M, Lecrenier MC, Steinhilber A, Niedzwiecka A, Wang YV, Dieu M, Azzollini D, Lie K, Lock EJ, Berntssen MHG, Renard P, Zagon J, Fumière O, van Loon JJA, Larsen T, Poetz O, Braeuning A, Palmblad M and Rasinger JD. Future feed control – Tracing banned bovine material in insect meal. Food Control. **2021**;128:108183.

[4] Pino LK, Searle BC, Bollinger JG, Nunn B, MacLean B and MacCoss MJ. The Skyline ecosystem: Informatics for quantitative mass spectrometry proteomics. Mass Spectrom Rev. **2020**;39(3):229-244.

[5] UniProt C. UniProt: the universal protein knowledgebase in 2021. Nucleic Acids Res. **2021**;49(D1):D480-D489.

# Part II

# Chapter 4

# Identification and Relative Abundance of Naturally Presented and Cross-Reactive Influenza A Virus MHC Class I-Restricted T Cell Epitopes

Hazem Hamza[1, 2], Michael Ghosh[1], Markus W. Löffler[1,3, 4, 5, 6], Hans-Georg Rammensee[1, 5, 6, 7], and Oliver Planz[1*]

[1] Institute for Immunology, University of Tübingen, Tübingen, Germany

[2] Virology Laboratory, Environmental Research Division, National Research Centre, Giza, Egypt.

[3] Institute for Clinical and Experimental Transfusion Medicine, Medical Faculty of Tübingen, Tübingen, Germany

[4] Centre for Clinical Transfusion Medicine, University Hospital Tübingen, Tübingen, Germany

[5] Cluster of Excellence iFIT (EXC2180) “Image-Guided and Functionally Instructed Tumor Therapies”, University of Tübingen, Tübingen, Germany.

[6] German Cancer Consortium (DKTK) and German Cancer Research Center (DKFZ), partner site Tübingen, Tübingen, Germany.

[7] Cluster of Excellence CMFI (EXC2124) "Controlling Microbes to Fight Infections", University of Tübingen, Tübingen, Germany

* Corresponding author

*Emerg Microbes Infect. 2024;13(1):2306959 PMID:38240239 DOI:10.1080/22221751.2024.2306959*

## Disclosure of authorship contribution

HH was involved in all parts of this study. All experimental work was planned and performed by HH. MG performed the LC-MS/MS data acquisition. HH further performed the LC-MS/MS data processing using the vendor-specific software Proteome Discoverer 1.4. HH performed the data analysis, data visualization and drafted the manuscript. Further information is provided in the “Author Contribution” section at the end of this chapter/manuscript.

## Abstract

Cytotoxic T lymphocytes are key for controlling viral infection. Unraveling CD8+ T cell-mediated immunity to distinct influenza virus strains and subtypes across prominent HLA types is relevant for combating seasonal infections and emerging new variants. Using an immunopeptidomics approach, naturally presented influenza A virus-derived ligands restricted to HLA-A*24:02, HLA-A*68:01, HLA-B*07:02, and HLA-B*51:01 molecules were identified. Functional characterization revealed multifunctional memory CD8+ T cell responses for nine out of sixteen peptides. Peptide presentation kinetics was optimal around 12 hours post infection and presentation of immunodominant epitopes shortly after infection was not always persistent. Assessment of immunogenic epitopes revealed that they are highly conserved across the major zoonotic reservoirs and may contain a single substitution in the vicinity of the anchor residues. These findings demonstrate how the identified epitopes promote T cell pools, possibly cross-protective in individuals and can be potential targets for vaccination.


## Introduction

Efforts to control influenza virus infection are mainly based on the annual adaptation and reformulation of vaccines according to the predominant circulating strains. Influenza viruses exhibit a relatively high mutational rate since the hetero-trimeric RNA-dependent RNA polymerase (RdRp) complex lacks proof-reading activity [1,2]. Accumulating point mutations, in particular within the major surface protein, hemagglutinin (HA), constantly generate virus mutants and the exchange of vRNA segments upon infection with multiple strains also facilitates emerging variants [1,3]. Influenza vaccines against the H3N2 subtype have been implicated with poor protection, according to subtype measurements [4]. This could be due to the tremendous mismatch between circulating and egg-adapted strains used for vaccine production [5,6]. Broadly-neutralizing antibodies (bnAbs) against the major surface proteins, either the stalk or HA head domain, have great potential to protect against seasonal influenza virus infections and could provide near-universal protection [7,8], however, bnAbs-escape mutant viruses have recently been reported [9,10].

Cytotoxic T lymphocytes (CTLs) are key for controlling infectious diseases and cancer. Human leukocyte antigen (HLA) molecules are a determinant factor of CD8+ T cells recognition and

can drive long-lasting memory post-priming with specific immunogenic epitopes [11-13]. In 2013, during the H7N9 outbreak in China, it was reported that the rapid recovery of patients coincided with early prominent H7N9-specific CD8+ T cell responses, while those patients with late CD8+/CD4+ T cell recruitment showed prolonged hospitalization [14]. In turn, in absence of bnAbs, pre-existing immunity mediated by cross-reactive CD8+ T cells recognizing conserved epitopes may have the capacity to promote recovery from infection and minimize disease severity upon emergence of novel variants [11,12,15]. Given that current influenza vaccines lack CD8+ T and NK cell activation [16], broadly reactive vaccines that can efficiently induce CD8+ T cell immunity against different influenza virus strains and subtypes would be desirable particularly for high-risk populations. The optimal design of peptide-based vaccines is mainly attributed to unveiling the factors underlying the immunogenicity of peptides and the magnitude of the immune response. It is seemingly evident that the relative abundance of peptides presented by MHC class I plays a pivotal role, in particular, during the course of natural infection in triggering the immune response hierarchies [17,18].

Herein, we characterize the immunological landscape of CD8+ T cells recognizing different influenza A virus (IAV) strains at different time points after infection of Human lung adenocarcinoma cells (Calu-3). Using immunopeptidomics, novel HLA class I-restricted (HLA-I) IAV ligands were identified in the context of HLA-A*24:02, HLA-A*68:01, HLA-B*07:02 and HLA-B*51:01 alleles. The identified HLA-I peptides were further screened for their in vitro immunogenicity using peripheral blood mononuclear cells (PBMCs) obtained from healthy donors expressing the respective HLA alleles. Nine out of sixteen peptides were recognized by T cells from healthy individuals, with multifunctional effector functions (TNF, CD107a, IFN-γ) and five ligands proved immunodominant. A conservation analysis revealed that two epitopes were highly conserved among zoonotic reservoirs (≥95%), while the other epitopes contained minor substitutions, 1-2 amino acids (AA) away from the peptide-anchor residues, which hardly affect binding affinity. The identified epitopes can potentially provide cross-protection across distinct IAV strains and subtypes. Moreover, the incorporation of such highly conserved CD8+ T cell epitopes into a broadly reactive T cell-inducing vaccine may achieve long-term heterosubtypic protection and match newly emerging strains.

## Materials and methods

### Cells and viruses

Calu-3 cells (ATCC® HTB-55) were cultured in Minimum Essential Media (MEM) supplemented with 1% Penicillin/Streptomycin (P/S), 10% fetal bovine serum (FBS), 2 mM L-glutamine, 1 mM sodium pyruvate and 1% non-essential AA. Calu-3 cells express HLA-A*24:02, HLA-A*68:01, HLA-B*07:02, HLA-B*51:01, and HLA-C*15:02 alleles. The HLA typing information of the Calu-3 cell line was retrieved from the TRON Cell Line Portal [19]. Madin-Darby canine kidney cells (MDCK II, ATCC® CRL2936™) were grown in IMDM medium and used for IAV propagation. The following IAV strains were used: A/Puerto Rico/8/34 (H1N1/PR8), A/Victoria/03/75 (H3N2/Victoria), and A/Fukui/20/2004 (H3N2/Fukui). For virus stocks preparation, MDCK II cells were infected with each strain and incubated for 1 h at 37 °C. The inocula were removed, and cell monolayers overlaid with infection media (1X DMEM supplemented with 1% P/S, 0.3% bovine serum albumin (BSA), and 1 μg $ml^{-1}$ TPCK-treated trypsin). After 48 to 72 h post infection (hpi), cell culture supernatants containing viruses were clarified by centrifugation, aliquoted, and stored at - 80°C. Virus titers were determined by standard plaque assay protocol.

### Direct infection of cells

Approximately $1 \times 10^8$ Calu-3 cells were infected with each of the IAV strains at an MOI of 4 and the infection rate was determined as described below to ensure that a minimum 50% of the cells were infected. After 1 h incubation at 37 °C, the inocula were removed, cell monolayers washed with phosphate-buffered saline (PBS), and overlaid with infection media (1X DMEM supplemented with 1% P/S, 0.3% BSA, and 1 μg $ml^{-1}$ TPCK-treated trypsin). At 3, 6, 9, 12, and 24 hpi, the cells were harvested using enzyme-free cell dissociation buffer (Gibco), washed twice times with cold PBS, and stored at - 80 °C.

### Determination of infection rate and HLA-I surface expression

HLA-I surface expression was evaluated using QIFIKIT quantitative flow cytometric assay kit (Agilent Dako, Denmark), according to the manufacturer's instructions. In brief, Calu-3 infected cells were stained with the pan-HLA-I-specific monoclonal antibody (mAb) W6/32 (produced in-house) in triplicates or IgG isotype control (BioLegend, San Diego, CA, USA). Subsequently, secondary staining with FITC-conjugated rabbit-anti-mouse F(ab')2 fragments

(Agilent Dako) was carried out alongside QIFIKIT quantification beads (Agilent Dako). For the infection efficiency rate, infected cells were fixed and permeabilized using Foxp3 Staining Buffer Set (eBioscience™, Invitrogen, CA, USA) followed by intracellular staining of IAV nucleoprotein (NP) step with FITC-conjugated anti-IAV NP monoclonal antibody (clone D67J; Invitrogen). Flow cytometric acquisition was performed on a BD FACSCanto II system (BD Biosciences, Franklin Lakes, NJ, USA), and the acquired data were analyzed by FlowJo 10.3 (FlowJo LLC, BD). The complete workflow is illustrated in (Fig. 1a).

**Immune precipitation of HLA-I-peptide complexes and peptide isolation**

HLA-I molecules from cell pellets were isolated using the standard immunoaffinity purification procedure as previously described [20,21]. Briefly, frozen cells were lysed using 10 mM CHAPS (AppliChem, Darmstadt, Germany) buffer prepared in PBS, containing a complete protease inhibitor (Roche, Mannheim, Germany). The cell lysates were homogenized by applying pulsed sonification. Thereafter, the HLA-I molecules were purified from lysates by immunoaffinity chromatography with the pan-HLA class I specific W6/32 antibody coupled to CNBr-activated sepharose (GE Healthcare, Chicago, IL, USA). HLA-associated peptides were eluted with 0.2% TFA followed by ultrafiltration of the eluate using 3-kDa Amicon filter units (Merck Millipore, Billerica, MA, USA). Desalting and concentration steps were accomplished by ZipTip C18 (Merck Millipore) and 0.1% TFA, and elution was performed with 32% Acetonitrile (AcN)/0.2% TFA. The final volume of the eluate was reduced by vacuum centrifugation.

**Characterization of naturally presented HLA-I Ligands by LC-MS/MS**

Purified HLA ligands were separated by reverse-phase high-performance liquid chromatography (HPLC; UltiMate 3000 RSLCnano system, Dionex, Sunnyvale, CA, USA) using a 75 µm × 2 cm trapping column and a 25 cm length and 50 µm separation column (Thermo Fisher Scientific, Waltham, MA, USA) subsequently, applying a gradient ranging from 2.4 to 32 % AcN over 90 min with a flow rate of 175 nl/min. For MS/MS, a top-five collision-induced dissociation (CID) method generating ion trap MS/MS spectra in the mass range 400–650 m/z was used with an online coupled mass spectrometer (LTQ Orbitrap XL, Thermo Fisher Scientific).

**Database search and spectral annotation**

Data were processed against concatenated FASTA sequences containing the reviewed UniProt human proteome as well as the IAV proteome of the strains used for this study (viewed January 2020) by applying the Sequest HT algorithm in the Proteome Discoverer 1.4 software (Thermo Fisher Scientific). Precursor mass tolerance was set to 5 ppm, fragment mass tolerance was set to 0.5 Da, and oxidized methionine was allowed as a dynamic modification. Percolator-assisted false discovery rate (FDR) algorithm [22] was implemented at a target value of q ≤ 0.05 (5% FDR), search engine rank =1, and peptide lengths were limited to 8–12 AA. All identified peptides were annotated to their respective HLA motifs using both NetMHCpan 4.0 [23] and SYFPEITHI [24] databases. Cutoff values of $IC_{50}$ ≤ 500 nM, percentile rank ≤ 2% for NetMHCpan 4.0, and a normalized SYFPEITHI score ≥ 50 % were applied. Peptides fulfilling the cut-off criteria of either or both prediction tools were designated as predicted and tested in PBMCs from healthy donors with the respective HLA allele.

**Label-free quantification of HLA ligands**

To determine the abundance of presented IAV-derived ligands over the infection time course, the label-free quantification (LFQ)-method was used as previously described by Nelde et al. [25]. Briefly, prior to the LC-MS/MS analysis, the total number of cells for each infection time point was normalized and LC-MS/MS analysis was performed in five technical replicates for each sample. The relative quantification of HLA ligands was performed by calculating the area under the curve (AUC) of the corresponding precursor-extracted ion chromatograms using Proteome Discoverer 1.4 (Thermo Fisher Scientific). To contend with the common LFQ and data-dependent acquisition (DDA) MS proteomics issues [26-28], the LFQ strategy was implemented by lowering FDR cut-offs and using matching between runs to reduce missing values in quantitation. High-quality peptide spectrum matches were filtered for 5% FDR and subsequently screened for binding affinity to the respective HLA molecules.

**Peptide synthesis**

Peptides were synthesized and provided by the Department of Immunology, Tübingen, Germany. Peptide synthesis was performed by the standard 9-fluorenylmethyloxycarbonyl/tert-butyl (Fmoc/tBu) method using an automated peptide synthesizer (Liberty Blue, CEM, Matthews, NC, USA). The identity and purity of peptides were evaluated by reversed-phase HPLC (e2695, Waters, Milford MA, USA) coupled online hybrid

mass spectrometry (LTQ Orbitrap XL, Thermo Fisher Scientific). Synthesized peptides were used in functional experiments.

**Human biomaterials and ethics statement**

Samples from healthy blood donors with matching HLA alleles were kindly provided by the Institute of Clinical and Experimental Transfusion Medicine (University of Tübingen) after obtaining informed consent documented in writing, according to the principles of the Declaration of Helsinki and conforming with applicable laws and regulations. This project has been reviewed and approved by the Ethics Committee at the Medical Faculty of the Eberhard Karls University Tübingen and the University Hospital Tübingen (Project no. 887/2020BO2 and 200/2021BO2).

**T cell culture**

PBMCs were isolated by SepMate™ tubes for layering Lymphoprep™ density gradient media (STEMCELL Technologies, Vancouver, Canada). Obtained cells were cryopreserved and stored in the vapor phase of liquid nitrogen. Vials of frozen PBMCs were thawed at 37 °C and cells rested overnight before stimulation. Cell culture was performed with IMDM media supplemented with 5 % heat-inactivated human serum (Sigma-Aldrich, Steinheim, Germany), 1% P/S, 25 µg $ml^{-1}$ gentamicin, and 50 µM β-mercaptoethanol with 5% $CO_2$ at 37 °C in a humidified incubator.

**IFN-γ ELISpot Assay**

IFN-γ ELISpot assays were performed after 12-day peptide stimulation (as described below) along with suitable controls. In contrast, *ex vivo* ELISpot was carried out 24 h after thawing the cells. Briefly, for IFN-γ ELISpot PBMCs were stimulated for 24 h after thawing with 1 µg $ml^{-1}$ IAV peptides of interest and control peptides. IL-2 (R&D Systems, Minneapolis, MN, USA) was added at a final concentration of 20 IU $ml^{-1}$ on days 2, 5, and 7. On day 12, cells were harvested and IFN-γ ELISpot was performed by seeding PBMCs at a final count of $10^5$ cells/well onto MultiScreen$_{HTS}$-HA nitrocellulose plates (Millipore). Subsequently, cells were incubated for 24 h following stimulation with candidate peptides and controls. Phytohemagglutinin (PHA) (Sigma-Aldrich), at a final concentration of 15 µg $ml^{-1}$ was used as a positive control. The following peptides were used as negative controls: DPYKATSAV human MUC16$_{6326–6334}$ (B*51); TPGPGVRYPL HIV Nef$_{128–137}$ (B*07), GSEELRSLY HIV POL$_{71–79}$ (A*01), RLRPGGKKK HIV GAG$_{20–28}$

(A*03). DMSO was used as a negative control for HLA-A*68:01 and HLA-A*24:02. The spot counts corresponding to IFN-γ producing cells were determined using ImmunoSpot® S5 analyzer (CTL, Cleveland, OH, USA) and ImmunoSpot software® ver. 5 (CTL). T cell responses were considered positive when results fulfilled the following criteria: each test well contains at least 10 spots, and the mean number of replicates is threefold higher than the mean spot count of the negative control. According to the recognition frequency among tested donors, the tested peptides were grouped into 3 different categories: negative group (0% response rate in any donor), subdominant group (<50% recognition frequency), and dominant group (≥50% recognition frequency).

**Intracellular cytokine staining**

The functionality of peptide-specific T cells was analyzed by ICS. PBMCs were stimulated with individual peptides at a final concentration of 10 μg $ml^{-1}$ and incubated for 12 h in the presence of GolgiStop (BD Biosciences), Brefeldin A (Sigma-Aldrich), and FITC mouse anti-human CD107a mAb (1:100, clone H4A3, BD Bioscience). Ionomycin and PMA (Sigma-Aldrich) served as a positive control. Thereafter, cells were stained for surface markers with PerCP anti-human CD8a (1:100 dilutions, clone RPA-T8, BioLegend) and APC-Cy™7 mouse anti-human CD4 (1:100, clone RPA-T4, BD Bioscience) mAb in addition to using LIVE/DEAD™ Fixable Aqua Stain to discriminate viable cells (1:400 dilutions, Invitrogen, Waltham, MA, USA). After incubation, a fixation/permeabilization step with Cytofix/Cytoperm solution (BD Biosciences) was added and the cells were further stained with PE anti-human IFN-γ (1:200 dilutions, clone B27, BioLegend) and Pacific Blue™ anti-human TNF-α (1:120, clone MAB11, BioLegend) mAb. Data were acquired by BD FACSCanto II flow cytometry (BD Biosciences) using FACS DIVA software (BD Biosciences). The gating strategy applied for the evaluation of flow cytometry-acquired data is provided in Supplementary materials (suppl. Fig. 1).

**HLA-Tetramer staining**

The frequency of peptide-specific $CD8^+$ T cells was evaluated by tetramer staining after incubation of PBMCs with respective PE-labeled HLA-peptide tetramer complexes. Briefly, PBMCs were cultured, as described above, and the HLA-multimers (ImmunAware, Hørsholm, Denmark) were added at a final concentration of 30 nM, according to the manufacturer's instruction and incubated for 20 min at room temperature. Cells were further washed twice with PBS and stained with LIVE/DEAD™ Fixable Aqua Stain (1:400 dilutions, Invitrogen) for 20

min at 4 °C. The antibody cocktail of cell surface markers PerCP anti-human CD8a (1:100 dilutions, clone RPA-T4, BioLegend) and APC-Cy™7 mouse anti-Human CD4 (1:100, clone RPA-T4, BD Bioscience) mAb was added for 20 min at 4 °C. Following mAb incubation, cells were analyzed by flow cytometry (FACSCanto II, BD Biosciences). The gating strategy applied for the evaluation of flow cytometry-acquired data is provided in Supplementary materials (suppl. Fig. 2). Due to sample constraints, staining was carried out only for peptides that elicited a high recognition frequency in the ELISpot assay.

**Conservation analysis**

To assess the conservation of the immunogenic peptides among human, swine, and avian influenza viruses, the exact sequence match of each peptide was evaluated in unique protein sequences of HA, MP, NP, PB1, and PB2 of all IAV subtypes retrieved from influenza research database (IRD) and National Center for Biotechnology Information (NCBI). Sequence homology and AA substitution rates were estimated using the IRD [29]. To visualize the AA substitutions, full-length sequences of MP, PB2, PB1, NP, and HA genes were aligned using MAFFT ver. 7 [30,31]. The phylogenetic relationship was evaluated with the Neighbor-Joining method. The evolutionary distances were computed using the Jukes-Cantor model, and the variation rate among sites was modeled with a gamma distribution. Bootstrap values were calculated out of 1000 replicates. Trees were visualized and annotated using Evolview ver. 3 [32]. Sequence logos were generated using Seq2Logo-2.1 [33] by applying the default setting; logo type Kullback–Leibler with coloring scheme by physicochemical properties and Hobohm1 clustering method.

**Software and statistical analysis**

Proteome Discoverer 1.4 (Thermo Fisher Scientific) software was used to analyze the MS/MS data. Mapping of the immunogenic T cell epitopes onto IAV proteins was performed using UCSF ChimeraX software [34]. ELISpot data were analyzed with ImmunoSpot software® ver. 5 (CTL). Flow cytometric data were analyzed using FlowJo version 10 (FlowJo LLC, BD). Workflow illustrations were created with BioRender.com Alterations of the HLA-I surface expression were evaluated using Brown-Forsythe ANOVA with Dunnett's T3 multiple comparisons correction. Statistical analysis was conducted using GraphPad Prism ver. 9.3 and $p$ values $<0.05$ were considered statistically significant. Where applicable, statistical details for each experiment are described in the corresponding figure legends.

**Data availability**

The MS/MS data have been deposited to the ProteomeXchange consortium repository (http://proteomecentral.proteomexchange.org) via the PRIDE partner repository [35] with the dataset identifier PXD035241.

## Results

**Identification of IAV-derived HLA-I ligands**

Although many IAV-derived $CD8^+$ T cell epitopes have been previously identified, their identification was primarily achieved by epitope prediction and screening of T cell responses. Here, a mass spectrometry-based (LC-MS/MS) immunopeptidomics approach was applied to increase the spectrum of MHC-I-presented IAV-derived peptides after infection of a human lung adenocarcinoma cell line (Calu-3).

To assess the features and kinetics of the naturally presented HLA-I peptides, the immunopeptidomes of Calu-3 cells were examined at different time points post infection with different IAV strains. Different viruses downregulate MHC-I surface expression [36-39]. Thus, as a first step, the HLA-I surface expression profile and the infection rates were determined (Fig. 1a-d). The expression of HLA-I molecules was similar after infection with H1N1/PR8 and H3N2/Fukui strains with mean expression levels of 246,847 (PR8) and 242,753 (Fukui) molecules/cell compared to the untreated Calu-3 cells (263,502 molecules/cell), despite the variance in infection rates. Whereas a significant ($p = 0.0046$) downregulation (221,341 molecules/cell) was observed after infection with H3N2/Victoria strain. We assume that the viral interference with the HLA-I expression may be virus/subtype-specific.

Calu-3 cells were infected with either H1N1/PR8, H3N2/Victoria and H3N2/Fukui strains followed by isolation of naturally presented HLA-I peptides and LC-MS/MS assessment at time points 3, 6, 9, 12, 24 hpi (Fig. 2a). A total of 16 IAV-derived MHC-I peptides were identified as predicted binders for HLA-A*24:02, HLA-A*68:01, HLA-B*07:02, and HLA-B*51:01 alleles (suppl. Table 1). Among these newly characterized peptides, four were derived from the HA protein, one each from M1, NS1, NS2, and PB1-F2 proteins, two from NP protein, and three each from PB1 and PB2 (suppl. Table 1). The $M1_{EAM}$ peptide was identified both in H1N1/PR8

and H3N2/Victoria infected cells. $HA_{VYR}$ was determined in H3N2/Victoria and H3N2/Fukui infected cells, whilst the rest of the HLA-I peptides were solely identified in either of the IAV subtype-infected cells.

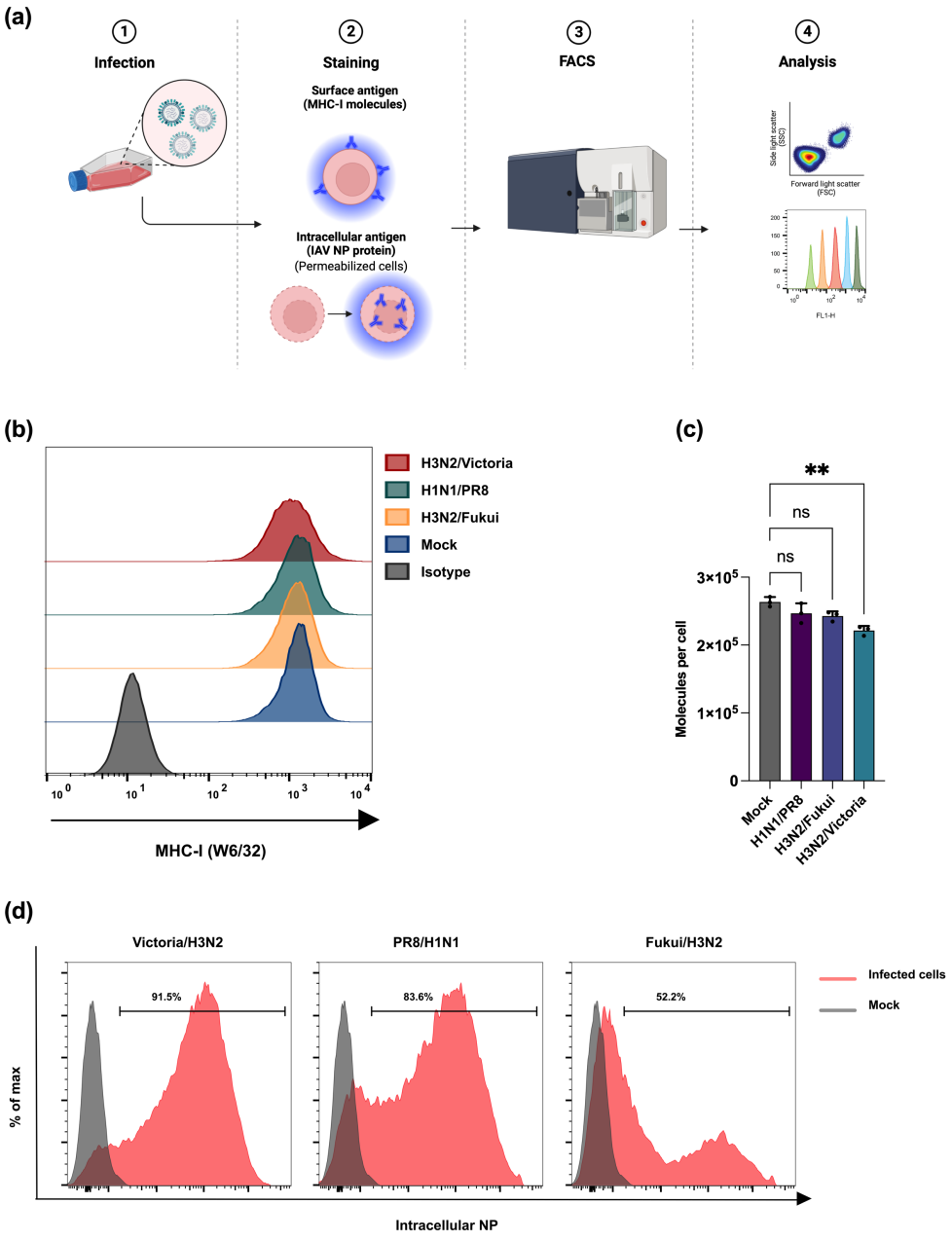


***Figure 1: Infection rates and MHC-I expression in Calu-3 cells. Cells were mock-treated or infected with different IAV strains.*** ***(a)*** *Schematic representation of MHC-I quantification and evaluation of IAV infection rate.* ***(b)*** *Cell surface expression of MHC-I molecules was quantified by staining with pan-HLA-I antibody (W6/32) and analyzed by flow cytometry at 24 hpi.* ***(c)*** *Alterations of the MHC-I surface expression were evaluated using QIFIKIT quantitative bead-based assay. Statistical differences were assessed using Brown-Forsythe ANOVA with Dunnett's T3 multiple comparisons correction* ***(d)*** *Post*

*infection, the cells were permeabilized for intracellular staining of IAV nucleoprotein (NP). The results are representative of two independent experiments (n=2).*

**Kinetics of IAV peptide presentation following infection of Calu-3 cells**

Next, we evaluated the kinetics of HLA presentation and relative abundance of the sixteen IAV-derived peptides during infection (Fig. 2a). After H1N1/PR8 infection, eight peptides were determined. Three peptides were identified at 6 hpi ($HA_{LPY}$, $NS1_{TMA}$, and $PB2_{GTA}$), suggesting that neither structural nor non-structural IAV protein-derived peptides have presentation preferences at early time points, whilst most of the remaining peptides could only be determined at 9 hpi, e.g. the $NP_{NLN}$ epitope was first identified at 12 hpi (Fig. 2b).

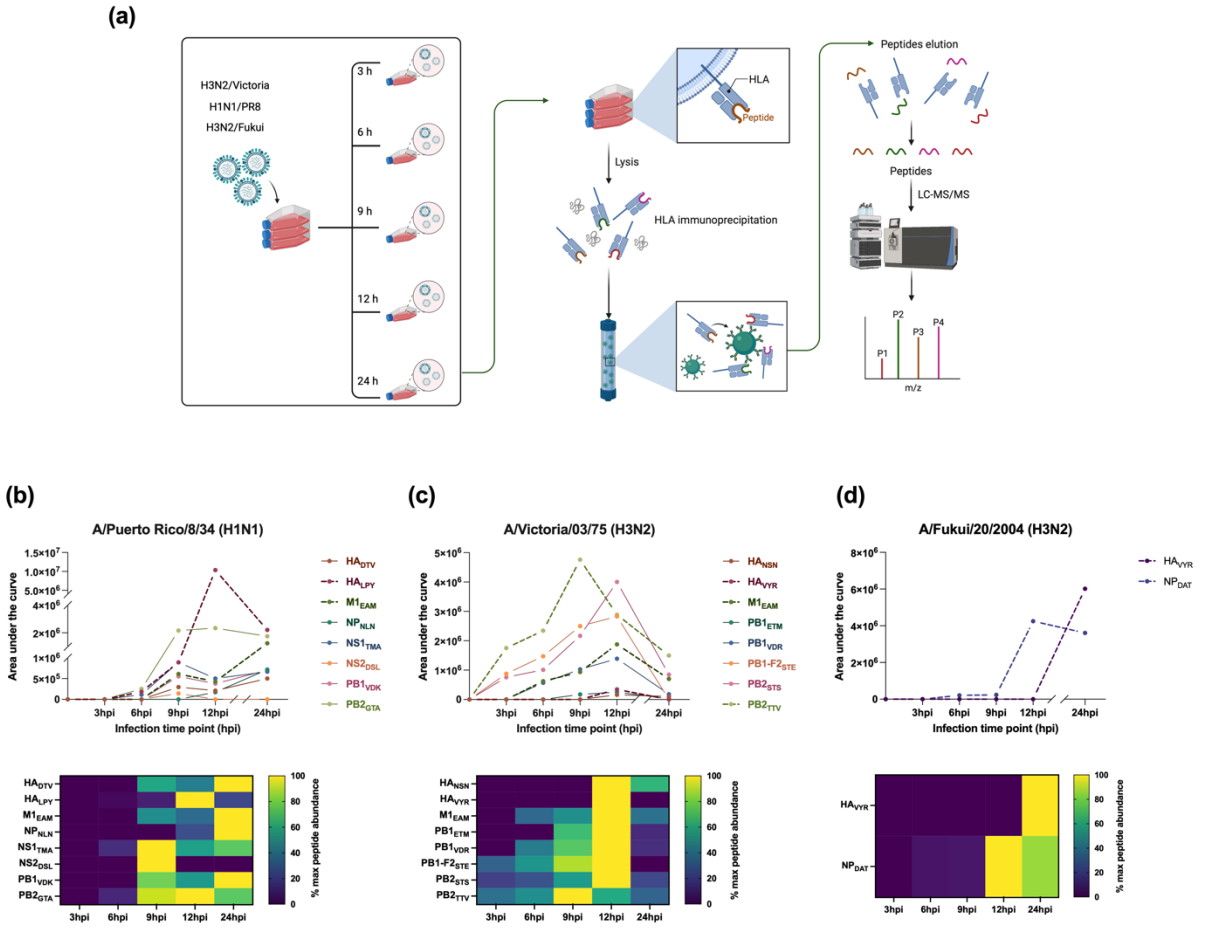


***Figure 2: Identification and presentation kinetics of IAV-derived ligands.*** ***(a)*** *Schematic representation of epitope mapping workflow. Calu-3 cells were infected with different IAV strains representing both H1N1 and H3N2 subtypes. HLA-peptide complexes were isolated from the cell lysates of infected cells at 3, 6, 9, 12, and 24 hpi by immunoaffinity chromatography with the pan-HLA class I-specific W6/32 antibody coupled to CNBr activated sepharose. HLA-peptide complexes were eluted by acidic elution*

*followed by desalting and concentration steps. The HLA ligands were further analyzed by HPLC tandem mass spectrometry (MS/MS).* ***(b-d)*** *The presentation kinetics of HLA-I-bound peptides isolated from infected Calu-3 cells during the infection time course are shown in the upper panel and the area under the curve (AUC) is presented as a percentage of maximum levels detected over the time course (lower panel). Dashed lines indicate the immunodominant epitopes. The MS/MS data were processed using proteome discoverer software V. 1.4, analyzed, and visualized using GraphPad prism software ver. 9.3.*

In Calu-3 cells, infected with the H3N2/Victoria strain, eight peptides were identified. Already at 3 hpi, PB1-F2$_{STE}$, PB2$_{STS}$, and PB2$_{TTV}$ peptides were presented, while most of the remaining peptides were first identified at 9 hpi. All peptides showed peak presentation at 12 hpi, except for the PB2$_{TTV}$ peptide, which peaked at 9 hpi. Interestingly, the M1$_{EAM}$ peptide was presented by the H1N1/PR8 and H3N2/Victoria infected cells but showed different presentation profiles in both earlier time points and altered peak expression (Fig. 2b, c).

Only two peptides were identified after infection with strain H3N2/Fukui. The NP$_{DAT}$ peptide was first observed at 6 hpi and reached its peak level of presentation at 12 hpi. Notably, the HA$_{VYR}$ epitope that was also presented by Calu-3 cells infected with H3N2/Victoria was observed only at 24 hpi (Fig. 2d).

Overall, most peptides were first identified between 6 to 9 hpi and peaked at 12 hpi. Not all viral protein segments were represented among the identified peptides. Taken together, the frequency and presentation kinetics showed a disparity between different peptides.

**IFN-γ ELISpot assay establishes IAV-derived HLA-I ligands as T cell epitopes**

All IAV peptides were analyzed with either SYFPEITHI or NetMHCpan 4.0 to assign their putative HLA-I restriction (suppl. Table 1). Thereafter, the peptides were tested for immunogenicity in at least eight different HLA-matched healthy blood donors using a 12-day IFN-γ ELISpot assay.

NP$_{DAT}$ and HA$_{LPY}$ were found to be the most immunogenic ligands for HLA-B*51 with 100% and 85.7% recognition rates, respectively (Fig. 3 a-b; suppl. Table 1). Moreover, HA$_{VYR}$, the only identified HLA-A*24-restricted ligand showed a 76.9% recognition rate (Fig. 3 c, d; suppl. Table 1), while the M1$_{EAM}$ and PB2$_{TTV}$ were proven immunodominant epitopes for HLA-A*68:01 and revealed a similar recognition frequency 66.7% (Fig. 3 e-g; suppl. Table 1). PB2$_{GTA}$ and PB2$_{STS}$,

spanning the same AA positions with two AA substitutions, were found to be subdominant epitopes for HLA-A*68:01 and presented quite similar recognition rates accounting for 41.7% and 33.3% respectively, as well as the $PB1_{ETM}$ exhibiting a recognition rate at 33.3%. It was observed that the $NP_{NLN}$ epitope was least recognized at a rate of 16.7% among the other HLA-A*68:01 epitopes, whilst the remainder of the identified peptides did not show immunogenic properties.

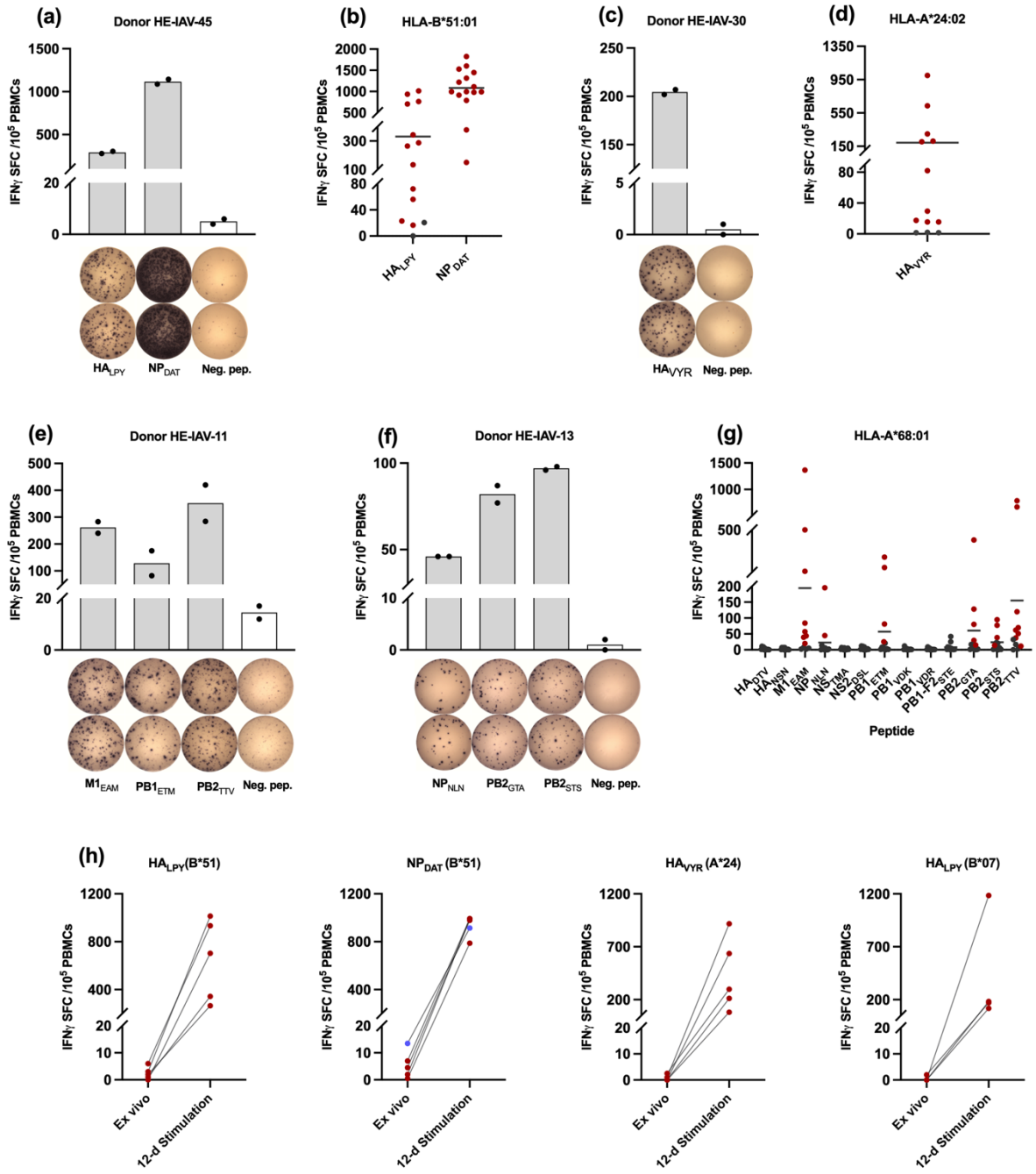


***Figure 3: Immunological characterization of naturally presented IAV-derived T cell epitopes by IFN-γ ELISpot assay***. *Representative ELISpot assays after 12-day in vitro stimulation of PBMCs isolated from*

*HLA-B*51* ***(a-b)****, HLA-A*24* ***(c-d)****, and HLA-A*68* ***(e-g)*** *-matched donors. Bars indicate mean spot counts of technical duplicates. The cumulative analysis of screening results was summarized in scatter plots* ***(b)****,* ***(d)****, and* ***(g)****. Each data point represents one single donor tested within one single experiment. Shown are the mean IFN-γ spot forming cells (SFCs) from two technical replicates of each tested donor normalized to the negative control. Irrelevant HLA-matched peptides, either HIV-derived peptides, human self-peptides, or DMSO served as a negative control. Horizontal lines represent the mean values of all tested donors. Positively tested donors are depicted by red circular shapes and negatively tested donors are shown by grey circular shapes.* ***(h)*** *Comparison between IFN-γ SFCs from ELISpot assays in an ex vivo setting and after 12-day stimulation. Four to five donors that showed a high T cell response in the 12-day ELISpot assay for the dominant epitopes* $NP_{DAT}$*,* $HA_{LPY}$ *(B*51), and* $HA_{VYR}$ *(A*24) were retested in the ex vivo system. Paired data points represent one single donor tested within one single experiment. HLA-A*68 restricted dominant epitopes were not included due to sample limitations.* $HA_{LPY,}$ *as HLA-B*07 binder, was also included in the analysis. Shown are the mean IFN-γ SFCs from two technical replicates of each tested donor normalized to the respective negative control. Data points in blue color represent donors that showed T-cell responses in both experimental settings. Data were analyzed and visualized using GraphPad Prism software ver. 9.3.*

To preclude potential competing effects during the 12-day stimulation assay among the tested peptides, *ex vivo* IFN-γ ELISpot assay was performed (Fig. 3h). Four to five donors that showed a strong T cell response in the 12-day ELISpot assay for the immunodominant epitopes $NP_{DAT}$, $HA_{LPY}$ (B*51) and $HA_{VYR}$ (A*24) were reassessed with the *ex vivo* system. However, we were unable to test the HLA-A*68:01 restricted immunodominant epitopes due to limited availability of sample materials. The results showed that the memory T cell response was either lacking or marginal, when compared with the 12-day setting upon pre-stimulation (Fig. 3h). Moreover, the $NP_{DAT}$ epitope only elicited low but detectable responses in one HLA-B*51:01 positive donor when compared to the respective results after 12-day stimulation. Altogether, in contrast to the minimal IFN-γ production towards the immunogenic peptides in the *ex vivo* system, the 12-day culture intensified the $CD8^+$ T cell immune response substantially, insofar as the epitope-specific memory $CD8^+$ T cells were shown as expandable.

**Functional assessment of IAV-specific memory T cells**

Next, HLA tetramer staining alongside intra-cellular cytokine staining (ICS) was carried out to assess the multi-functionality and peptide-specificity of T cells previously investigated by ELISpot assays.

Using ICS, TNF, IFN-γ, and CD107a were determined to assess the multifunctionality of memory T cells, following stimulation with IAV-peptides (Fig. 4 a-c, e-h; Suppl. Fig. 3 a). IFN-γ-specific T cell populations responding to the HLA-A*68-restricted peptides, were 0.1-2.1%, (Fig. 4e). Likewise, the HLA-A*24-restricted peptides elicited T cells in a similar frequency (Fig. 4f). Moreover, the HLA-B*51:01 immunodominant epitopes revealed specific T cell populations ranging from 0.1 to 3.6% for the $HA_{LPY}$ peptide and reaching 17.2% for the $NP_{DAT}$ peptide (Fig. 4g). Notably, the $NP_{DAT}$ epitope elicited the strongest $CD8^+$ T cell responses, corroborating respective ELISpot results.

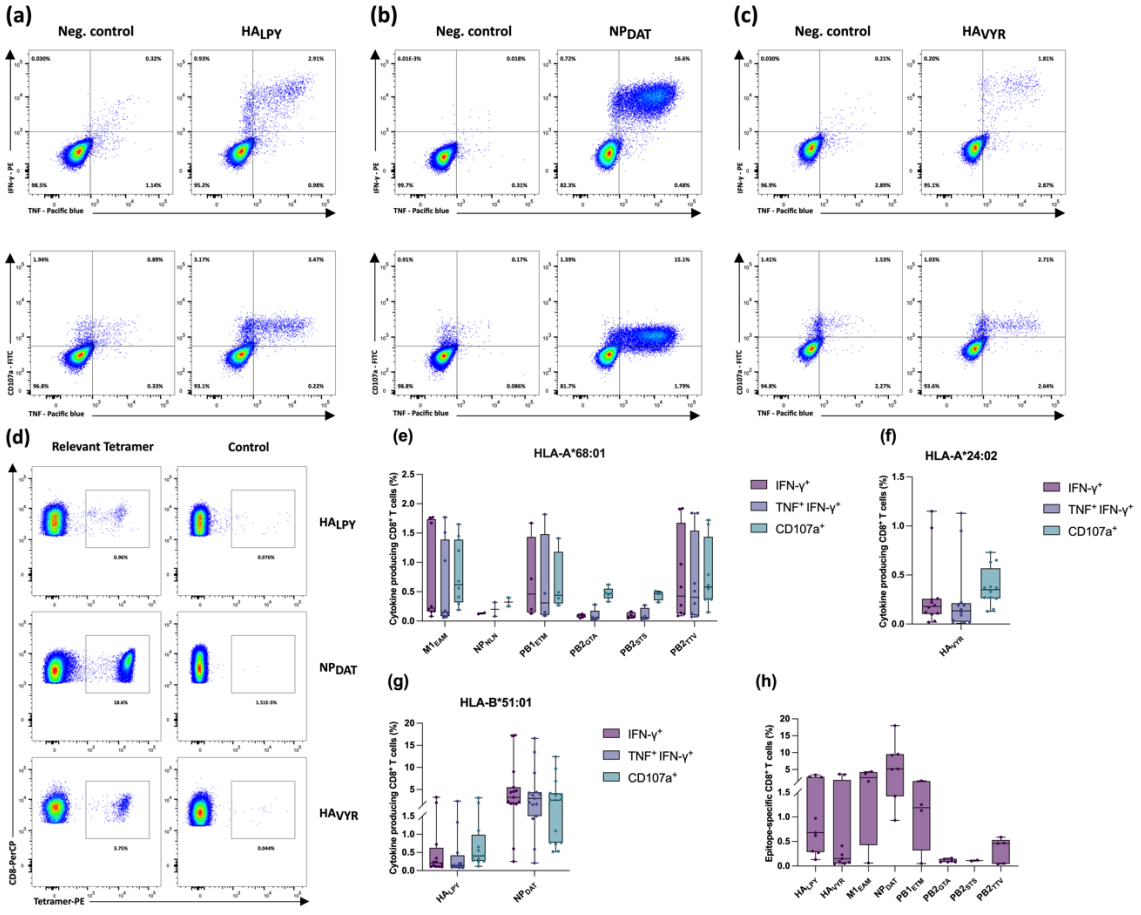


***Figure 4: IAV-derived T cell epitopes are multifunctional.*** ***(a-d)*** *Representative intracellular IFN-γ, TNF-α, and CD107a staining of PBMCs isolated from healthy HLA-matched donors exhibiting HLA-B*51 (**a, b**), HLA-A*24 (**c**), after 12-day stimulation with IAV-derived HLA class I peptides evaluated by flow cytometry. (**d**) representative tetramer staining after 12-day amplification of $CD8^+$ T cells, derived from HLA-matched donors; HLA-B*51 and HLA-A*24. Irrelevant tetramers were used as a negative control.* ***(e-g)*** *Box and whisker plots represent a cumulative percentage of $CD8^+$ IFN-$\gamma^+$, $CD8^+$ IFN-$\gamma^+$ TNF-$\alpha^+$, or $CD8^+$ $CD107a^+$ (**h**) and the frequency of epitope-specific $CD8^+$ T cells evaluated by tetramer staining.*

*Boxes extend from the 25th to 75th percentiles, whiskers represent minimum to maximum, and the horizontal plotted lines are the median values. The indicated percentages represent the frequency of T-cell responses post stimulation with the test peptide minus the negative control of the respective donor. Each data point represents one single donor tested within one single experiment. Data were analyzed and visualized using GraphPad Prism software ver. 9.3 and FlowJo software ver. 10.3. The gating strategies applied for the flow cytometry-based analysis presented in this figure are depicted in the supplements (suppl. Fig. 1 and Fig.2).*

HLA multimer staining was carried out for all but one epitope, $NP_{NLN}$, due to sample constraints (Fig. 4 d, h; Suppl. Fig. 3 b). Robust epitope-specific recognition was demonstrated for all tested tetramers except for $PB2_{GTA}$ and $PB2_{STS}$. The strongest response was consistently observed for $NP_{DAT}$, reaching up to 19.3% tetramer-positive CD8+ T cells, followed by $M1_{EAM}$, $HA_{VYR}$ and $HA_{LPY}$ (eliciting 3.4-4.4%).

Generally, the predicted HLA restriction was confirmed by tetramer staining for all immunogenic peptides. The multifunctional T cell recognition frequencies for IAV-derived epitopes varied profoundly between donors as well as peptides. Moreover, it was shown that the T cell immune response evoked by IAV-specific epitopes was mainly driven by $CD8^+$ T cells in all tested donors.

**HLA cross-reactivity and mismatch analysis**

The NetMHCpan 4.0 prediction results revealed that some peptides were assigned to different HLA-I allotypes (suppl. Table 2). To avoid potential false positives, the following restrictions were applied for donor selection: HLA-B*07$^+$/B*51$^-$, for peptide $HA_{LPY}$, and HLA-A*03$^+$/A*68:01$^-$ for peptides $HA_{NSN}$ and $PP2_{TTV}$, whilst peptide $PB1\text{-}F2_{STE}$ was tested in two different settings HLA- A*01$^+$/A*03$^-$/A*68:01$^-$ and HLA-A*01$^-$/A*03$^+$/A*68:01$^-$. The 12-day ELISpot and ICS results revealed that all peptides with putative HLA-A*68 restriction proved unable to bind to more than one HLA allotype (Fig. 5 a-b). Interestingly, HLA-B*07:02$^+$ donors showed strong IFN-γ immune response in ELISpot with 45% T cell recognition frequency against $HA_{LPY}$ peptide (Fig. 5 c). Moreover, the ICS data corroborated the 12-day ELISpot assay results (Fig. 5d-e) and demonstrated that the immune response was mediated by $CD8^+$ T cells. The $HA_{LPY}$ tetramer staining results were positive in eight of the tested donors (Fig. 5f,g). $HA_{LPY}$ epitope was further tested by *ex vivo* ELISpot assay in 5 donors, who showed a strong T cell response after 12-day stimulation. The result revealed that none of the donors elicited

immune response (Fig. 3h). Ultimately, the ELISpot as well as the ICS results demonstrated that peptides that induced T cell responses are restricted to one distinct HLA-I allotype with the exception of $HA_{LPY}$ peptide that is restricted to two prominent HLA-I allelic products (B*51 and B*07), providing broader coverage in population harboring at least one of these alleles.

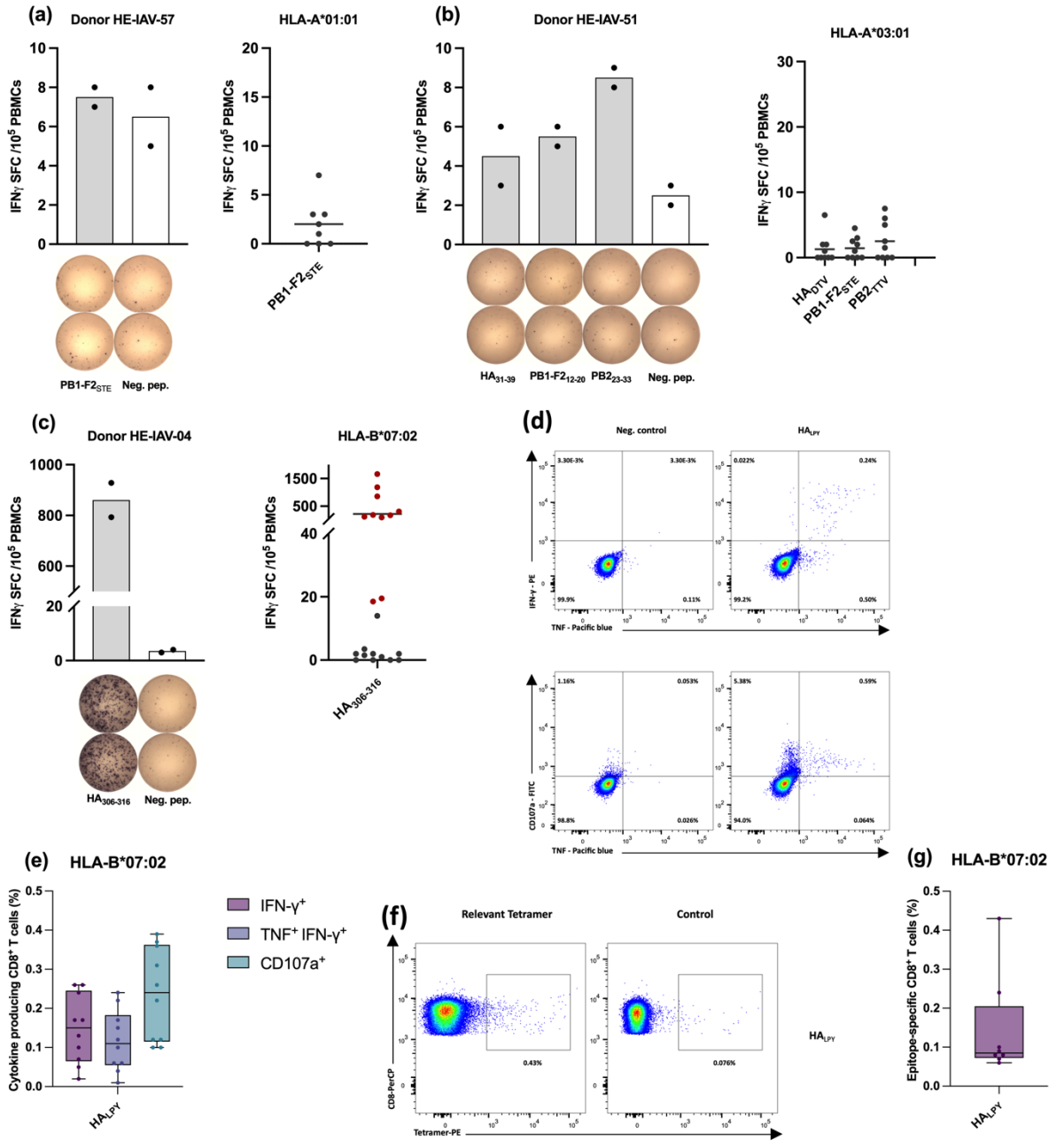


***Figure 5: Immunological characterization of naturally presented IAV-derived T cell epitopes by IFN-γ ELISpot assay****. Representative ELISpot assay after 12-day in vitro stimulation of PBMCs isolated from HLA-A*01* ***(a)****, HLA-A*03* ***(b)****, and HLA-B*07* ***(c)*** *-matched donors. Bars indicate mean spot counts of technical duplicates. The cumulative analysis of screening results was summarized in scatter plots* ***(a-c)****. Each data point represents one single donor tested within one single experiment. Shown are the*

*mean IFN-γ spot forming cells (SFCs) from two technical replicates of each tested donor normalized to the respective negative control. Horizontal lines represent the mean values of all tested donors. Positively evaluated donors are depicted by red circular shapes and negatively tested donors are shown by grey circular shapes.* ***(d-e)*** *Representative intracellular IFN-γ, TNF-α, and CD107a staining of PBMCs obtained from healthy HLA-matched donors (HLA-B*07), and tetramer staining* ***(f-g)*** *after 12-day amplification of $CD8^+$ T cells derived from HLA-matched donors. Box and whisker plots represent a cumulative percentage of $CD8^+$ IFN-$\gamma^+$, $CD8^+$ IFN-$\gamma^+$ TNF-$\alpha^+$ or $CD8^+$ CD107$a^+$* ***(e)*** *and the frequency of epitope-specific $CD8^+$ T cells evaluated by tetramer staining* ***(g)****. Boxes extend from the $25^{th}$ to $75^{th}$ percentiles, whiskers represent minimum to maximum, and the horizontal plotted lines are the median values. The indicated percentages represent the frequency of T-cell responses post stimulation with the test peptide minus the negative control of the respective donor. Each data point represents one single donor tested within one single experiment. The gating strategies applied for the flow cytometry-based analysis presented in this figure are depicted in the supplements (suppl. Fig. 1 and Fig.2).*

**Epitope conservation analysis across the zoonotic reservoir**

Sequence variation of IAV internal proteins exists among the zoonotic reservoirs, even though they exhibit a higher degree of conservation compared to the surface HA and NA proteins.

Therefore, a point mutation analysis was conducted for each epitope in more than 30,000 human IAV sequences, 6000 swine IAV sequences, and 10,000 avian IAV sequences. It was observed that the most highly conserved epitope was $PP2_{TTV}$; accounting for 100%, 96.8%, and 99% similarity in human, swine, and avian IAV sequences respectively, with total sequences conservation in 62,503 of 62,938 (99.3%) (Fig. 6 a-f).

Peptide $NP_{NLN}$ showed the second-leading conservation rate; at 92.4% in human, and 98% in both swine and avian IAV strains (Fig. 6 a-f). In terms of immunogenicity, it was determined to be the least immunogenic peptide by ELISpot assay (Fig. 3 g, suppl. Table 1). The most immunogenic peptides, $NP_{DAT}$ and $HA_{VYR}$, (suppl. Table 1, Fig. 3 d-g) were poorly conserved, especially concerning avian IAV sequences (1.8% and 2.4%, respectively), but they had dissimilar conservation scores accounting for 42.5% and 98.6% in human IAV strains; 82 % and 42.3% in swine IAV strains, respectively (Fig. 6 a-f). Conversely, $M1_{EAM}$ had nominal sequence identity in human and swine IAV strains, while it was highly conserved in avian IAV strains with a 79.4% homology score (Fig. 6 a-f). Moreover, $HA_{LPY}$ comprised at least one amino acid substitution leading to a minimal conservation rate of < 0.1% in each reservoir. Similarly,

$PB1_{ETM}$ was not conserved at all among swine IAV strains, while it showed conservation scores of 70% and 46.9% in both avian and human IAV strains, respectively.

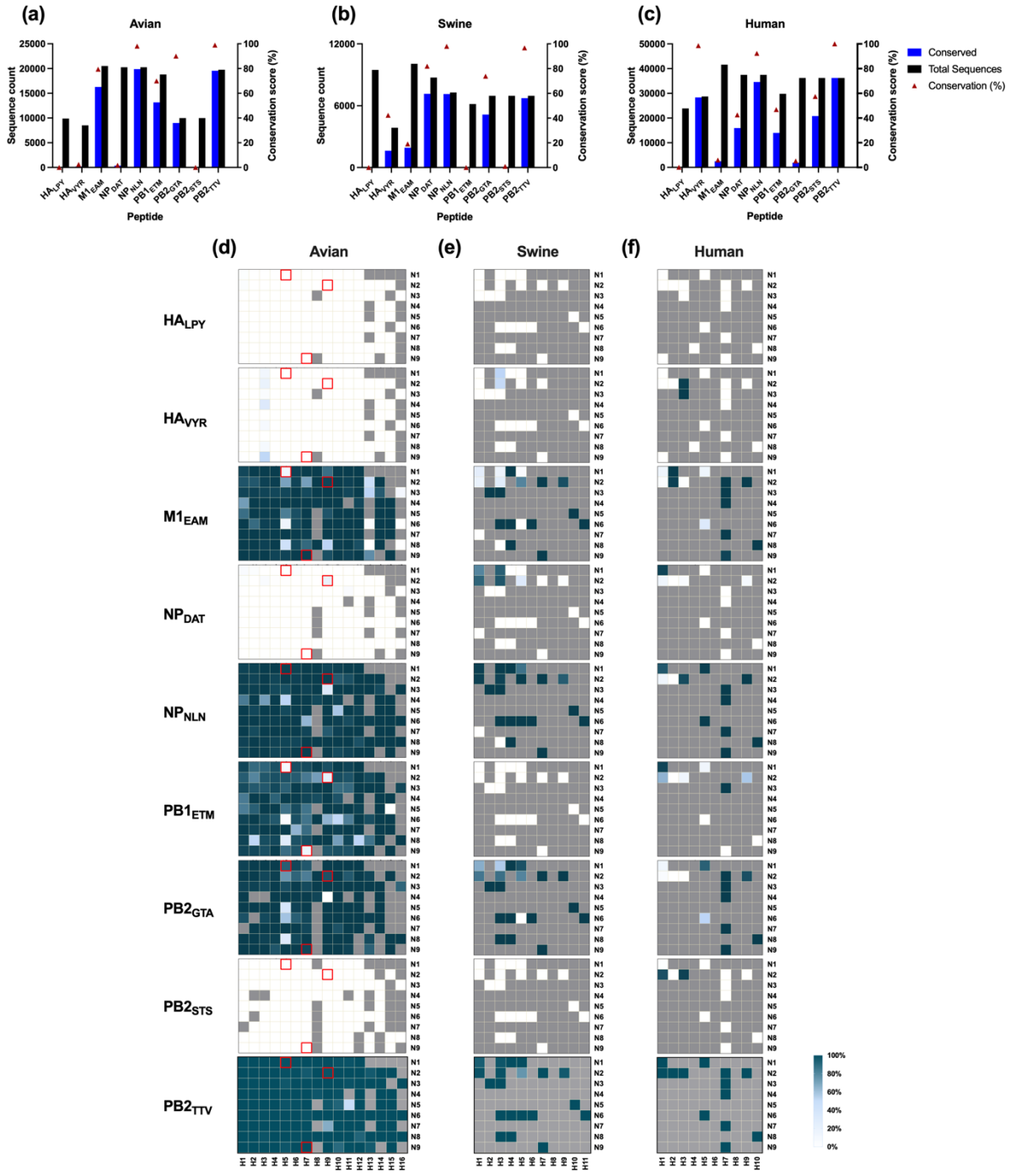


***Figure 6: HLA-I epitope conservation analysis in human, swine, and avian zoonotic reservoirs****. Bar graphs represent the number of identical sequences (blue), in all available IAV strains sequences (black) in avian (**a**), swine (**b**), and human (**c**). The conservation score (%) is depicted as superimposed red triangles. The distribution of conserved sequences across IAV subtypes is shown in heatmaps for avian (**d**), swine (**e**), and human sequences (**f**). The color scale represents the conservation index (%), which is*

*indicated as 0% (white color) to 100% (Dark slate gray color); the grey color indicates no sequences were available. Sequences with unknown hemagglutinin (H) or neuraminidase (N) were not included in the heatmaps. Red boxes indicate avian strains associated earlier with potential pandemics. Data were visualized using GraphPad Prism software ver. 9.3.*

Although $PB2_{GTA}$ and $PB2_{STS}$ showed comparable response rates by ELISpot assay to HLA-A*68:01, both peptides had identical sequences with two interchangeable AAs (suppl. Table 1). Moreover, $PB2_{GTA}$ proved to be highly conserved in avian and swine IAV strains but had a lower conservation score in human strains. Inversely, $PB2_{STS}$ had a minimal number of identical sequences in avian and swine IAV strains but exhibited an increased conservation rate in human sequences (Fig. 6 a-f).

Considering the potential for a pandemic threat of the H5N1, H9N2, and H7N9 subtypes, regions on heatmaps were marked by red boxes indicating the conservation of the tested epitopes in these highly relevant strains (Fig. 6 d-f).

**Amino acid substitutions close to anchor residues do not affect the binding of the IAV peptides under consideration**

Next, we extended the conservation analysis to assess AA substitutions aiming to reveal the mutational dissimilarities and to estimate the influence of respective substitutions on peptide binding affinity. The positions of the immunogenic peptides were also mapped onto the crystal structure of IAV proteins (Fig. 7 a-f).

Notably, peptides $NP_{NLN}$ and $PB2_{TTV}$ carried one single mutation in a nominal number of human H2N2 and swine IAV sequences respectively, which resulted in different peptide sequence variants, although those peptides showed the highest degree of homology (Fig. 8 a-b). In both peptides, most substitutions were I30V or K33R for peptide $PB2_{TTV}$ and A146T for peptide $NP_{NLN}$ (Suppl. Fig. 4 a-b). These substitutions were in the vicinity of the N- and C-terminal anchor residues and did not affect the peptide binding affinity to respective HLA molecules as predicted by the NetMHCpan algorithm.

For the highly immunogenic $NP_{DAT}$ peptide, sequence variations are mainly restricted to one AA substitution in human subtypes, (H3N2 and H2N2) and most avian IAV strains, while two AA substitutions were also observed, to a lesser extent, in the avian subtypes (Fig. 8 c). The

predominant substitutions were A131S as well as the I136L/M at the C-terminal anchor residue, but these amino acids are tolerated at the P9 position of the peptide binding groove and the ligand sequence variants harboring these substitutions exhibit strong binding affinity. A limited number of deleterious AA changes A128T and I136R were observed at both anchor residues of the $NP_{DAT}$ peptide (Suppl. Fig. 4 c). Likewise, a comparable substitution pattern was observed for $PB1_{ETM}$ attributed to single AA changes in human (H3N2, H2N2), avian (H5N1, H7N9, H9N2), and most swine strains (Fig. 8 d). The prevailing substitutions were M111I and V113K/A without influence on binding affinity (Suppl. Fig. 4 d).

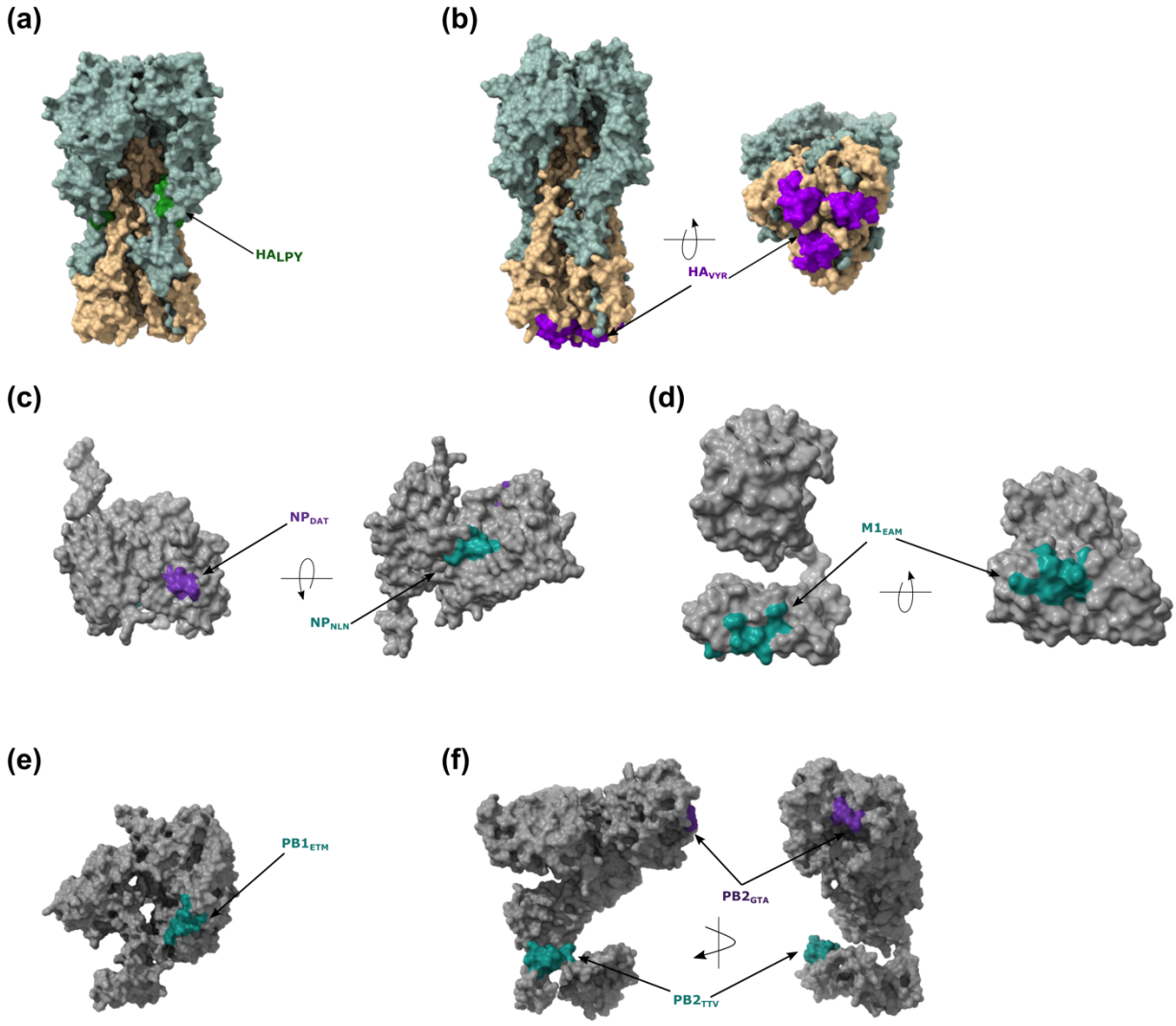


***Figure 7: Mapping of the immunogenic T cell epitopes onto IAV proteins****. The location of T cell epitopes is mapped on the crystal structure of IAV proteins obtained from the Protein Data Bank (PDB).* ***(a)*** *$HA_{LPY}$ (1RU7),* ***(b)*** *$HA_{VYR}$ (6CEX),* ***(c)*** *$NP_{DAT}$ and $NP_{NLN}$ (2IQH),* ***(d)*** *$M1_{EAM}$ (7JM3), $PB1_{ETM}$ (6RR7), and* ***(f)*** *$PB2_{GTA/STS}$ and $PB2_{TTV}$. Molecular graphics and analyses were performed with UCSF ChimeraX software.*

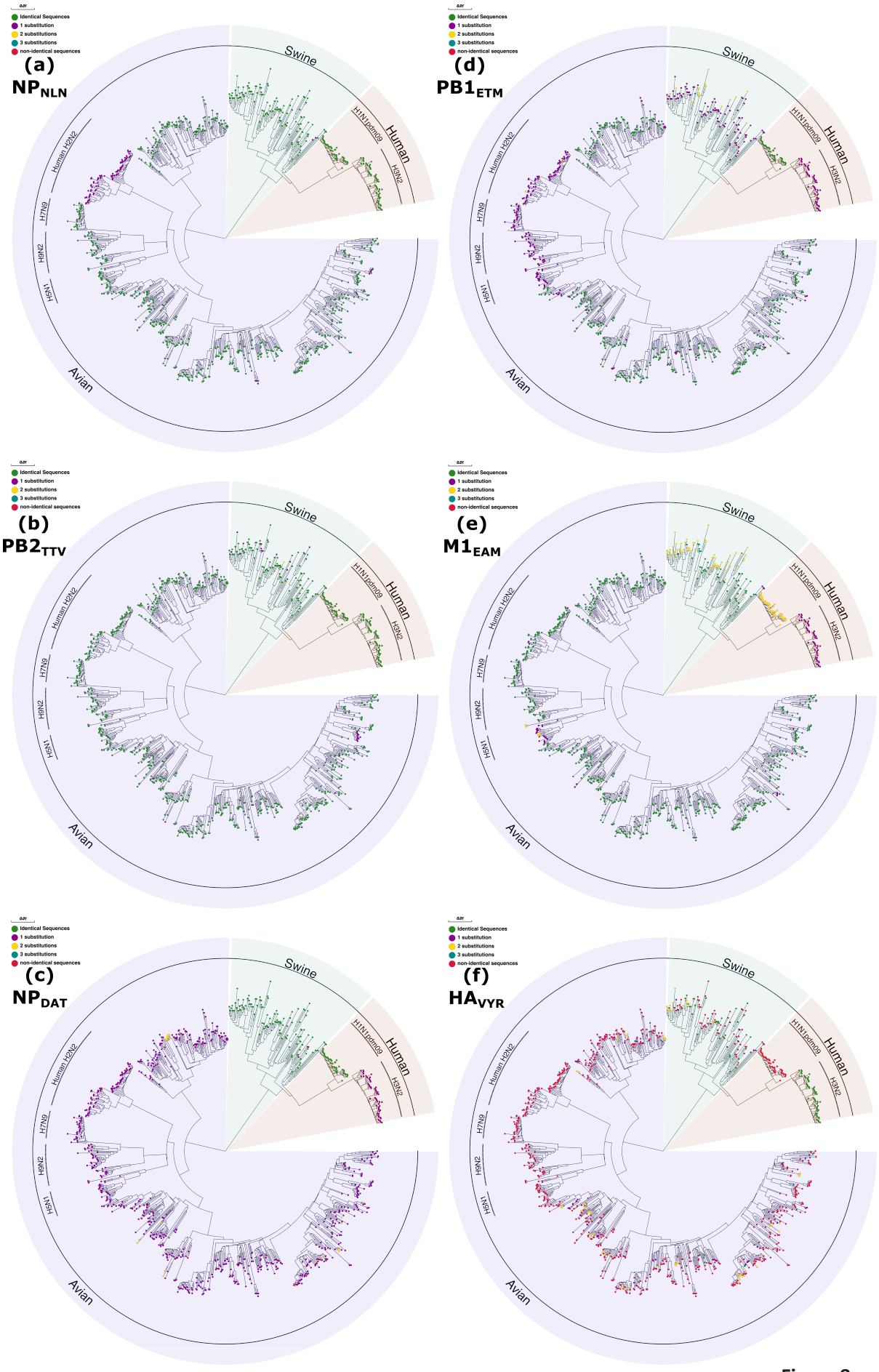


**Figure 8 continued**

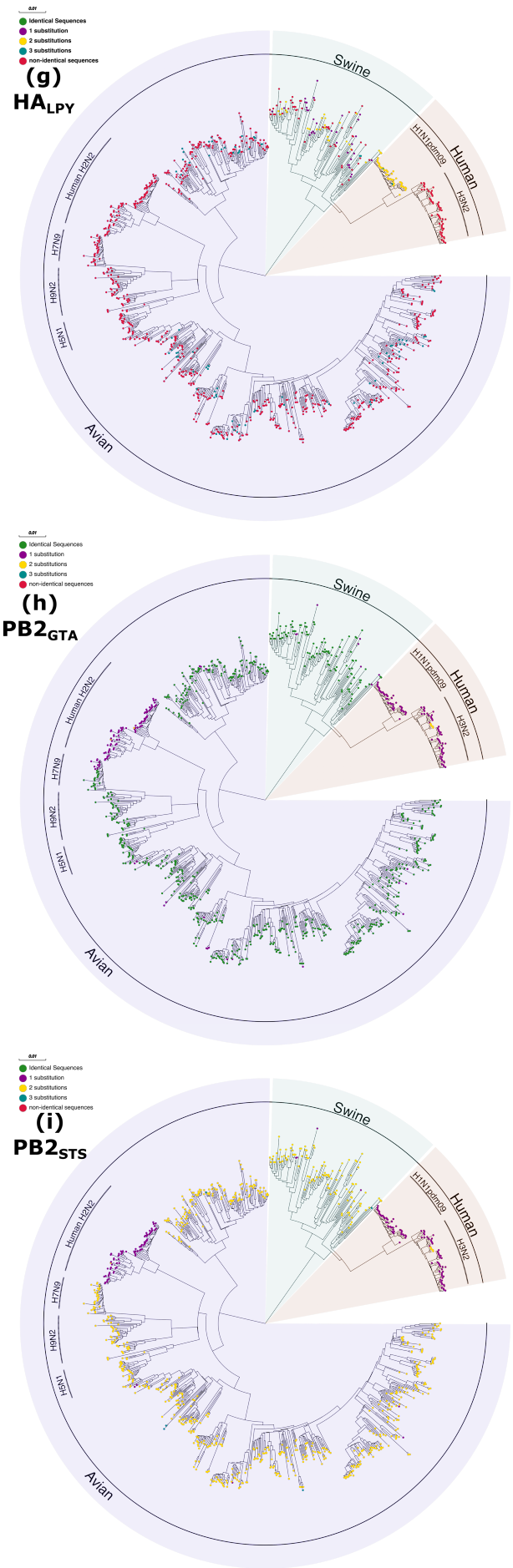


***Figure 8: Amino acid substitutions do not affect the peptide anchor residues.*** *Details of the substitutional divergence of all identified epitopes are depicted in the phylogenetic trees **(a-i)**. Sequence homology and amino acid substitution rates were estimated using the influenza research database by applying the point mutation analysis algorithm. The phylogenetic relationship was evaluated with the Neighbor-Joining method. The evolutionary distances were computed using the Jukes-Cantor model, and the variation rate among sites was modeled with a gamma distribution. Epitopes with identical sequences are designated in green; the number of amino acid substitutions is color-coded, and red color represents sequences that harbor more than 3 substitutions. Major IAV lineages and strains associated earlier with potential pandemics are indicated.*

Peptide $M1_{EAM}$ showed one to two AA changes in human, avian and swine IAV strains (Fig. 8 e). These substitutions were mainly V205I, S207N, A209T or Q208K and did not affect the anchor residues. Additionally, deleterious residues A202M and R210M/S/T were notable at P2 and P9 anchor positions in a scant number of peptide binding motifs (Suppl. Fig. 4 e).

This was also particularly striking for the $HA_{VYR}$ peptide in which the majority of avian, swine IAV sequences, as well as human H1N1 and H2N2, encompassed more than three mutations (namely non-identical sequences) (Fig. 8 f). The predominant substitutions were not at the anchor residues, except, F517I/L/M and I517V/Y/S mutations, which were found at the P9 C-terminus anchor residue, while the latter was deleterious for binding (Suppl. Fig. 4 f). The peptide $HA_{LPY}$ sequence showed diverse mutations in swine, human, and avian strains (Fig. 8 g). To the most extent, substitutions were rather distant from the anchor residues, nevertheless, preferred substitutions L306M/K at the P1 position and I316V/M at the P9 C-terminal anchor residue were also observed (Suppl. Fig. 4 g). These substitutions within $HA_{VYR}$ and $HA_{LPY}$ peptides marginally affected their binding affinity.

$PB2_{GTA}$ and $PB2_{STS}$ ligands showed one AA substitution in H1N1, H2N2, and H3N2 human subtypes (Fig. 8 h-i). The $PB2_{STS}$ sequence was attributed to two mutations in avian and swine sequences, while $PB2_{GTA}$ showed a high conservation level in both reservoirs except for a limited number of avian H7N9 sequences harboring single mutations. These substitutions, mainly S682G and A684S, were particularly found in IAV human subtypes (Suppl. Fig. 4 h).

Together, these analyses revealed that most epitopes are highly conserved in the major zoonotic reservoirs and can be attributed to a single mutation except for $HA_{VYR}$ and $HA_{LPY}$ epitopes. The results demonstrated that, in terms of conservation, epitope-specific $CD8^+$ T cells can confer broad recognition and thus potential reactivity against different IAV subtypes across the zoonotic reservoirs.

## Discussion

The relevance of Influenza virus clearance driven by $CD8^+$ T cells following infection is underscored and has been well-investigated in mouse models and humans [11,12,40]. In humans, antigen recognition mediated by $CD8^+$ T cells is dependent on the expression of HLA alleles, which are widely divergent between individuals. So far, different IAV-restricted $CD8^+$ T

cell epitopes have been described, for the most prevalent HLA alleles [11,12,41]. Nonetheless, further studies are imperative to fully explore the spectrum of $CD8^+$ T cell recognition towards influenza viruses for possible inclusion in T cell-based vaccine approaches.

This immunopeptidomic analysis aimed to identify IAV-derived peptides restricted to different HLA allotypes, HLA-A*24:02, HLA-A*68:01, HLA-B*07:02, and HLA-B*51:01, presented on the cell surface of Calu-3 cells following infection with H1N1/PR8, H3N2/Victoria and H3N2/Fukui strains at different infection time points. While a number of viruses, e.g., HIV and Herpesviruses are implicated to modulate MHC-I expression and interfere with MHC-I ligand presentation [37,39,42,43], herein, we investigated the modulation associated with IAV infection. The data revealed that altering the MHC-I surface expression post IAV infection likely depends on the virus/subtype and/or the cell line used. This inference is substantiated by the fact that two IAV strains, H1N1/PR8, and H3N2/Fukui, do not significantly change the MHC-I surface expression, whilst infection with H3N2/Victoria alters the expression profile. An earlier report demonstrated that IAV and influenza B viruses (IBV) alter the expression profile at a late stage of infection [44].

The Immunopeptidomic analysis revealed 16 naturally presented peptides exhibiting a high predicted binding affinity for HLA-A*68:01 (13 peptides), HLA-A*24:02 (1 peptide), and HLA-B*51:01 (2 peptides). The presentation kinetics demonstrated also that most peptides were detectable between 6-9 hpi and reached their peak at 12 hpi and that a substantial presentation early post infection for immunodominant epitopes is not always persistent. Our findings are in line with an earlier report indicating that the presentation kinetics of different ligands peaked between 6.5 - 9.5 hpi and were independent of antigen expression kinetics [45]. IAV manifest temporal regulation of gene expression at the translational level, and this is mirrored by the role of these proteins in the viral replication cycle [46,47]. Although immunopeptidomics was performed at different time points following infection, still several viral proteins were lacking as source proteins among the identified HLA-I ligands. These observations corroborate immunopeptidomics studies that identified different HLA-A*24–restricted peptides mostly annotated to PB2 and PB1 viral proteins without any presentation of either M1 or NA protein [48]. In contrast, Wu and colleagues identified naturally presented HLA-I-restricted IAV ligands comprising all IAV protein segments [45]. Collectively, the significance of viral ligand presentation following direct infection remains controversial.

Apparently, the antigen presentation is correlated to the degradation of viral proteins rather than protein expression.

Nine out of sixteen putative epitopes were functionally assessed and proved to be immunogenic, among which 5 epitopes were determined as immunodominant. The sporadic or weak T cell responses to certain peptides could be correlated to either the low avidity TCRs or the TCR-pMHC-I being in reversed docking mode, limiting the ability of naïve T cells to drive strong immune responses [49,50].

So far, in a preceding immunopeptidomics study, Habel and colleagues described two ligands ($PB2_{TTV}$ and $PB2_{GTA}$) as weak binders to HLA-A*11 and nonimmunogenic [51]. However, in our study both peptides as well as $PB2_{STS}$, the $PB2_{GTA}$-variant, were identified as strong binders to HLA-A*68, based on the *in silico* prediction algorithms and elicited $CD8^+$ T cell responses as confirmed by functional validation experiments. Of note, there are discrepancies between the accuracy of prediction algorithms and can result in ambiguity in the predicted MHC restriction. Also, *in silico* prediction tools may disregard several peptides that were experimentally validated on T cell level. So, it should be noted that ligands binding prediction does not necessarily correlate with their immunogenicity and cannot be used as a sole parameter. Similarly, Hensen and colleagues identified the HLA-A*24-restricted epitope, $HA_{VYR}$, as a weak binder of HLA-A*24:02 and did not reveal immunogenic characteristics during validation whereas we defined this epitope as a strong binder and an immunodominant epitope with polyfunctional characteristics [48].

The presentation of CTL epitopes can be affected by AA substitutions within the HLA ligand sequence. Mutations in CTL epitopes, in particular at an anchor residue, can result in loss of $CD8^+$ T cell recognition since the epitope no longer match the specific TCR [52-55]. In this context, our data showed that most epitopes are highly conserved in the major zoonotic reservoirs and alterations can be attributed to single AA substitutions, in particular for the $NP_{DAT}$ epitope, in the vicinity of the anchor residues without affecting the binding affinity. In addition, HA-derived epitopes showed the lowest conservation score with more than 3 AA changes and predominant substitutions located distant from the anchor residues. Nevertheless, other mutations were found at either P2 or the PΩ terminus, but these substitutions are preferable at this position. Earlier reports examined the variation of AA

sequences within the relatively conserved NP protein and showed that substitutions within NP-derived $CD8^+$ T cells epitopes at the anchor position P2 with deleterious AA resulted in the loss of epitope recognition and affected the virus-specific CTL response [54,56]. Further reports explored additional AA variations within other NP-derived epitopes that show signs of antigenic drift and revealed that the CTL clones elicit cross-reactive immune responses against heterosubtypic variants of the epitope [57]. Taken together, our data indicate that, in terms of conservation, epitope-specific $CD8^+$ memory T cells can confer cross-reactivity against multiple IAV subtypes across zoonotic reservoirs.

In summary, several IAV-derived epitopes were identified, thereby broadening the knowledge beyond the few previously characterized IAV-derived epitopes. These epitopes represent promising targets for T cell-based vaccination alongside other epitopes that could confer heterosubtypic protection in individuals, particularly against newly emerging variants and in the absence of any preexisting neutralizing antibody response.

### *Limitations of the study*

The results of this study should be interpreted in the context of their technical limitations. The immunopeptidome profiling has been carried out *in vitro*, in an infected tumor cell line. Nevertheless, testing the immunogenicity of the identified peptides in HLA-matched donors in an *ex vivo* setting supports their *in vivo* relevance and natural HLA peptides presentation. Second, the LC-MS/MS-based analysis has technical limitations and is prone to intrinsic biases. Hence, the lack of detection of other possibly immunogenic peptides is conceivable. We assume that performing the analysis with different IAV subtypes and at multiple infection time points may facilitate the identification of additional IAV epitopes. However, further studies with different IAV subtypes as well as cell lines expressing different HLA alleles are a prerequisite for the identification of additional epitopes.

### *Acknowledgments*

We would like to thank Prof. Dr. Cécile Gouttefangeas, Department of Immunology, University of Tübingen, for helpful discussions, and Martin Laure, Claudia Falkenburger, Ulrich Wulle and Beate Pömmerl for technical support. H. Hamza received a Ph.D. fellowship from the German Academic Exchange Service (DAAD) and the Egyptian Ministry of Higher Education and Scientific Research.

### Author Contributions

Conceptualization: H.H. and O.P.; methodology: H.H. and M.G.; formal analysis: H.H.; investigation: H.H. and O.P.; resources: O.P.; H.-G.R.; writing – original draft: H.H. and O.P.; writing – review & editing: H.H., M.G., M.W.L., H.-G.R. and O.P; visualization: H.H; supervision: H.H. and O.P.; project administration: H.H and O.P, and M.W.L.; funding acquisition: O.P.

### Competing Interests

None to declare.

## References

[1] Taubenberger JK and Morens DM. The Pathology of Influenza Virus Infections. Annual Review of Pathology: Mechanisms of Disease. **2008**;3(1):499-522.

[2] Sanjuán R, Nebot MR, Chirico N, Mansky LM and Belshaw R. Viral Mutation Rates. Journal of Virology. **2010**;84(19):9733-9748.

[3] Lauring AS and Andino R. Quasispecies theory and the behavior of RNA viruses. PLoS pathogens. **2010**;6(7):e1001005.

[4] Belongia EA, Simpson MD, King JP, Sundaram ME, Kelley NS, Osterholm MT and McLean HQ. Variable influenza vaccine effectiveness by subtype: a systematic review and meta-analysis of test-negative design studies. The Lancet Infectious Diseases. **2016**;16(8):942-951.

[5] Wu NC, Lv H, Thompson AJ, Wu DC, Ng WWS, Kadam RU, Lin C-W, Nycholat CM, McBride R, Liang W, Paulson JC, Mok CKP and Wilson IA. Preventing an Antigenically Disruptive Mutation in Egg-Based H3N2 Seasonal Influenza Vaccines by Mutational Incompatibility. Cell Host & Microbe. **2019**;25(6):836-844.e5.

[6] Zost SJ, Parkhouse K, Gumina ME, Kim K, Perez SD, Wilson PC, Treanor JJ, Sant AJ, Cobey S and Hensley SE. Contemporary H3N2 influenza viruses have a glycosylation site that alters binding of antibodies elicited by egg-adapted vaccine strains. Proceedings of the National Academy of Sciences. **2017**;114(47):12578-12583.

[7] Guthmiller JJ, Han J, Utset HA, Li L, Lan LY-L, Henry C, Stamper CT, McMahon M, O'Dell G, Fernández-Quintero ML, Freyn AW, Amanat F, Stovicek O, Gentles L, Richey ST, de la Peña AT, Rosado V, Dugan HL, Zheng N-Y, Tepora ME, Bitar DJ, Changrob S, Strohmeier S, Huang M, García-Sastre A, Liedl KR, Bloom JD, Nachbagauer R, Palese P, Krammer F, Coughlan L, Ward AB and Wilson PC. Broadly neutralizing antibodies target a haemagglutinin anchor epitope. Nature. **2022**;602(7896):314-320.

[8] Paules CI, Marston HD, Eisinger RW, Baltimore D and Fauci AS. The Pathway to a Universal Influenza Vaccine. Immunity. **2017**;47(4):599-603.

[9] Guthmiller JJ, Han J, Li L, Freyn AW, Liu STH, Stovicek O, Stamper CT, Dugan HL, Tepora ME, Utset HA, Bitar DJ, Hamel NJ, Changrob S, Zheng N-Y, Huang M, Krammer F, Nachbagauer R, Palese P, Ward AB and Wilson PC. First exposure to the pandemic H1N1 virus induced broadly neutralizing antibodies targeting hemagglutinin head epitopes. Science Translational Medicine. **2021**;13(596):eabg4535.

[10] Park J-K, Xiao Y, Ramuta MD, Rosas LA, Fong S, Matthews AM, Freeman AD, Gouzoulis MA, Batchenkova NA, Yang X, Scherler K, Qi L, Reed S, Athota R, Czajkowski L, Han A, Morens DM, Walters K-A, Memoli MJ, Kash JC and Taubenberger JK. Pre-existing immunity to influenza virus hemagglutinin stalk might drive selection for antibody-escape mutant viruses in a human challenge model. Nature medicine. **2020**;26(8):1240-1246.

[11] La Gruta NL and Turner SJ. T cell mediated immunity to influenza: mechanisms of viral control. Trends in Immunology. **2014**;35(8):396-402.

[12] Sridhar S, Begom S, Bermingham A, Hoschler K, Adamson W, Carman W, Bean T, Barclay W, Deeks JJ and Lalvani A. Cellular immune correlates of protection against symptomatic pandemic influenza. Nature Medicine. **2013**;19(10):1305-1312.

[13] Janssens Y, Joye J, Waerlop G, Clement F, Leroux-Roels G and Leroux-Roels I. The role of cell-mediated immunity against influenza and its implications for vaccine evaluation. Frontiers in immunology. **2022**;13:959379.

[14] Wang Z, Wan Y, Qiu C, Quiñones-Parra S, Zhu Z, Loh L, Tian D, Ren Y, Hu Y, Zhang X, Thomas PG, Inouye M, Doherty PC, Kedzierska K and Xu J. Recovery from severe H7N9 disease is associated with diverse response mechanisms dominated by CD8+ T cells. Nature communications. **2015**;6(1):6833.

[15] Hayward AC, Wang L, Goonetilleke N, Fragaszy EB, Bermingham A, Copas A, Dukes O, Millett ER, Nazareth I, Nguyen-Van-Tam JS, Watson JM, Zambon M, Flu Watch G, Johnson AM and McMichael AJ. Natural T Cell-mediated Protection against Seasonal and Pandemic Influenza. Results of the Flu Watch Cohort Study. American journal of respiratory and critical care medicine. **2015**;191(12):1422-31.

[16] Koutsakos M, Wheatley AK, Loh L, Clemens EB, Sant S, Nussing S, Fox A, Chung AW, Laurie KL, Hurt AC, Rockman S, Lappas M, Loudovaris T, Mannering SI, Westall GP, Elliot M, Tangye SG, Wakim LM, Kent SJ, Nguyen THO and Kedzierska K. Circulating T(FH) cells, serological memory, and tissue compartmentalization shape human influenza-specific B cell immunity. Sci Transl Med. **2018**;10(428).

[17] Croft NP, Smith SA, Wong YC, Tan CT, Dudek NL, Flesch IEA, Lin LCW, Tscharke DC and Purcell AW. Kinetics of Antigen Expression and Epitope Presentation during Virus Infection. PLoS pathogens. **2013**;9(1):e1003129.

[18] Tscharke DC, Croft NP, Doherty PC and La Gruta NL. Sizing up the key determinants of the CD8+ T cell response. Nature Reviews Immunology. **2015**;15(11):705-716.

[19] Scholtalbers J, Boegel S, Bukur T, Byl M, Goerges S, Sorn P, Loewer M, Sahin U and Castle JC. TCLP: an online cancer cell line catalogue integrating HLA type, predicted neo-epitopes, virus and gene expression. Genome Med. **2015**;7:118.

[20] Kowalewski DJ and Stevanović S. Biochemical Large-Scale Identification of MHC Class I Ligands. In: van Endert P, editor. Antigen Processing: Methods and Protocols. Totowa, NJ: Humana Press; 2013. p. 145-157.

[21] Falk K, Rotzschke O, Stevanovic S, Jung G and Rammensee HG. Allele-specific motifs revealed by sequencing of self-peptides eluted from MHC molecules. Nature. **1991**;351(6324):290-6.

[22] Käll L, Canterbury JD, Weston J, Noble WS and MacCoss MJ. Semi-supervised learning for peptide identification from shotgun proteomics datasets. Nat Methods. **2007**;4(11):923-5.

[23] Jurtz V, Paul S, Andreatta M, Marcatili P, Peters B and Nielsen M. NetMHCpan-4.0: Improved Peptide-MHC Class I Interaction Predictions Integrating Eluted Ligand and Peptide Binding Affinity Data. Journal of immunology. **2017**;199(9):3360-3368.

[24] Rammensee H, Bachmann J, Emmerich NP, Bachor OA and Stevanovic S. SYFPEITHI: database for MHC ligands and peptide motifs. Immunogenetics. **1999**;50(3-4):213-9.

[25] Nelde A, Kowalewski DJ, Backert L, Schuster H, Werner JO, Klein R, Kohlbacher O, Kanz L, Salih HR, Rammensee HG, Stevanović S and Walz JS. HLA ligandome analysis of primary chronic lymphocytic leukemia (CLL) cells under lenalidomide treatment confirms the suitability of lenalidomide for combination with T-cell-based immunotherapy. Oncoimmunology. **2018**;7(4):e1316438.

[26] Lazar C, Gatto L, Ferro M, Bruley C and Burger T. Accounting for the Multiple Natures of Missing Values in Label-Free Quantitative Proteomics Data Sets to Compare Imputation Strategies. J Proteome Res. **2016**;15(4):1116-25.

[27] Stead DA, Paton NW, Missier P, Embury SM, Hedeler C, Jin B, Brown AJ and Preece A. Information quality in proteomics. Brief Bioinform. **2008**;9(2):174-88.

[28] Liu H, Sadygov RG and Yates JR, 3rd. A model for random sampling and estimation of relative protein abundance in shotgun proteomics. Anal Chem. **2004**;76(14):4193-201.

[29] Zhang Y, Aevermann BD, Anderson TK, Burke DF, Dauphin G, Gu Z, He S, Kumar S, Larsen CN, Lee AJ, Li X, Macken C, Mahaffey C, Pickett BE, Reardon B, Smith T, Stewart L, Suloway C, Sun G, Tong L, Vincent AL, Walters B, Zaremba S, Zhao H, Zhou L, Zmasek C, Klem EB and Scheuermann RH. Influenza Research Database: An integrated bioinformatics resource for influenza virus research. Nucleic Acids Res. **2017**;45(D1):D466-D474.

[30] Kuraku S, Zmasek CM, Nishimura O and Katoh K. aLeaves facilitates on-demand exploration of metazoan gene family trees on MAFFT sequence alignment server with enhanced interactivity. Nucleic Acids Res. **2013**;41(Web Server issue):W22-8.

[31] Katoh K, Rozewicki J and Yamada KD. MAFFT online service: multiple sequence alignment, interactive sequence choice and visualization. Brief Bioinform. **2019**;20(4):1160-1166.

[32] Subramanian B, Gao S, Lercher MJ, Hu S and Chen WH. Evolview v3: a webserver for visualization, annotation, and management of phylogenetic trees. Nucleic Acids Res. **2019**;47(W1):W270-W275.

[33] Thomsen MC and Nielsen M. Seq2Logo: a method for construction and visualization of amino acid binding motifs and sequence profiles including sequence weighting, pseudo counts and two-sided representation of amino acid enrichment and depletion. Nucleic acids research. **2012**;40(Web Server issue):W281-7.

[34] Goddard TD, Huang CC, Meng EC, Pettersen EF, Couch GS, Morris JH and Ferrin TE. UCSF ChimeraX: Meeting modern challenges in visualization and analysis. Protein Sci. **2018**;27(1):14-25.

[35] Perez-Riverol Y, Csordas A, Bai J, Bernal-Llinares M, Hewapathirana S, Kundu DJ, Inuganti A, Griss J, Mayer G, Eisenacher M, Pérez E, Uszkoreit J, Pfeuffer J, Sachsenberg T, Yilmaz S, Tiwary S, Cox J, Audain E, Walzer M, Jarnuczak AF, Ternent T, Brazma A and Vizcaíno JA. The PRIDE database and related tools and resources in 2019: improving support for quantification data. Nucleic Acids Res. **2019**;47(D1):D442-d450.

[36] Blagoveshchenskaya AD, Thomas L, Feliciangeli SF, Hung C-H and Thomas G. HIV-1 Nef Downregulates MHC-I by a PACS-1- and PI3K-Regulated ARF6 Endocytic Pathway. Cell. **2002**;111(6):853-866.

[37] Petersen JL, Morris CR and Solheim JC. Virus evasion of MHC class I molecule presentation. J Immunol. **2003**;171(9):4473-8.

[38] Cohen GB, Gandhi RT, Davis DM, Mandelboim O, Chen BK, Strominger JL and Baltimore D. The Selective Downregulation of Class I Major Histocompatibility Complex Proteins by HIV-1 Protects HIV-Infected Cells from NK Cells. Immunity. **1999**;10(6):661-671.

[39] Compeer EB, Flinsenberg TW, van der Grein SG and Boes M. Antigen Processing and Remodeling of the Endosomal Pathway: Requirements for Antigen Cross-Presentation [Review]. Frontiers in immunology. **2012**;3:37.

[40] Krammer F, Smith GJD, Fouchier RAM, Peiris M, Kedzierska K, Doherty PC, Palese P, Shaw ML, Treanor J, Webster RG and García-Sastre A. Influenza. Nature Reviews Disease Primers. **2018**;4(1):3.

[41] Thomas PG, Keating R, Hulse-Post DJ and Doherty PC. Cell-mediated protection in influenza infection. Emerg Infect Dis. **2006**;12(1):48-54.

[42] Kasper MR and Collins KL. Nef-mediated disruption of HLA-A2 transport to the cell surface in T cells. J Virol. **2003**;77(5):3041-9.

[43] Piguet V, Wan L, Borel C, Mangasarian A, Demaurex N, Thomas G and Trono D. HIV-1 Nef protein binds to the cellular protein PACS-1 to downregulate class I major histocompatibility complexes. Nature cell biology. **2000**;2(3):163-7.

[44] Koutsakos M, McWilliam HEG, Aktepe TE, Fritzlar S, Illing PT, Mifsud NA, Purcell AW, Rockman S, Reading PC, Vivian JP, Rossjohn J, Brooks AG, Mackenzie JM, Mintern JD, Villadangos JA, Nguyen THO and Kedzierska K. Downregulation of MHC Class I Expression by Influenza A and B Viruses [Original Research]. Frontiers in immunology. **2019**;10:1158.

[45] Wu T, Guan J, Handel A, Tscharke DC, Sidney J, Sette A, Wakim LM, Sng XYX, Thomas PG, Croft NP, Purcell AW and La Gruta NL. Quantification of epitope abundance reveals the effect of direct and cross-presentation on influenza CTL responses. Nature communications. **2019**;10(1):2846.

[46] Gale M, Jr., Tan SL and Katze MG. Translational control of viral gene expression in eukaryotes. Microbiol Mol Biol Rev. **2000**;64(2):239-80.

[47] Krammer F and Palese P. Orthomyxoviridae: The Viruses and Their Replication. In: Howley PM, Knipe DM, editors. Fields Virology: Emerging Viruses. Vol. Seventh edition. Philadelphia: Wolters Kluwer Health; 2020. p. 1224-1337.

[48] Hensen L, Illing PT, Bridie Clemens E, Nguyen THO, Koutsakos M, van de Sandt CE, Mifsud NA, Nguyen AT, Szeto C, Chua BY, Halim H, Rizzetto S, Luciani F, Loh L, Grant EJ, Saunders PM, Brooks AG, Rockman S, Kotsimbos TC, Cheng AC, Richards M, Westall GP, Wakim LM, Loudovaris T, Mannering SI, Elliott M, Tangye SG, Jackson DC, Flanagan KL, Rossjohn J, Gras S, Davies J, Miller A, Tong SYC, Purcell AW and Kedzierska K. CD8+ T cell landscape in Indigenous and non-Indigenous people restricted by influenza mortality-associated HLA-A*24:02 allomorph. Nature communications. **2021**;12(1):2931.

[49] Gras S, Chadderton J, Del Campo Claudia M, Farenc C, Wiede F, Josephs Tracy M, Sng Xavier YX, Mirams M, Watson Katherine A, Tiganis T, Quinn Kylie M, Rossjohn J and La Gruta Nicole L. Reversed T Cell Receptor Docking on a Major Histocompatibility Class I Complex Limits Involvement in the Immune Response. Immunity. **2016**;45(4):749-760.

[50] Cukalac T, Chadderton J, Zeng W, Cullen JG, Kan WT, Doherty PC, Jackson DC, Turner SJ and La Gruta NL. The Influenza Virus–Specific CTL Immunodominance Hierarchy in Mice Is Determined by the Relative Frequency of High-Avidity T Cells. The Journal of Immunology. **2014**;192(9):4061-4068.

[51] Habel JR, Nguyen AT, Rowntree LC, Szeto C, Mifsud NA, Clemens EB, Loh L, Chen W, Rockman S, Nelson J, Davies J, Miller A, Tong SYC, Rossjohn J, Gras S, Purcell AW, Hensen L, Kedzierska K and Illing PT. HLA-A*11:01-restricted CD8+ T cell immunity

against influenza A and influenza B viruses in Indigenous and non-Indigenous people. PLoS pathogens. **2022**;18(3):e1010337.

[52] Rammensee H-G, Friede T and Stevanović S. MHC ligands and peptide motifs: first listing. Immunogenetics. **1995**;41(4):178-228.

[53] Rammensee H-G. Chemistry of peptides associated with MHC class I and class II molecules. Current Opinion in Immunology. **1995**;7(1):85-96.

[54] Berkhoff EG, Boon AC, Nieuwkoop NJ, Fouchier RA, Sintnicolaas K, Osterhaus AD and Rimmelzwaan GF. A mutation in the HLA-B*2705-restricted NP383-391 epitope affects the human influenza A virus-specific cytotoxic T-lymphocyte response in vitro. J Virol. **2004**;78(10):5216-22.

[55] Rimmelzwaan GF, Boon AC, Voeten JT, Berkhoff EG, Fouchier RA and Osterhaus AD. Sequence variation in the influenza A virus nucleoprotein associated with escape from cytotoxic T lymphocytes. Virus Res. **2004**;103(1-2):97-100.

[56] Berkhoff EG, Geelhoed-Mieras MM, Verschuren EJ, van Baalen CA, Gruters RA, Fouchier RA, Osterhaus AD and Rimmelzwaan GF. The loss of immunodominant epitopes affects interferon-gamma production and lytic activity of the human influenza virus-specific cytotoxic T lymphocyte response in vitro. Clin Exp Immunol. **2007**;148(2):296-306.

[57] Gras S, Kedzierski L, Valkenburg SA, Laurie K, Liu YC, Denholm JT, Richards MJ, Rimmelzwaan GF, Kelso A, Doherty PC, Turner SJ, Rossjohn J and Kedzierska K. Cross-reactive CD8+ T-cell immunity between the pandemic H1N1-2009 and H1N1-1918 influenza A viruses. Proceedings of the National Academy of Sciences of the United States of America. **2010**;107(28):12599-604.

## Supplementary materials

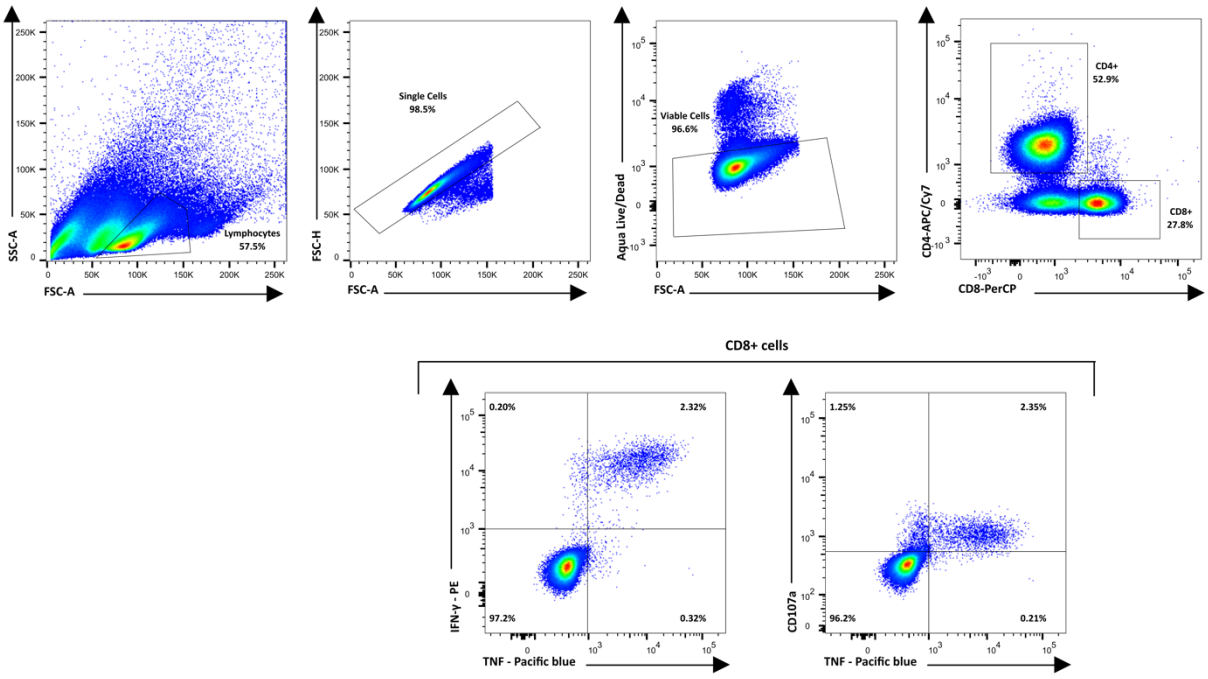


***Supplementary Figure 1: Gating strategy for flow cytometry-based intracellular cytokines staining.*** *The first gate (FSC-A vs. SSC-A) shows lymphocyte identification, which is further gated to single cells (FSC-A vs. FSC-H) and subsequently gated to identify viable cells (FSC-A vs. Aqua live/dead). The identified populations of CD4+ and CD8+ cells were evaluated for their cytokine production (TNF-Pacific Blue vs. IFN-γ-PE) alongside their degranulation (TNF-Pacific Blue vs. CD107a-FITC).*

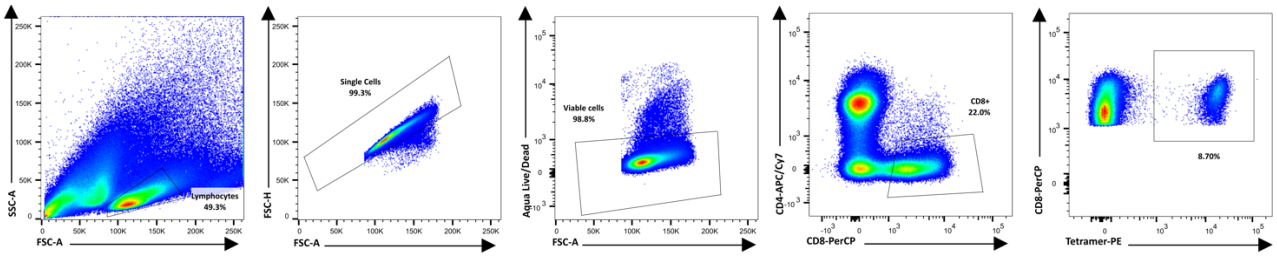


***Supplementary Figure 2: Gating strategy for flow cytometry-based tetramer staining.*** *The first gate (FSC-A vs. SSC-A) shows lymphocyte identification. Singlet cells were identified using the forward and side scatters and further gated to exclude dead cells (FSC-A vs. Aqua live/dead). The identified CD8+ cell population was evaluated to estimate the epitope-specific CD8+ T cells (CD8-PerCP vs. Tetramer-PE).*

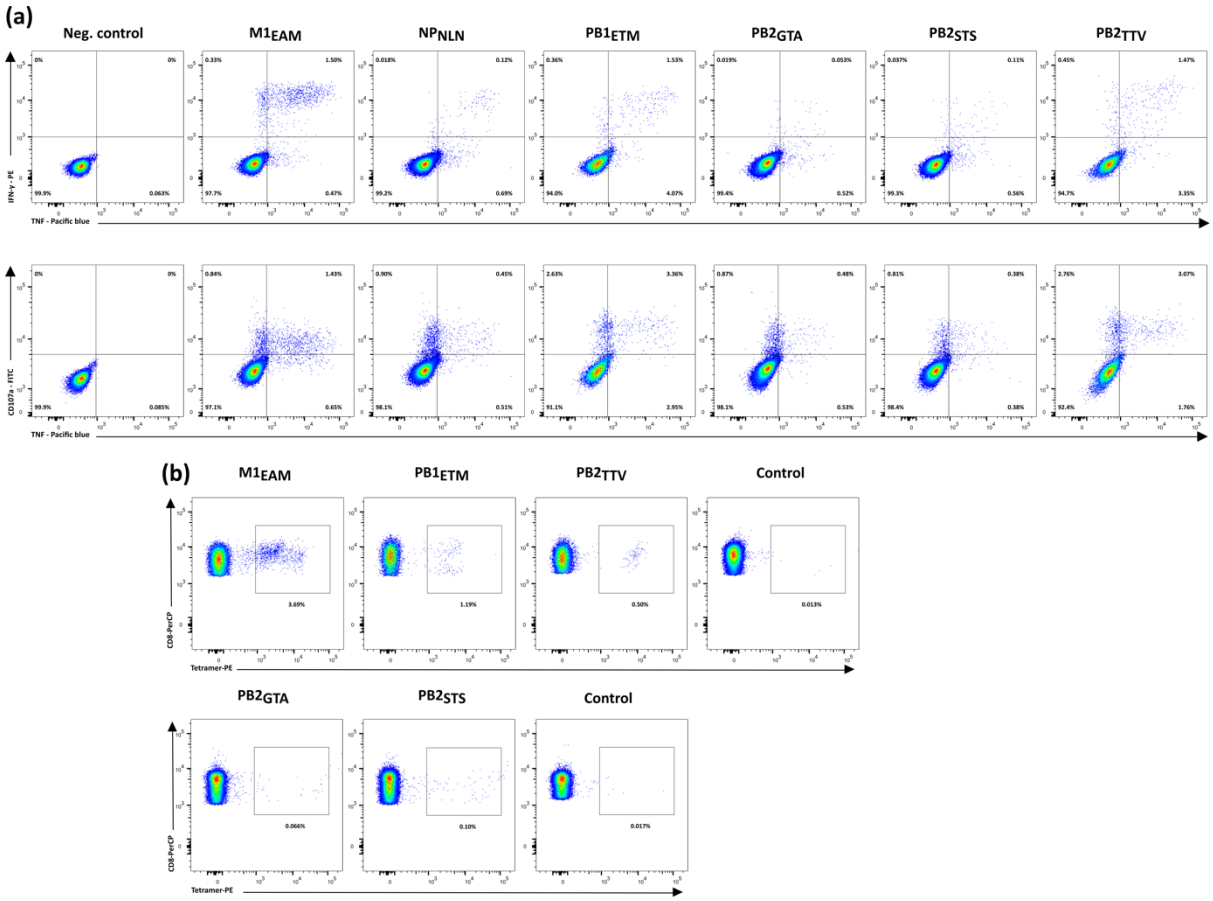


***Supplementary Figure 3: IAV-derived T cell epitopes are multifunctional.*** *Representative (a) intracellular IFN-γ, TNF-α, and CD107a staining (b) tetramer staining of PBMCs isolated from healthy HLA-A*68:01-matched donors after 12-day stimulation with IAV-derived HLA class I peptides evaluated by flow cytometry-based analysis.*

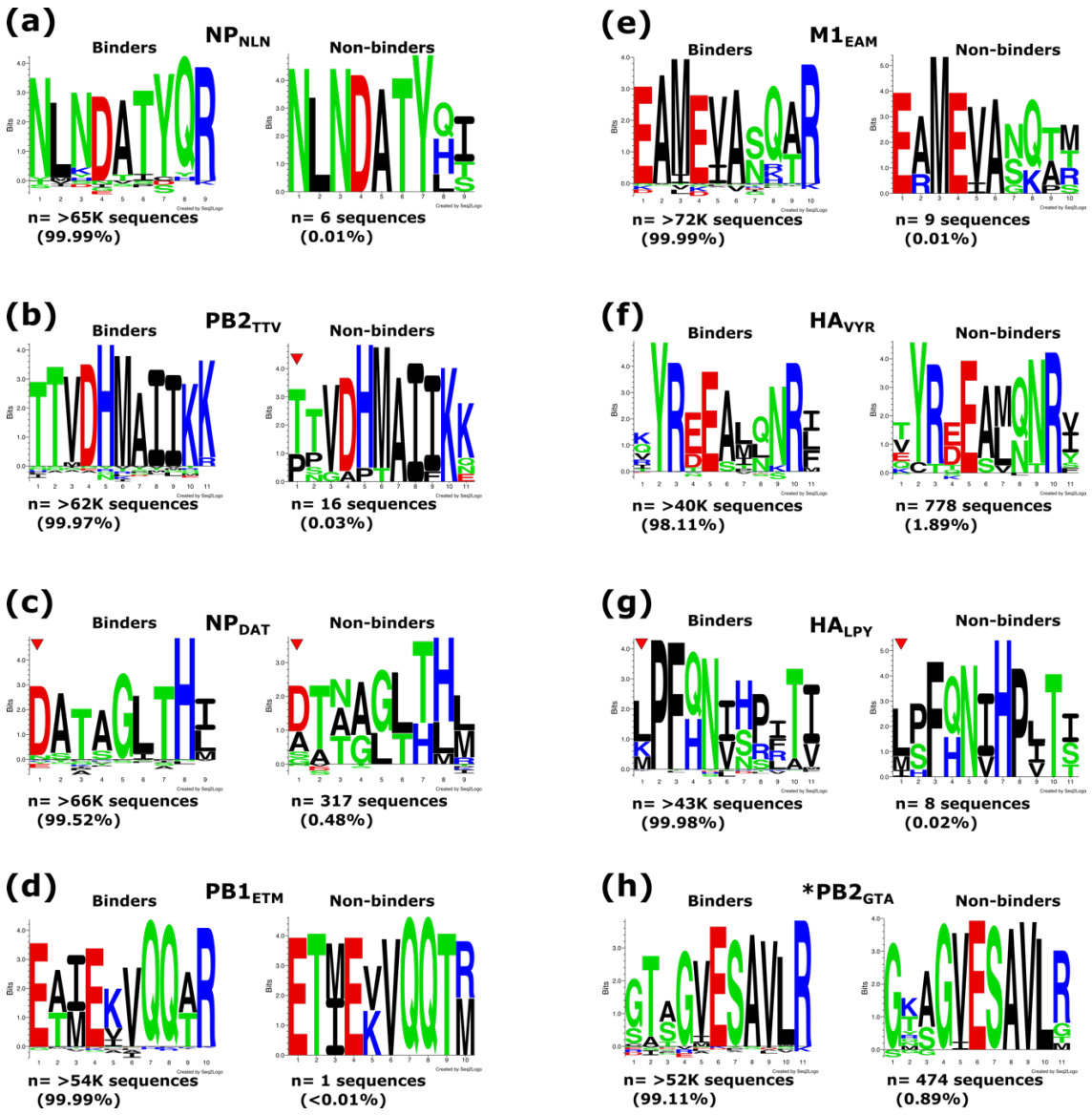


***Supplementary Figure 4: Amino acid substitutions exhibit an imperceptible effect on the peptides anchor residues.*** *Sequence logos of amino acid binding motifs and sequence variants profiles showing the frequency of residues at different positions (a-h). Both binder and non-binder motifs panels were categorized according to NetMHCpan 4.0. The "n" represents the number of sequence variants found for each epitope. Sequence motifs were generated using Seq2Logo-2.1 by applying the default setting; logo type Kullback–Leibler with coloring scheme by physicochemical properties and Hobohm1 clustering method. Letters represent amino acid codes, and their heights are proportional to frequencies, big stacks represent conservations and small stacks represent divergence. The x-axis shows amino acid positions, the y-axis reports the content of different residues at each position. Amino acids at the P1 position that echo the P2 anchor preferences are indicated by red arrows.*

**Supplementary Table 1: Summary of IAV-derived peptides identified by LC-MS/MS.**

| Peptide ID | Source protein | Protein accession | Sequence | Position | HLA restriction | ELISpot response rate % | | Tetramer staining |
|---|---|---|---|---|---|---|---|---|
| | | | | | | 12-d stimulation | Ex vivo | |
| **HA$_{DTV}$** | HA | P03452 | DTVDTVLEK | 31-39 | A*68:01 | 0.0 (0/12) | nt | nt |
| **HA$_{LPY}$** | HA | P03452 | LPYQNIHPVTI | 306-316 | B*51:01 | 85.7 (12/14) | 0.0 | Positive |
| **HA$_{NSN}$** | HA | P03435 | NSNGNLIAPR | 263-272 | A*68:01 | 0.0 (0/12) | 0.0 | nt |
| **HA$_{VYR}$** | HA | D8KQT3 | VYRDEALNNRF | 507-517 | A*24:02 | 76.9 (10/13) | 0.0 | Positive |
| **M1$_{EAM}$** | M1 | P03485 | EAMEVASQAR | 201-210 | A*68:01 | 66.7 (8/12) | nt | Positive |
| **NP$_{DAT}$** | NP | D8KQT4 | DATAGLTHI | 128-136 | B*51:01 | 100 (15/15) | 20.0 (1/5) | Positive |
| **NP$_{NLN}$** | NP | P03466 | NLNDATYQR | 142-150 | A*68:01 | 16.7 (2/12) | nt | nt |
| **NS1$_{TMA}$** | NS1 | P03496 | TMASVPASR | 80-88 | A*68:01 | 0.0 (0/12) | nt | nt |
| **NS2$_{DSL}$** | NS2 | P03508 | DSLGEAVMR | 43-51 | A*68:01 | 0.0 (0/12) | nt | nt |
| **PB1$_{ETM}$** | PB1 | P31341 | ETMEVVQQTR | 109-118 | A*68:01 | 33.3 (4/12) | nt | Positive |
| **PB1$_{VDK}$** | PB1 | P03431 | EVVQQTRVDK | 112-121 | A*68:01 | 0.0 (0/12) | nt | nt |
| **PB1$_{VDR}$** | PB1 | P31341 | EVVQQTRVDR | 112-121 | A*68:01 | 0.0 (0/12) | nt | nt |
| **PB1-F2$_{STE}$** | PB1-F2 | H9XIJ4 | STEHINIQK | 12-20 | A*68:01 | 0.0 (0/12) | nt | nt |
| **PB2$_{GTA}$** | PB2 | P03428 | GTAGVESAVLR | 682-692 | A*68:01 | 41.7 (5/12) | nt | Positive |

| Peptide ID | Source protein | Protein accession | Sequence | Position | HLA restriction | ELISpot response rate % | | Tetramer staining |
|---|---|---|---|---|---|---|---|---|
| **PB2$_{STS}$** | PB2 | P31345 | STSGVESAVLR | 682-692 | A*68:01 | 33.3 (4/12) | nt | Positive |
| **PB2$_{TTV}$** | PB2 | P31345 | TTVDHMAIIKK | 23-33 | A*68:01 | 66.7 (8/12) | nt | Positive |

nt: not tested.

**Supplementary Table 2: Summary of IAV-derived epitopes showing predicted affinity to multiple HLAs.**

| Peptide ID | Protein | Protein accession | Sequence | Position | ELISpot response rate % | | Actual HLA | Tested HLA | NetMHC Rank | Intracellular staining | Tetramer staining |
|---|---|---|---|---|---|---|---|---|---|---|---|
| | | | | | 12-d stimulation | Ex vivo | | | | | |
| **HA$_{DTV}$** | HA | P03452 | DTVDTVLEK | 31-39 | 0.0 (0/9) | nt | A*68:01 | A*03:01 | 1.948 | Negative | nt |
| **PB1-F2$_{STE}$** | PB1-F2 | H9XIJ4 | STEHINIQK | 12-20 | 0.0 (0/9) | nt | A*68:01 | | 0.503 | Negative | nt |
| **PB2$_{TTV}$** | PB2 | P31345 | TTVDHMAIIKK | 23-33 | 0.0 (0/9) | nt | A*68:01 | | 0.718 | Negative | nt |
| **PB1-F2$_{STE}$** | PB1-F2 | H9XIJ4 | STEHINIQK | 12-20 | 0.0 (0/9) | nt | A*68:01 | A*01:01, A*03:01 | 1.142 | Negative | nt |
| **HA$_{LPY}$** | HA | P03452 | LPYQNIHPVTI | 306-316 | 45.5 (10/22) | 0.0 | B*51:01 | B*07:02 | 1.4974 | CD8 | Positive |

nt: not tested.

# General Discussion

Effective prevention and treatment of influenza rely on the development of vaccines and antiviral drugs. Like other RNA viruses, influenza viruses exploit a high rate of mutations as well as reassortment that significantly attributed to their evolution. Continuous accumulation of point mutations modifies the genome sequence, allowing the virus to generate a multitude of genetic and antigenic variants. Moreover, the segmented genome facilitates the exchange of vRNA segments between different viruses during co-infection, resulting in the emergence of new viruses with altered characteristics [1]. Thus, annual reformulation of vaccines is necessary to match the circulating strains that either mutated or lost the targets recognized by preexisting neutralizing antibody response, leading to a high number of non-responders [2-5]. Using vaccination solely is not at all sufficient to control influenza. On the other hand, antiviral therapy is an essential component in the fight against the disease. Nevertheless, the currently available anti-influenza drugs are very limited, not very effective, and prone to resistance. Accordingly, there is an urgent demand for the development of novel antiviral drugs and finding alternatives to currently used approaches [4-6].

Influenza viruses also rely on crucial host factors, including cellular signaling pathways e.g. Raf/MEK/ERK signaling cascade. Importantly, these factors are not encoded by the virus and are thus not susceptible to mutations caused by the RdRp. During infection, the virus triggers the Raf/MEK/ERK signaling pathway, which enhances efficient replication by boosting RdRp activity. The key role played by the Raf/MEK/ERK signaling pathway in the context of influenza viruses suggests the potential to target this pathway for novel anti-influenza strategy.

In the realm of repurposing drugs, the antiviral potential of the MEK inhibitor, zapnometinib (previously designated ATR-002, PD0184264) was investigated. The results revealed that zapnometinib can effectively impair the replication of different IAV strains and subtypes. Earlier studies also reported MEK inhibition demonstrated strong antiviral activity against a wide range of IAV and IBV strains, including the highly pathogenic H5N1 avian influenza viruses [7-9]. On the other hand, Baloxavir Marboxil (BXA), the recently licensed polymerase inhibitor, demonstrates efficacy not only against human IAV and IBV but also against avian and swine subtypes. Although BXA is robust as a single-dose antiviral drug, its use has led to a significant level of viral resistance [10-13]. Given that the emergence of DAA-resistant strains is a major

challenge, the inhibitory activity of zapnometinib was assessed against H1N1 and H3N2 strains carrying the BXA resistance-associated PA-I38T mutation. The findings validated the indirectly antiviral-acting host-targeting MEK inhibitor could overcome viral resistance of IAV-carrying substitutions mounted against the directly acting antiviral BXA.

However, In the context of treating seasonal influenza, adverse effects are frequently regarded as the primary concern when inhibiting cellular signaling pathways. These concerns could be mitigated by either administering short-term treatment to IV-infected patients or by considering a combinatorial strategy with other DAA drugs. This approach can help to lower the dosage while still having a potent antiviral effect [14]. Moreover, it can overcome the resistance issue associated with the licensed DAA monotherapy as well as minimize dose-related toxicity and maximize clinical benefits [15]. Along this line, the synergistic potential of combinatorial treatment with zapnometinib and BXA was investigated. Compared to monotherapy, this combination treatment demonstrated more efficient reduction of the IAV titer and exhibited synergistic effect when both compounds were used at concentrations below their individual therapeutic levels.

Present investigations are shedding light on the immunomodulatory potential of MEK inhibitors [16-18]. A primary focus of the research was to examine the potential beneficial effects of zapnometinib's immunomodulatory effect *in vivo*, in addition to its antiviral activity. The immunomodulatory effect of zapnometinib was investigated in an ALI model that, on one hand, mirrors a severe hyperinflammatory condition, and on the other hand, remains unaffected by the pathogen infection dynamics. This model characteristic is crucial for distinguishing between direct anti-inflammatory effects and indirect effects primarily resulting from the reduction in pathogen levels. The results emphasize that zapnometinib treatment led to a significant decrease in hyperinflammatory cytokine responses, highlighting the drug’s immunomodulatory effectiveness. These findings provide the first *in vivo* validation of earlier *in vitro* research showing that zapnometinib modulates the proinflammatory gene expression response while having minimal effect on genes associated with the antiviral type I interferon (IFN) response [19].

In summary, the investigations emphasize vital insights to advance the development of zapnometinib, offering a promising therapeutic approach for managing respiratory infections.

Furthermore, the study sheds light on the dual impact of zapnometinib, encompassing both viral load reduction and modulation of the immune response.

On the other hand, when recapping influenza vaccines, current seasonal inactivated influenza vaccines induce antibodies targeting the HA head domain and thereby conferring strain-specific immunity. However, these antibodies are ineffective in providing cross-protection due to the persistent antigenic drift of the influenza viruses' surface proteins [20]. Given that current influenza vaccines have no impact on $CD8^+$ and innate T cells activation, cytotoxic CD8+ T cells confer cross-protection against seasonal IAVs, IBVs, pandemic, and avian IAVs [21-24]. CTLs are milestones for the management of infectious diseases. HLA molecules are key determinants of antigen recognition mediated by $CD8^+$ T cell recognition and can promote long-lasting memory post-priming with particular immunogenic epitopes [2,21,25]. Thus, broadly reactive vaccines that can harness the potential of $CD8^+$ T cell cross-protective immunity against different influenza virus strains and subtypes would be desirable, particularly for high-risk populations.

The effective design of peptide-based vaccines primarily lies in unveiling the factors that influence peptide immunogenicity and the magnitude of the immune response. Notably, the relative abundance of peptides presented by MHC-I plays a crucial role, particularly, during natural infection in provoking the hierarchy of immune responses [26-28].

Immunopeptidomics primarily focuses on identifying tumor antigens, in addition to the identification of viral epitopes. Here, a mass spectrometry-based (LC-MS/MS) immunopeptidomics approach was implemented to broaden the repertoire of MHC-I-presented peptides derived from IAV following infection of Calu-3 cells. Also, the investigation aimed to analyze the characteristics and temporal dynamics of naturally occurring HLA-I peptides restricted to different HLA allotypes, HLA-A*24:02, HLA-A*68:01, HLA-B*07:02, and HLA-B*51:01, expressed on the cell surface of Calu-3 cells following infection with H1N1/PR8, H3N2/Victoria and H3N2/Fukui strains at different infection time points.

Several viruses, including HIV, Adenoviruses and Herpesviruses, are linked to the regulation of MHC-I expression and interference of MHC-I ligand presentation [29-35]. A previous report also highlighted alterations in expression profiles by IAV and IBV during the late stage of infection [36]. Thus, the modulation of the HLA-I surface expression profile associated with

IAV infection was investigated. The data indicated that, following influenza virus infection, the expression of HLA-I molecules exhibited distinct patterns depending on the viral strain. The expression of HLA-I molecules remained consistent for H1N1/PR8 and H3N2/Fukui strains, while a significant downregulation occurred after infection with the H3N2/Victoria strain. These findings suggest that IAV interference with HLA-I expression may be specific to the virus strains/subtypes.

Immunopeptidomic analyses unveiled sixteen naturally presented peptides with high predicted binding affinity for HLA-A*68:01 (13 peptides), HLA-A*24:02 (1 peptide), and HLA-B*51:01 (2 peptides). Among these newly characterized peptides, four originated from the HA protein, with one each from M1, NS1, NS2, and PB1-F2 proteins. Additionally, two peptides were derived from the NP protein, while three each originated from PB1 and PB2. These peptides exhibited distinct presentation kinetics, being most detectable between 6-9 hours post infection (hpi) and reaching their peak at 12 hpi. These results are consistent with an earlier report which indicated that the peak presentation kinetics of various ligands occurred between 6.5 and 9.5 hpi and were not influenced by the kinetics of antigen expression [37].

IAV demonstrates temporal regulation of gene expression at the translational level, which mirrors the role of these proteins in the viral replication cycle [38-42]. However, certain viral proteins were notably absent as source proteins among the identified HLA-I ligands, despite performing ligandome analysis at various time points following infection. These findings corroborate immunopeptidomics studies that pinpointed distinct HLA-A*24–restricted peptides, primarily associated with PB2 and PB1 proteins, while notably excepting M1 or NA protein presentation [43]. In contrast, another study revealed naturally occurring HLA-I-restricted IAV ligands that encompass all IAV protein segments [37]. Thus, the significance of viral ligand presentation following direct infection remains controversial, and it appears that antigen presentation is more closely correlated with the degradation of viral proteins instead of their expression.

Notably, there are variations exist in the precision of prediction algorithms, leading to potential ambiguity in the MHC restriction prediction. Additionally, *in silico* prediction tools may overlook certain peptides that have been experimentally validated at the T cell level. Thus, all identified IAV-derived peptides were experimentally tested, and nine out of sixteen

putative epitopes were confirmed to be immunogenic. Among these, five epitopes were assigned as immunodominant. Moreover, the sporadic or weak T cell responses to certain epitopes may be attributed to either low-avidity TCRs or the reversed docking mode of TCR-pMHC-I interactions, which can restrict the capacity of naïve T cells to mount a robust immune response [44,45]. Therefore, it is important to recognize that the *in silico* binding prediction of ligands does not always correspond to the ligands' immunogenicity and cannot be solely relied upon as a parameter. Collectively, the ELISpot and ICS results revealed that most peptides triggering T cell responses are restricted to a single HLA-I allotype. However, the $HA_{LPY}$ epitope stands out by being restricted to two prominent HLA-I alleles (HLA-B*07:02 and HLA-B*51:01), thus offering broader coverage in populations possessing at least one of these alleles.

The presentation of CTL epitopes can be affected by AA substitutions within the HLA ligand sequence. Mutations occurring in CTL epitopes, particularly at anchor residues, may result in a loss of recognition by CD8+ T cells, as the epitope no longer precisely matches the specific TCR [46-50]. In this context, the data revealed that most epitopes remain highly conserved in major zoonotic reservoirs. Although some epitope sequence variants were observed, these can often be attributed to single AA substitutions, which occur in the vicinity of the anchor residues without significantly affecting binding affinity. Collectively, in the context of conservation, the data imply that epitope-specific CD8+ memory T cells have the potential to exhibit cross-reactivity against various IAV subtypes across different zoonotic reservoirs.

In summary, multiple IAV-derived epitopes comprising different viral protein segments were characterized, thereby expanding the knowledge beyond the limited set of previously known IAV-derived epitopes. Alongside other epitopes that may confer heterosubtypic protection, these specific epitopes hold promise as targets for T cell-based vaccination particularly against newly emerging variants, even when there are no preexisting neutralizing antibody responses.

**References**

[1] Lauring AS and Andino R. Quasispecies theory and the behavior of RNA viruses. PLoS pathogens. **2010**;6(7):e1001005.

[2] La Gruta NL and Turner SJ. T cell mediated immunity to influenza: mechanisms of viral control. Trends in Immunology. **2014**;35(8):396-402.

[3] Ludwig S. Disruption of virus-host cell interactions and cell signaling pathways as an anti-viral approach against influenza virus infections. Biological chemistry. **2011**;392(10):837-47.

[4] He F, Leyrer S and Kwang J. Strategies towards universal pandemic influenza vaccines. Expert review of vaccines. **2016**;15(2):215-25.

[5] Naesens L, Stevaert A and Vanderlinden E. Antiviral therapies on the horizon for influenza. Current opinion in pharmacology. **2016**;30:106-115.

[6] Watanabe T and Kawaoka Y. Influenza virus-host interactomes as a basis for antiviral drug development. Current opinion in virology. **2015**;14:71-8.

[7] Ludwig S, Wolff T, Ehrhardt C, Wurzer WJ, Reinhardt J, Planz O and Pleschka S. MEK inhibition impairs influenza B virus propagation without emergence of resistant variants. FEBS letters. **2004**;561(1-3):37-43.

[8] Droebner K, Pleschka S, Ludwig S and Planz O. Antiviral activity of the MEK-inhibitor U0126 against pandemic H1N1v and highly pathogenic avian influenza virus in vitro and in vivo. Antiviral research. **2011**;92(2):195-203.

[9] Haasbach E, Muller C, Ehrhardt C, Schreiber A, Pleschka S, Ludwig S and Planz O. The MEK-inhibitor CI-1040 displays a broad anti-influenza virus activity in vitro and provides a prolonged treatment window compared to standard of care in vivo. Antiviral research. **2017**;142:178-184.

[10] Takashita E, Kawakami C, Morita H, Ogawa R, Fujisaki S, Shirakura M, Miura H, Nakamura K, Kishida N, Kuwahara T, Mitamura K, Abe T, Ichikawa M, Yamazaki M, Watanabe S, Odagiri T and On Behalf Of The Influenza Virus Surveillance Group Of J. Detection of influenza A(H3N2) viruses exhibiting reduced susceptibility to the novel cap-dependent endonuclease inhibitor baloxavir in Japan, December 2018. Euro Surveill. **2019**;24(3).

[11] Checkmahomed L, M'Hamdi Z, Carbonneau J, Venable MC, Baz M, Abed Y and Boivin G. Impact of the Baloxavir-Resistant Polymerase Acid I38T Substitution on the Fitness of Contemporary Influenza A(H1N1)pdm09 and A(H3N2) Strains. J Infect Dis. **2020**;221(1):63-70.

[12] Gubareva LV, Mishin VP, Patel MC, Chesnokov A, Nguyen HT, De La Cruz J, Spencer S, Campbell AP, Sinner M, Reid H, Garten R, Katz JM, Fry AM, Barnes J and Wentworth

DE. Assessing baloxavir susceptibility of influenza viruses circulating in the United States during the 2016/17 and 2017/18 seasons. Euro Surveill. **2019**;24(3).

[13] Omoto S, Speranzini V, Hashimoto T, Noshi T, Yamaguchi H, Kawai M, Kawaguchi K, Uehara T, Shishido T, Naito A and Cusack S. Characterization of influenza virus variants induced by treatment with the endonuclease inhibitor baloxavir marboxil. Scientific reports. **2018**;8(1):9633.

[14] Planz O. Development of cellular signaling pathway inhibitors as new antivirals against influenza. Antiviral research. **2013**;98(3):457-468.

[15] Govorkova EA and Webster RG. Combination chemotherapy for influenza. Viruses. **2010**;2(8):1510-29.

[16] Houde N, Beuret L, Bonaud A, Fortier-Beaulieu SP, Truchon-Landry K, Aoidi R, Pic E, Alouche N, Rondeau V, Schlecht-Louf G, Balabanian K, Espeli M and Charron J. Fine-tuning of MEK signaling is pivotal for limiting B and T cell activation. Cell Rep. **2022**;38(2):110223.

[17] Verma V, Jafarzadeh N, Boi S, Kundu S, Jiang Z, Fan Y, Lopez J, Nandre R, Zeng P, Alolaqi F, Ahmad S, Gaur P, Barry ST, Valge-Archer VE, Smith PD, Banchereau J, Mkrtichyan M, Youngblood B, Rodriguez PC, Gupta S and Khleif SN. MEK inhibition reprograms CD8(+) T lymphocytes into memory stem cells with potent antitumor effects. Nat Immunol. **2021**;22(1):53-66.

[18] Li D, March ME, Gutierrez-Uzquiza A, Kao C, Seiler C, Pinto E, Matsuoka LS, Battig MR, Bhoj EJ, Wenger TL, Tian L, Robinson N, Wang T, Liu Y, Weinstein BM, Swift M, Jung HM, Kaminski CN, Chiavacci R, Perkins JA, Levine MA, Sleiman PMA, Hicks PJ, Strausbaugh JT, Belasco JB, Dori Y and Hakonarson H. ARAF recurrent mutation causes central conducting lymphatic anomaly treatable with a MEK inhibitor. Nature medicine. **2019**;25(7):1116-1122.

[19] Schreiber A, Viemann D, Schöning J, Schloer S, Mecate Zambrano A, Brunotte L, Faist A, Schöfbänker M, Hrincius E, Hoffmann H, Hoffmann M, Pöhlmann S, Rescher U, Planz O and Ludwig S. The MEK1/2-inhibitor ATR-002 efficiently blocks SARS-CoV-2 propagation and alleviates pro-inflammatory cytokine/chemokine responses. Cell Mol Life Sci. **2022**;79(1):65.

[20] Koutsakos M, Illing PT, Nguyen THO, Mifsud NA, Crawford JC, Rizzetto S, Eltahla AA, Clemens EB, Sant S, Chua BY, Wong CY, Allen EK, Teng D, Dash P, Boyd DF, Grzelak L, Zeng W, Hurt AC, Barr I, Rockman S, Jackson DC, Kotsimbos TC, Cheng AC, Richards M, Westall GP, Loudovaris T, Mannering SI, Elliott M, Tangye SG, Wakim LM, Rossjohn J, Vijaykrishna D, Luciani F, Thomas PG, Gras S, Purcell AW and Kedzierska K. Human CD8(+) T cell cross-reactivity across influenza A, B and C viruses. Nat Immunol. **2019**;20(5):613-625.

[21] Sridhar S, Begom S, Bermingham A, Hoschler K, Adamson W, Carman W, Bean T, Barclay W, Deeks JJ and Lalvani A. Cellular immune correlates of protection against symptomatic pandemic influenza. Nature medicine. **2013**;19(10):1305-12.

[22] Quinones-Parra SM, Clemens EB, Wang Z, Croom HA, Kedzierski L, McVernon J, Vijaykrishna D and Kedzierska K. A Role of Influenza Virus Exposure History in Determining Pandemic Susceptibility and CD8+ T Cell Responses. J Virol. **2016**;90(15):6936-6947.

[23] Koutsakos M, Wheatley AK, Loh L, Clemens EB, Sant S, Nussing S, Fox A, Chung AW, Laurie KL, Hurt AC, Rockman S, Lappas M, Loudovaris T, Mannering SI, Westall GP, Elliot M, Tangye SG, Wakim LM, Kent SJ, Nguyen THO and Kedzierska K. Circulating T(FH) cells, serological memory, and tissue compartmentalization shape human influenza-specific B cell immunity. Sci Transl Med. **2018**;10(428).

[24] Wang Z, Wan Y, Qiu C, Quiñones-Parra S, Zhu Z, Loh L, Tian D, Ren Y, Hu Y, Zhang X, Thomas PG, Inouye M, Doherty PC, Kedzierska K and Xu J. Recovery from severe H7N9 disease is associated with diverse response mechanisms dominated by CD8+ T cells. Nature communications. **2015**;6(1):6833.

[25] Janssens Y, Joye J, Waerlop G, Clement F, Leroux-Roels G and Leroux-Roels I. The role of cell-mediated immunity against influenza and its implications for vaccine evaluation. Frontiers in immunology. **2022**;13:959379.

[26] Croft NP, Smith SA, Wong YC, Tan CT, Dudek NL, Flesch IEA, Lin LCW, Tscharke DC and Purcell AW. Kinetics of Antigen Expression and Epitope Presentation during Virus Infection. PLoS pathogens. **2013**;9(1):e1003129.

[27] Tscharke DC, Croft NP, Doherty PC and La Gruta NL. Sizing up the key determinants of the CD8+ T cell response. Nature Reviews Immunology. **2015**;15(11):705-716.

[28] La Gruta NL and Turner SJ. T cell mediated immunity to influenza: mechanisms of viral control. Trends Immunol. **2014**;35(8):396-402.

[29] Blagoveshchenskaya AD, Thomas L, Feliciangeli SF, Hung C-H and Thomas G. HIV-1 Nef Downregulates MHC-I by a PACS-1- and PI3K-Regulated ARF6 Endocytic Pathway. Cell. **2002**;111(6):853-866.

[30] Petersen JL, Morris CR and Solheim JC. Virus Evasion of MHC Class I Molecule Presentation. The Journal of Immunology. **2003**;171(9):4473-4478.

[31] Cohen GB, Gandhi RT, Davis DM, Mandelboim O, Chen BK, Strominger JL and Baltimore D. The Selective Downregulation of Class I Major Histocompatibility Complex Proteins by HIV-1 Protects HIV-Infected Cells from NK Cells. Immunity. **1999**;10(6):661-671.

[32] Compeer EB, Flinsenberg TW, van der Grein SG and Boes M. Antigen Processing and Remodeling of the Endosomal Pathway: Requirements for Antigen Cross-Presentation [Review]. Frontiers in immunology. **2012**;3:37.

[33] Piguet V, Wan L, Borel C, Mangasarian A, Demaurex N, Thomas G and Trono D. HIV-1 Nef protein binds to the cellular protein PACS-1 to downregulate class I major histocompatibility complexes. Nature cell biology. **2000**;2(3):163-7.

[34] Li L, Santarsiero BD and Bouvier M. Structure of the Adenovirus Type 4 (Species E) E3-19K/HLA-A2 Complex Reveals Species-Specific Features in MHC Class I Recognition. Journal of immunology. **2016**;197(4):1399-407.

[35] Kasper MR and Collins KL. Nef-mediated disruption of HLA-A2 transport to the cell surface in T cells. J Virol. **2003**;77(5):3041-9.

[36] Koutsakos M, McWilliam HEG, Aktepe TE, Fritzlar S, Illing PT, Mifsud NA, Purcell AW, Rockman S, Reading PC, Vivian JP, Rossjohn J, Brooks AG, Mackenzie JM, Mintern JD, Villadangos JA, Nguyen THO and Kedzierska K. Downregulation of MHC Class I Expression by Influenza A and B Viruses [Original Research]. Frontiers in immunology. **2019**;10:1158.

[37] Wu T, Guan J, Handel A, Tscharke DC, Sidney J, Sette A, Wakim LM, Sng XYX, Thomas PG, Croft NP, Purcell AW and La Gruta NL. Quantification of epitope abundance reveals the effect of direct and cross-presentation on influenza CTL responses. Nature communications. **2019**;10(1):2846.

[38] Gale M, Jr., Tan SL and Katze MG. Translational control of viral gene expression in eukaryotes. Microbiol Mol Biol Rev. **2000**;64(2):239-80.

[39] Krammer F and Palese P. Orthomyxoviridae: The Viruses and Their Replication. In: Howley PM, Knipe DM, editors. Fields Virology: Emerging Viruses. Vol. Seventh edition. Philadelphia: Wolters Kluwer Health; 2020. p. 1224-1337.

[40] Zhang L, Wang Y, Shao Y, Guo J, Gao GF and Deng T. Fine Regulation of Influenza Virus RNA Transcription and Replication by Stoichiometric Changes in Viral NS1 and NS2 Proteins. J Virol. **2023**;97(5):e0033723.

[41] Min JY, Li S, Sen GC and Krug RM. A site on the influenza A virus NS1 protein mediates both inhibition of PKR activation and temporal regulation of viral RNA synthesis. Virology. **2007**;363(1):236-43.

[42] Zhu Z, Fan H and Fodor E. Defining the minimal components of the influenza A virus replication machinery via an in vitro reconstitution system. PLoS Biol. **2023**;21(11):e3002370.

[43] Hensen L, Illing PT, Bridie Clemens E, Nguyen THO, Koutsakos M, van de Sandt CE, Mifsud NA, Nguyen AT, Szeto C, Chua BY, Halim H, Rizzetto S, Luciani F, Loh L, Grant EJ, Saunders PM, Brooks AG, Rockman S, Kotsimbos TC, Cheng AC, Richards M, Westall GP, Wakim LM, Loudovaris T, Mannering SI, Elliott M, Tangye SG, Jackson DC, Flanagan KL, Rossjohn J, Gras S, Davies J, Miller A, Tong SYC, Purcell AW and Kedzierska K. CD8+ T cell landscape in Indigenous and non-Indigenous people restricted by influenza mortality-associated HLA-A*24:02 allomorph. Nature communications. **2021**;12(1):2931.

[44] Cukalac T, Chadderton J, Zeng W, Cullen JG, Kan WT, Doherty PC, Jackson DC, Turner SJ and La Gruta NL. The Influenza Virus–Specific CTL Immunodominance Hierarchy in

Mice Is Determined by the Relative Frequency of High-Avidity T Cells. The Journal of Immunology. **2014**;192(9):4061-4068.

[45] Gras S, Chadderton J, Del Campo Claudia M, Farenc C, Wiede F, Josephs Tracy M, Sng Xavier YX, Mirams M, Watson Katherine A, Tiganis T, Quinn Kylie M, Rossjohn J and La Gruta Nicole L. Reversed T Cell Receptor Docking on a Major Histocompatibility Class I Complex Limits Involvement in the Immune Response. Immunity. **2016**;45(4):749-760.

[46] Berkhoff EG, Boon AC, Nieuwkoop NJ, Fouchier RA, Sintnicolaas K, Osterhaus AD and Rimmelzwaan GF. A mutation in the HLA-B*2705-restricted NP383-391 epitope affects the human influenza A virus-specific cytotoxic T-lymphocyte response in vitro. J Virol. **2004**;78(10):5216-22.

[47] Rimmelzwaan GF, Boon AC, Voeten JT, Berkhoff EG, Fouchier RA and Osterhaus AD. Sequence variation in the influenza A virus nucleoprotein associated with escape from cytotoxic T lymphocytes. Virus Res. **2004**;103(1-2):97-100.

[48] Rammensee H-G, Friede T and Stevanović S. MHC ligands and peptide motifs: first listing. Immunogenetics. **1995**;41(4):178-228.

[49] Rammensee H-G. Chemistry of peptides associated with MHC class I and class II molecules. Current Opinion in Immunology. **1995**;7(1):85-96.

[50] Berkhoff EG, Geelhoed-Mieras MM, Verschuren EJ, van Baalen CA, Gruters RA, Fouchier RA, Osterhaus AD and Rimmelzwaan GF. The loss of immunodominant epitopes affects interferon-gamma production and lytic activity of the human influenza virus-specific cytotoxic T lymphocyte response in vitro. Clin Exp Immunol. **2007**;148(2):296-306.

# Abbreviations

| | |
|---|---|
| **A549** | Human lung adenocarcinoma cells |
| **AA** | Amino acid |
| **AIV** | Avian influenza viruses |
| **ALI** | Acute lung injury |
| **ARDS** | Acute respiratory distress syndrome |
| **AUC** | Area under the curve |
| **bnAbs** | Broadly-neutralizing antibodies |
| **BSA** | Bovine serum albumin |
| **BXA** | Baloxavir acid |
| **BXM** | Baloxavir marboxil |
| **Calu-3** | Human lung adenocarcinoma cells |
| **$CC_{50}$** | 50% cytotoxicity concentration |
| **CD107a** | Lysosomal Associated Membrane Protein 1 |
| **cHA** | Chimeric HA |
| **CI** | Combination index |
| **CID** | Collision-induced dissociation |
| **COBRA** | Computationally optimized broadly reactive antigen |
| **CPE** | Cytopathic effect |
| **CSS** | Clinical severity status |
| **CTL** | Cytotoxic T lymphocytes |
| **DAA** | Direct-acting antiviral |
| **DDA** | Data-dependent acquisition |
| **$D_m$** | Median effect dose |
| **DMEM** | Dulbecco's modified eagle medium |
| **DMSO** | Dimethyl sulfoxide |
| **DNA** | Deoxyribonucleic acid |
| **dpi** | Day post infection |
| **DR** | Dose reduction |
| **DRI** | Dose reduction index |
| **$EC_{50}$** | Half maximal effective concentration |
| **ELISpot** | Enzyme-linked immunospot |
| **FACS** | Fluorescence-activated cell sorting |
| **FBS** | Fetal bovine serum |
| **FDA** | US Food and Drug Administration |
| **FDR** | False discovery rate |
| **FFU** | Focus-forming unit |
| **HA** | Hemagglutinin |
| **HEK 293T** | Human embryonic kidney cells |
| **HLA** | Human leukocyte antigen |
| **HLA-I** | Human leukocyte antigen class I |
| **HPAI** | Highly pathogenic avian influenza |
| **hpi** | Hours post infection |
| **HSA** | Highest single agent model |
| **HTA** | Host-targeted antiviral |
| **IAV** | Influenza A virus |
| **IBV** | Influenza B virus |
| **$IC_{50}$** | Half-maximal inhibitory concentration |
| **ICS** | Intracellular cytokine staining |
| **ICV** | Influenza C virus |
| **IDV** | Influenza D virus |
| **IFIT-1** | Interferon Induced Protein With Tetratricopeptide Repeats 1 |
| **IFN** | Interferon |

| | |
|---|---|
| **IFN-γ** | Interferon gamma |
| **IgG** | Immunoglobulin G |
| **IgG-HRP** | Immunoglobulin G conjugated to horseradish peroxidase |
| **IMDM** | Iscove's modified dulbecco's medium |
| **IRD** | Influenza research database |
| **IV** | Influenza virus |
| **LC-MS/MS** | Liquid chromatography-tandem mass spectrometry |
| **LFQ** | Label-free quantification |
| **LLOQ** | Lower limit of quantification |
| **LNP** | Lipid nanoparticle |
| **LTQ** | Linear trap quadrupole |
| **LTQ** | Linear trap quadrupole |
| **M1** | Matrix protein 1 |
| **M2** | Matrix protein 2 |
| **mAB** | Monoclonal antibody |
| **mABs** | Monoclonal antibodies |
| **MAPK** | Mitogen-activated protein kinase |
| **MDCK II** | Madin-darby canine kidney cells |
| **MEM** | Minimum essential medium |
| **MHC-I** | Major histocompatibility complex class I |
| **MOI** | Multiplicity of infection |
| **MRC-5** | Human fibroblast lung cells |
| **mRNA-LNP** | mRNA–lipid nanoparticle |
| **MS** | Mass spectrometry |
| **MS/MS** | Tandem mass spectrometry |
| **NA** | Neuraminidase |
| **NAI** | Neuraminidase inhibitors |
| **NCBI** | National Center for Biotechnology Information |
| **NI** | Neuraminidase-inhibiting activity |
| **nM** | Nanomolar |
| **nm** | nanometer |
| **NP** | Nucleoprotein |
| **nt** | not tested |
| **OD** | Optical density |
| **P/S** | Penicillin/Streptomycin |
| **PA** | Polymerase acidic protein |
| **pAbs** | Polyclonal antibodies |
| **PB1** | Influenza polymerase basic protein 1 |
| **PB2** | Influenza polymerase basic protein 2 |
| **PBMCs** | Peripheral blood mononuclear cells |
| **PBS** | Phosphate-buffered saline |
| **PDB** | Protein data bank |
| **PE** | Phycoerythrin |
| **pfu** | Plaque-forming unit |
| **PHA** | Phytohemagglutinin |
| **PMA** | Phorbol-12-myristate-13-acetate |
| **PVDF** | Polyvinylidene fluoride |
| **RBS** | Receptor-binding site |
| **RdRp** | RNA-dependent RNA polymerase |
| **RNA** | Ribonucleic acid |
| **SA** | Sialic acid |
| **SD** | Standard deviation |
| **SEM** | Standard error of the mean |
| **SFCs** | Spot forming cells |
| **SI** | Selectivity index |
| **SOC** | Standard-of-care |

| | |
|---|---|
| **$TCID_{50}$** | 50% tissue culture infectious dose |
| **TCR** | T-cell receptor |
| **TMB** | Tetramethylbenzidine |
| **TMPRSS2** | Transmembrane protease, serine 2 |
| **TNF** | Tumor necrosis factor |
| **TPCK** | N-tosyl-L-phenylalanine chloromethyl ketone |
| **Vero E6** | African green monkey kideny cells |
| **vRNA** | Viral RNA |
| **vRNP** | Viral ribonucleoproteins |
| **VYR** | Virus yield reduction assay |
| **WHO** | World Health Organization |
| **WT** | Wild type |
| **µM** | Micromolar |

# Acknowledgements

I want to thank Prof. Hans-Georg Rammensee for giving me the opportunity to study and work in the Department of Immunology. Of course, I would like to express my respect for creating a unique work and research atmosphere. The collaborative environment at the Department fostered my work and made this project possible.

I extend my sincere appreciation to my supervisor Prof. Oliver Planz for his insightful guidance and unwavering support. From the inception of this project until my thesis defense, his invaluable feedback and discussions shaped my research and writing. I am also thankful to Olli's group members for their collaborative spirit.

I would like to thank Prof. Stefan Stevanović, for his support as a supervisor before his retirement and his group, particularly, Michi Ghosh and Ana Marcu for their support during mass spectrometry analysis.

I also want to thank our technical support team, Beate, Claudia, and Ulrich, for always having time to support us and making the working environment better for all of us.

The administrative staff at the Department of Immunology deserve recognition for their prompt assistance with paperwork, scheduling, and logistical matters. Their efficiency allowed me to focus on my research. Thank you!

Foremost, I would like to express my heartfelt gratitude to my parents, brothers, and sisters, for their unwavering support and encouragement throughout this journey. Their love and belief in me kept me going during challenging times. There are no words that can thank you enough for everything you have done for me.

In loving memory of my father, whose absence is felt profoundly. Your encouragement and belief in my abilities fueled my pursuit of knowledge. Your legacy endures through my unwavering dedication to this work.